Novel tools for polymer monolithic capillary column production and chromatographic application

For the award of Doctor of Philosophy

David Collins

Student no: 96562048
School of Chemical Sciences

Under the supervision of:

Dr. Ekaterina Nesterenko
Prof. Brett Paull
Dr. Dermot Brabazon

April 2013

Declaration

I hereby certify that this material, which I now submit for assessment on the programme of study leading to the award of Doctor of Philosophy is entirely my own work, that I have exercised reasonable care to ensure that the work is original and does not to the best of my knowledge breach any law of copyright, and has not been taken from the work of others save to the extent that such work has been cited and acknowledged within the text of my work.

Signed:_____ Date:_____

Candidate ID No:_____

Table of Contents

Chapter 1. Introduction

Chapter 2. Development of a capillary and microbore scale column heater based on a thermoelectric array

Chapter 3. Chromatographic evaluation and application of a capillary and microbore scale column heater based on a thermoelectric array

Chapter 4. Photo-initiated monoPLOT column fabrication and evaluation

Chapter 6. In-process layer measurement for monoPLOT column fabrication

List of awards

1. Recipient of 2013 Society of Chemical Industry Wesley Cocker Award.
2. Recipient of Dublin City University Faculty of Science and Health Outstanding Graduate Researcher Award 2012.
3. Recipient of 2012 Royal Society of Chemistry Ronald Belcher Award for outstanding achievement in the area of high temperature capillary LC and capillary LC related instrumentation development.
4. Nominated for American Chemical Society Division of Analytical Chemistry Award for Young Investigators in Separation Science 2012.
5. Nominated for best poster prize at Separation Science Asia 2011, Singapore.
6. Nominated for best poster prize at CASi 2010, Dublin, Ireland.

List of patents and invention disclosures

1. Collins, D.; Nesterenko, E.; Heery, B.; Paull, B., US Patent of Dublin City University entitled “Column heater”, published by the USPTO December 20th, 2012 under publication number US-2012-0318782-A1
2. Collins, D.; Nesterenko, E.; Heery, B.; Paull, B., British Patent Application No. 1109528.8 "Capillary column curing system". HMC Ref: D07-396-53GB, 7th June 2011.
3. Collins, D.; Nesterenko, E.; Heery, B.; Paull, B., US Patent of Dublin City University entitled “Capillary column curing system", published by the USPTO December 13th, 2012 under publication number US-2012-0315023-A1
4. Collins, D.; Nesterenko, E.; Paull, B.; Invention disclosure of Dublin City University entitled “monoPLOT column fabrication through laminar flow thermal initiation”, March 2012.

List of publications

1. Collins, D.; Nesterenko, E.; Brabazon, D.; Paull, B.; "Fabrication of bonded monolithic porous layer open tubular (monoPLOT) columns in wide bore capillary by laminar flow thermal initiation", *Chromatographia*, (2013), 76, pp. 581-589.

2. Collins, D.; Nesterenko, E.; Brabazon, D.; Paull, B.; "In-process phase growth measurement technique in the fabrication of monolithic porous layer open tubular (monoPLOT) columns using capacitively coupled contactless conductivity", *The Analyst*, (2013), 138, pp. 2540-2545.

3. Collins, D., "Exploring High Temperature LC", *Laboratory News*, Oct 2012.

4. Collins, D.; Nesterenko, E.; Brabazon, D.; Paull, B.; "Controlled UV photo-initiated fabrication of monolithic porous layer open tubular (monoPLOT) capillary columns for chromatographic applications", *Anal. Chem*., (2012), 84, 7, pp. 3465–3472.

5. Collins, D., "The Heat Is On", *LCGC, E-Separation Solutions*, January 2012.

6. Collins, D.; Nesterenko, E.; Connolly, D.; Vasquez, M.; Macka, M.; Brabazon, D.; Paull, B., "Versatile capillary column temperature control using a thermoelectric array based platform", *Anal. Chem.*, (2011), 83, 11, pp. 4307–4310.

7. Collins, D.; Connolly, D.; Macka, M.; Paull, B., "Application of dynamic temperature gradients and profiles for capillary LC through the application of a new thermoelectric array based column heater", *Chromatography Today*, (Aug/Sep 2010), pp 30–31.

List of oral presentations

1. Collins, D., Nesterenko, E., Brabazon, D., Paull, B., "Exploring high temperature liquid chromatography", *Lab Innovations 2012 – Royal Society of Chemistry Lecture*, Birmingham, invited talk.

2. Collins, D., Nesterenko, E., Brabazon, D., Paull, B., "Controlled uv photo-initiated fabrication of monolithic porous layer open tubular (monoplot) capillary columns for chromatographic applications", *Analytical Conference of Siberia and Far East 2012,* Krasnoyarsk, invited talk.

3. Collins, D., Nesterenko, E., Brabazon, D., Paull, B., "Novel tools for polymer monolithic capillary column production and chromatographic application", *Analytical Research Forum*, 2012, Durham, invited talk.

4. Paull, B., Connolly, D., Nesterenko, P., Nesterenko, E., Alwael, H., Collins, D., Peristyy, A., Duffy, E., He, X., "Application of Metallic and Carbonaceous Nano-particle Modified Phases in Micro-extraction and Liquid Chromatography", *38th International Symposium on High Performance Liquid Phase Separations and Related Techniques 2012*, Anaheim, invited talk.

5. Nesterenko, E., Collins, D., Thompson, R., Clarke, P., O'Connor, B., Brabazon, D., Paull, B., "MonoPLOT columns for micro-solid phase extraction and LC of proteins", *36th International Symposium on Capillary Chromatography,* 2012, Riva del Garda, oral presentation.

6. Collins, D., Nesterenko, E., Connolly, D., Thompson, R., Clarke, P., O'Connor, B., Paull, B., "Production, characterisation and application of monoPLOT open tubular capillary columns", *11th Asia-Pacific International Symposium on Microscale Separations and Analysis*, 2011, Hobart, invited talk.

7. Nesterenko, E., Moyna, A., Collins, D., Yavorskyy, A., Connolly, D., Paull, B., "Ion-exchange monoPLOT columns for micro solid-phase extraction", *23nd International Ion Chromatography Symposium 2011*, Rhode Island, oral presentation.

8. Collins, D., Nesterenko, E., Connolly, D., Macka, M., Brabazon, D., Paull, B., "Investigation of Temperature Effects on Monolithic Ion Exchangers Using an Advanced Peltier Array Based Capillary Column Heater", *22nd International Ion Chromatography Symposium 2010*, Cincinnati, oral presentation.

9. M.Vázquez, D. Collins, E. Nesterenko, D. Brabazon, B. Paull, Preparation of monoliths in glass/silicon microfluidic chips as stationary phases and frits for column packing, *28th International Symposium on Chromatography 2010*, Valencia, oral presentation.

10. Collins, D., Nesterenko, E., Connolly, D., M., Macka, M., Brabazon, D., Paull, B., "The application of dynamic temperature profiles and gradients from a peltier array based platform to the fabrication and application of capillary HPLC columns", *28th International Symposium on Chromatography 2010*, Valencia, oral presentation.

List of poster presentations

1. Collins, D., Nesterenko, E., Brabazon, D., Paull, B., "Controlled UV photo-initiated fabrication of monolithic porous layer open tubular (monoPLOT) capillary columns for chromatographic application", *36th International Symposium on Capillary Chromatography*, 2012, Riva del Garda, poster presentation.

2. Collins, D., Nesterenko, E., Connolly, D., Brabazon, D., Paull, B., "Complex Rapid Temperature Programming For Capillary And Microscale Liquid Chromatography Through The Application Of Direct Contact Thermoelectric Module Arrays", *Chem50 Symposium*, 2011, Hobart, poster presentation.

3. Collins, D., Nesterenko, E., Connolly, D., Brabazon, D., Paull, B., "Complex Rapid Temperature Programming For Capillary And Microscale Liquid Chromatography Through The Application Of Direct Contact Thermoelectric Module Arrays", *Separation Science Asia 2011*, Singapore, poster presentation.

4. Collins, D., Nesterenko, E., Connolly, D., Brabazon, D., Paull, B., "Complex Rapid Temperature Programming For Capillary And Microscale Liquid Chromatography Through The Application Of Direct Contact Thermoelectric Module Arrays", *36th International Symposium on High Performance Liquid Phase Separations and Related Techniques 2011*, Budapest, poster presentation.

5. Ben Azouz, A., He, X., Vazquez, M., Nesterenko, E., Collins, D., Nesterenko, P., Paull, B., Brabazon, D., "Carbon and polymer monolith focussed ion beam serial sectioning and imaging for 3D surface reconstruction and morphological parameter evaluation", *36th International Symposium on High Performance Liquid Phase Separations and Related Techniques 2011*, Budapest, poster presentation.

6. Collins, D., Nesterenko, E., Connolly, D., Macka, M., Brabazon, D., Paull, B., "Dynamic rapid temperature programming for capillary and microscale liquid chromatography", *Conference on Analytical Sciences Ireland 2011*, Dublin, poster presentation.

7. M. Vázquez, D. Collins, E. Nesterenko, D. Brabazon, B. Paull, A novel method for in situ preparation of monolithic stationary phases in specific areas of microfluidic channels by thermally initiated polymerisation, *UNCSR Symposium 2010*, Dublin, poster presentation.

8. Collins, D., Nesterenko, E., Connolly, D., M., Macka, M., Brabazon, D., Paull, B., "The application of dynamic temperature profiles and gradients from a peltier array based platform to the fabrication and application of capillary HPLC columns", *UNCSR Symposium 2010*, Dublin, poster presentation.

9. Collins, D., Connolly, D., Vazquez, M., Macka, M., Brabazon, D., Paull, B., "Generation and control of temperature gradients and longitudinal profiles along LC capillary columns through the use of Peltier arrays and infra red thermal imaging", *35th International Symposium on High Performance Liquid Phase Separations and Related Techniques 2010*, Boston, poster presentation.

List of figures

Figure 1.8 – SEM images of the carbon monolith at different magnifications, (a) 600X and (b) 20,000X.

Figure 1.9 – SEM images of polyacrylamide hybrid monoliths.

Figure 1.10 – SEM image of a silica layer formed in a 15 μm ID capillary.

Figure 1.11 – Separation of anisole isomers (1. toluene, 2. anisole, 3. 3-Nitroanisole, 4. 4-Nitroanisole, 5. 2-Nitroanisole). Column dimensions: 6m x 15 um ID. Mobile phase: n-heptane/1,4-dioxane 95/5 (v/v) in isocratic mode. Linear flow rate was calculated to be 3.6 mm/s. UV detection at 225 nm.

Figure 1.12 – SEM image of a PS-DVB PLOT column prepared in a 10 μm ID fused silica capillary.

Figure 1.13 – Dependence on capillary diameter of the morphology of photo-polymerised monoliths derived from a variety of polymerisation mixtures resulting in different macropore sizes (decreasing macropore size M1 to M4). No surface treatment was used on the fused-silica capillaries.

Figure 1.14 – Base peak chromatogram from the microSPE-nano-LC/ESI-MS analysis of a 4-ng tryptic in-gel digest of a single SDS-PAGE cut of M. acetivorans, separated on a 4.2 m x 10 μm ID PLOT column. A 4 cm x 50 μm ID PS-DVB monolithic column was used as the microSPE pre-column.

Figure 1.15 – SEM images of a 50 um ID capillary coated under stationary conditions (A) and revolving at 100 rpm (B).

Figure 1.16 – CEC separation of thiourea and benzene derivatives, (1. thiourea, 2. benzene, 3. methylbenzene, 4. ethylbenzene, 5. propylbenzene, and 6. butylbenzene) at 60 C with pressurised flow (inlet pressure = 5,000 Pa) and EOF (20 kV). Column: 40 cm x 20 um ID EDMA monoPLOT column with a 0.5 μm layers, photo-grafted with META. Mobile phase: 40:60% ACN:Tris buffer (10 *mM*, pH 8). UV detection at 200 nm.

Figure 1.17 – Separation of 8 proteins (1. ribonuclease, 2. insulin, 3. cytochrome C, 4. horseradish peroxidase, 5. carbonic anhydrase, 6. enolase, 7. alcohol dehydrogenase and 8. phosphorylase) on a diol functionalised monoPLOT column. Column: 51 cm x 50 µm ID, 5 µm layer. Mobile phase: A: 0% ACN, 0.1% TFA; B: 90% ACN, 0.1% TFA. Gradient elution: 0.0–20.0 min from 100% A to 100% B; 20.0–20.1 min from 100% B to 100% A;20.1–60 min 100% A, pH 1.9. Flow rate = 0.4 mL/min.

Figure 1.18 – Analysis of phenylurea pesticides (1. fenuron, 2. metoxuron, 3. chlortoluron, 4. diuoron, 5. isoproturon, 6. linuron, and 7. chloroxuron) on a Zorbax StableBond-C18 column (50 mm x 2.1 mm ID, 1.8 µm d_p). Mobile phase: ACN/water (30:70%). DAD detection at 245 nm.

Figure 1.19 – Separation of polymer additives by isothermal elution at 50 8C (A) and by a temperature program from 100 to 150 °C (B). Column, 3 mm Hypersil ODS, 100 A, 0.32 mm ID x 69 cm. Mobile phase: DMF–acetonitrile (10:90%), flow rate = 5 ml/min. UV detection at 280 nm.

Figure 1.20 – Band broadening due to thermal effects: (a) ideal case, no thermal effects; (b) effect of incoming mobile phase that is at a lower temperature than the column; (c) effect of frictional heating; (d) combined effects of cold incoming mobile phase and frictional heating. An oven temperature of 70 °C is assumed.

Figure 1.21 – Comparison of separations of Leu-Pro performed at (a) 23 °C and (b) 1 °C on a LiChrosorb RP-18 250 x 4.6 mm ID (d_p 10 µm) column at a flow rate of 2.0 ml/mm. Mobile phase: 0.050 M phosphate in MeOH, pH 6.0 (10:90%). UV detection at 210 nm.

Figure 1.22 – Separation of Val-Pro-Leu isomers at (a) room temperature, mobile phase MeOH with 0.05 M phosphate (pH 7.0) (15:85%), flow rate 2.0 ml/mm, at (b) -0.1 °C, mobile phase MeOH – phosphate buffer (pH 7.0) (20:80%), flow rate 2.0 ml/mm, and at (c) -11 °C, flow-rate 1.8 ml/min. Column = Pecosphere C_{18} 33 cm x 4.6 mm ID (d_p 3 µm). UV detection at 210 nm.

Figure 1.23 – The influence of loading temperature on enrichment-column focusing of Irganox 1076 (60 ng) when using a loading flow rate of 5 μL/min and an injection volume of 500 μL.

Figure 1.24 – Separation of o-phythalaldehyde derivatives of amino acid esters with step gradient elution at −10 °C; 5.4% diethylether in hexane (0 – 23.8 min) → 26.5% diethylether in hexane (23.8 – 40.0 min) → 50.0% diethylether in hexane (40.0 – 50.0 min).

Figure 1.25 – Plate height vs. linear velocity at various temperatures for moderately retained solutes. Experimental conditions: 3 μm ZirChrom-PS column, 5 cm x 4.6 mm ID, 40% ACN/60% water, △ = 25 °C, octanophenone, k = 3.87, ▽ = 80 °C decanophenone, k = 3.15, □ = 120 °C, decanophenone, k = 5.70, ○ = 150 °C, decanophenone, k = 1.65.

Figure 1.26 – Van't Hoff plot of polystyrenes, demonstrating the impact of temperature on the retention of compounds with different molecular mass.

Figure 1.27 – Effect of temperature on the separation of caffeine derivatives (1, hypoxantine; 2, theobromine; 3, theophilline; 4, caffeine; 5, ß-hydroxy-ethyltheophilline). Column: ZirChrom-DB-C_{18} 50 mm x 4.6 mm: (a) 25 ◦C, flow rate = 1 mL/min, water–methanol 60:40% (v/v); (b) 150 ◦C, flow rate = 7 mL/min, water.

Figure 1.28 – Effect on of temperature on resolution. Separation of benzene and six steroids (1. benzene; 2. hydrocortisone; 3. cortisone; 4. prednisolone; 5. dexamethasone; 6. hydrocortisone acetate; and 7. testosterone) on a NIPAAm-BMA-DMAPAAm (IBD) terminally-modified column at (a) 10 °C,and (b) 50 °C. Mobile phase: H_2O. Flow rate = 1.0 mL/min. UV detection at 254 nm.

Figure 1.29 – Effect of temperature on (a) dielectric constant, (b) surface tension and (c) viscosity for pure water, and water/acetonitrile and water/methanol mixtures.

Figure 1.30 – Separation of (a) alkylbenzenes at 190 °C at 4 ml/min and (b) phenylalkanols at 170 °C at 1 ml/min on C_{18} bonded ethylene bridged hybrid column.

Figure 1.31 – Green chromatography of a sulfonamide mixture (1. sulfamethazine, 2. sulfamethizole, 3. sulfachlorpyridazine, and 4. sulfamethoxine) on a Hypercarb column 100 mm x 3 mm ID (d_p 5 µm), at various conditions, (a) isocratic 50% B, isothermic 50 °C; (b) solvent program 50 to 100% B in 5 min, isothermic 50 °C; (c) isocratic 50% B, temperature program: initial 40 °C, hold 0–2 min, ramp 40–180 °C at 20 °C/min. Flow rate = 0.5 mL/min. Mobile phase: A, 0.1% acetic acid in water, B, 0.1% acetic acid in ethanol. DAD detection at 273 nm. Inset: MS peak area under conditions (b) and (c).

Figure 1.32 – Separations of a protein mixture (1. ribonuclease, 2. insulin; and 3. α-chymotrypsin) performed on a HC-C_8 phase at 120 °C, (A) injection made immediately after column equilibration at 120 °C; (B) after 24 hr; (C) after 50 hr. Conditions: 120 °C, 5 mL/min, injection volume 1 µL. Solvent (A) 0.1% TFA in water; solvent (B) 0.067% TFA in ACN. Linear gradient from 10 to 90% B in 0.3 min (dwell time is 0.2 min). UV detection at 220 nm.

Figure 1.33 – Effect of the inlet solvent temperature on separation. Flow rate = 2 ml/min, incoming and oven temperatures shown in figure.

Figure 1.34 – Column temperature lag during a temperature program from 40 °C to 200 °C at 40 °C/min, after an initial hold 1 min. The column was 4.6mm internal diameter x 150 mm long. Mobile phase: H_2O, flow rate = 3 mL/min, and was maintained in a liquid state by applying 250 psi backpressure to the column outlet. The mobile phase preheater was programmed to track the oven temperature.

Figure 2.1 – Schematic of TEC module (cooling mode).

Figure 2.2 – TEC module structure.

Figure 2.3 – Mk.1 prototype TEC column heater, showing control board (a), heat exchanger (b), Peltier module and thermistor (c), column (d), and fan (e).

Figure 2.4 – 12 x 12 mm Peltier response for temperature vs input current.

Figure 4.15 – SEM image of a non-uniform porous PS-DVB layer inside a 100 µm ID polyimide coated capillary due to non-homogenous light.

Figure 4.16 – Chemical structure of (a) H-Nu 815 and (b) borate V.

Figure 4.17 – SEM images of porous PS-DVB layers formed inside a 100 µm ID polyimide coated capillary. Polymerisation mixture: 12 %wt styrene, 12 %wt vinylbenzene chloride, 15.5 %wt divinylbenzene, (a) 15 %wt acetonitrile, 20 %wt isopropanol, 22 %wt 1-decanol, and (b) 18 %wt acetonitrile, 39 %wt 1-decanol. In both cases the amount of initiator was the same, 0.5 %wt H-Nu 815, 0.5 %wt borate V, and 2.5 %wt MPPTFB (with respect to monomers). Polymerisation conditions: Exposed to 2 mW/cm2 of IR light at 830 nm for 4 hrs.

Figure 4.18 – Comparison of polymer layer thickness and %wt of MPPTFB in the polymerisation mixture. Polymerisation mixture: 12 %wt styrene, 12 %wt vinylbenzene chloride, 16 %wt divinylbenzene, 18 %wt acetonitrile, 40 %wt 1-decanol, 0.5 %wt H-Nu 815, 0.5 %wt borate V, and varying %wt TFB (with respect to monomers). Polymerisation conditions: Exposed to 2 mW/cm2 of IR light at 830 nm for 4 hrs.

Figure 4.19 – SEM images of PS-DVB polymer layer formed within a 100 µm ID capillary using (a) 0.5% wt, (b) 1.5 %wt, and (c) 2.5% wt TFB. Polymerisation mixture and conditions as per Figure 4.18.

Figure 4.20 – Separation of ten proteins (1. INS, 2. Rnase B, 3. TRY, 4. Rnase A, 5. Cyt C, 6. MB, 7. HRP, 8. PP2, 9. CA, and 10. Con A) at varying flow rates using a 45 min gradient from 1 to 90% acetonitrile: flow rate (a) 0.5 µL/min, (b) 0.4 µL/min, (c) 0.3 µL/min, (d) 0.2 µL/min, and (e) 0.1 µL/min. Column: 60 cm x 50 µm ID BuMA-EDMA monoPLOT column, layer thickness ~2 µm. Mobile phase: ACN/H_2O gradient from 1 to 90% with 0.1% TFA. UV detection at 214 nm.

Figure 6.9 – (a) C4D response recorded during polymerisation of a ~400 nm layer inside a 50 µm ID capillary and (b) SEM image of fabricated layer. Polymerisation conditions: mixture = BuMA/EDMA with 1% 10 *mM* NaCl, temperature = 60 °C, linear flow rate = 1.0 mm/s. Change in C4D response was recorded as 3.3 mV, corresponding to a theoretical layer thickness of 370 nm. (c) C4D response recorded during polymerisation of a ~3.3 µm layer inside a 100 µm ID capillary and (d) SEM image of fabricated layer. Polymerisation conditions: mixture was PS-DVB with 1% 10 *mM* NaCl, temperature = 60 °C, linear flow rate = 0.5 mm/s. Change in C4D response was recorded as 63.8 mV, corresponding to a theoretical layer thickness of 2.98 µm.

Figure 6.10 – Relationship between effective capillary ID and C4D response, showing both bare capillary (□) and capillary with monoPLOT layer (○).

Figure 6.11 – SEM image of overpolymerised BuMA-EDMA monoPLOT column fabricated from a polymerisation mixture containing 2 %wt of 10 *mM* NaCl.

List of tables

List of abbreviations

ACN – acetonitrile

ABS – acrylonitrile butadiene styrene

AFM – atomic force microscopy

AIBN – azobisisobutyronitrile

borate V – butyltriphenyl-borate

BuMA – butyl methacrylate

BVPE – 1,2-bis(*p*-vinylphenyl)ethane

CA – carbonic anhydrase

CEC – capillary electrochromatography

CME – capillary micro extraction

Con A – concanavalin A

Cyt C – cytochrome C

CZE – capillary zone electrophoresis

DAD – diode array detector

DAP – dimethoxy-2-phenyacetophenone

DNA – deoxyribonucleic acid

DVB – divinylbenzene

EDMA – ethylene dimethacrylate

ETV – electrothermal vaporisation

EW – evanescent wave

GC – gas chromatography

GMA – glycidylmethacrylate

GUI – graphical user interface

H-Nu 815 – 2-[2-[2-chloro-3-[(1,3-dihydro-1,1,3-trimethyl-2H-benz[e]indol-2-ylidene) ethylide- ne]-1-cyclohexen-1-yl]ethenyl]-1,1,3-tri-methyl-1H-benz[e]indolium

HPLC – high performance liquid chromatography

HRP – horseradish peroxydase

ICP – inductively coupled plasma

ID – internal diameter

INS – insulin

IR – infra red

LC – liquid chromatography

LED – light emitting diode

LMA – lauryl methacrylate

LPD – liquid phase deposition

MB – myoglobin

MeOH – methanol

monoPLOT – monolithic porous layer open tubular

MPPTFB – N-methoxy-4-phenylpyridinium tetrafluoroborate

MS – mass-spectrometry

NDSA – naphthalenedisulphonic acid

OD – outer diameter

ODS – octadecyl silica

OT – open tubular

PAH – polyaromatic hydrocarbon

PCR – polymerase chain reaction

PEEK – polyether ether ketone

PID – proportional integral derivative

PLOT – porous layer open tubular

PP2 – phosphatase B

PS-DVB – polystyrene-divinylbenzene

RNase A – ribonuclease A

RNase B – ribonuclease B

ROC – rate of change

RP – reversed phase

RSD – relative standard deviation

sC4D – scanning capacitively coupled contactless conductivity detection

SEM – scanning electron microscopy

SFI – Science Foundation Ireland

SNR – signal to noise ratio

SPME – solid-phase micro extraction

TEC – thermoelectric cooler

TEOS – tetraethylorthosilicate

TFA – trifluoroacetic acid

THF – tetrahydrafuran

TIR – total internal reflection

TRY – Trypsin

uHPLC/UPLC – ultra high performance liquid chromatography

UV – ultraviolet

VI – virtual instrument

WCOT – wall-coated polymeric coatings

Acknowledgements

I would firstly like to thank my wife Caitríona for her support, patience, and encouragement during my studies, and for also proof reading the manuscript.

I would like to thank my three supervisors, Dr. Ekaterina Nesterenko, Prof. Brett Paull, and Dr. Dermot Brabazon, and also Prof. Apryll Stalcup. Without their advice, guidance and direction none of this would have been possible.

Abstract

Though the vast majority of routine separations in liquid chromatography (LC) are performed on standard-bore columns, in recent years there has been significant interest in micro-format LC systems, resulting in the development of capillary and micro-bore scale columns and instrumentation. Capillary scale LC separations provide lower mobile phase consumption and facilitate the analysis of smaller sample volumes, whilst simultaneously offering the possibility of fast analysis times and potentially higher separation efficiency. Furthermore, reducing the diameter of the column reduces the dilution of the sample as it passes through the column, thus improving detection sensitivity. Several novel instrument developments and approaches for capLC are discussed in this work, including their design, implementation, evaluation and application.

One of the current trends in both standard and capillary format LC is the utilisation of high temperatures, including temperature programmed separations, as well as the application of thermally responsive stationary phases. However, most commercially available column ovens cannot provide the high ramp rates, sectioned heating or high temperatures that may be required. In an attempt to address these issues, several prototypes of a novel segmented column heater, based on thermoelectric (TEC) modules for capillary and micro-bore LC were developed. The devices had a broad operating temperature range with a fast heating rate, allowing very rapid temperature programming, with precise and isolated zoned column temperature control. To demonstrate application, the developed systems were applied to reversed-phase and ion-exchange mode capillary separations. The devices were

further applied to the fabrication of monolithic stationary phases via thermally-initiated polymerisation.

Interest in capillary LC has also focused on separations utilising porous layer open tubular (PLOT) columns. Such columns with an organic porous polymer monolithic layer (monoPLOT) offer significant potential for LC applications arising from variation of surface chemistry and simple surface modification procedures, high flow-through permeability and low column backpressure. However, monoPLOT columns can be difficult to fabricate, and column to column reproducibility is often poor. The production of long monoPLOT columns suitable for use in gas chromatography adds further difficulties. Furthermore, there are currently no methods for in-process control during monoPLOT column fabrication, with existing approaches relying on empirical or experimental data resulting in poor repeatability.

Two techniques which allow the fine control of monoPLOT layer thickness and morphology were developed, and were based on both photo- and thermal-initiated polymerisation approaches. In the first case, an automated technique using a UV/IR reactor with a capillary feed-through system was utilised for the automated fabrication of both UV- and IR-initiated polymer monoPLOT columns. Relationships between direct exposure times, intensity and layer thickness were determined, as were the effects of capillary delivery rate (indirect exposure rate), and multiple exposures on the layer thickness and axial distribution of the layer. In the second instance, polymer monoPLOT columns were fabricated using a novel laminar flow thermal-initiation method, allowing tight control over layer thickness and morphology. In this case, relationships between polymerisation mixture

linear flow velocity and layer thickness were investigated, as was the effect on layer porosity and structure.

Lastly, two methods for in-process layer measurement during monoPLOT column fabrication were developed, using optical absorbance and capacitively coupled contactless conductivity respectively, significantly improving column to column reproducibility.

CHAPTER 1. INTRODUCTION

(1.1) STATIONARY PHASES FOR CAPILLARY LIQUID CHROMATOGRAPHY

(1.2) TEMPERATURE EFFECTS IN LIQUID CHROMATOGRAPHY

Current trends in analytical chemistry in general, and liquid chromatography (LC) in particular, are towards the miniaturisation of instrumentation, greener chemistry, reduction of hazardous solvent waste and increasing the separation speed [1-6]. Although systems that accommodate standard bore columns continue to dominate in routine separations in LC, the past 15 years has seen a significant amount of development in the area of micro-scale separations, leading to what is commonly termed today 'capillary' liquid chromatography, since separations performed at this scale offer many benefits over stand-bore systems. Perhaps two of the most obvious advantages of capillary LC are the cost savings to be gained from reduced running costs, and the reduced environmental impact of using less solvent. Comparing a standard bore and capillary column, the saving in solvent volume will be relative to the square of the proportion of column radii, so a considerable cost saving can be made. Compared with 4.0 – 4.6 mm standard bore columns, capillary column diameters are significantly smaller at 10 – 250 μm. Previously, the term 'Capillary LC' referred to columns of diameter 100 – 500 μm, and 'Nano-LC' between 10 and 100 μm, however the term has become more generalised, broadly describing all sizes of capillary up to around 250 μm ID.

In terms of separation performance there are also considerable gains to be made. Analyte diffusion is reduced (diffusion increasing proportionally with the square of the column radius), providing potential for improvements in resolution, efficiency and mass sensitivity due to reduced dilution of the sample [7], however conversely, increased diffusion may provide potential for improvement in resolution and efficiency for coated capillary column formats. This increase in mass sensitivity facilitates the separation of very small amounts of sample [8,9], a factor that is of huge benefit in the fields of proteomics, forensics, bio-

separations, etc., where often only minute amounts of individual analytes are available. Another advantage of capillary columns, which is often overlooked, is the reduced amount of stationary phase within the column, allowing easier exploration into new stationary phase development [6]. Often, new and novel stationary phases require either expensive materials and/or synthesis. Reducing the amount of stationary phase required for the investigation of chemical structure and selectivity, column stability etc., further reduces the cost and provides increased accessibility to the development of chromatographic materials.

Temperature too can be applied more easily to capillary LC than to standard bore separations. Due to their small ID, capillary columns have a lower thermal mass and so equilibrate to temperature changes more quickly, allowing the application of rapid temperature programming. This, and other advantages of capillary columns specifically regarding temperature applications, and the effect of temperature itself in the chromatographic process, make up the first two experimental Chapters of this work.

A further advantage of reducing column diameters can be seen in hyphenated techniques, such as LC-MS, particularly electrospray ionisation mass spectrometry, which benefits from increased sensitivity through the use of low column flow rates [10]. Electrospray ionisation can be performed with flow rates as high as 500 μL/min, however the highest sensitivity is achieved using much lower flow rates in the low μL/min and nL/min range [6,11].

1.1 Stationary phases for capillary liquid chromatography

Capillary columns come in three different formats; particle packed [12], monolithic [4,13,14], and open tubular (OT) columns [93,113]. Particulate column beds are still the most popular due to their high efficiency and good batch-to-batch reproducibility. Monolithic phases are characterised by high flow-through permeability, usually without significant impact on efficiency at increased flow rates, whilst OT columns can offer very low backpressures. Each of these column formats can be prepared in a range of materials, most common of which are silica, organic polymers, and organic-silica hybrids. However, metal oxide and carbonaceous substrates may also be used. Each of these may be modified with a very wide range of functionalities.

1.1.1 Particle packed stationary phases

Particle packed capillary columns offer several advantages over their standard bore counterparts. As particles become smaller and smaller, separation efficiency increases dramatically with low plate heights and flat van Deemter curves possible [15-17]. Particle packed columns typically exhibit high surface areas giving high sample capacities. However, these advantages come at the cost of extremely high column back pressures, typical values being between 500 and 1200 bar, however, over 5000 bar has also been reported [6]. Separations performed at such pressures are usually termed Ultra High Performance Liquid Chromatography (uHPLC or UPLC). Such high pressures demand the use of smaller bore columns with low volumes, capable of withstanding such high pressures, and require the use of high pressure pumping equipment capable of delivering flow at extreme pressures [18]. However, due to such high back pressures, separations

performed on packed columns must be performed at low flow rates and as such can take an excessive amount of time. Furthermore, fabricating frits for particle packed columns at capillary scale presents significant challenges [19-20] and the narrow diameter of capillary also makes packing the column a difficult task.

The material type and size of particles can vary considerably. Typically, particles are either silica or polymer based, with silica particles being the most common, however polymer particles are becoming more and more popular in recent years [4,21,22]. The structure of silica particles used in modern HPLC can be either porous [23], non-porous [24] or superficially porous [25], sizes ranging from sub-µm to approximately 10 µm, and are typically spherical in structure. Pore sizes too can vary considerably and commercially available particles can have pore sizes from 50 to over 1000 Å. Polyethylene [26,27] and polypropylene [27] are the most common polymer based particles, however, polystyrene [28,30], polymethacrylate [29,30], polyhydroxymethacrylate [30], and polyvinyl alcohol [30] are also used. In addition to silica and polymer particles, cellulose, agarose, dextrin, and chitosan, and ceramic particles such as hydroxyapatite and zirconia are sometimes used in certain modes of LC, however, to a much lesser extent.

1.1.2 Monolithic stationary phases

Following renewed interest in capillary electrochromatography (CEC) in the mid to late 1990's there has been a surge of interest in the application of monolithic materials in separation science, and today monoliths find application in many modes of chromatography.

As discussed earlier, particle packed columns have been used in chromatography for more than 30 years and in capillary format they still remain the most popular among commercially available columns. However, the separation performance of such a column is mainly determined by the particle size and distribution. The quality of the column is also determined by the homogeneity of the packed bed itself and the packing of particles within a column, and in particular capillary columns, can be very challenging indeed [9,16]. In contrast to particle packed columns, monolithic columns are made of a single piece of porous material, usually organic [31-36] or inorganic [37-39] polymers. Monoliths present an attractive alternative to particle packed columns [40-41] primarily due to their low back pressure, high permeability and convection dominated mass transfer. Additionally, since the monolith is chemically attached to the walls of the capillary, there is no need for a column frit.

The first monolithic columns were fabricated in the 1970s by Ross *et.al.* [42] from polyurethane. Shortly after, Knox and Bristow [8] suggested that the presence of large communicating pores would provide a network through which the mobile phase could flow. As a result of the increased hydrodynamic flow the speed of the separation would also increase. They further suggested that the surface area required for the adsorption and desorption processes could be obtained by creating mesopores on the surface of the monolithic structure.

Such a porous structure allows the application of higher flow rates in comparison with packed columns. Additionally, since the inlet bed settling is absent in these columns, the reliability, reproducibility and lifetime of the column is potentially increased and efficiency

is maintained over the lifetime of the column. Monolithic stationary phases can be classified by the monolithic material itself; e.g. silica, organic polymers, metal oxide, carbon, and organic-silica hybrid monoliths.

1.1.2.1 Silica monolithic stationary phases

Compared with polymer monoliths, silica monoliths have a larger surface area, are very mechanically stable, and demonstrate excellent resistance to swelling or shrinkage in solvents [43-44]. The silica monolithic structure can be characterised by the lowest theoretical plate height, shown to be approximately 5 μm (185,000 N/m) [52], while Leinweber *et.al.* showed that the performance of monolithic columns can be comparable to a column packed with 1 μm particles [45]. However, unlike polymer monoliths the fabrication process for silica monoliths is a complicated procedure [43] and their operation is limited due to their narrow working pH range. The preparation of silica based monoliths progressed in 1990s with the invention of silica rod columns [46-47]. A synthetic route to silica monolith production was developed by Nakanishi and Soga [48] and applied by Tanaka [49]. The method was based on the hydrolysis and polycondensation of tetramethosysilane in the presence of poly(sodium styrenesulphonate) or polyethylene oxide, which was used as template. A later method based on the packing of fused silica capillaries with octadecyl silica (ODS) particles followed by thermal treatment to form monolithic columns was suggested by Horvath *et al.* [50]. After sintering, the monolithic column was octadecylated *in-situ* with dimethyloctadecylchlorosilane. Further improvements of this technique used hybrid silanes [51].

The sol-gel process, described above [48], typically involves phase separation due to the polymer template and sol-gel transition due to polycondensation of the silica precursor, which leads to a continuous silica network with a defined pore structure. Further thermal treatment results in monolithic silica columns with a bimodal pore structure consisting of macro- (or through-pores) and mesopores in the silica skeleton. This method allows independent control of the pore size. It is possible to prepare monolithic silica columns with macropores in the range of 1 – 8 μm, while keeping the size of mesoropores constant at 13 nm. In 2000 the first commercially available silica monolithic column, the Chromolith column, was presented by Merck KGaA [52]. A typical scanning electron microscopy (SEM) image of a porous monolithic silica is shown in Figure 1.1.

(a) 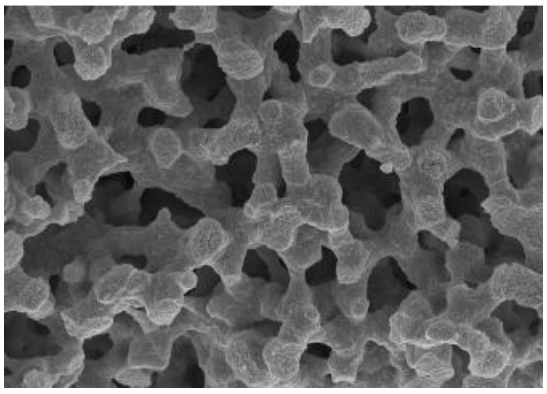 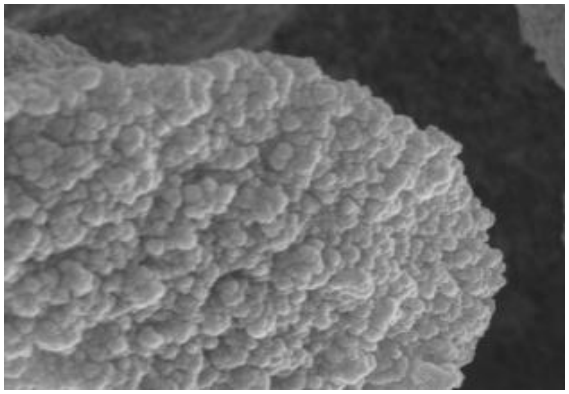 (b)

Figure 1.1 – SEM images of a silica monolith, (a) the typical porous structure with macropores, and (b) the mesoporous structure of the silica skeleton. Reproduced from [51].

Silica-based monoliths in capillary format have also been recently prepared, the general method for their fabrication being the same as for standard-bore columns. Tanaka *et al.* have demonstrated the preparation of capillary based silica monoliths which exhibit high permeability, high surface area, with a user defined pore size [53-56]. An advantage of this

technique over that for standard bore columns is that since the monolith is prepared *in-situ* in the fused silica capillary, the monolith itself is chemically bound to the walls. This eliminates the problem of wall effects that are typical for standard bore silica monolith columns which are encased in column housing after all rod fabrication steps are completed [51,57]. A good example showing the superior performance of capillary monolithic silica column over its standard bore counterpart is presented in Figure 1.2.

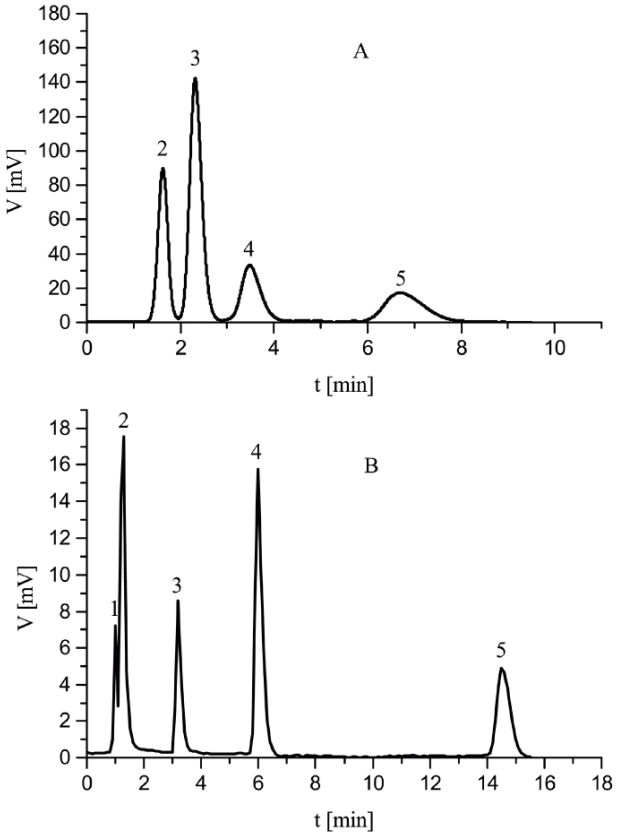

Figure 1.2 – Separation of isomeric naphthalenedisulphonic acids (NDSA) (1. uracil, 2. 1,5-NDSA, 3.,6-NDSA, 4. 1,3-NDSA, and 5. 1,7-NDSA) on silica-based monolithic columns, (A) Chromolith Performance RP 18e, 4.6 mm ID, flow rate = 1 mL/min, and (B) Chromolith CapRod RP 18e, 100 μm ID, flow rate = 1.3 μL/min. UV detection: 225 nm. Mobile phase: 0.4 M Na_2SO_4 in water. Reproduced from [58].

In Figure 1.2, chromatograms showing the separation of isomeric naphthalenedisulphonic acids on a standard bore (4.6 mm ID) and capillary columns (100 μm ID) are presented. Both columns were reversed-phase (RP) ODS monolithic phases with the same morphology (pore size and surface area). It can clearly be seen the peak efficiency and resolution were much higher for the capillary column, and allow the separation of peaks that co-eluted on the standard bore column.

1.1.2.2 Polymer monolithic phases

Compared with particle packed columns, polymer monoliths generally have a lower efficiency (particularly for small molecules) and loading capacity [59]. An interesting comparison was presented by Moravcova *et al.* [58], who performed separations of alkylbenzenes on particulate and monolithic polymethacrylate capillary columns using the same separation conditions, including flow rate. The two chromatograms of the separations are shown in Figure 1.3, and it can be seen that the efficiency was higher for the particle-packed column.

Generally, this type of polymeric stationary phases is applied to the separation of proteins or high molecular weight compounds [43], however recently, several authors have also shown relatively high efficiency separations of small molecules [60,61]. The main disadvantages of polymer monoliths, which are common to nearly all polymer stationary phases, are relatively poor mechanical (and in some cases structural) stability, and swelling or shrinkage in some solvents [43]. However, polymer monoliths have several advantages over other types of stationary phase.

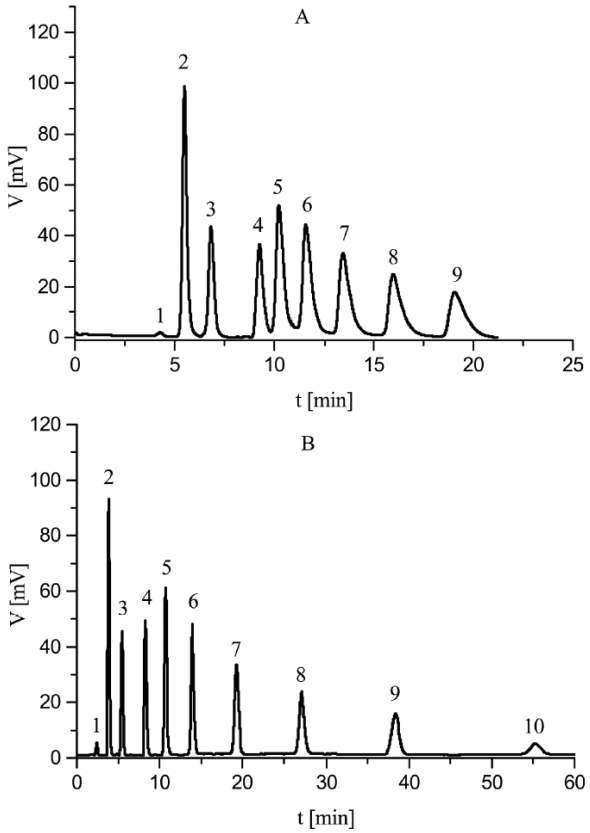

Figure 1.3 – Separation of alkylbenzenes (1. uracil, 2. benzyl alcohol, 3. benzaldehyde, 4. benzene, 5. toluene, 6. ethylbenzene, 7. propylbenzene, 8. butylbenzene, 9. amylbenzene, and 10. hexylbenzene) on a (A) polymethacrylate monolithic capillary column at flow rate = 2.1 μL/min, and on (B) particulate Superspher RP-8 capillary column at flow rate = 2.2 μL/min (B). Mobile phase: 30:70% H_2O/ACN. UV detection at 254 nm. Reproduced from [58].

Apart from the general advantages of monolithic phases, such as low backpressures and high flow through permeability, the physical structure (pore, mesopore and globule sizes) of the polymer monolith can be highly developed and is readily tailored for specific types of separation or analyte. Furthermore, the surface chemistry of the polymer monolith can be easily varied for specific functionality using simple surface modification procedures which can be carried out *in-situ*, making them ideal for use in capillary and microchip formats. Polymeric stationary phases are also highly chemically stable even under harsh conditions,

for example at extreme pH values and/or high temperatures. In their work on micro-bore titanium housed polymer monoliths, Nesterenko *et al.* demonstrated excellent column stability by separating acetophenone, benzene, toluene and naphthalene at high temperatures (100 °C), repeatedly over a 55 hr period [62]. They further separated nine pesticides on the same 100mm × 0.8mm ID column at 70 °C.

These properties mean that although there continues to be a huge interest in polymer monolithic phases in LC, this type of stationary phase (albeit in OT format) is also suitable for use in gas chromatography (GC), where high flow rates and temperatures are common, and where stationary phase stability is paramount. Monolithic columns were initially used in GC almost 35 years ago [63-65] however their use was overshadowed by the introduction of OT columns [66] and so did not attract much interest. Recently, Svec and Kurganov [68] applied both polymer and silica columns to GC, showing that monolithic phases allowed very fast separations while providing column efficiencies comparable to that of particle packed columns. They concluded that monolithic columns have many advantages in GC, and in particular polymer monoliths are likely to attract most attention, enabling the analysis of compounds which contain a large percentage of water such as environmental samples.

Most commonly, polymer monoliths act as reversed-phase substrates and are generally fabricated through free-radical polymerisation methods, the most common approaches being thermal- and photo-initiation techniques [67]. For both methods the approach is similar, with the suitable functional monomers being polymerised in the presence of appropriate porogens and the desired amount of free-radical initiator.

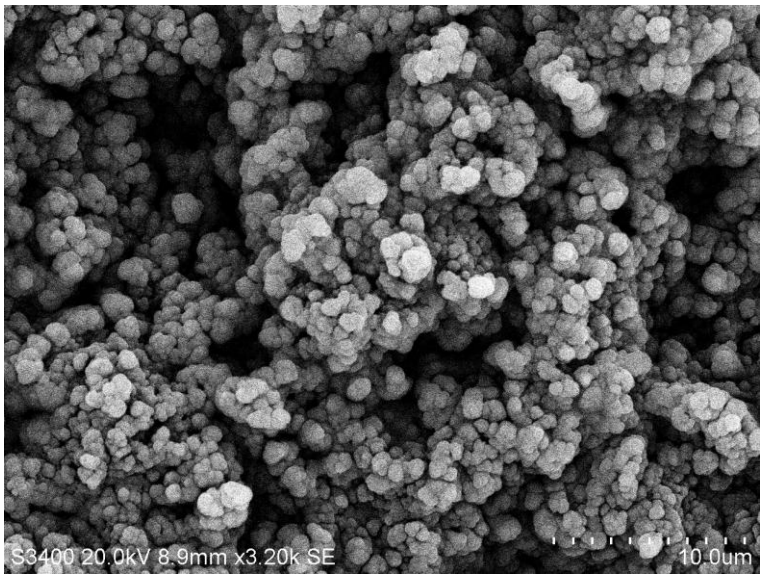

Figure 1.4 – SEM image of a polystyrene-divinylbenzene (PS-DVB) polymer monolith.

The empty capillary was filled with the polymerisation mixture and exposed to the required amount of energy in the form of light or heat for photo- and thermal-initiation, respectively. Both polymerisation time and energy can be varied to obtain different monolithic structures with different morphologies and surface area. The reaction rate for free-radical polymerisation is not a simple function of temperature, or light intensity as the process consists of several steps [69,70]. Most important is the rate of initiation, which is highly dependant on energy applied, since the half-life of initiators decreases with an increase in temperature or light intensity. As a result, the decomposition rate of the initiator, the number of radicals produced, the formation of a larger number of polymerisation nuclei, and consequently the overall polymerisation rate are higher at elevated temperatures or light intensities. In this case, as the formation of new polymerisation centres is faster than the growth of globules, the supply of monomers runs low fast and the number of globules is large, but their size stays small which leads to smaller voids between globules. This means

that higher polymerisation initiation energies will lead to the formation of smaller pore and globule sizes.

The duration of polymerisation also has a significant effect upon the morphology and the pore size of the resultant monolith. Longer polymerisation times lead to the formation of larger monolith globules resulting in smaller voids between them, and as a result leads to smaller pores and a higher density of the monolith [69]. Greiderer *et al.* [71] showed how polymerisation time can significantly affect the stationary phase morphology and subsequent efficiency on 1,2-bis(*p*-vinylphenyl)ethane (BVPE) columns. After 60 mins polymerisation the structure possessed a bimodal pore distribution (macro and mesopores were present) providing much higher surface area (102 m^2/g), more suitable to the separation of small molecules. However, the structural integrity of the resultant monolith was weak, leading to rapid column degradation [72]. On the contrary, long polymerisation times under the same conditions led to the formation of a monolithic structure with a significantly smaller surface area (32 m^2/g) [71], with such a change in monolith morphology significantly affecting the efficiency. The difference in separation efficiency between stationary phases prepared during 60 min and 300 min polymerisation can be clearly seen in Figure 1.5. Longer polymerisation times led to the formation of larger globules and subsequently lower surface area. A separation performed on this column exhibited poor peak shape despite the use of gradient elution.

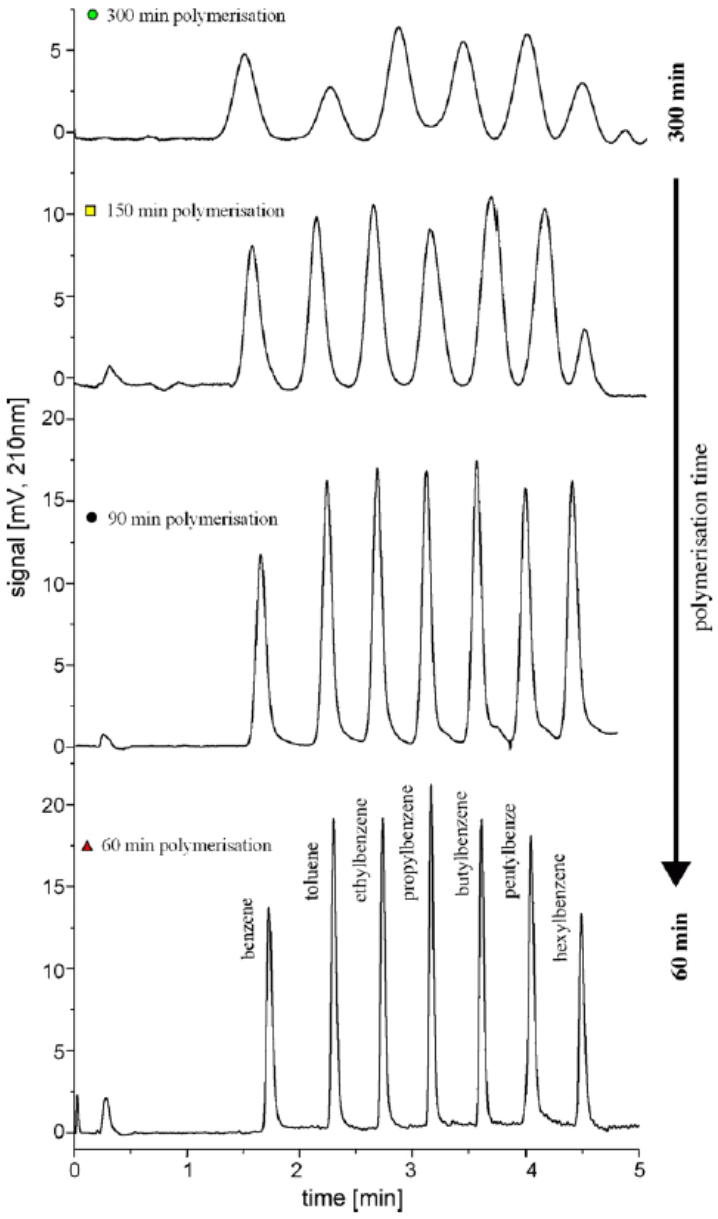

Figure 1.5 – *Effect of polymerisation time on the separation efficiency of monolithic BVPE capillary columns for alkylbenzenes (1. benzene, 2. toluene, 3. ethylbenzene, 4. propylbenzene, 5. butylbenzene, 6. pentylbenzene and 7. hexylbenzene). Separation conditions were identical in each case: solvent: (A) H_2O; (B) ACN, gradient: 30–100% B in 5 mins, flow rate: 10 µl/min. UV-detection: 210 nm. Reproduced from [71].*

1.1.2.3 Metal oxide monolithic phases

Another type of monolithic phase are those composed of a metal oxide (*i.e.* zirconia, alumina, titania) monolith. Compared with silica or polymer monoliths, metal oxide phases offer excellent chemical and mechanical stability, even at high temperatures [73]. Metal oxide monoliths built on titania supports have been reported [74-76], however, zirconia (ZrO_2) is probably the most common metal oxide support for chromatographic applications and stationary phases based on this material are readily available [74,77-80].

Work on metal oxide monoliths was first reported by Wu *et al.* in 1999 [81]. In this work, a capillary column was packed with zirconia particles, the particles themselves being effectively glued together in a polybutadiene matrix. Other approaches involve the fabrication of a silica monolith which is then coated with a metal oxide such as zirconia [82] or titania [83]. In their work, Hoth *et al.* fabricated zirconia and hafnia (HfO_2) metal oxide monoliths using an approach somewhat similar to one that is used for the fabrication of silica monoliths. It was based on the hydrolysis of zirconium or hafnium chlorides followed by polycondensation of zirconia or hafnia, respectively. This was done in the presence of propylene oxide which was added to induce polymerisation. Figure 1.6(a) and (b) show SEM images the fabricated hafnia and zirconia monolith respectively, clearly showing the monolith morphology and flow through pores.

(a)

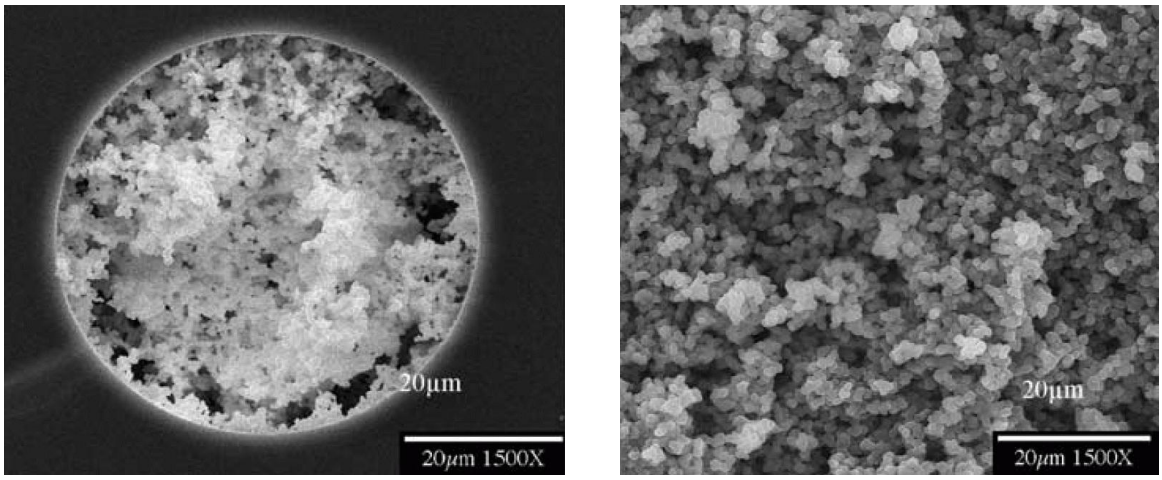

(b)

Figure 1.6 – Scanning electron microscopy (SEM) images of (a) hafnia-monolith inside a 50 µm ID. column and (b) of a zirconia monolithic pellet. Reproduced from [73]

Hoth *et al.* further fabricated a 29 cm hafnia monolithic column in 50 µm ID capillary and tested its suitability by successfully separating pyridine, pyrazole and imidazole (see Figure 1.7).

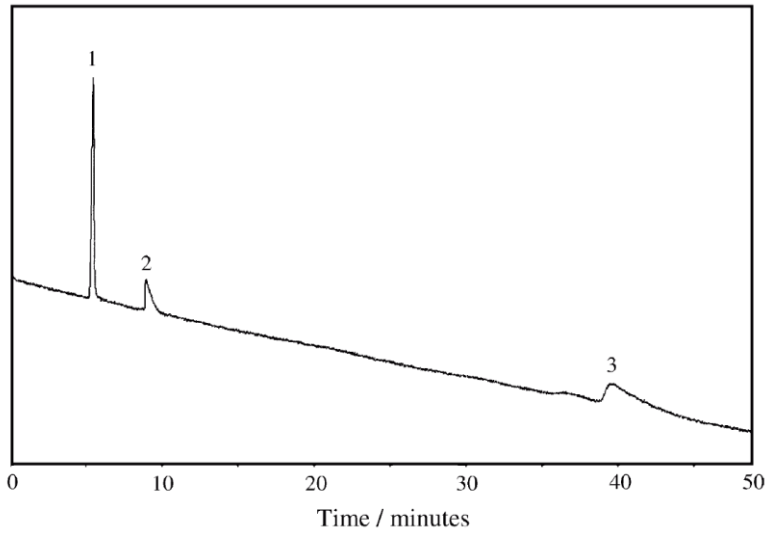

Figure 1.7 – Separation of three components (1. pyridine, 2. pyrazole, and 3. imidazole) on a hafnia monolithic column. Column: 29 cm x 50 µm ID (21 cm effective length). Mobile phase: 5 mM phosphate buffer pH 7.1. UV detection at 214 nm. Reproduced from [73]

1.1.2.4 Carbon monolithic phases

Although many works on carbon monoliths exists, very few deal with their applications in chromatography [84,85]. Carbon monoliths have generated a lot of interest due to their excellent adsorption properties and although their synthesis is straight forward, usually done via a templating method, they are difficult to manufacture in a format useful for LC. Firstly, the pyrolysis process is carried out at very high temperatures, typically >1200 °C, and secondly, the carbon monolith is prone to shrinkage as it undergoes pyrolysis [86] and so will simply detach from the walls of the column even if the column housing can withstand such high temperatures. Where attempts to apply carbon monoliths to chromatographic separations were performed, such monoliths had to be encased in a column housing after the completion of all fabrication steps, which can be very technically challenging.

To date, the vast majority of works on carbon monoliths in the area of separation science has been performed on standard-bore monoliths. Nevertheless, a recent work by Shi *et al.* [86] showed the fabrication and application of carbon monoliths to solid phase micro extraction (SPME). In this work the carbon monolith was prepared via a polymerisation – carbonisation method, using a PS-DVB polymer monolithic structure as the base monolith. Carbonisation was then performed through pyrolysis at 900 °C for 5 hrs. The resultant carbon monolith was observed to have a bimodal pore structure – see Figure 1.8.

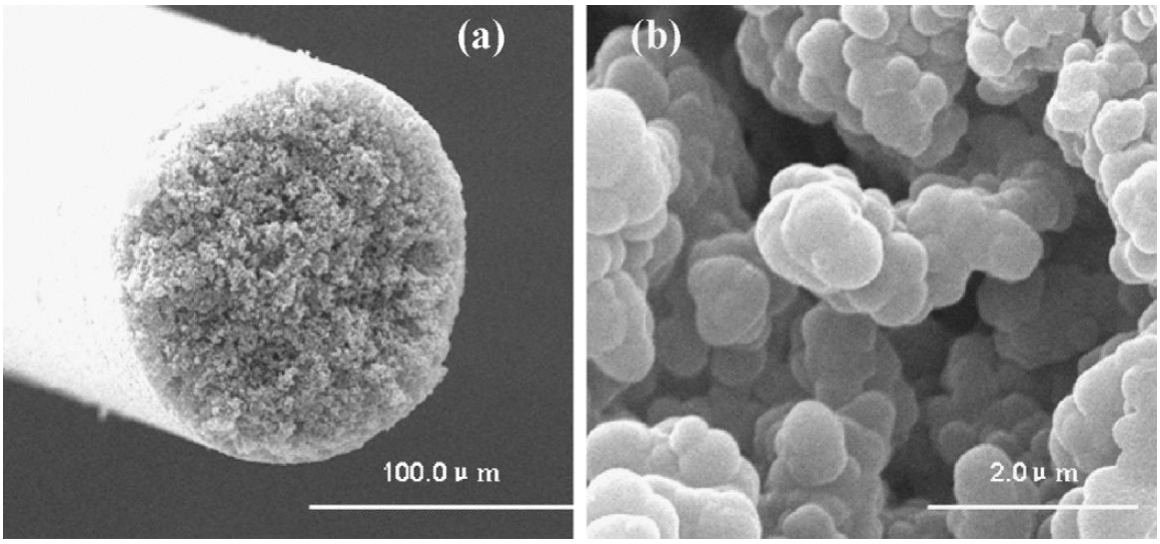

Figure 1.8 – SEM images of the carbon monolith at different magnifications, (a) 600X and (b) 20,000X. Reproduced from [86].

Shi *et al.* performed SPME directly on the carbon monolithic rod, using it for the extraction of phenols after which they injected the sample onto a GS-MS. In comparison to commercially available SPME fibres the group found that their monolithic carbon rod resulted in a faster extraction equilibrium and a higher extraction capacity.

1.1.2.5 Organic-silica hybrid monoliths

As discussed, both silica and polymer based monoliths have many advantages and disadvantages: the first have excellent mechanical stability, high surface area and efficiency, but are chemically active, while the latter exhibit great chemical stability even at extreme pH, but are prone to shrinkage and swelling in certain solvents. Attempts to combine the advantages of both types of materials and reduce the impact of negative factors have resulted in the development of organic-silica phases.

The first organic-silica hybrid monoliths were introduced by Hayes and Malik [87] in 2000. Compared with polymer and silica monoliths, organic-silica phases exhibit a higher mechanical and pH stability, are less prone to shrinkage during fabrication [88], and are generally more straight forward in their production [89]. They can be produced through the simultaneous hydrolysis and condensation of organo-functionalised trialkoxysilanes (providing the desired functional groups) and tetraalkoxysilanes (such as tetramethoxysilane) which result in the formation of a hybrid silica matrix with the organic functionalities covalently incorporated (Figure 1.9). The organic moieties are attached via Si-C linkages, which are more hydrolytically stable than Si-O which is typically used in attaching functional groups to the surface of the silica matrix. The entire process can be carried out via one or two step catalysis.

(a) 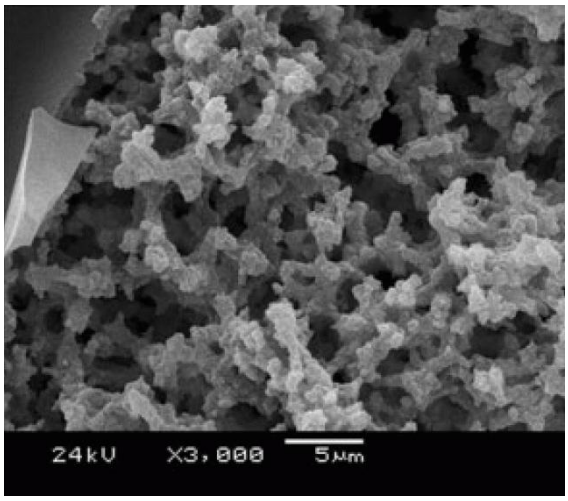

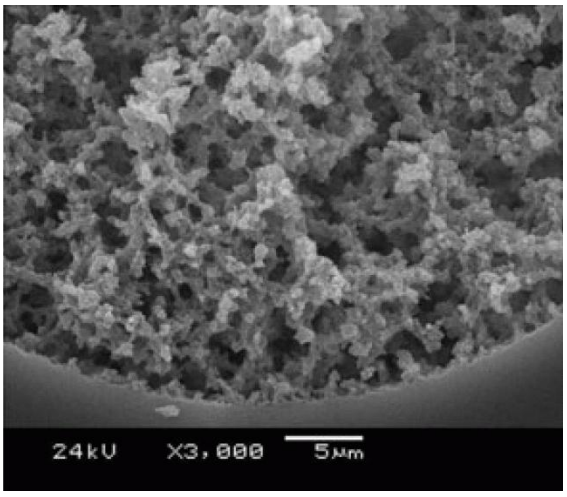

(b)

Figure 1.9 – SEM images of polyacrylamide hybrid monoliths. Reproduced from [43].

Due to their properties, organic-silica monolithic phases can be used for a broad range of applications. They are commonly used in capillary LC for the separation of drugs [90], polyaromatic hydrocarbons [91] and protein digests [92].

1.1.3 Open tubular columns

Open tubular columns possess a layer of stationary phase around the inside circumference of the column, while maintaining an open void in the centre. This type of column was initially proposed for GC by Golay [93] over 50 years ago and following this pioneering development, OT capillary GC has practically replaced packed-column GC for most analytical applications, with porous layer open tubular (PLOT) columns now well-established as a common OT column format [68].

By the late 1970s, following the work done by Tsuda *et al.* [94], OT columns were also finding application in micro-bore LC [95,96] and although they continue to be used in some capillary LC applications, predominantly they are used in GC [97], capillary electrophoretic methods such as capillary zone electrophoresis (CZE), and capillary electrochromatographic methods such as CEC [98-103]. There are numerous publications on the design, performance, and properties [94,104-109] of OT columns and also comparisons with particle packed phases [110,111]. In LC, OT columns have several advantages over packed columns, the main advantages being low column back pressure and fast analysis times. Other sometimes overlooked advantages include reduced solvent consumption and small sample volumes [112]. Additionally, in contrast with particle packed columns, the high permeability of OT columns permits the use of much longer columns. However, compared to OT GC columns, the diameters of OT LC columns must be 10^2 – 10^3 times smaller in order to gain comparable efficiencies. This necessary reduction in diameter is due to the much reduced diffusion coefficients in the liquid and stationary phases and as a result the benefit of reduced backpressure is often lost due to use of very long columns [141]. Theoretical models [113-114] have shown that OT columns

can provide high resolution, fast separations, with superb efficiencies. In their recent work, Causon *et al.* showed that a 5 μm ID porous silica OT column would be superior in terms of kinetic performance compared with packed columns of the same dimensions [114].

Open-tubular structures within capillaries can be further divided into two categories. The phase itself may be comprised of a non-porous layer (film coating, or immobilised non-porous particles) [110,115] or PLOT structures containing a layer of porous material. A variation of the latter type are monolithic porous layer open tubular (monoPLOT) columns which have the stationary phase covalently bound to the capillary wall, resulting in a very stable structure. Porous layer structures can provide high capacity due to their higher surface area as compared with non-porous, wall-coated polymeric coatings (WCOT). However, the commercial techniques used in the formation of all such stationary phases upon the walls of capillary columns are of course highly proprietary.

A common approach for the fabrication of PLOT columns is to immobilise a layer of stationary phase particles onto the inner wall of the column [116]. Deposition of solid layers of adsorbents for PLOT column production required very stable suspensions of particles to be immobilised. A frequent problem in the manufacture of such columns can be blockage of the PLOT column after coating procedures. Since in many cases stationary phase is not chemically bonded to the column wall, the stability of the layer ultimately depends on the constant nature of the forces that hold it to the column wall, which can be reduced with an increase of temperature and pressure which is a common problem in GC. This can lead to a gradual loss of adsorbed stationary phase as well as sudden break up and wash off the column. This effect is commonly known as column bleed.

However, column bleed can be reduced or eliminated completely if the stationary phase is chemically bonded onto the capillary wall and this can only be achieved via *in-situ* fabrication. In comparison with other types of OT capillary columns, the range of bonded porous layer stationary phases is rather limited. This relative lack of bonded polymeric PLOT columns for use in GC, and indeed capillary LC, is due mainly to the many challenges associated with the controllable manufacture of such columns of varying dimensions.

The past decade has seen an extensive amount of work done in the development of bonded polymer OT (particularly monoPLOT) phases for use in capillary LC. Like full monolithic phases, PLOT columns can be fabricated from a variety of different materials, for example silica, titanium oxide, and both organic and inorganic polymers.

1.1.3.1 Silica PLOT columns

Silica PLOT columns were first fabricated by Tock *et al.* by the precipitation of pre-gelled polyethoxysilane from solution in both a dynamic and static coating procedure [117,118]. However, the resultant phases had a low porosity and consequently poor retention and capacity. Some years later Crego *et al.* formed thick film layers inside capillaries through the hydrolytic *in-situ* polycondensation of tetraethylorthosilicate (TEOS), and although the resultant separations were promising, retention capacity was poor [115]. More recently, Colón *et al.* developed TEOS and C_{18}-TEOS phases for OT reversed-phase LC [119-121] and electrochromatography [122-123], with unmodified silicon dioxide surfaces having been used to generate efficiencies up to 1 million theoretical plates in chip [124,125], single [126] and multipath [127] capillary formats. Further recent work by Forster *et al.* [128]

investigated the fabrication of a sol-gel derived silica PLOT column in various column sizes, 100, 50, and 15 μm ID. The authors found that only a thin layer of silica could be formed in the 100 and 50 μm ID capillary, with most of the particles aggregating and falling to the bottom of the capillary due to gravity. However, in the 15 μm ID capillary the authors were able to fabricate a covalently attached layer of silica (see Figure 1.10). The prepared column was subsequently successfully applied to the normal-phase separation of anisole isomers (see Figure 1.11).

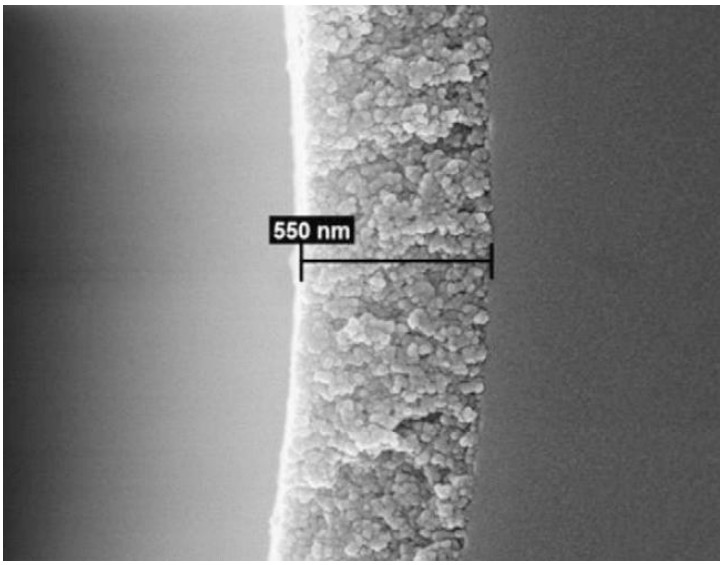

Figure 1.10 – SEM image of a silica layer formed in a 15 μm ID capillary. Reproduced from [128].

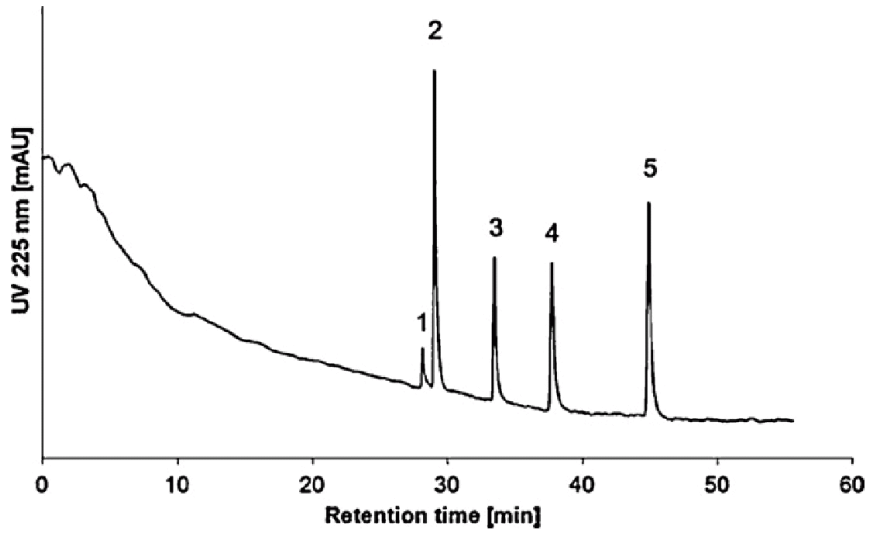

Figure 1.11 – Separation of anisole isomers (1. toluene, 2. anisole, 3. 3-Nitroanisole, 4. 4-Nitroanisole, 5. 2-Nitroanisole). Column dimensions: 6m x 15 um ID. Mobile phase: n-heptane/1,4-dioxane 95/5 (v/v) in isocratic mode. Linear flow rate was calculated to be 3.6 mm/s. UV detection at 225 nm. Reproduced from [128].

1.1.3.2 Titanium dioxide

In the last 10 years there has been interest in titanium dioxide particle packed phases [129,130] for screening complex biological mixtures, etc. as this type of phase has several advantages over silica based columns [131,132]. There is little work reported on titania columns in OT format, however in recent years titania OT capillary columns have been applied to capillary microextraction (CME) [133], and for the enrichment of phosphopeptides [134]. In their work to apply titania monoPLOT columns to CME, Wu *et al.* [133] fabricated a thin layer of mesoporous titania on the inside of a fused silica capillary by means of a sol-gel technique, in order to preconcentrate V, Cr and Cu found in human urine and lake water. The authors reported high sensitivity and selectivity when combined with electrothermal vaporisation inductively coupled plasma mass spectrometry (ETV-ICP-MS) [135].

More recently, Lin *et al.* [136] fabricated an OT titania based column through the deposition of TiO_2 nano-particles on the inside of a fused silica capillary by liquid phase deposition (LPD), using the column to successfully concentrate phosphopeptides. This fabrication technique involves filling the capillary with a precursor solution consisting of $(NH_4)_2TiF_6$ and H_3BO_3 followed by immersion in a water bath at 35 °C for 16 hrs for LPD. After LPD and washing of the capillary, the layer was aged by calcinating the TiO_2 nano-particle structure by heating it to 300 °C for 2 hrs. The resultant column was used as an in-tube SPME device followed by direct infusion MS detection for the isolation and analysis of phosphopeptides from tryptic digest of phosphoproteins. The authors reported that the TiO_2 films were still stable even after several hundred extractions.

1.1.3.3 Polymer PLOT columns

Polymer monolithic PLOT columns, with a solid porous structure similar to fully polymerised monolithic columns, are generally fabricated using either photo- or, more frequently, thermally-initiated free radical polymerisation. However, unlike fully polymerised monolithic columns, OT polymer monolith formats can present significant challenges in their synthesis. The primary difficulty in their fabrication lies in controlling the rate of polymerisation so that only a polymer layer is formed, while at the same time ensuring that the morphology of the layer is not adversely affected. It is well known that the morphology of the monolithic structure is highly dependant on the rate of polymerisation [69]. In this respect, since thermally initiated polymerisation is a slower process than photo-initiated fabrication, it is perhaps more suited to the fabricated of this type of polymeric structure.

A significant amount of work on thermally-initiated polymerisation of PLOT columns has been carried out by Karger *et al*. [137-141]. In these studies the authors prepared 10 μm ID columns for multi-dimensional [139] and hyphenated LC-MS [138,141] through the polymerisation of a PS-DVB mixture in fused silica capillaries at 74 °C for 16 hrs. Figure 1.12 shows an SEM of the resultant polymer monolithic layer.

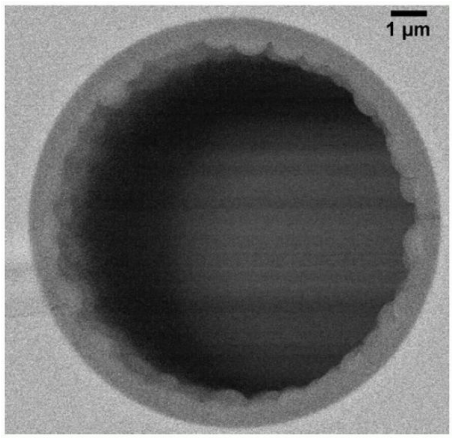

Figure 1.12 – SEM image of a PS-DVB PLOT column prepared in a 10 μm ID fused silica capillary. Reproduced from [138]

The diameter of the capillary further plays a large part in the success of fabrication, i.e. as capillary bore size increases it becomes increasingly difficult to form a porous layer structure. In a recent work, Nischang *et al.* [142] investigated the effect of capillary diameter on polymerisation within the confined space of a capillary. They found that the ease of fabrication of the porous polymer monolith is directly aided by an increase in surface-to-volume ratio of the capillary, i.e. the larger the bore of the capillary, the easier it is to fabricate a porous monolith in the whole volume of the capillary. Conversely, the smaller this ratio, the easier it becomes to form a bonded porous layer, retaining an open

tubular structure. Figure 1.13 shows their findings in different capillary sizes using different monomer mixtures, with decreasing macropore sizes from M1 to M4.

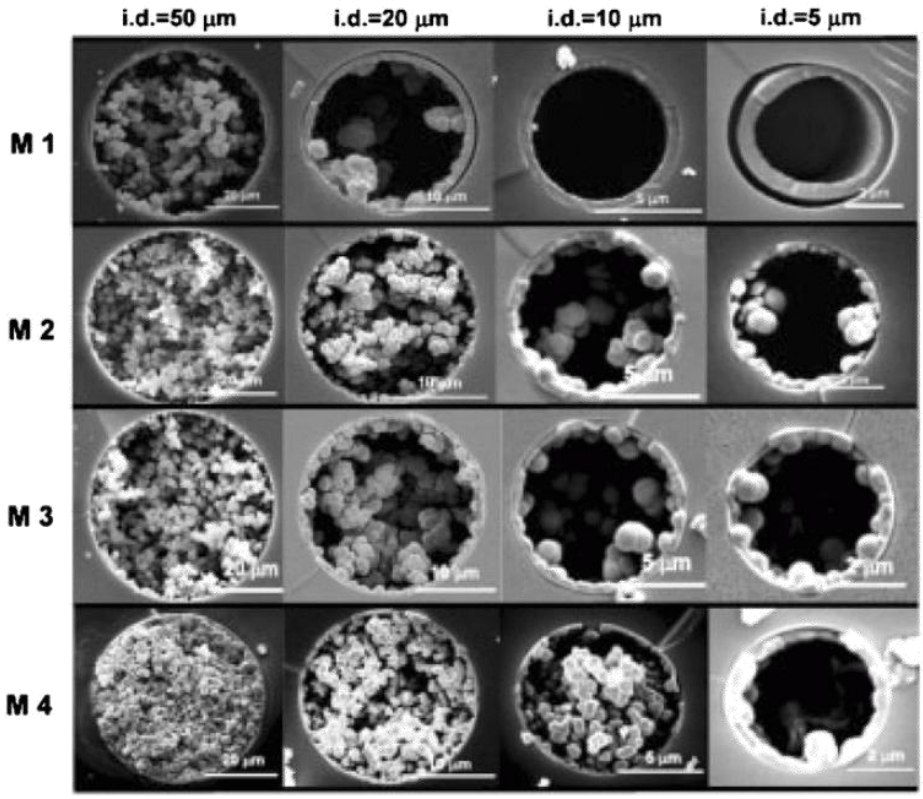

Figure 1.13 – Dependence on capillary diameter of the morphology of photo-polymerised monoliths derived from a variety of polymerisation mixtures resulting in different macropore sizes (decreasing macropore size M1 to M4). No surface treatment was used on the fused-silica capillaries. Reproduced from [142].

An excellent example of the separation power of a 4.2 m x 10 µm ID PS-DVB PLOT column is shown in Figure 1.14. In this example the authors identified over 3000 unique peptides covering 566 proteins, achieving detection levels in the attomole to sub-attomole level. Peak capacity was reported to be in the region of approximately 400. However, the

disadvantage of using such narrow bore columns is extremely high backpressure even at very low flow rate (~200 bar at 20 nl/min).

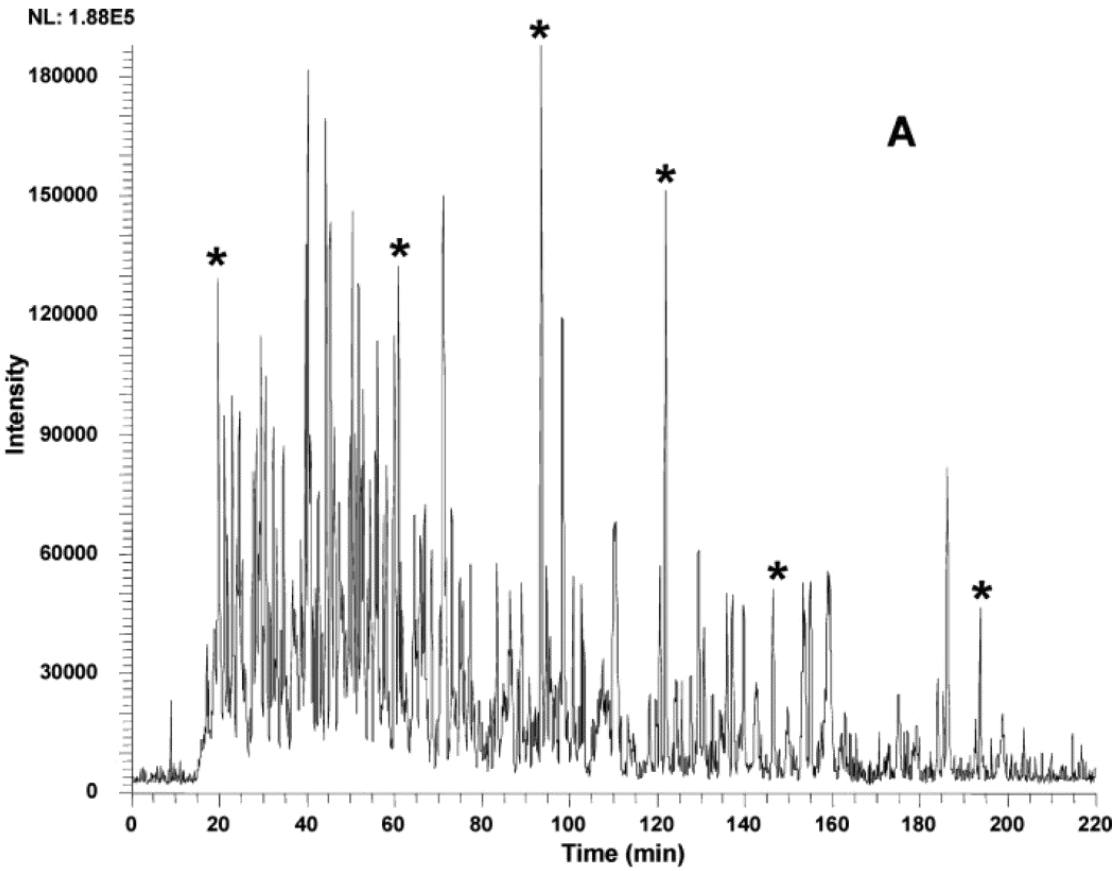

Figure 1.14 – Base peak chromatogram from the microSPE-nano-LC/ESI-MS analysis of a 4-ng tryptic in-gel digest of a single SDS-PAGE cut of M. acetivorans, separated on a 4.2 m x 10 µm ID PLOT column. A 4 cm x 50 µm ID PS-DVB monolithic column was used as the microSPE pre-column. Reproduced from [141].

The other common approach for free radical polymerisation is through photo-initiation. Although photo-initiated polymerisation is somewhat easier to apply than thermally-initiated polymerisation, it has some disadvantages. Firstly, the rate of photo-initiated reaction is much faster than thermally-initiated, making it difficult to control the rate of

polymerisation sufficiently in order to form a monolithic porous layer structure. Secondly, inhomogeneity of the incident light may cause non-uniform layer growth within the capillary, and so it is vital that the light used to initiate polymerisation is homogenous from all sides of the capillary. Furthermore, photo-initiated polymerisation of certain compounds (PS-DVB for example) or within certain types of capillary (such as polyimide-coated capillary) can be difficult as the compounds or material may absorb at the wavelength being used. Conversely, photo-initiated polymerisation can be achieved over a wide range of wavelengths suited to particular initiators [143]. It is also highly controllable, since the power (intensity) of the light can be changed rapidly. Most importantly, due to the many variable parameters of photo-initiation it is possible to tightly control monolith morphology, and in the case of PLOT columns, the thickness of the layer.

In the work by Eeltink *et al.* [144] the authors fabricated a 20 and 50 µm ID butyl methacrylate (BuMA) – ethylene dimethacrylate (EDMA) PLOT columns with layer thicknesses between approximately 0.5 and 1.0 µm by exposing a capillary filled with polymerisation mixture to 254 nm light for 2 min. The initial resultant porous monolithic layer exhibited poor homogeneity, being significantly thicker on the side facing the light source of a standard UV chamber (see Figure 1.15(a)). The authors then repeated the experiment but rotated the capillary at 100 rpm during polymerisation, resulting in a highly homogenous layer (see Figure 1.15(b)). Using a 40 cm x 20 µm column with a 0.5 µm layer, the authors performed CEC separations of thiourea and benzene derivatives, demonstrating a rapid high efficiency separation (up to 400,000 plates/m) at 60 °C , which can be seen in Figure 1.16.

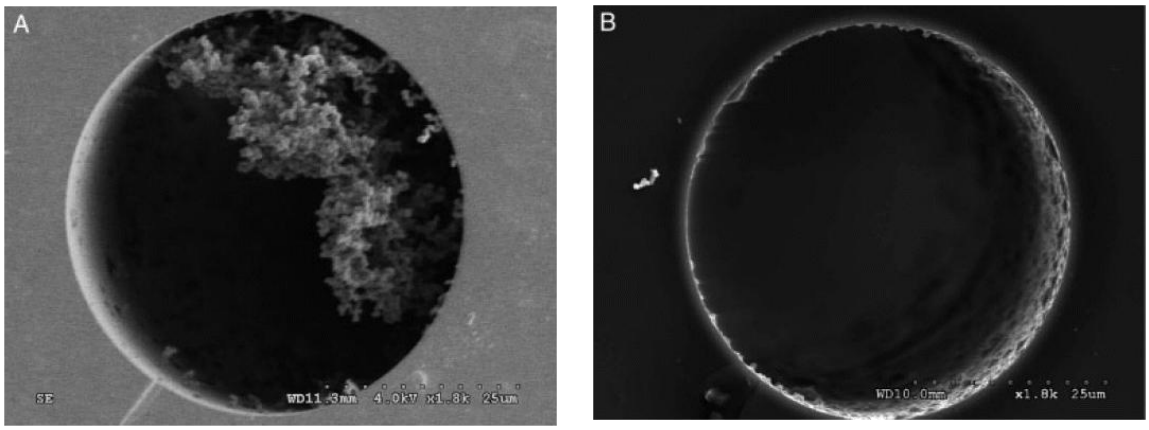

Figure 1.15 – SEM images of a 50 um ID capillary coated under stationary conditions (A) and revolving at 100 rpm (B). Reproduced from [144].

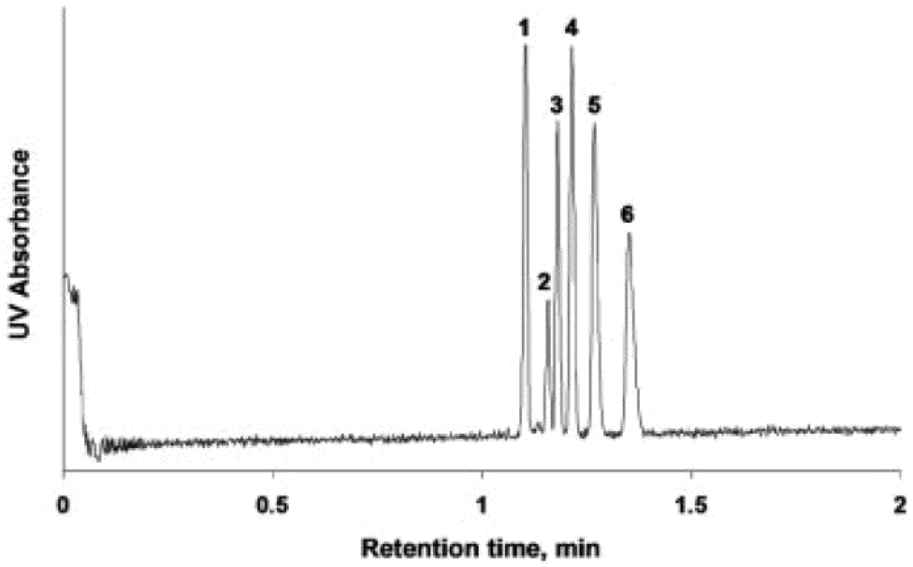

Figure 1.16 – CEC separation of thiourea and benzene derivatives, (1. thiourea, 2. benzene, 3. methylbenzene, 4. ethylbenzene, 5. propylbenzene, and 6. butylbenzene) at 60 C with pressurised flow (inlet pressure = 5,000 Pa) and EOF (20 kV). Column: 40 cm x 20 um ID EDMA monoPLOT column with a 0.5 μm layers, photo-grafted with META. Mobile phase: 40:60% ACN:Tris buffer (10 mM, pH 8). UV detection at 200 nm. Reproduced from [144].

Two other notable studies which attempted to address the problem of non-uniform layer growth were presented by Abele *et al.* [145] and Nesterenko *et al.* [146]. In the first instance the authors used a highly novel technique, polymerising a porous layer inside 25, 50 and 100 µm ID capillaries through the application of an evanescent light wave. Evanescent wave (EW) polymerisation had previously been suggested for the fabrication of submicron layers [147,148], however it had never been previously applied to synthesis within a capillary.

In order to achieve this, the authors placed a 365 nm UV light emitting diode (LED) at the end of a Teflon coated capillary filled with a glycidylmethacrylate – ethylenedimethacrylate (GMA–EDMA) polymerisation mixture, ensuring the incident light shone axially on the capillary, and successfully fabricated porous polymer layers between 2 and 25 µm. This is possible since the refractive index of the Teflon coating is lower than that of the fused silica, ensuring total internal reflection (TIR) along the length of the capillary. However, the authors emphasised, that the technique is not applicable to the fabrication of porous layer in polyimide coated capillary since the refractive index of polyimide is higher than that of fused silica. Another downside of this approach is the limited length of layer which can be formed due to the absorption of the light and losses in the fused silica medium and the authors were only able to fabricate a monoPLOT column of approximately 7 cm.

The approach by Nesterenko *et al.* [146] was proven to be more effective in the fabrication of longer monoPLOT columns, and in this work the authors were able to produce 50 µm ID columns of approximately 27 cm. This was achieved by repeatedly passing a 365 nm light

source over a capillary filled with GMA–EDMA polymerisation mixture. Although the incident light was from one side only, the capillary was placed on a highly reflective surface. The authors noted that by 'scanning' the capillary in this way it was possible to produce a highly uniform layer due to the incident light causing a moving evanescent light wave along the length of the capillary. The authors used two prepared columns joined together (total length 51 cm) to perform separation of a test mixture of proteins, which is presented in Figure 1.17. Importantly, the pressure drop across the column of less than 1.5 MPa shows a great potential of such columns to low pressure capillary chromatography.

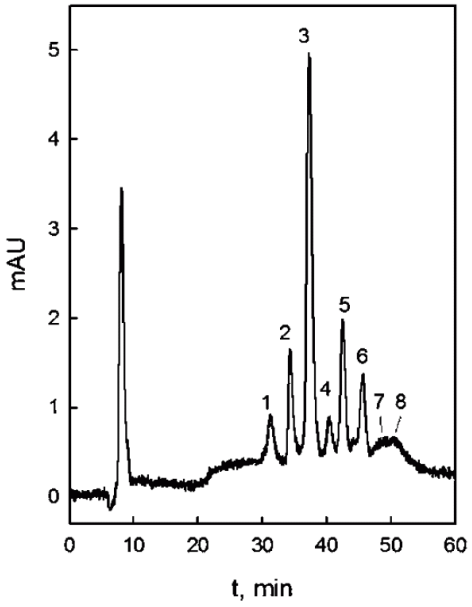

Figure 1.17 – Separation of 8 proteins (1. ribonuclease, 2. insulin, 3. cytochrome C, 4. horseradish peroxidase, 5. carbonic anhydrase, 6. enolase, 7. alcohol dehydrogenase and 8. phosphorylase) on a diol functionalised monoPLOT column. Column: 51 cm x 50 µm ID, 5 µm layer. Mobile phase: A: 0% ACN, 0.1% TFA; B: 90% ACN, 0.1% TFA. Gradient elution: 0.0–20.0 min from 100% A to 100% B; 20.0–20.1 min from 100% B to 100% A;20.1–60 min 100% A, pH 1.9. Flow rate = 0.4 mL/min. UV detection at 210 nm. Reproduced from [146]

1.2 Temperature effects in liquid chromatography

Temperature is an important, yet often neglected, separation parameter in liquid chromatography. Precise control of column temperature can, and has been, used to manipulate run times, improve peak efficiency and resolution, increase analyte signal-to-noise ratios, reduce mobile phase solvent consumption, and even change peak elution order [149-152]. Isobaric temperature programming can also be a promising alternative to gradient elution in cases where the required range of the elution strength is not too wide, for instance, for the separation of closely related macromolecules [153]. Varying temperature has been shown to both reduce overall retention and, in cases, improve selectivity for smaller molecules in both reversed-phase [154] and in ion exchange chromatography [155-157], and greatly affect the retention and resolution of biomolecules [158,159].

In recent years, the limits of high performance liquid chromatography have been pushed further and further, and the importance of temperature on the chromatographic process has become paramount in achieving the best possible results. Temperature programming is one of the major tools at the disposal of chromatographers in the quest for faster analysis, specifically when it comes to capillary and micro-scale separations due to their low thermal mass, high thermal conductivity, and thus fast thermal equilibration times. One area where temperature programmed chromatography plays an important role is in rapid chromatography, with faster separations being one of the driving forces behind the continuous development of the field, particularly in capillary scale LC. Higher temperatures generally reduce the viscosity of the mobile phase, reducing backpressure, and allowing the application of higher flow rates, which when combined with a reduction in retention (as in reversed-phase chromatography for example), means that run times can be significantly

shortened. Two examples of how the application of high temperature can be used to reduce run times are shown in Figures 1.18 and 1.19. In Figure 1.18 the separation time was reduced from 11 mins to approximately 2 mins, as the reduced viscosity of the mobile phase also allowed the application of a higher flow rate; 0.85 mL/min at 80 °C compared to only 0.35 mL/min at 40 °C. An improvement in efficiency can also be seen.

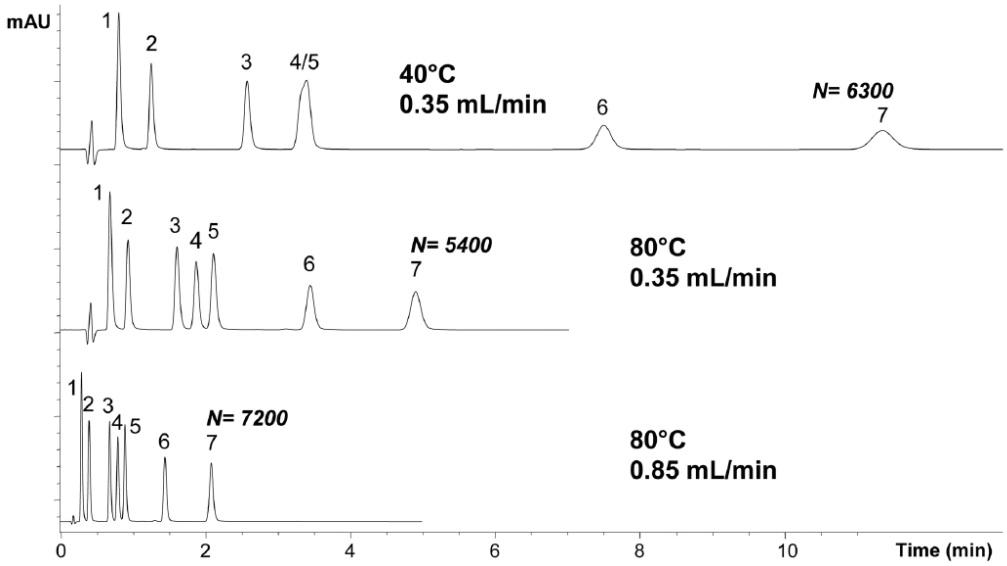

Figure 1.18 – Analysis of phenylurea pesticides (1. fenuron, 2. metoxuron, 3. chlortoluron, 4. diuoron, 5. isoproturon, 6. linuron, and 7. chloroxuron) on a Zorbax StableBond-C18 column (50 mm x 2.1 mm ID, 1.8 µm d_p). Mobile phase: ACN/water (30:70%). DAD detection at 245 nm. Reproduced from [160].

High temperature liquid chromatography has also been developed as an example of "green chemistry", and many practitioners have employed critically heated water as the mobile phase with some considerable success [161-163]. Temperature has been used in various methods with thermally responsive materials, most common of which are polymers [153-155] These materials range in function from changing hydrophobicity (trap and release)

with temperature to mechanical action (through swelling or contraction).

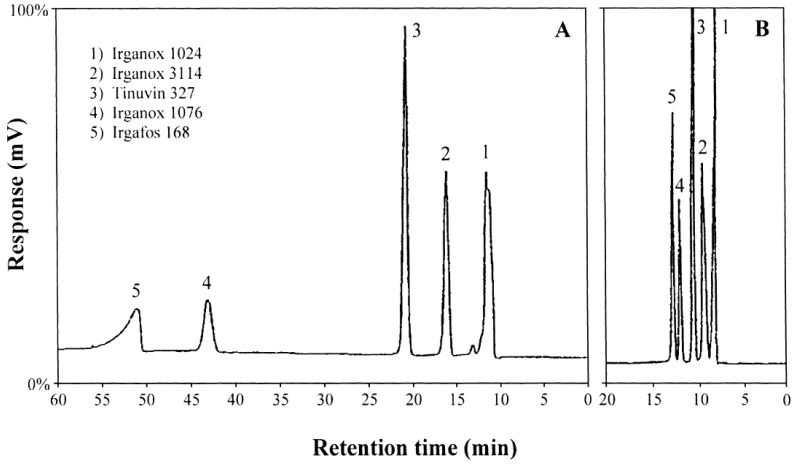

Figure 1.19 – Separation of polymer additives by isothermal elution at 50 8C (A) and by a temperature program from 100 to 150 °C (B). Column, 3 mm Hypersil ODS, 100 A, 0.32 mm ID x 69 cm. Mobile phase: DMF–acetonitrile (10:90%), flow rate = 5 ml/min. UV detection at 280 nm. Reproduced from [164].

Conversely, poor temperature control during the separation process may have the opposite effect to many of those benefits that can be seen in high temperature separations, namely shifting retention times, and ultimately resulting in a loss of efficiency. Figure 1.20 shows the theoretical effect of column and eluent temperature, and of frictional heating within the column on band broadening. Depending on the type of column, mobile phase, and separation parameters, small differences in temperature along the column can have a dramatic impact on the results. Even separations performed at room temperature can be adversely affected by poor temperature control of the column compartment and/or the mobile phase. These negative effects become particularly evident in uHPLC, where frictional heating of the mobile phase can occur due to the density of the packed particles.

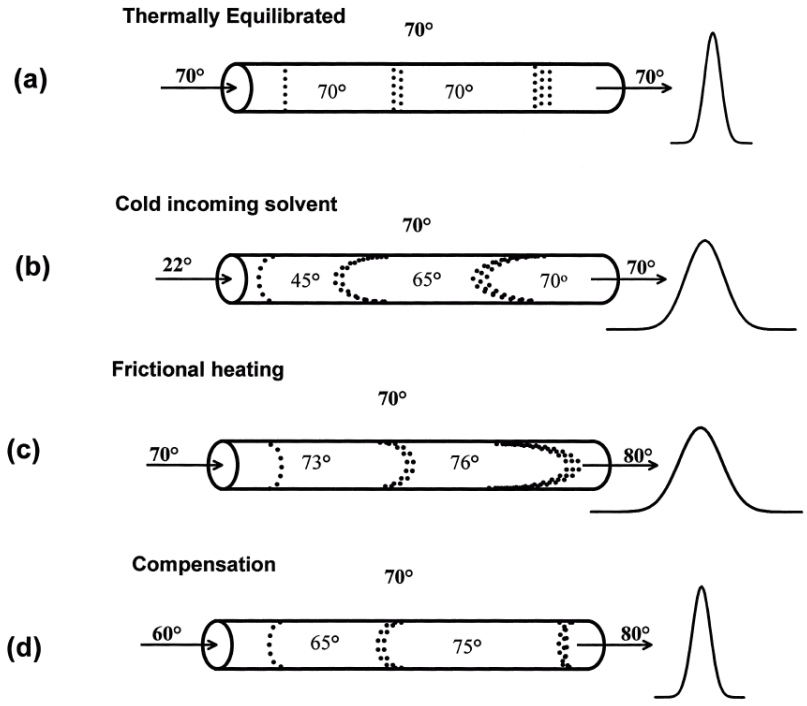

Figure 1.20 – Band broadening due to thermal effects: (a) ideal case, no thermal effects; (b) effect of incoming mobile phase that is at a lower temperature than the column; (c) effect of frictional heating; (d) combined effects of cold incoming mobile phase and frictional heating. An oven temperature of 70 °C is assumed. Reproduced from [165]

High pressure separations can cause excessive frictional heating of the mobile phase with longitudinal temperature gradients within the column increasing to the point that the column outlet temperature can be over 10 °C higher than the column inlet [166,167]. In these instances precise temperature control and regulation of the entire column is of considerable importance.

1.2.1 Low temperature chromatography

1.2.1.1 Sub-ambient chromatographic separations

The application of temperature to liquid chromatography is not simply limited to ambient temperatures and above. There has also been much work done on sub-ambient and even sub-zero separations. Chromatography in the sub-ambient region and down to around 0 °C is uncommon except in cases where the analytes to be separated are thermolabile at ambient temperature [168-171]. However, besides the separation of thermally sensitive analytes, there are a few other cases where separations at sub-ambient temperatures may be necessary. An example of this can be seen in the separation of some biological species which might undergo chemical reactions or conformational change at room temperature, for example some biologically active peptides [172-176]. Diagnosing such reactions and their interplay with chromatographic retention is often done through increasing the flow rate, and usually co-eluting peaks at lower flow rates will gain some resolution at higher flow rate. However, for solutes that undergo such on-column reactions, the effect of temperature on the chromatographic process can be much more dramatic as compared with the effects of flow rate. It has been shown, that for a simple model using proline dipeptides, a separation done at 1 °C resulted in two otherwise co-eluting peaks (at 23 °C) being completely resolved, with an increase in resolution, efficiency and sensitivity [172], as shown in Figure 1.21.

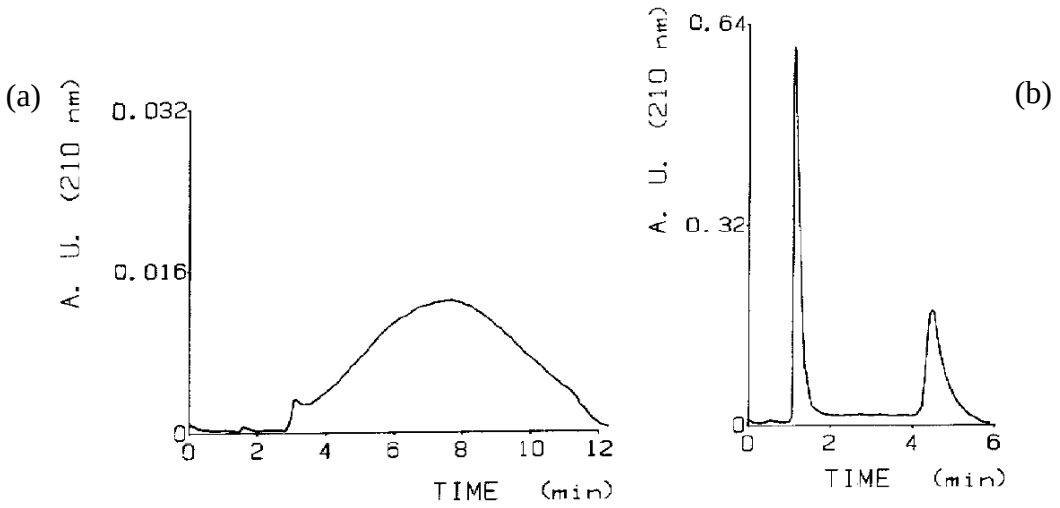

Figure 1.21 – Comparison of separations of Leu-Pro performed at (a) 23 °C and (b) 1 °C on a LiChrosorb RP-18 250 x 4.6 mm ID (d_p 10 μm) column at a flow rate of 2.0 ml/mm. Mobile phase: 0.050 M phosphate in MeOH, pH 6.0 (10:90%). UV detection at 210 nm. Reproduced from [172].

Similar work has also been carried out on analytes of biologically active peptides containing 1-prolyl down to temperatures as low as -15 °C. In this case rapid isomer interconversion between cis- and trans-isomeric forms of the prolyl peptide was shown to result in classical secondary equilibrium effects in the peak shapes [173] as can be seen from Figure 1.22. A detailed examination of the dynamic effects of secondary equilibria on the chromatographic process was performed by Melander *et al.* [174] and an improvement in the separation of many other biological analytes at sub-ambient temperatures has also been reported [175,176].A more common application for sub ambient temperature in LC is on-column focusing. This is achieved by holding the column inlet at a low temperature, typically less than 5 ºC. This effectively allows solute enrichment at the head of the column and previous works [177-184] have shown sample volumes to be increased by a factor of 10^3 simply by employing this method [178].

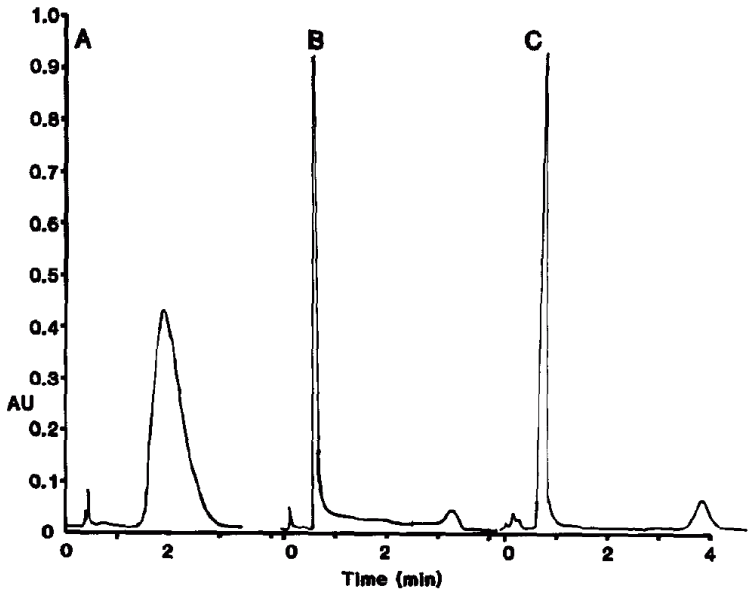

Figure 1.22 – Separation of Val-Pro-Leu isomers at (a) room temperature, mobile phase MeOH with 0.05 M phosphate (pH 7.0) (15:85%), flow rate 2.0 ml/mm, at (b) -0.1 °C, mobile phase MeOH – phosphate buffer (pH 7.0) (20:80%), flow rate 2.0 ml/mm, and at (c) -11 °C, flow rate 1.8 ml/min. Column = Pecosphere C_{18} 33 cm x 4.6 mm ID (d_p 3 μm). UV detection at 210 nm. Reproduced from [173].

In their study, Molander *et al* [178] evaluated column focusing efficiency by injecting large, 500 µL samples onto the column at different temperatures, applying the same loading flow rate, and using peak height measurements as an indicator of focusing efficiency. As it can be seen from Figure 1.23, the peak heights significantly increased with temperature decrease from 20 °C to 5 °C. Greibrokk *et al.* also demonstrated several examples of solute focusing through the application of temperature gradients which started at some low initial temperature, typically between 5 and 7 ºC [177-184]. After the desired amount of sample is injected onto the column the temperature is ramped up, subjecting the sample to programmed gradient elution.

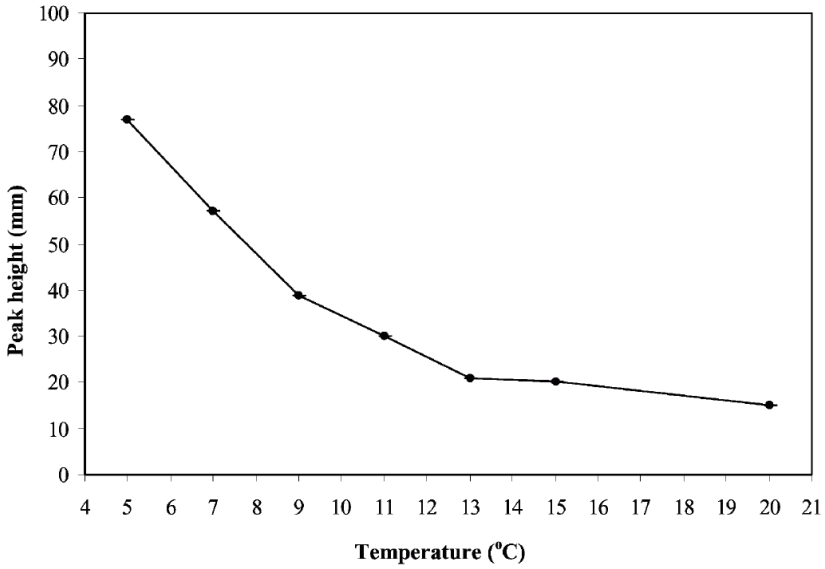

Figure 1.23 – The influence of loading temperature on enrichment-column focusing of Irganox 1076 (60 ng) when using a loading flow rate of 5 µL/min and an injection volume of 500 µL. Reproduced from [178]

By using this method the authors demonstrated that the use of sub-ambient temperatures was an effective way of loading large sample volumes onto analytical columns and improving the limits of detection particularly for trace determination. This method is particularly suited to capillary scale columns.

1.2.1.2 Sub-zero °C chromatographic separations

In comparison with high temperature chromatography, there are much fewer studies reporting on sub-zero liquid chromatography, with much of the published work at these temperatures being in the area of liquid-liquid extractions and preparative methods prior to separation on a chromatographic column [185]. An interesting work undertaken at sub-zero temperatures describes affinity chromatography using Sepharose-bound L-trialanine p-nitroanilide for the affinity binding of porcine pancreatic elastase, which was adsorbed in a

hypersaline medium at −14 °C and eluted with a mobile phase of 50% (v/v) ethylene glycol[186].

One of the most exciting applications of sub-zero temperatures in LC is in the area of ice chromatography [187-198] which uses only water ice as the stationary phase [193,198-201] at temperatures between -5 °C to almost -20 °C. Ice based chromatography presents a simple stationary phase on which it is possible to carry out normal phase separations and several compounds, including estrogens, amino acids, and acyclic polyethers, have all been successfully separated by this method with hexane-based mobile phases. Okada *et al.* [198] performed a separation of nine amino acids using just ice as the stationary phase and a mobile phase of diethylether in hexane. The separation was performed at –10 °C and is shown in Figure 1.24.

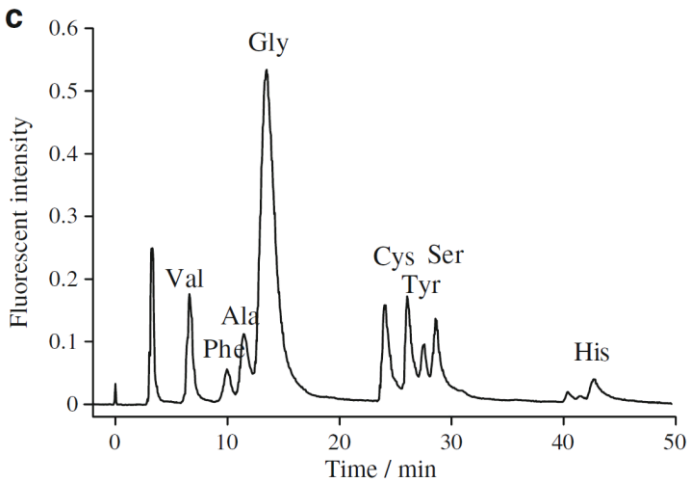

Figure 1.24 – Separation of o-phythalaldehyde derivatives of amino acid esters with step gradient elution at −10 °C; 5.4% diethylether in hexane (0 – 23.8 min) → 26.5% diethylether in hexane (23.8 – 40.0 min) → 50.0% diethylether in hexane (40.0 – 50.0 min). Reproduced from [198].

However, the application of sub 0 °C temperatures to the chromatographic process is not simply confined to the creation of stationary phases or as a parameter in the chromatographic process. Freezing has also been used to create “ice-valves” in micro-fluidic platforms to control flow [202].

Recently Eghbali *et al.* [203] demonstrated analyte trapping on the end of a column which was applied to separations of large bio-molecules, in this case proteins and peptides. This was achieved by cooling the end segment of a reversed phase column to approximately -20 °C. The authors noted that biological analytes such as these typically have large retention enthalpies, thus temperature has a significant effect on their retention behaviour.

1.2.2 High temperature chromatography

Historically, the use of elevated temperatures in liquid chromatography did not generate much interest and was certainly not widely used, even though the benefits of performing separations at higher than ambient temperatures have been well known for over 40 years [204,205]. Two exceptions to this were its application in size exclusion and ion-exchange chromatography [164], but for the most part, the role of temperature in the chromatographic process was often one of simple thermostatting rather than being employed as a useful chromatographic tool. Part of the reason for this was due to the lack of commercially available column ovens capable of high temperatures, but more significantly it was because thermally stable stationary phases simply did not exist. In addition, during the latter half of the last century pumping technology was developing quickly and improvements in pumping control and mixing was enabling the use of reproducible, compositional mobile

phase gradients with the result that high temperature separations attracted very little attention. As recently as 1996, a publication [206] reported that half of all HPLC systems being sold did not come with a column oven. In the past few decades however, column technology has moved on considerably and in recent years there has been renewed interest in high temperature LC, particularly given the growing popularity of microbore and capillary scale LC. The low thermal mass of these small columns allows for almost instantaneous thermal transfer and today the use of higher than ambient temperatures is recognised as a valuable tool in LC, particularly in reversed-phase separations. Currently most modern liquid chromatographs are sold complete with integrated column oven compartments, most being capable of heating to at least 80 °C. There have been a number of comprehensive reviews and book chapters published on the subject of high temperature LC [151,160,164,207-212].

1.2.2.1 Application of temperature

Nowadays most commercially available LC systems come with some degree of column heating, usually in the form of a column compartment, however some instruments also offer extended compartments which house not only the column, but also the injector and inlet tubing. In general LC applications, temperature can be applied to the column in a number of ways. The column can be heated by direct contact through heating blocks (direct contact), by being immersed in a water bath (or by using a water jacket), or through the use of an air bath or circulating air oven [207,211,231]. Clearly, the most efficient of these approaches is the water bath or water jacket due to their superior heating capacity, however direct contact systems come a close second, their major limitation being in the way the column contacts the heating blocks. Unfortunately, water bath systems are seriously limited

by the temperature gradients which they can achieve, while water jacket systems fare only slightly better due to their smaller thermal mass. Air bath systems can provide fast thermal gradients, depending on the efficiency of the system, and most circulating air ovens give thermal response times of approximately 30 °C/min. In this respect, direct contact systems out perform other types of column oven. Provided the contact between the column and the heating block(s) is thermally efficient, extremely high ramp rates have been reported. Furthermore, some groups have modified GC column heaters for use with capillary scale columns - GC column heaters providing ramp rates of up to 1800 °C/min [213].

1.2.2.2 The effect of temperature on LC separations

The effect of a temperature increase on the separation efficiency is described in the following pages. It is well known that diffusion coefficients in the mobile (D_m) and stationary (D_s) phases are highly dependent on temperature (eq. (1.1) and (1.2)):

$$D_m \propto \frac{\sqrt{\psi_2 M_2}}{\eta . V_1^{0.6}} T$$

eq. (1.1)

$$D_s = \frac{D_m . \varepsilon_t . \delta}{\tau}$$

eq.(1.2)

where T is temperature, M_2 is molecular weight of solvent, V_1 is molar volume of solute, η is viscosity of mobile phase, Ψ_2 is association factor of solvent, ε_t is porosity, δ is constrictivity, and τ is tortuosity.

The terms B (longitudinal diffusion) and C (mass transfer) of the van Deemter equation (eq.1.3) are both related to the diffusion coefficients in mobile and stationary phases which it turn are affected by temperature.

$$H_u = A + \frac{B}{u} + Cu$$

eq. (1.3)

Looking firstly at the B-term, it can be rewritten as:

$$\frac{B}{u} = \frac{\sigma^2}{L}$$

eq. (1.4)

where B is the longitudinal diffusion coefficient, u is the linear velocity of the mobile phase, σ^2 is variance resulting from diffusion and L is column length. This can be further shown as:

$$\frac{\sigma^2}{L} = \frac{2D_m}{u}$$

eq. (1.5)

where D_m is the diffusion coefficient of solute in mobile phase. The C-term can be presented as:

$$C_u = (C_s + C_m)u$$

eq. (1.6)

where C is the coefficient of resistance to mass transfer, C_s is the coefficient of mass transfer in the stationary phase and C_m is the coefficient of mass transfer in the mobile

phase. The mass transfer terms also can be described relative to the diffusion coefficients in the mobile and stationary phase respectively:

$$C_s = \frac{2k'}{3(k'+1)^2} \cdot \frac{d^2}{D_s}$$

eq. (1.7)

$$C_m = \frac{1+6k'+11k'^2}{24(k'+1)^2} \cdot \frac{r^2}{D_m}$$

eq.(1.8)

where *k'* is capacity factor, *d* is thickness of stationary phase, *r* is column radius, D_m is diffusion coefficient of solute in mobile phase, and D_s is diffusion coefficient of solute in stationary phase.

There have been many studies showing the advantages of high temperature separations across different modes of liquid chromatography [149,150,152,214]. The most obvious advantage of running a separation at higher than ambient temperatures is the reduction in column backpressure due to a decrease in mobile phase viscosity. The drop in pressure means that the user can run at higher flow rates, therefore increasing the speed of the separation. Importantly, the use of elevated flow rates in conjunction with increased column temperatures has much less of an impact on separation efficiency. The effect on temperature on efficiency at different flow rates is presented in Figure 1.25, and it can be seen that at high linear velocities where the C-term is the dominant contributor to theoretical plate height, the van Deemter curve remains shallow. Due to improved mass transfer at elevated temperatures, the cost to column efficiency from running at higher than optimal flow rates is greatly reduced.

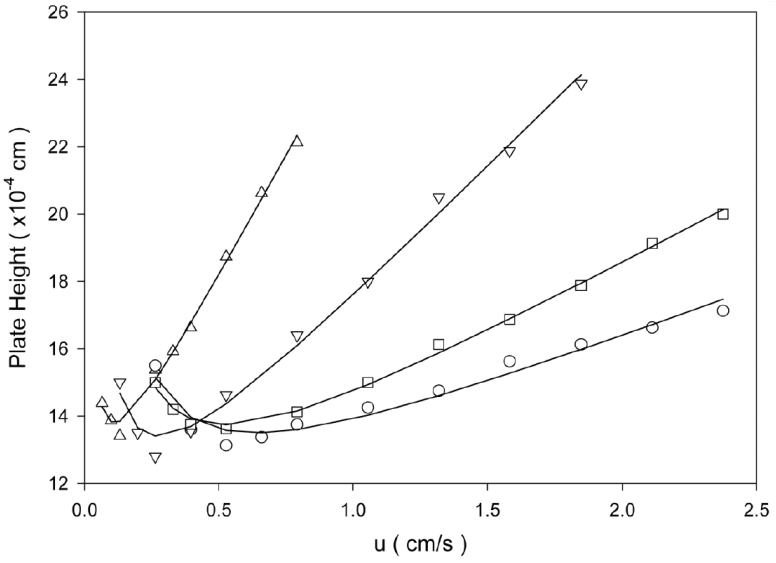

Figure 1.25 – Plate height vs. linear velocity at various temperatures for moderately retained solutes. Experimental conditions: 3 µm ZirChrom-PS column, 5 cm x 4.6 mm ID, 40% ACN/60% water, △ = 25 °C, octanophenone, k = 3.87, ▽ = 80 °C decanophenone, k = 3.15, □ = 120 °C, decanophenone, k = 5.70, ○ = 150 °C, decanophenone, k = 1.65. Reproduced from [151].

In addition to this, there is a relationship between temperature and analyte retention, which is described by the van't Hoff equation (eq. (1.11)), and is derived from general thermodynamic equation:

$$\ln K = \frac{-\Delta H^0}{RT} + \frac{\Delta S^0}{T}$$

eq. (1.9)

Where ΔH^0 is the enthalphy of adsorption, R is the gas constant, T, is absolute temperature in kelvin, ΔS^0 is the enthropy of adsorption and K is the equilibrium constant [215]. The equilibrium constant K is proportional to the retention factor k according to the following equation:

$$\ln K = \ln k\varphi$$

eq. (1.10),

where φ is the phase ratio (V_s/V_m). Thus the relation between retention factor and temperature can be written as:

$$\ln k = \frac{-\Delta H^0}{RT} + \frac{\Delta S^0}{T} + \ln \varphi$$

eq.(1.11)

Figure 1.26 shows the practical application of the relationship between retention factor and temperature for eight different polystyrenes of increasing molecular mass, showing that adjusting the temperature may significantly affect the retention and selectivity. Faster flow rates and lower retention factors mean that run times can be considerably shorter in comparison to separations carried out at room temperature; up to 50 times faster in some instances [216].

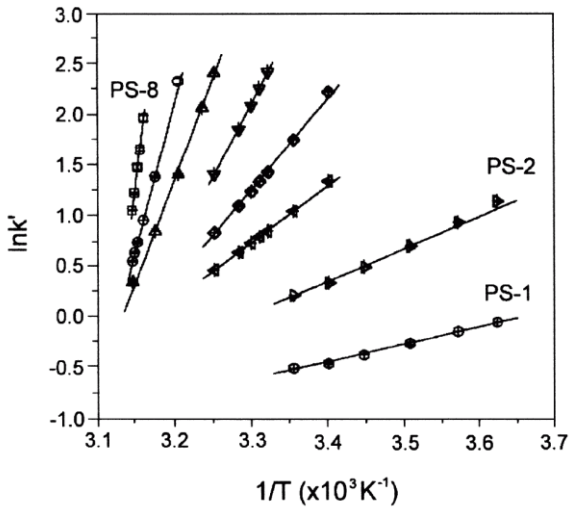

Figure 1.26 – Van't Hoff plot of polystyrenes, demonstrating the impact of temperature on the retention of compounds with different molecular mass. Reproduced from [164].

In addition to decreasing the analysis time, the use of high temperature has many other significant effects. Improvement of peak shape and column efficiency have been reported for a variety of stationary phases including zirconia [209,217], carbonaceous sorbents such as Hypercarb [218], organic polymers [219] and bare silica [220]. As described earlier, analyte diffusivity increases at higher temperatures which improves column efficiency due to improved mass transfer. Figure 1.27 shows a separation of caffeine derivatives on a zirconia-based column at 25 °C and 150 °C, with a significant improvement in peak shape and efficiency at the higher temperature.

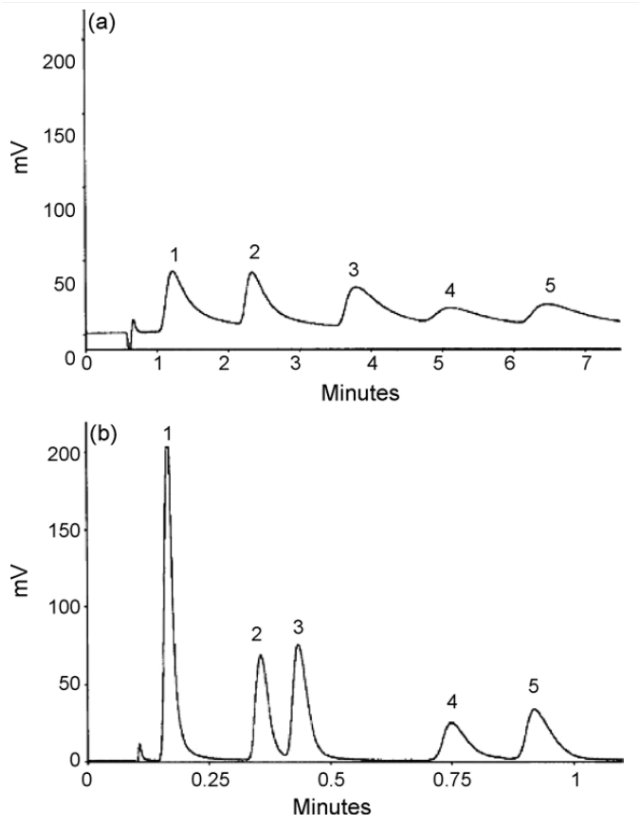

Figure 1.27 – Effect of temperature on the separation of caffeine derivatives (1, hypoxantine; 2, theobromine; 3, theophilline; 4, caffeine; 5, ß-hydroxy-ethyltheophilline). Column: ZirChrom-DB-C_{18} 50 mm x 4.6 mm: (a) 25 ◦C, flow rate = 1 mL/min, water–methanol 60:40% (v/v); (b) 150 ◦C, flow rate = 7 mL/min, water. Reproduced from [231].

Separation selectivity and resolution can be significantly improved and so peaks that co-elute at room temperature can often be separated at higher temperatures or through the application of thermal gradients (also known as temperature programming). A good example of the effect of temperature of peak selectivity is presented in Figure 1.28, which shows a separation of a mixture of six steroids at different temperatures. Additionally in many instances the analyte signal-to-noise ratio can also be increased [209,211].

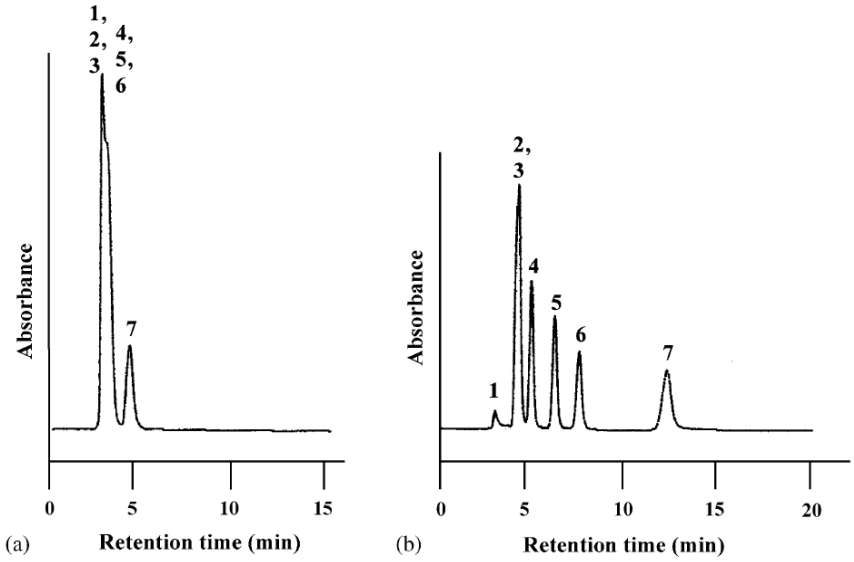

Figure 1.28 – Effect of temperature on resolution. Separation of benzene and six steroids (1. benzene; 2. hydrocortisone; 3. cortisone; 4. prednisolone; 5. dexamethasone; 6. hydrocortisone acetate; and 7. testosterone) on a NIPAAm-BMA-DMAPAAm (IBD) terminally-modified column at (a) 10 °C,and (b) 50 °C. Mobile phase: H_2O. Flow rate = 1.0 mL/min. UV detection at 254 nm. Reproduced from [221].

Isobaric (constant pressure) separations are also possible using temperature programming and this offers an excellent alternative to solvent gradient elution where the required range of the elution strength is not very wide.

1.2.2.3 Water-only separations

Higher temperature reduces the dielectric constant of water, so hotter water begins to take on the characteristics of an organic solvent [222]. Figure 1.29 shows the effect of temperature on the dielectric constant, surface tension, and viscosity of pure water, and on water/acetonitrile and water/methanol mixtures.

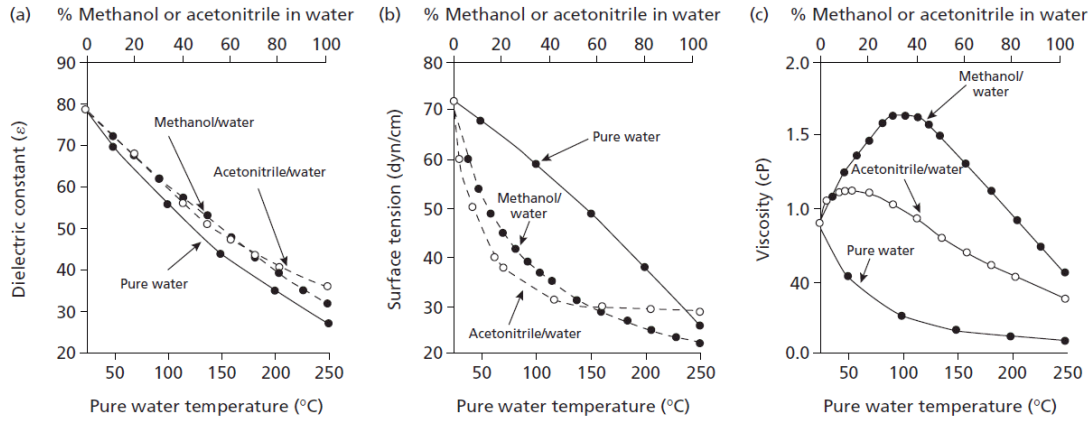

Figure 1.29 – Effect of temperature on (a) dielectric constant, (b) surface tension and (c) viscosity for pure water, and water/acetonitrile and water/methanol mixtures. Reproduced from [222].

This means that as higher temperatures are used, less organic solvent within the mobile phase is required for the separation. Indeed, a growing application of high temperature LC is within the area of 'green' chemistry, where only pure water is used as the mobile phase for reversed-phase separations [210,230]. Two excellent recent examples are shown in Figure 1.30, where Smith *et al.*, [230] separated a mixture of alkylbenzenes and phenylalkanols using superheated water as the mobile phase at temperatures up to 190 °C on a C_{18} bonded ethylene bridged hybrid column.

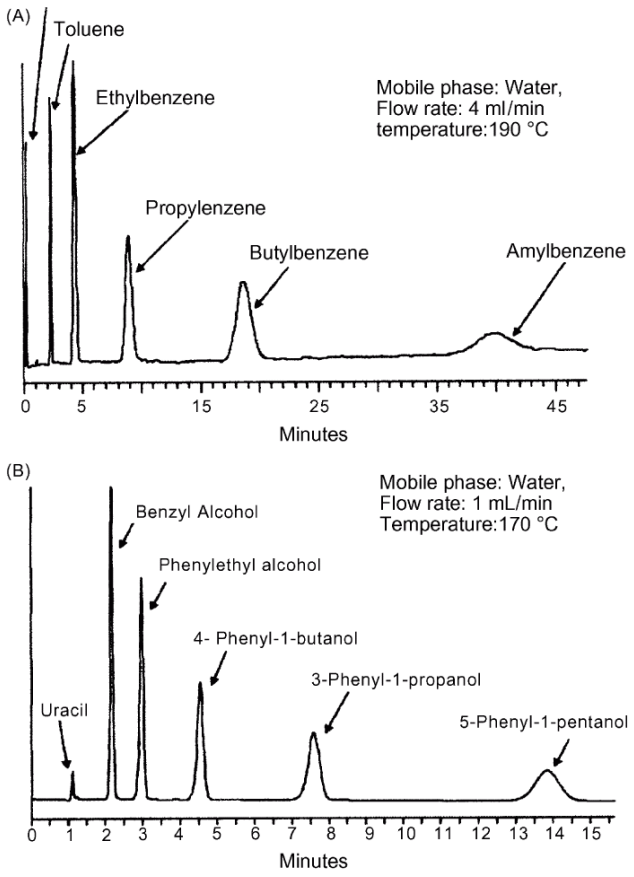

Figure 1.30 – Separation of (a) alkylbenzenes at 190 °C at 4 ml/min and (b) phenylalkanols at 170 °C at 1 ml/min on C_{18} bonded ethylene bridged hybrid column. Reproduced from [230].

Kephart and Dasgupta [223] performed separations using superheated water, and in this work the authors investigated up to the boundary of supercritical water, successfully separating several *n*-butyl-benzenes at temperatures up to 370 °C. This work is of particular interest as several observations regarding the technical difficulties with operating at such high temperatures were made. The authors noted that supercritical water was a highly aggressive solvent and at 370 °C caused catastrophic failure of fused silica capillaries within only 1 hr of use. The presence of a silica pre-saturator extended the lifetime of the column to 10 hrs, however, such a short column lifetime is of very limited use. Even at 250

°C the lifetime of the capillary was approximately 3 days when used without the silica pre-saturator. Later Causon *et al*. [224] studied the stability of a poly(divinylbenzene) monolithic column when using pure water at temperatures up to 250 ◦C and showed that the monolith was stable and attached to the inner walls of the capillary for up to 30 h of operating at 220 ◦C.

Several comparisons [225-227] of solvent composition against temperature have shown that a 1% increase in MeOH concentration was equivalent to an increase in temperature of around 4ºC. Other comparisons have been made with acetonitrile-water mobile phases with similar results. The combination of solvent and temperature gradients together, and indeed the simultaneous use of the two, is considered to be a highly effective way to control peak retention and selectivity. In general, it is the entropy dominated separations that will benefit most from temperature programming over solvent gradient programming.

1.2.2.4 The effect of temperature on detection sensitivity

In addition to the many advantages of applying high temperature to the separation itself, there are also some other positive aspects which are not so obvious, particularly concerning the detector. Often, in the course of high temperature LC, post-column cooling is required prior to UV or fluorescence detection, however there have been many studies done which show that high mobile phase temperatures improved detector response, particularly for evaporative light scattering detectors [209]. High eluent temperatures are also of benefit when using LC-MS and studies have shown many advantages including reduced run times and improved sensitivity and detection[228,229]. Figure 1.31 shows a series of chromatograms of a separation of sulfonamides under various conditions, including a

solvent and temperature program. However, the inset in the figure shows the MS peak area for each compound under solvent and temperature programming conditions, and the improvement in sensitivity, particularly for peak 4, can clearly be seen.

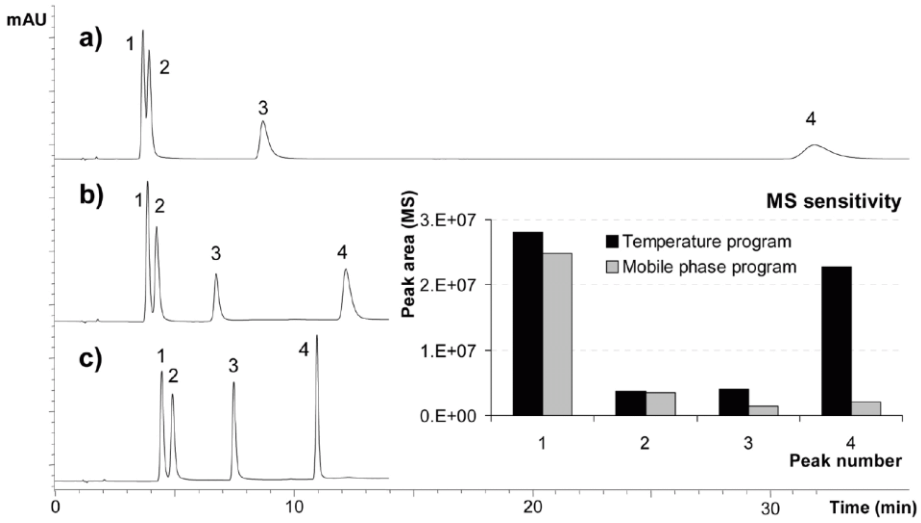

Figure 1.31 – Green chromatography of a sulfonamide mixture (1. sulfamethazine, 2. sulfamethizole, 3. sulfachlorpyridazine, and 4. sulfamethoxine) on a Hypercarb column 100 mm x 3 mm ID (d_p 5 µm), at various conditions, (a) isocratic 50% B, isothermic 50 °C; (b) solvent program 50 to 100% B in 5 min, isothermic 50 °C; (c) isocratic 50% B, temperature program: initial 40 °C, hold 0–2 min, ramp 40–180 °C at 20 °C/min. Flow rate = 0.5 mL/min. Mobile phase: A, 0.1% acetic acid in water, B, 0.1% acetic acid in ethanol. DAD detection at 273 nm. Inset: MS peak area under conditions (b) and (c). Reproduced from [160].

1.2.2.5 Stationary phase and analyte stability at elevated temperatures

There continues to be a widespread reluctance to use high temperature mainly due to the popularity of silica based stationary phases and their intolerance to water-based eluents at elevated temperatures. Silica based phases have a reputation as being notoriously unstable when used at elevated temperatures, and in some cases even short term exposure to high temperatures may permanently degrade the column [156,158]. High temperatures often increase the solvating strength of the mobile phase, and (both non-bonded and bonded) coatings may be easily removed. The aggressive use of temperature, even with just water as the mobile phase, can lead to rapid degradation of the stationary phase [159]. The underlying supports of the stationary phase can also be attacked causing the structure to either collapse or simply wash off the column (column bleed), a condition that is most common in GC. Occasionally a column may be conditioned by cycling the column temperature under flow or by flushing the column with a strong mobile phase at high temperature. However, depending on the type of column there may be a loss of stationary phase, reducing both capacity and efficiency and ultimately resulting in the destruction of the column. Having said this, there are many columns now commercially available that have excellent thermal stability and which demonstrate excellent reproducibility when used at elevated temperatures. In addition, even separations done on silica columns which are prone to degradation at elevated temperatures can often benefit from temperature programming provided the upper temperature limits are not excessive. Over 100 ºC most silica based C_{18} phases will rapidly degrade [231]; however, once the temperature is kept below 70 ºC, most reversed-phase columns will experience no problems whatsoever. On the other hand, phases such as cross-linked polystyrene, graphitic carbon, and zirconia (to name a few) have demonstrated excellent stability at temperatures exceeding 240 ºC

[211,231]. Analyte stability may also be affected by the application of high temperatures particularly if the analyte in question is a thermally labile species. Many compounds (especially biomolecules and bio-active compounds) will undergo rapid degradation at elevated temperatures and this is probably the main reason that high temperature LC has yet to be accepted by the wider pharmaceutical industry. However, the occurrence of on-column degradation depends not only on the reaction rate of the analyte at the given conditions, but also the length of time which the analyte is exposed to these conditions [232]. Theoretically, any on-column reaction might be rendered insignificant if the increase in the analyte's reaction rate at high temperatures was offset by the reduction in the time that the analyte spends in the column [233]. Although the compound might degrade at the applied temperature, the combined effects of reduced retention and higher flow rate might well result in the analyte eluting before it has time to degrade. A recent study illustrated this particularly well by separating three proteins at 120 ºC on a silica based column using a mobile phase consisting of 0.1% TFA [234], shown in Figure 1.32. This further highlights the importance of very rapid temperature programming in LC.

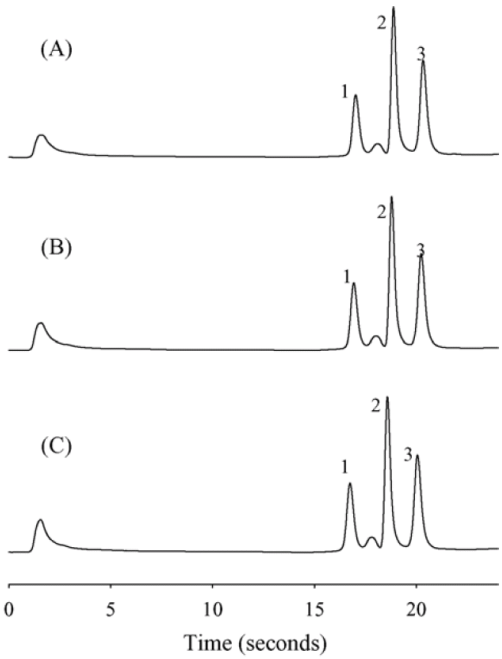

Figure 1.32 – Separations of a protein mixture (1. ribonuclease, 2. insulin; and 3. α-chymotrypsin) performed on a HC-C_8 phase at 120 °C, (A) injection made immediately after column equilibration at 120 °C; (B) after 24 hr; (C) after 50 hr. Conditions: 120 °C, 5 mL/min, injection volume 1 µL. Solvent (A) 0.1% TFA in water; solvent (B) 0.067% TFA in ACN. Linear gradient from 10 to 90% B in 0.3 min (dwell time is 0.2 min). UV detection at 220 nm. Reproduced from [234].

1.2.2.6 The effect of eluent pre-heating and post-column thermostating

There are a number of considerations that must be taken into account besides the stability of the column and analytes in question. The effect of difference between temperature of the inlet mobile phase and the column temperature is shown in Figure 1.33. It can clearly be seen that the difference of ~16 °C significantly affects peak shape, causing them to split, while fine temperature adjustment results in excellent peak shape and complete resolution of all peaks of the test mixture. In order to minimise band broadening the mobile phase should be pre-heated to within at least 6 ºC of the column temperature and this is especially critical for columns larger than 2 mm in diameter [165,235-238].

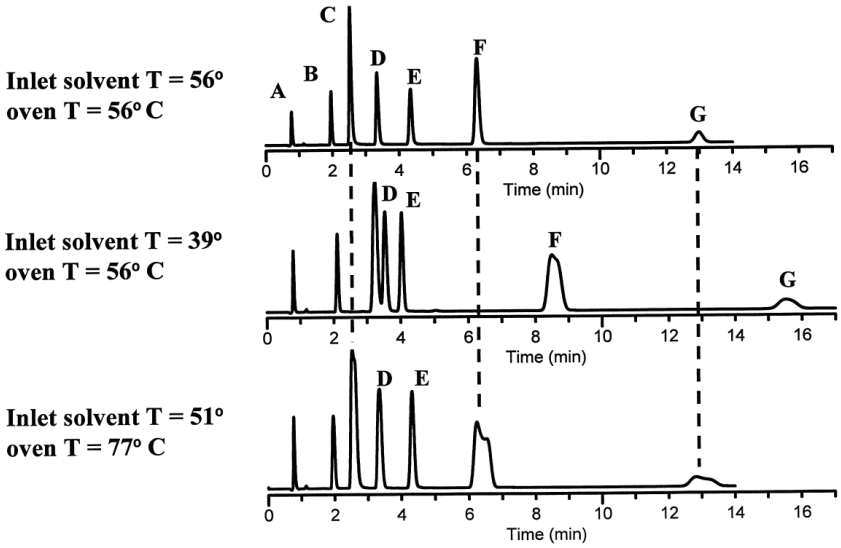

Figure 1.33 – Effect of the inlet solvent temperature on separation. Flow rate = 2 ml/min, incoming and oven temperatures shown in figure. Reproduced from [165].

Likewise, at the column exit, the eluent should be temperature controlled depending on the mode of detection being employed. For most standard optical detectors the mobile phase may need to be cooled prior to entering the detector. At higher temperatures a pressure restrictor (usually just a coil or section of narrow bore tubing or capillary) will often be required between the column and detector, the purpose of which is to prevent the mobile phase from boiling before it has a chance to cool sufficiently [151,211,238]. If the column ID is too large (typically >2 mm) then there will be considerable thermal lag, so rapid temperature programming will not work effectively and will probably cause band broadening (this can occur due to axial and/or radial temperature gradients within the column). An excellent example of this is presented in Figure 1.34, reproduced from the work by Jones [207]. In this example the author applied a temperature program to a 4.6 mm ID stainless steel housed column, heating at 40 °C/min from 40 °C to 200 °C. The author recorded the temperature at the start, middle, and exit of the column, comparing it to the

actual temperature of the column oven. As can be seen from the figure, some areas of the column suffers from excessive thermal lag, between 45 – 50 °C in some instances.

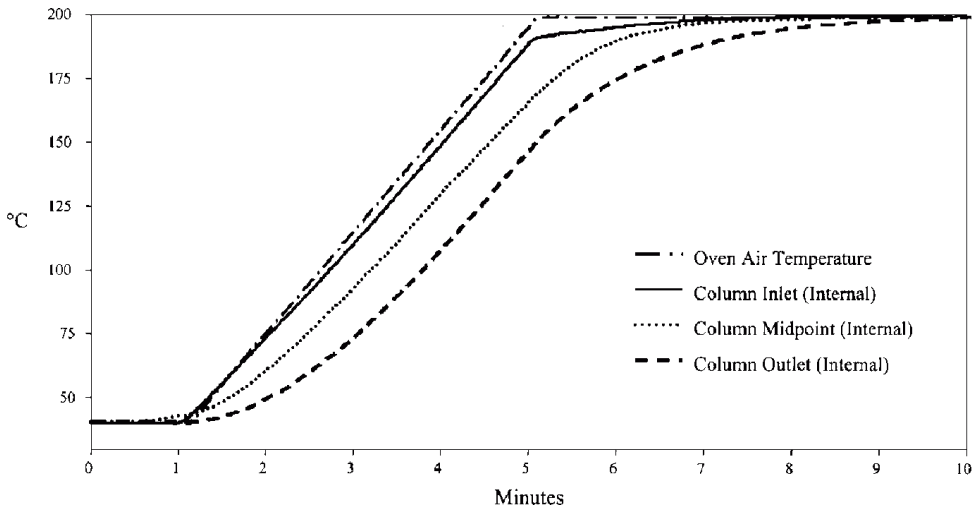

Figure 1.34 – Column temperature lag during a temperature program from 40 °C to 200 °C at 40 °C/min, after an initial hold 1 min. The column was 4.6mm internal diameter x 150 mm long. Mobile phase: H_2O, flow rate = 3 mL/min, and was maintained in a liquid state by applying 250 psi backpressure to the column outlet. The mobile phase preheater was programmed to track the oven temperature. Reproduced from [207].

The next decade promises to be very exciting with regard to high temperature LC, particularly as the boundaries of what is possible are constantly being pushed further. Although the application of elevated temperatures may not become common place across all modes, it is most likely, given that it is such a useful tool, that temperature programming will become the norm. Having said this, there is a worldwide push towards reducing solvent consumption and separations carried out at high temperature is the logical solution. With the market moving towards greener and faster separations we will probably see the sizes of analytical columns becoming smaller and smaller, more suited to rapid temperature

programming and high temperatures. In addition, with mass spectrometers becoming more affordable, we can expect an increase in the use of LC-MS in analytical labs, a technique which benefits from the application of elevated temperatures.

1.3 Conclusions

Capillary scale LC offers many benefits over standard bore separations and continues to grow in popularity in many different modes of chromatography. Furthermore, the extensive work done in the area of monolithic stationary phases over the past 15 years has added a further dimension to LC separations and capillary LC in particular. With the trend towards smaller column sizes and rapid separations, there exists a need for capillary scale instrumentation, not only in analytical sense, but also as an aid for the development and fabrication of capillary columns. The work carried out in the following Chapters of this thesis aims to address this need for new and novel instrumentation. The design, development, and application of a rapid direct contact column oven suitable for capillary and micro-bore scale LC is presented. Additionally, extensive work on the fabrication of monoPLOT columns through both photo- and thermal-initiation is carried out, with an emphasis on control of the procedure and column reproducibility.

Reference list

1. Novotny, M., *Anal. Chem.*, (1988), 60, 8, pp. 500.
2. Chervet, J.P.; Ursem, M.; Salzmann, J.B., *Anal. Chem.*, (1996), 68, pp. 1507.
3. Desmet, G.; Eeltink, S., *Anal. Chem.*, (2013), 85, pp. 543.
4. Gritti, F.;, Guiochon, G.; *J. Chromatogr. A.*, (2012), 1228, pp. 2.
5. Kiplagat, I.; Kuban, P.;Pelcova, P.; Kuban, V., *J. Chromatogr. A*, (2010), 1217, pp. 5116.
6. Saito, Y.; Jinno, K.; Greibrokk, T., *J. Sep. Sci*., (2004), 27, pp. 1379.
7. Vissers, J.P.C.; Claessens, H.A.; Cramers, C.A., *J. Chromatogr. A*, (1997), 779, pp. 1.
8. Bristow, P.A.; Knox, J.H.; *Chromatographia*, (1977), 10, 6, pp. 279.
9. Vissers, J.P.C, *J. Chromatogr. A*, (1999), 856, 1, pp. 117.
10. Hopfgartner, G.; Bean, K.; Henion, J.J.; *J. Chromatogr.*, (1993), 647, pp. 51.
11. Banks, J.F.; *J. Chromatogr.*, (1996), 743, pp. 99.
12. Patel, K. D.; Jerkovich, A. D.; Link, J. C.; Jorgenson, J. W., *Anal. Chem.*, (2004), 76, pp. 5777.
13. Svec, F.; Frechet, J. M. J., *Anal. Chem.*, (1992), 64, pp. 820.
14. Minakuchi, H.; Nakanishi, H.; Soga, N.; Ishizuka, N.; Tanaka, N., *Anal. Chem.*, (1996), 68, pp. 3498.
15. Lippert, J.A.; Xin, B.; Wu, N.; Lee, M.L., *J. Microcol. Sep.*, (1999), 11, pp. 631.
16. MacNair, J.E.; Lewis, K.C.; Jorgenson, J., *Anal. Chem.*, (1997), 69, pp. 983.
17. MacNair, J.E.; Lewis, K.C.; Jorgenson, J., *Anal. Chem.*, (1999), 71, pp. 700.
18. Bruns, S.; Grinias, J.P.; Blue, L.E.; Jorgenson, J.W.; Tallarek, U.; *Anal Chem*, (2012), 84, pp. 4496.

19. D'Orazio, G.; Fanali, S.; *J. Chromatogr. A*, (2012), 1232, pp. 176.
20. Chen, C.J.; Chen, W.Y.; Tseng, M.C.; Chen, Y.R.; *Anal. Chem.*, (2012), 84, pp. 297.
21. Koyama, T.; Terauchi, K., *J. Chromatogr. B*, (1996), 679, 1, pp. 31.
22. Perrier-Cornet, R.; Heroguez, V.; Thienpont, A.; Babot, O.; *et al., J. Chromatogr. A*, (2008), 1179, 1, pp. 2.
23. http://www.merckmillipore.com/ireland/chemicals/chromolith-performance-si-100-4-6-mm/, (accessed Feb 2013).
24. http://www.glantreo.com/nonporoussilica.php, (accessed Feb 2013).
25. http://www.glantreo.com/coresilicaparticles.php, (accessed Feb 2013).
26. http://www.sigmaaldrich.com/catalog/product/supelco/567416U/, (accessed Feb 2013).
27. http://www.millipore.com/userguides/tech1/00107545pu, (accessed Feb 2013).
28. http://www.welchmat.com/english/productview.aspx?StkNo=15, (accessed Feb 2013).
29. http://www.separations.us.tosohbioscience.com/Products/HPLCColumns/ReversedPhase/PolymerbasedColumns/, (accessed Feb 2013).
30. http://www.futecs.com/shodex/subpage/08.html, (accessed Feb 2013).
31. Hutchinson, J.P.; Zakaria, P.; Bowie, A.R.; Macka, M.; Avdalovic, N.; Haddad, P.R., *Anal. Chem.*, (2005), 77, pp. 407.
32. Svec, F.; *J. Sep. Sci.*, (2004), 27, pp. 747.
33. Ueki, Y.; Umemura, T.; Li, J.; Odake, T.; Tsunoda, K., *Anal. Chem.*, (2004) 76, pp. 7007.
34. Viklund, C.; Svec, F.; Frechet, J.M.J.; Irgum, K., *Chem. Mater*., (1996), 8, pp.

744.

35. Zakaria, P.; Hutchinson, J.P.; Avdalovic, N.; Liu, Y.; Haddad, P.R., *Anal. Chem*., (2005), 77, pp. 417.
36. Zabka, M.; Minceva, M.; Rodrigues, A.E., *J. Biochem. Biophys. Methods*, (2007), 70, pp. 95.
37. Cabrera, K.; Wieland, G.; Lubda, D.; Nakanishi, K.; Soga, N.; Minakuchi, H.; Unger, K.K.; *TrAC*, (1998), 17, pp. 50.
38. Cabrera, K.; *J. Sep. Sci*., (2004), 27, pp. 843.
39. Ishizuka, N.; Kobayashi, H.; Minakuchi, H.; Nakanishi, K.; Hirao, K.; Hosoya, K.; Ikegami, T.; Tanaka, N.; *J. Chromatogr. A*, (2002), 960, pp. 85.
40. Rozenbrand. J; van Bennekom, W.P., *J. Sep. Sci*., (2011), 34, pp.1934.
41. Wu, R.; Hu, L.G.; Wang, F.J.; Ye, M.L.; Zou, H., *J. Chromatogr. A*, (2008), 1184, pp. 369.
42. Ross W.D.;, Jefferson, R.T.; *J. Chromatogr. Sci*., (1970), 8, 7, pp. 386.
43. Liang, Y.; Zhang, L.; Zhang, Y., *Anal. Bioanal. Chem.*, (2013) 405, pp. 2095.
44. Nunez, O.; Nakanishi, K.; Tanaka, N., *J. Chromatogr. A*, (2008), 1191, pp. 231.
45. Leinweber, F.C.; Tallarek, U., *J. Chromatogr. A*, (2003), 1006, pp. 207.
46. Nakanishi, K.; Minakuchi, H.; Soga, N.; Tanaka, N., *J. Sol-Gel. Sci. Technol*., (1997), 8, pp. 547.
47. Cabrera, K.; Wieland, G.; Lubda, D.; Nakanishi, K., *et al., TrAC*, (1998), 17, pp. 50.
48. Nakanishi, K.; Soga, N., *J. Am. Ceram. Soc*., (1991), 74, 10, pp. 2518.
49. Minakuchi, H.; Nakanishi, K.; Soga, N.; Ishizuka, N.; Tanaka, N., *Anal.Chem.*, (1996), 68, pp. 3498.

50. Asiaie, R.; Huang, X.; Farnan, D.; Horvath, C., *J. Chromatogr. A*, (1998), 806, pp. 251.

51. Cabrera, K., *J. Sep. Sci.*, (2004), 27, pp. 843.

52. Lubda, D.; Cabrera, K.; Kraas, W.; Schaefer, C.; Cunningham, D., *LC-GC Europe*, (2001), 14, 12, pp. 2.

53. Nunez, O.; Ikegami. T.; Kajiwara, W.; Miyamoto, K.; *et al*., *J. Chromatogr. A*, (2007), 1156, pp. 35.

54. Nunez, O.; Ikegami. T.; Miyamoto, K.; Tanaka, N., *J. Chromatogr. A*, (2007), 1175, pp. 7.

55. Soonthorntantikul, W.; Leepipatpiboon, N.; Ikegami, T.; Tanaka, N.; Nhujak, T., *J. Chromatogr. A*, (2009), 1216, pp. 5868.

56. Hara, T.; Makino, S.; Watanabe, Y.; Ikegami, T.; Cabrera, K.; Smarsly, B.; Tanaka N, *J. Chromatogr. A*, (2010), 1217, pp. 89.

57. Siouffi, A.M., *J. Chromatogr. A*, (2003), 1000, pp. 801.

58. Moravcova, D.; Jandera, P.; Urban, J.; Planeta, J., *J. Sep. Sci.*, (2004), 27, pp. 789.

59. Nesterenko, E.; Yavorska, O.; Macka, M.; Yavorskyy, A.; Paull, B., *Anal. Methods*, (2011), 3, pp. 537.

60. Lin, Z.; Huang, H.; Sun, X.; Lin, Y.; Zhang, L.; Chen, G., *J. Chromatogr. A*, (2012), 1246, pp. 90.

61. Huang, H.; Lin, Z.; Lin, Y.; Sun, X.; Xie, Y.; Zhang, L.; Chen, G., *J. Chromatogr. A*, (2012), 1251, pp. 82.

62. Nesterenko, E. P.; Nesterenko, P. N.; Connolly, D.; Lacroix, F.; Paull, B., *J. Chromatogr. A*, (2010), 1217, pp. 2138.

63. Ross, W.D.; Jefferson, R.T., *J. Chromatogr. Sci.*, (1970), 8, pp. 386.

64. Schnecko, H.; Bieber, O., *Chromatographia*, (1971), 4, pp. 109.

65. Hileman, F.D.; Sievers, R.E; Hess, G.G.; Ross, W.D., *Anal. Chem.*, (1973), 45, pp. 1126.

66. Dandenau, R.D.; Zerenner, E.H.; *J. High Resolut. Chromatogr.*, (1979), 2, pp. 351.

67. Svec, F., J. Chromatogr. A, (2010), 1217, pp. 902.

68. Svec, F.; Kurganov, A.A., *J. Chromatogr. A*, (2008), 1184, pp. 281.

69. Svec, F.; Tennikova, T.B.; Deyl, Z., Monolithic Materials: Preparations, Properties and Applications, 1st edition, Elsevier: Amsterdam, (2003), 773 p.

70. Svec, F.; Frechet, J.M.J., *Macromolecules*, (1995), 28, pp. 7580.

71. Greiderer, A.; Trojer, L.; Huck, C.W.; Bonn, G.K., *J. Chromatogr. A*, (2009), 1216, pp. 7747.

72. Trojer, L.; Bisjak, C.P.; Wieder, W.; Bonn, G.K., *J. Chromatogr. A*, (2009), 1216, pp. 6303.

73. Hoth, D.C., *J. Chromatogr. A*, (2005), 1079, pp. 392.

74. Silva, C.R.; Airoldi, C.; Collins, K.E.; Collins, C.H., *LC–GC*, (2004), 22, pp. 632.

75. Kimura, Y.; Shibasaki, S.; Morisato, K.; Ishizuka, N., *et al*., *Anal. Biochem*., (2004), 326, pp. 262.

76. Sekiguchi, Y.; Mitsuhashi, N.; Inoue, Y.; Yagisawa, H.; Mimura, T., *J. Chromatogr. A*, (2004), 1039, pp. 71.

77. http://www.zirchrom.com, (accessed Feb 2013).

78. Nawrocki, J.; Dunlap, C.; McCormick, A.; Carr, P.W., *J. Chromatogr. A*, (2004), 1028, pp. 1.

79. Nawrocki, J.; Dunlap, C.; Li, J.; Zhao, J., *et al*., *J. Chromatogr. A*, (2004), 1028, pp. 31.

80. C.J. Dunlap, C.V. McNeff, D. Stoll, P.W. Carr, *Anal. Chem*., (2001), 73, pp. 598.

81. Wu, N.; Tang, Q.; Shen, Y.; Lee, M.L., *Chromatographia*, (1999), 49, 7, pp. 431.

82. Shi, Z.G.; Feng, Y.Q.; Xu, L.; Zhang, M.; Da, S.L., *Talanta*, (2004), 63, pp. 593.

83. Miyazaki, S.; Miah, M.Y.; Shintani, Y.; Kuroha, T.; Nakanishi, K., *J. Sep. Sci.*, (2005), 28, pp. 39.

84. Liang, C.; Dai, S.; Guiochon, G.; *Anal. Chem.*, (2003), 75, pp. 4904.

85. Eltmimi A.H.; Barron L.; Rafferty A.; Hanrahan J.P., *et al.*, *J. Sep. Sci.*, (2010), 33, 9, pp. 1231.

86. Shi, Z.; Chen, F.; Xing, J.; *et al.*, *J. Chromatogr. A*, (2009), 1216, pp.5333.

87. Hayes, J.D.; Malik, A., *Anal. Chem*., (2000), 72, 17, pp. 4090.

88. Colon, L.A.; Li, L.;, *Adv. Chromatogr.*,(2008), 46, pp. 391.

89. Siouffi, A.M., *J. Chromatogr. A, (*2003), 1000, pp. 801.

90. Li, L.; Colon, L.A., *J. Sep. Sci*, (2009), 32, pp. 2737.

91. Roux, R.; Jaoude, M.A.; Demesmay, C.; *J. Chromatogr. A,* (2009), 1216, pp. 3857–3863.

92. Wu, M.H.; Wu, R.A.; Wang, F.J.; Ren, L.B., *et al*., *Anal. Chem.*, (2009), 81, pp. 3529.

93. Golay, M.J.E., *Gas Chromatography*, Coates, V.J., Ed. Academic Press: New York, (1958), pp. 1.

94. Tsuda, T.; Hibi, K.; Nakanishi, T.; Takeuchi, T.; Ishii, D.; *J. Chromatogr.*, (1978). 158, pp. 227.

95. Tsuda, T.; Novotny, M., *Anal. Chem*., (1978), 50, pp. 632.

96. Ishii, D.; Asai, K.; Hibi, K.; Jonokuchi, T.; Nagaya, M., *J. Chromatogr*., (1977), 144, pp. 157.

97. Halasz, I.; Horvath, C.; *Nature*, (1963), 197, pp. 71.

98. Yu, C.; Svec, F.; Frechet, J.M.J., *Electrophoresis*, (2000), 21, pp. 120.

99. Zaidi, S.A.; Cheong, W.J., *Electrophoresis*, (2009), 30, pp. 1603.

100. Chen, J.L.; Lin, Y.C.; *J. Chromatogr. A*, (2010), 1217, pp. 4328.

101. Tan, Z.J.; Remcho, V.T., *J. Microcolumn. Sep.*, (1998), 10, pp. 99.

102. Yang, L.; Guihen, E.; Holmes, J.D.; Loughran, M., *et al.*, *Anal. Chem.*, (2005), 77, pp. 1840.

103. Huang, X.; Zhang, J.; Horvath, C., *J. Chromatogr. A*, (1999), 858, pp. 91.

104. Ishii, D.; Takeuchi, T., *J. Chromatogr. Sci*., (1980), 18, pp. 462.

105. Jorgenson, J.; Guthrie, E.J., *J. Chromatogr.*, (1983), 255, pp. 335.

106. Dluzneski, P.R.; Jorgenson, J.W.; *J. High Resolut. Chromatogr*., (1988), 11, pp. 332.

107. Tijssen, R.; Bleumer, J.P.A.; Smit, A.L.C.; van Kreveld, M.E., *J. Chromatogr.*, (1981), 218, pp. 137.

108. Yang, F., *J. High Resolut. Chromatogr*., (1980), 3, pp. 589.

109. Yang, F., *J. Chromatogr. Sci*., (1982), 20, pp. 241.

110. Guiochon, G., *Anal. Chem.*, (1981), 53, pp. 1318.

111. Knox, J.H., *J. Chromatogr. Sci*., (1980), 18, pp. 453.

112. Maskarinec, M.; Sepaniak, M.; Baichunas, A.; Vargo, J., *Clin. Chem.*, (1984), 30, 9, pp. 1473.

113. Knox, J.H.; Gilbert, M.T., *J. Chromatogr.*, (1979), 186, pp. 405.

114. Causon, T.J.; Shellie, R.A.; Hilder, E.F.; Desmet, G.; Eeltink, S., *J. Chromatogr. A*, (2011), 1218, pp. 8388.

115. Crego, A.L.; Diezmasa, J.C.; Dabrio, M.V., *Anal. Chem.*, (1993), 65, pp. 1615.

116. de Zeeuw, J., *LC-GC*, (2011), 24, pp. 38.

117. Tock, P.P.H.; Boshoven, C.; Poppe, H.; Kraak, J.C.; *J. Chromatogr.*, (1989), 477, pp. 95.

118. Tock, P.P.H.; Stegeman, G.; Peerbom, R.; Poppe, H.; Kraak, J.C.; Unger, K.K., *Chromatographia*, (1987), 24, pp. 617.

119. Guo, Y.; Colón, L.A., *Anal. Chem*., (1995), 67, pp. 2511.

120. Guo, Y.; Colón, L.A., *J. Microcolumn. Sep.*, (1995), 7, pp. 485.

121. Guo, Y.; Colón, L.A., *Chromatographia*, (1996), 43, pp. 477.

122. Rodríguez, S.A.; Colón, L.A., *Anal. Chim. Acta*, (1999), 397, pp. 207.

123. Rodríguez, S.A.; Colón, L.A., *Appl. Spectrosc*., (2001), 55, pp. 472.

124. De Malsche, W.; De Bruyne, S.; De Beek, J.O.; Sandra, P., *et al.*, *J. Chromatogr. A*, (2012), 1230, pp. 41.

125. De Malsche, W.; De Beek, J.O.; De Bruyne, S.; Gardeniers, H., *et al.*, *Anal. Chem.*, (2012), 84, pp. 1214.

126. Wang, X.; Wang, S.; Veerappan, V.; Byun, C.K.; *et al*., *Anal. Chem.*, (2008), 80, pp. 5583.

127. Daley, A.B.; Wright, R.D.; Oleschuk, R.D.; *Anal. Chim. Acta*, (2011), 690, pp. 253.

128. Forstera, S.; Kolmar, H.; Altmaier, S., *J. Chromatogr. A*, (2012), 1265, pp. 88.

129. Sekigushu, Y.; Mitsuhashi, N.; Inoue, Y.; Yagisawa, H.; Mimura, T., *J. Chromatogr. A*, (2004), 1039, pp. 71.

130. De Graauw, M., Phospho-proteomics, methods and protocols, Humana Press: New York, (2009), 328 p.

131. Kephart, T.S.; Dasgupta P.K., *Anal. Chim. Acta*, (2000), 414, pp. 71.

132. Nawrocki, J.; Dunlap. C.; McCormick, A.; Carr, P.W., *J. Chromatogr. A*, (2004), 1028, pp. 1.

133. Wu,Y.; Hu, B.; Hu, W.; Jiang, Z.; Li, B., *J. Mass Spectrom.*, (2007), 42, pp. 467.

134. Liang, S.S.; Makamba, H.; Huang. S.Y.; Chen, S.H., *J. Chromatogr. A*, (2006), 1116, pp. 38.

135. Jaoudé, M.A.; Randon, J., *Anal. Bioanal. Chem*., (2011), 400, pp. 1241.

136. Lin, B., Li, T.; Zhaob, Y.; Huangb, F., *et al.*, *J. Chromatogr. A*, (2008), 1192, pp. 95.

137. Luo, Q.; Yue, G.; Valaskovic, G.A.; Gu, Y.; Wu, S.L.; Karger, B.L., *Anal. Chem.*, (2007), 79, pp. 6174.

138. Luo, Q.; Wu, S.L.; Rejtar, T.; Karger, B.L., *J. Chromatogr. A*, (2009), 1216, pp. 1223.

139. Luo, Q.; Yue, G.; Valaskovic, G.A.; Gu, Y.; Wu, S.L.; Karger, B.L., *Anal. Chem.*, (2007), 79, pp. 6174.

140. Luo, Q.; Ge, Y.; Wu, S.L.; Rejtar, T.; Karger, B.L., *Electrophoresis*, (2008), 29, pp. 1604.

141. Yue, G.; Luo, Q.; Zhang, J.; Wu, S.; Karger, B.L., *Anal. Chem.*, (2007), 79, pp. 938.

142. Nischang, I.; Brueggemann, O.; Svec, F., *Anal. Bioanal. Chem.*, (2010), 397, pp. 953.

143. Walsh, Z.; Abele, S.; Lawless, B.; Heger, D.; Klan, P.; Breadmore, M.; Paull, B.; Macka, M., *Chem. Commun*., (2008), pp. 6504.

144. Eeltink, S.; Svec, F.; Frechet, J.M.J., *Electrophoresis*, (2006), 27, pp. 4249.

145. Abele, S.; Smejkal, P.; Yavorska, O.; Foret, F.; Macka, M., *Analyst*, (2010), 135,

pp. 477.

146. Nesterenko, E.; Yavorska, O.; Macka, M.; Yavorskyy, A.; Paull, B., *Anal. Methods*, (2011), 3, pp. 537.

147. Ecoffet, C.; Espanet, A.; Lougnot, D., *J. Adv. Mater.*, (1998), 10, pp. 411.

148. Espanet, A.; Ecoffet C.; Lougnot, D.J.; *J. Polym. Sci., Part A: Polym. Chem.*, (1999), 37, 13, pp. 2075.

149. Ooms, B., *LC-GC*, (1996), 14, pp. 306.

150. Chen, H.; Horvath, C. *J. Chrom. A*, (1995), 705, pp. 3.

151. Mcneff, C. V.; Yan, B.; Stoll, D. R.; Henry, R. A., *J. Sep. Sci.*, (2007), 30, pp. 1672.

152. Van de Merbel, N. C.; Giegold, S.; Teutenberg, T., *LC-GC*, (2007), 20, pp. 32.

153. Bazargan, V.; Stoeber, B., *J. Microelectromech. Syst*., (2010), 19, 1079.

154. Luo, Q. Z.; Mutlu, S.; Gianchandani, Y. B.; Svec, F.; Frechet, J. M. J., *Electrophoresis*, (2003), 24, pp. 3694.

155. Li, Z. M.; He, Q. H.; Ma, D.; Chen, H. W., *Anal. Chim. Acta*, (2010), 665, pp. 107.

156. Claessens, H.A.; van Straten, M.A., *J. Chromatogr. A*, (2004), 1060, pp. 23.

157. Wouters, B.; Bruggink, C.; Desmet, G.; Agroskin, Y.; Pohl, C.; Eeltink, S., *Anal. Chem.*, (2012), 84, pp. 7212.

158. Guillarme, D.; Russo, R.; Rudaz, S.; Bicchi, C.; Veuthey, J.L., *Curr. Pharm. Anal.*, (2007), 3, pp. 221.

159. He, P.; Yang, Y., *J. Chromatogr. A,* (2003), 989, pp. 55.

160. Vanhoenacker, G.; Sandra, P., *J. Sep. Sci.*, (2006), 29, pp. 1822.

161. Godin, J. P.; Hopfgartner, G.; Fay, L., *Anal. Chem.*, (2008), 80, pp. 7144.

162. Yang, Y.; Kondo, T.; Kennedy, T. J., *J. Chromatogr. Sci*., (2005), 43, pp. 518.

163. de Boer, A. R.; Alcaide-Hidalgo, J. M.; Krabbe, J. G.; Kolkman, J.; Boas, C. N. V.; Niessen, W. M. A.; Lingeman, H.; Irth, H., *Anal. Chem.*, (2005), 77, pp. 7894.

164. Greibrokk, T.; Andersen, T.; *J. Chromatogr. A*, (2003), 1000, pp. 743.

165. Wolcott, R.G.; Dolan, J.W.; Snyder, L.R.; Bakalyar, S., *J. Chromatogr. A*, (2000), 869, pp. 211.

166. Fallas, M.M.; Hadley, M.R.; McCalley, D.V, *J. Chromatogr. A*, (2009), 1216, pp. 3961.

167. de Villiers, A.; Lauer, H.; Szucs, R.; Goodall, S.; Sandra, P., *J. Chromatogr. A*, (2006), 1113, pp. 84.

168. Sellmann, D.; Jonk, E.; Reinecke, H.J.; Wurminghausen, T.; *Fresenius Zeitschrift fur Analytische Chemie*, (1979), 294, pp. 372.

169. Beyer, J.; Becker, H.; Martin, R.; *J. Liq. Chromatogr.*, (1986), 9, pp. 2433.

170. Henderson, D.; O'Conner, D.; Kirby, J.; Sears, C.; *J. Chromatogr. Sci.*, (1985), 23, pp. 477.

171. Henderson, D.; O'Conner, D.; *Adv. Chromatogr*., (1984), 23, pp. 65.

172. Henderson, D.; Horvath, C.; *J. Chromatogr.*, (1986), 368, pp. 203.

173. Henderson, D.; Mello, J.; *J. Chromatogr.*, (1990), 499, pp. 79.

174. Melander, W.R.; Lin, H.J.; Jacobson, J.; Horvath, C.; *J. Phys. Chem.*, (1984), 88, pp. 4527.

175. Jensen, W.; *J. Chromatogr.*, (1981), 204, pp. 407.

176. Wu, Y.; Wu, P., *Phytochem. Anal.*, (1991), 2, pp. 220.

177. Holm, A.; Molander, P.; Lundanes, E.; Greibrokk, T., *J. Sep. Sci*., (2003), 26, pp.

1147.

178. Molander, P.; Holm, A.; Lundanes, E.; Hegna, D.R.; Ommundsen, E.; Greibrokk, T., *Analyst*, (2002), 127, 7, pp. 892.

179. Molander, P.; Thomassen, A.; Kristoffersen, L.; Greibrokk, T.; Lundanes, E.; *J. Chromatogr. B*, (2002), 766, 1, pp. 77.

180. Skuland, I.L.; Andersen, T.; Trones, R.; Eriksen, R.B.; Greibrokk, T., *J. Chromatogr. A*, (2003), 1011, pp. 31.

181. Molander, P.; Gundersen, T.E.; Haas, C.; Greibrokk, T.; Blomhoff, R.; Lundanes, *J. Chromatogr. A*, (1999), 847, pp. 59.

182. Molander, P.; Thommesen, S.J.; Bruheim, I.A.; Gundersen, T.E.; Trones, R.; Greibrokk, T.; Lundanes, E.; *J. High Resolut. Chromatogr.*, (1999), 22, 9, pp. 490.

183. Molander, P.; Haugland, K.; Hegna, D.R.; Ommundsen, E.; Lundanes, E.; Greibrokk, T., *J. Chromatogr. A*, (1999), 864, pp. 103.

184. Molander, P.; Holm, A.; Lundanes, E.; Ommundsen, E.; Greibrokk, T., *J. High Resolut. Chromatogr*., (2000), 23, 11, pp. 653.

185. Yoshida, M.; Akane, A., *Anal. Chem*., (1999), 71, pp. 1918.

186. Balny, C.; Ledoucen, C.; Douzou, P.; Bieth, J.G., *J. Chromatogr.*, (1979), 168, pp. 133.

187. Supatashvili, G.D., *Geochemistry*, (1981), 11, pp. 1734.

188. Dash, J.G.; Haiying, F.; Wettlaufer, J.S., *Rep. Prog. Phys.*, (1995), 58, pp. 115.

189. Knight, C.A., *J. Geophys. Res.*, (1996), 101, pp. 12921.

190. Baker, M.B.; Dash, J.G., *J. Geophys. Res*., (1996), 101, pp. 12929.

191. Doppenschmidt, A.; Butt, H.J., *Langmuir*, (2000), 16, pp. 6709.

192. Conklin, M.H.; Bales, R.C., *J. Geophys. Res.*, (1993), 98, pp. 16851.

193. Tasaki, Y.; Tetsuo, O., Anal. Chem., (2009), 81, pp. 890.

194. Nada, H.; Furukawa, Y., *J. Crystal Growth*, (2005), 283, pp. 242.

195. Eisenberg, D.; Kauzmann, W., The Structure and Properties of Water, 1st edition, Oxford University Press: Oxford, (1969), 308 p.

196. Hobbs, P.V.; Ice Physics, 1st edition, Clarendon Press: Oxford, (1974), 837 p.

197. Tasaki, Y.; Okada T.; *J. Chromatogr. A*, (2008), 1189, pp. 72.

198. Okada, T.; Tasaki, Y., *Anal. Bioanal. Chem*., (2010), 396, pp. 221.

199. Dasgupta, P.K.; Youwen, M., *Anal. Chem*., (1997), 69, pp. 4079.

200. Shamoto, T.; Tasaki, Y.; Okada, T., *J. Am. Chem. Soc*., (2010), 132, pp. 13135.

201. Tasaki, Y.; Okada, T., *Anal. Chem.*, (2006), 78, pp. 4155.

202. Sgro, A.E.; Allen, P.B.; Chiu, D.T., *Anal. Chem.*, (2007), 79, pp. 4845.

203. Eghbali, H.; Koen, S.; Tienpont, B.; Eeltink, S., *et al.*, *Anal. Chem*., (2012), 84, pp. 2031.

204. Hesse, G., Engelhardt, H., *J. Chromatogr.*, (1966), 21, pp. 228.

205. Scott, R.; Lawrence, J.*; J. Chromatogr. Sci*., (1969), 7, pp. 65.

206. Zhu, P.L.; Dolan, J.W.; Snyder, L.R.; Djordjevic, N.M.; Hill, D.W.; Lin, J.T., Sander, L.C.; Van Heukelem, L., *J. Chromatogr. A*, (1996), 756, pp. 63.

207. Jones, B., *J. Liq. Chromatogr.*, (2007), 27, pp. 1331.

208. Tan, I.; Roohi, F.; Titirici M.M.; *Anal. Methods*, (2012), 4, pp. 34.

209. Guillarme, D.; Heinisch, S., *Sep. Purif. Rev.*, (2005), 34, pp. 181.

210. Coym, J.; Dorsey, J., *Anal. Lett.*, (2005), 37, 5, pp. 1013.

211. Teutenberg, T., *Anal. Chim. Acta*, (2009), 543, pp. 1.

212. Teutenberg, T., High Temperature Liquid Chromatography – A User's Guide for

Method Development, 1st edition, RSC Publishing: Cambridge, (2010), 220 p.

213. Luong, J.; Gras, R.; Mustacich, R.; Cortes, H., *J. Chromatogr. Sci*., (2006), 44, pp. 253.

214. Melander, W.R.; Horvath, C., High Performance Liquid Chromatography: Advances and Perspectives , 1st edition, Academic Press: New York, (1980), 341 p.

215. Jensen, D.S.; Teutenberg, T.; Clark, J.; *et al*., *LC-GC*, (2012), 30, 12, pp. 1046.

216. Teutenberg, T.; Wiese, S.; Wagner, P.; Gmehling, J., *J. Chromatogr. A*, (2009**)**, 1216, pp. 8470.

217. Mao, Y.; Carr, P.W., *Anal. Chem*. 72 (2000) 110–118.

218. Barrioulet, M.P.; Heinisch, S.; Rocca, J.L., *Spectra Anal*., (2007), 36, pp. 38.

219. Miller, D.J.; Hawthorne, S.B., *Anal. Chem.*, (1997), 69, pp. 623.

220. Bidlingmeyer, B.A.; Henderson, J., *J. Chromatogr. A*, (2004), 1060, pp. 187.

221. Ayano, E.; Nambu, K.; Sakamoto, C.; Kanazawa, H., *J. Chromatogr. A*, (2006), 1119, pp. 58.

222. Yang, Y., *LC-GC*, (2003), 16, 6A, pp. 37.

223. Kephart, T.S.; Dasgupta P.K., *Anal. Chim. Acta*, (2000), 414, pp. 71.

224. Causon, T.J.; Shellie, R.A.; Hilder, E.F., *Analyst*, (2009), 134, pp. 440.

225. Chen, M.H.; Horvath, C.; *J. Chromatogr. A*, (1997), 788, pp. 51.

226. Bowermaster, J.; McNair, H.; *J. Chromatogr. Sci*., (1984), 22, pp. 165.

227. Tran, J.V.; Molander, P.; Greibrokk, T.; Lundanes, E., *J. Chromatogr. Sci*., (2001), 24, pp. 930.

228. Pereira, L.; Aspey, S.; Ritchie, H., *J. Sep. Sci*., (2007), 30, pp. 1115.

229. Albert, M.; Cretier, G.; Guillarme, D.; Heinisch, S.; Rocca, J.L., *J. Sep. Sci.*,

(2005), 28, pp. 1803.

230. Smith, R., *J. Chromatogr. A*, (2008), 1184, pp. 441.

231. Heinisch, S.; Rocca, J.L., *J. Chromatogr. A*, (2009), 1216, pp. 642.

232. Thompson, J.D.; Carr, P., *Anal. Chem.*, (2002), 74, pp. 1017.

233. Antia, F.D.; Horvath, C., *J. Chromatogr*., (1988), 435, pp. 1.

234. Yang, X.; Ma, L.; Carr, P.W., *J. Chromatogr. A*, (2005), 1079, pp. 213.

235. Marin, S.J.; Jones, B.A.; Felix, W.D.; Clark, J., *J. Chromatogr. A*, (2004), 1030, pp. 255.

236. Thompson, J.D.; Brown, J.S.; Carr, P.W., *Anal. Chem*., (2001), 73, pp. 3340.

237. Fields, S.M.; Ye, C.Q.; Zhang, D.D.; Branch, B.R., *et al*., *J. Chromatogr. A*, (2001), 913, pp. 197.

238. Teutenberg, T.; Goetze, H.J.; Tuerk, J.; Ploeger, J., *et al*., *J. Chromatogr. A*, (2006), 1114, pp. 89.

CHAPTER 2.

DEVELOPMENT OF A CAPILLARY AND MICROBORE SCALE COLUMN HEATER BASED ON A THERMOELECTRIC ARRAY

Abstract

A new direct contact platform for the precise control of capillary column temperature based upon the use of individually controlled sequentially aligned thermoelectric (TEC) units is presented. The platform provides rapid temperature control for capillary and microbore liquid chromatography columns and allows simultaneous temporal and spatial temperature programming. In this work, two working prototypes were developed with an operating temperature range of 15 to 150 °C and 5 to 200 °C for the Mk.1 and Mk.2 prototypes, respectively. Ramp rates for both of these prototype column heaters were approximately 400 °C/min. A third, commercial prototype was also developed under funding from Science Foundation Ireland.

The systems were evaluated for a number of non-standard capillary based applications, such as the direct application of temperature gradients with both linear and non-linear profiles, including both static column temperature gradients and temporal temperature gradients, and the formation of in-capillary monolithic stationary phases with gradient polymerisation through precise temperature control.

Chapter 2 details the design, development, and testing of both the Mk.1 and Mk.2 column heaters and compares their performance to a commercially available column oven. Future work, including the development of a commercial prototype of the TEC column heater is also discussed.

Chromatographic applications and evaluation of the Mk.1 and Mk.2 column heaters are shown in Chapter 3.

Aims

The aim of the work presented in Chapter 2 was to design, develop, and build a segmented TEC based column heating and cooling unit. Due to its segmented design it can provide longitudinal and spatial temperature gradients. The proposed heating/cooling platform can also find use as a tool in various hyphenated techniques that demand minimal additional column band broadening and require temperatures or ramp rates outside the traditional operating envelope of conventional column ovens.

2.1 Introduction

Most commercially available LC systems offer some degree of column heating, usually in the form of a column compartment. Some instruments also offer extended compartments which house not only the column, but also the injector and inlet tubing, such as the TCC-3000SD and NCS-3500RS nano/cap systems from Dionex. Other systems also offer independently controlled heating zones within the column compartment, such as the Shimadzu Nexera range of instruments. Column temperature can be controlled in various ways: heating blocks, water jackets and baths, as well as the more common circulating air ovens. Heaters based upon water jackets and baths have been found to be the most efficient, due to their superior heat capacity. However, such column heaters generally exhibit a rather limited temperature range (though water can be replaced with other liquids with greater heat capacity for temperatures greater than 100 °C) and a prohibitively slow rate of heating and cooling, in applications where any form of temperature gradient is required. In the case of heating blocks, performance strongly depends on the degree of contact with the column, and in commercial examples where this close contact is maintained, these type of heaters are generally efficient in heat transfer [1] and also exhibit reasonable heating rates of approximately 20 – 30 °C/min. Circulating air ovens have a heating capacity that depends on the heating rate of the air and speed at which this heated air can be circulated around the column. This type of oven is suitable for isothermal operation (very limited in their heating and cooling rates, typically <10 °C/min) but not for rapid temperature programming – in practice they are the slowest and most inefficient. In addition, very few commercially available column ovens are capable of heating above 80 °C [2-6] while fewer still are capable of cooling below 10 °C [5]. Capillary and microscale HPLC lends itself very well to rapid heating and high-temperature operation, as the column mass is small and the

columns have thin walls (predominantly manufactured in fused silica housing), thus possessing low thermal mass and high thermal conductivity (~1.4 Wm/k). Currently however, there are very few column heaters specifically designed for both capillary and microscale HPLC, and those that do exist are very limited in heating rate and range. Moreover, none can provide the generation of longitudinal gradients and most have only limited temperature data acquisition capability [2-5]. Column heating/cooling platforms based upon thermoelectric units combine the advantages of direct contact ovens (fast thermal transfer rates) and of circulating air ovens (broad elevated temperature range). Indeed, rapid direct contact heating or cooling can be applied through an array of TEC modules, which would consist of many distinct thermally isolated zones, making it possible to generate both temporal and spatial temperature gradients. This approach introduces a number of novel features previously unavailable, including the ability to spatially apply heated or cooled zones for potential on-column thermally controlled trap and release applications, or to apply instant or dynamic temperature gradients to the column. In addition, such a heating/cooling platform could also find use as a tool in various hyphenated techniques that demand minimal extra column band broadening and require either high or low temperatures. Such precise and rapid localised control of temperature using single TEC modules has previously been reported in micro-fluidic platforms, mainly for control of fluid flow [7-10] but also for PCR amplification of DNA [11] and the thermally actuated trap and release from thermo-responsive polymer gels [12].

2.2 Experimental

2.2.1 Materials

For the development and construction of column heater prototypes Mk.1 to 3 the following materials were used:

- 12 x 12 mm single stage TEC units (TEC Microsystems GmbH, Berlin, Germany) were used in the Mk.1 and Mk.2 column heater. 30 x 30 mm single stage TEC units (Radionics Ltd., Dublin, Ireland) were used in the Mk.3 column heater.
- Rapid prototype parts were manufactured from Acrylonitrile butadiene styrene (ABS) and soluble support material (Laser Lines Ltd, Oxon, UK).
- Enclosures were designed in-house and manufactured by Advanced Design Ltd., (Wexford, Ireland).
- Raw materials (PEEK, Delrin, aluminium) were purchased from Alperton Engineering Ltd., (Dublin, Ireland).
- Fabricated parts were manufactured by WIC Contracting Ltd., (Dublin, Ireland).
- Electronic components were purchased from Radionics Ltd., (Dublin, Ireland), Farnell Ltd., Leeds, United Kingdom, and EPCOS AG, (Munich, Germany).
- Circuit boards were designed in-house and fabricated by Beta Layout Ltd., (Shannon, County Clare, Ireland).
- USB6009 cards (National Instruments UK & Ireland, Newbury, UK) were used for data acquisition. Coding for the devices was done through the LabView virtual instrument environment, 2009 version.
- A PicoLog ADC16 (Pico Technology, Cambridgeshire, UK) system was used for preliminary data acquisition.

- Power supplies for the column heaters were purchased from Komplett.ie, (Dublin, Ireland).
- AS1802 thermally conductive silicon was purchased from ACC Silicons, (Bridgwater, UK).
- Loctite 5910 high temperature silicon was purchased from Murphy Engineers Ltd., (Dublin, Ireland).
- Electrolube Thermal Bonding System (TBS) was purchased from Electrolube, (Derbyshire, UK).
- Heat sink compound was purchased from Radionics, (Dublin, Ireland).
- High temperature insulating material, Puren NE-B2 40 HT (Puren GMBH, Überlingen, Germany) was used for thermal insulation between the heating zones at their mountings.
- Teflon coated (15 μm thickness) fused silica capillary, 100 μm ID, 375 μm OD was purchased from Composite Metal Services Ltd., (Charlestown, UK).

2.2.2 Reagents

All chemicals were reagent or analytical grade purity.

For the fabrication of monolithic stationary phases the following reagents and chemicals were used:

- Lauryl methacrylate (LMA), ethylene dimethacrylate (EDMA), butyl methacrylate (BuMA), 1-propanol, 1,4-butanediol, 3-methoxysilylpropyl methacrylate, and UV-initiator dimethoxy-2-phenyacetophenone (DAP) were purchased from Sigma-Aldrich (Gillingham, UK).

- All solvents which were used for the preparation of HPLC mobile phases and for the synthesis and washing of prepared monoliths, namely, tetrahydrafuran (THF), acetonitrile (ACN), sodium hydroxide (NaOH), hydrochloric acid (HCl), and methanol (MeOH), were purchased from Lab Scan (Gliwice, Poland).
- Deionised water purified by a Milli-Q system (Millipore, Bedford, MA, USA) was utilised throughout the experiments.

2.2.3 Instrumentation

- For the temperature/pressure response studies a Dionex Ultimate 3000 nano-HPLC system (Dionex, Sunnyvale, CA, USA) was used, incorporating an FLM-3000 column compartment which was used only for the performance comparison with the TEC array module.
- Rapid prototype parts were printed on a Dimension SST 768 rapid prototyper (Dimension 3D Printers, MN, USA).
- The thermal camera used was an A20 Thermovision FLIR infra-red camera (FLIR Systems, West Malling, UK). Data acquisition and capture was done using FLIR Systems FSCAP, Ver 1.2.

2.2.4 Software

Software used in the development, design, and control of the column heaters are listed below:

- For data acquisition, Chromeleon 6.8 software (Dionex, Sunnyvale, CA, USA) was used.
- Mechanical design of the column heaters was done through AutoCAD 2006, (AutoDESK Ltd., Hampshire, UK) and Solidworks 2004 (Solidworks UK, Cambridge, UK).
- Electrical design of the column heaters was done through PSpice 9.1 student version (Cadence Design Systems, Berkshire, UK), and Target 3001 (TARGET 3001!, Eichenzell, Germany), a freeware open-source design and simulation package. Electrical drafting packages used also included Design Spark, a freeware package provided by Radionics Ltd.
- Control of the Mk.2 column heater was done through the LabView virtual environment, (National Instruments UK & Ireland, Newbury, UK).
- The Mk.3 column heater was controller through onboard PIC (Peripheral Interface Controller) control. The software was coded in C in the MpLab IDE (Integrated development Environment) obtained from Microchip Technology Inc., Arizona, USA, and complied using the CCS compiler, a freeware compiler (Custom Computer Services Inc., Wisconsin, USA).
- A PicKit2 (Radionics Ltd., Dublin, Ireland) was used to program the onboard PIC on the Mk.3 column heater.

– An Atmel AVR Mk.2 programmer (Radionics Ltd., Dublin, Ireland) was used to program the AVR microcontroller on the Mk.3 column heater touch screen.

2.2.5 Experimental procedures

2.2.5.1 Capillary silanisation

Fused silica capillaries were initially pretreated through activation of the surface silanol groups of the inner walls by sequential flushing with 1 *M* NaOH, deionised water, 0.1 *M* HCl, deionised water, and acetone. The pretreated capillary was silanised using a 50 %wt solution of trimethoxysilylpropyl methacrylate in toluene at 60 °C for 24 hrs. After silanisation the capillary was washed with acetone for 3 hrs.

2.2.5.2 Fabrication of reversed-phase columns (capillary format)

The LMA-EDMA column was prepared according to the procedure described by Eeltink *et al.*[13]. The monomer mixture consisted of 24 %wt LMA, 16 %wt EDMA, 45.5 %wt 1-propanol, 14.5 %wt 1,4-butanediol, and 0.4 %wt of dimethoxy-2-phenyacetophenone (with respect to monomers). The initiator (DAP) was weighed out into the mixture vessel, and the porogen mixture (1-propanol and 1,4-butanediol) was added, followed by the monomers. The mixture was vortexed and deoxygenated under a flow of nitrogen for 10 min. A desired length of 100 μm ID silanised capillary was filled with the monomer mixture and exposed to 2 J cm^2 of UV radiation. The resultant monolithic column was washed with MeOH to remove residual porogen and unreacted monomers.

2.3 Design and development

The primary design criteria for the column heater was to develop a platform which could not only provide dynamic, longitudinal, and spatial gradients along the length of the column, but also have a rapid response, further allowing the application of fast temperature programming. Columns with an internal diameter larger than ~2 mm can exhibit radial temperature gradients during temperature programming, particularly if the applied gradients are fast. This makes larger columns unsuitable for use with rapid temperature programming and so the design goal of the column heater was to accommodate smaller columns, specifically capillary and microbore scale. The second design requirement was to develop a system which had the capacity to take columns of a useful length and so the column heater was designed to take columns up to 130 – 150 mm long.

In order to provide segmented heating for longitudinal gradients it was necessary to use multiple individual heating elements and to achieve fast ramp rates these elements were required to have a low thermal mass, enabling them to equilibrate quickly to temperature changes. Furthermore, in order to provide fast negative ramp (cooling) rates the heating elements should be able to lose or pump thermal energy away quickly. An ideal type of heating/cooling element with these characteristics is the Peltier, or thermoelectric module. The Peltier effect is termed as the conversion of a difference in temperature between the two sides of the module into a potential difference or vice versa and is thermodynamically reversible depending on the applied polarity.

TEC modules are used extensively in the electronics industry, usually for cooling components that are prone to overheating. They do this by acting as a very effective heat

pump, drawing heat from one side of the device and emitting it on the other. The level of cooling that can be achieved by a TEC module depends on the amount of heat that can be drawn away from the hot side of the device and the ability of the attached heat-sink to dissipate the heat. The direction of heat transfer through the device depends on its polarity, so by simply switching the polarity of the TEC unit in the circuit, it is possible to both heat and cool the same side of each individual unit (see Figure 2.1). The modules selected for use in the TEC column heater were chosen based on their operational temperature range and low thermal mass, so the system response would be very fast.

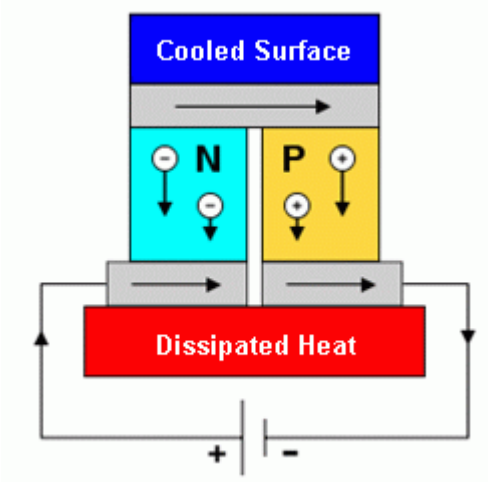

Figure 2.1 – Schematic of TEC module (cooling mode).

TEC modules are constructed of multiple P-N junctions, each junction containing two dissimilar metals, for example Cu & Fe (see Figure 2.2). The performance of the module is dependant on the property of the P-N junction and in the case of the TEC column heater bismuth-telluride Peltier modules were used. The contact surfaces of the device were ceramic (Al_2O_3).

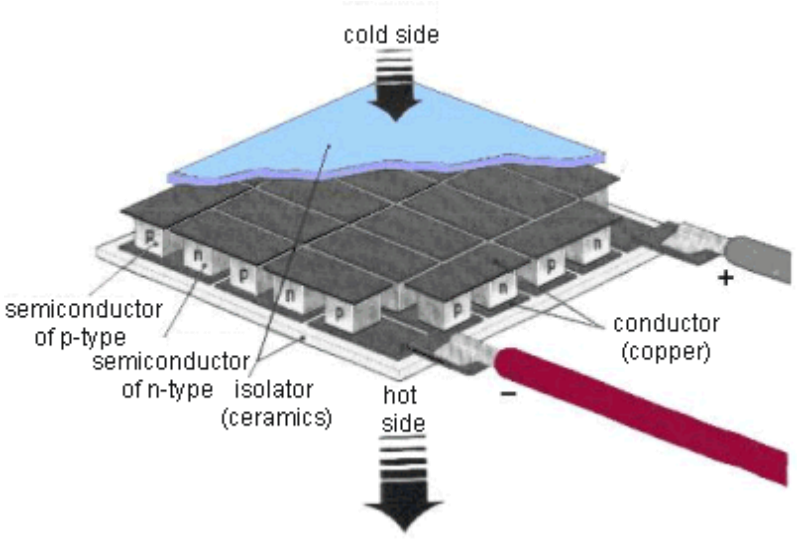

Figure 2.2 – TEC module structure.

Since the 'pumping' direction is dependant on polarity it allows both heating and cooling on the same side of each module. Some TEC modules can also be used over very broad temperature ranges, from sub-zero to >200 °C. The solder melt temperature of the TEC modules used in all three iterations of the developed column heater was 230 °C so the upper temperature limit was set to 200 °C for all three devices.

2.3.1 Mk.1 Column heater

The Mk.1 prototype of the TEC column heater was constructed from a single dimension array made up of ten individual single stage 12 x 12 mm TEC modules, thus allowing the generation of complex and dynamic temperature profiles and gradients along the array. The total length of the array was 130 mm. The modules were arranged so that there was a gap of approximately 0.5 mm between each one, thermally isolating it from its neighbour. Each TEC module was wired independently so that both heating and cooling could take place

simultaneously and independently along the array. For the prototype device, the capillary column was attached to the array of TEC modules using commercially available thermal paste, ensuring good thermal conductivity between the TEC module surfaces and the column. This prototype was compatible with capillary scale columns and micro-fluidic chips. The low thermal mass of the capillary columns attached using the thermal paste meant any radial thermal gradients, which could possibly occur in larger diameter columns, were negligible in this instance. Since the thermal paste was not an adhesive, it also allowed for the easy removal of the column. Temperature control of the device was achieved by monitoring the temperature of each individual TEC unit. A thermistor mounted on the surface of each unit measured the surface temperature and the data was fed to a basic data acquisition circuit which collected data from each segment of the module. Temperature control was achieved through simple thermostat switches, one for each TEC module.

The system used a simple forced air cooled heat exchanger to dissipate heat during cooling operations (see Figure 2.3). During operation below ambient temperature or during cooling mode, air is passed from the heat exchanger through a series of fins attached to the bottom surface of each TEC unit (the hot side of the modules), and so by dissipating this heat it allows the working surface of the unit to cool.

The Mk.1 prototype had an input voltage of between 2 and 5 V_{DC}, drawing a maximum current of up to 15 A. For this early prototype the useful operating range of the device was kept to 15 – 150 °C. To operate at temperatures above 150 °C more complex control and

power circuitry was required – the objective of the 1st prototype was for a proof of principle study and so the design was kept reasonably simple.

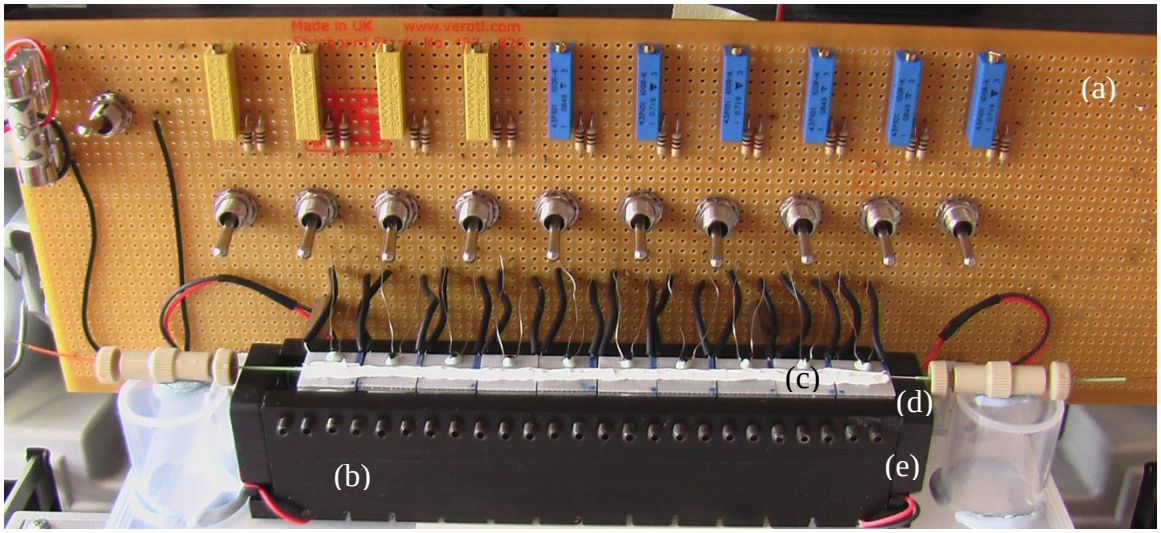

Figure 2.3 – Mk.1 prototype TEC column heater, showing control board (a), heat exchanger (b), Peltier module and thermistor (c), column (d), and fan (e).

Likewise, to achieve temperatures below 15 °C a more efficient heat exchanger was required as thermal sinking occurred at higher currents. Thermal sinking occurs when the module cannot lose enough heat to the heat exchanger and so begins to heat up due to either resistive heating or simply due to heat sinking through the device from the hot side. A graph of the response curve for temperature against input current for the 12 x 12 mm TEC modules is shown in Figure 2.4. The red area highlights the inefficiency of this early heat exchanger and operating inside this region resulted in thermal sinking of the module. Thus, during cooling operations, current to each individual TEC module was limited to 350 mA.

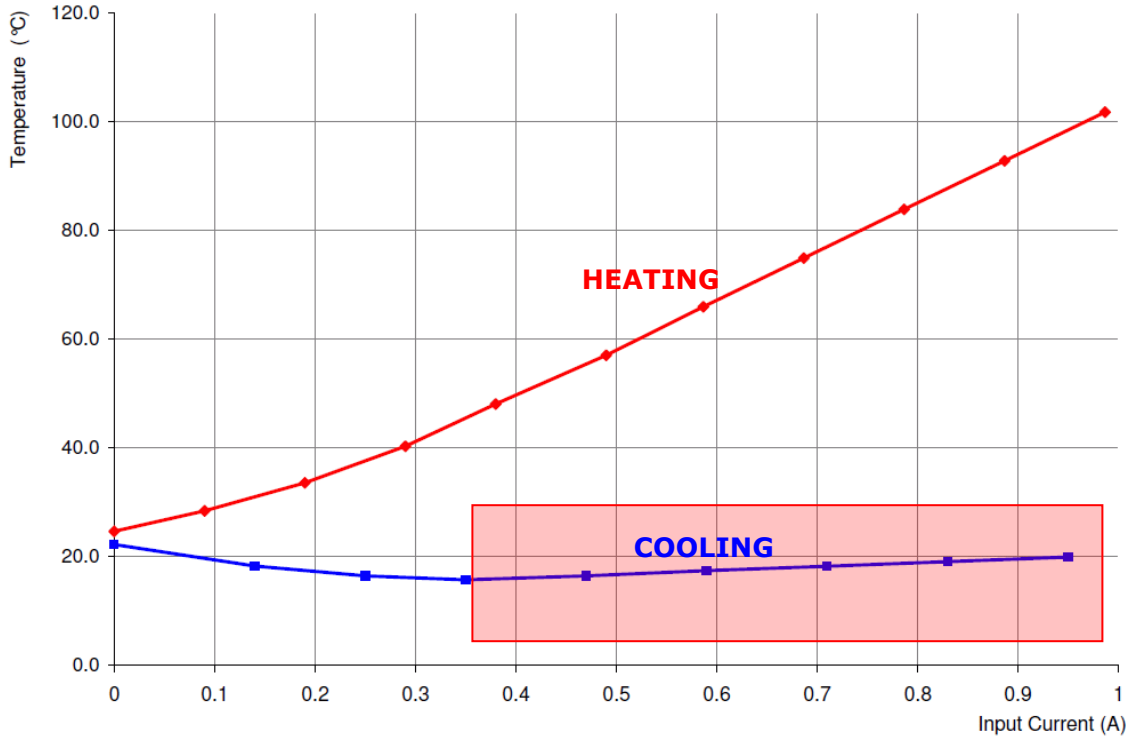

Figure 2.4 – 12 x 12 mm Peltier response for temperature vs input current.

2.3.2 Mk.2 Column heater

The Mk.2 prototype column oven was designed to be an improvement over the Mk.1 prototype, both in terms of performance and versatility. The Mk.2 column heater could accommodate columns up to 150 mm long and 8 mm in diameter as well as column fittings. In this design, pairs of TEC modules contacted the column from both sides ensuring a more uniform radial temperature profile, see Figure 2.5. The TEC modules are mounted in 'jaws' which open to a maximum width of 30mm.

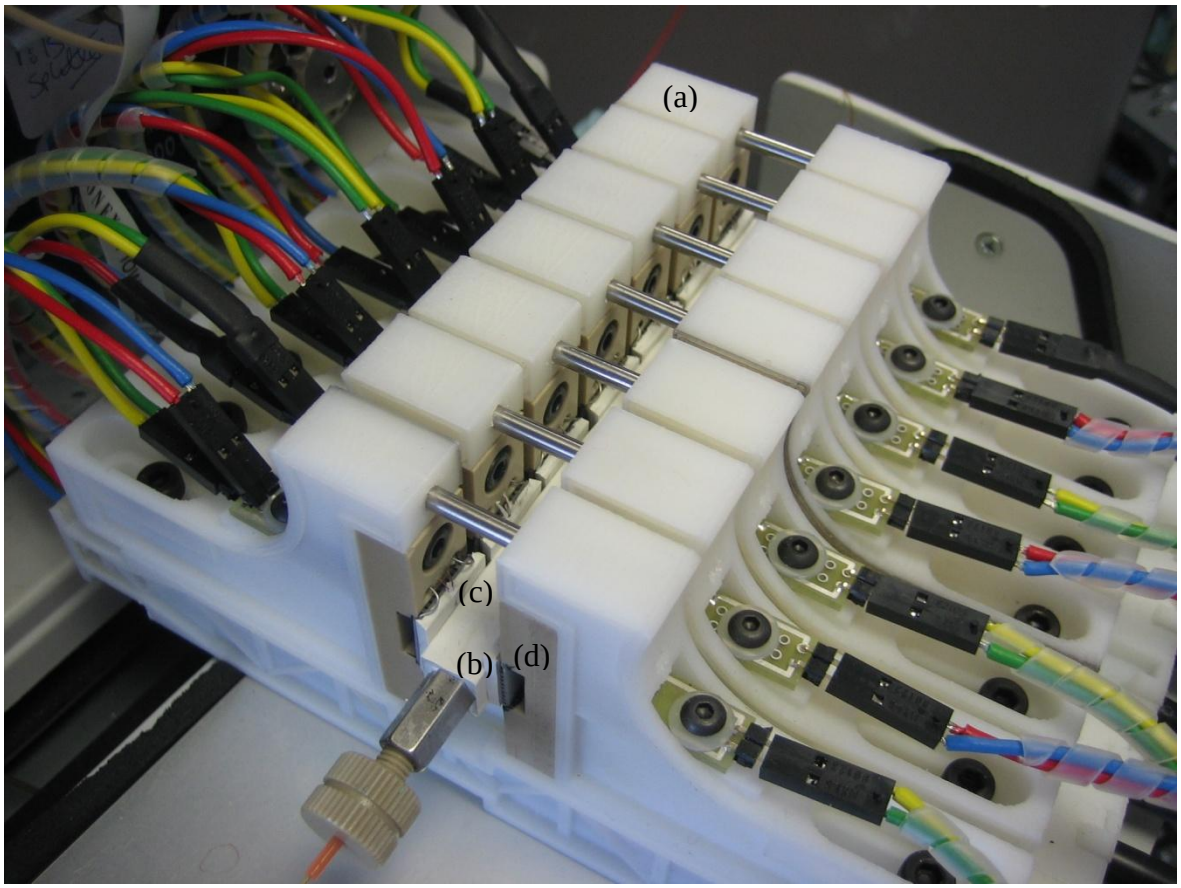

Figure 2.5 – Mk.2 TEC column heater prototype set up with 7 channels (~90 mm long), showing heat exchanger (a), column (b), silicon pad with embedded thermistor (c), and TEC module (d).

Column contact was provided using soft thermally conductive silicon gel pads, ensuring excellent thermal transfer between the array and column, see Figure 2.6. For large columns (as shown in Figure 2.5), the column itself was encased in thermally conductive silicon to ensure proper thermal transfer. This approach also allowed the column fittings to be heated and cooled along with the column. Temperature feedback was provided by a thermistor which was embedded in the silicon gel pads close to the column contact surface. For each module, and thus each pair of pads, one thermistor provided the temperature process value.

Each pair of TEC modules was individually controlled and monitored through dedicated closed-loop control, in this case proportional-integral-derivative (PID) loops.

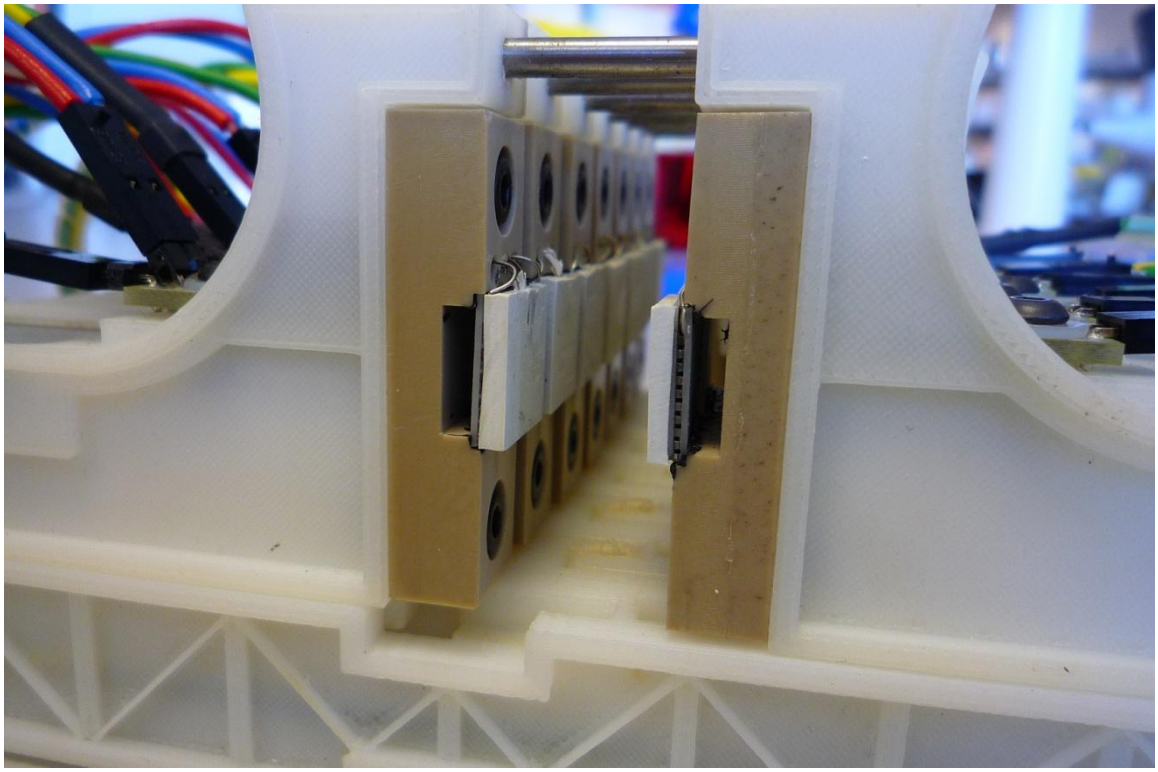

Figure 2.6 – Detail of thermally conductive silicon gel pads which contact the column.

PID controllers are a generic control loop feedback mechanism, widely used in industry for control applications. Each control loop constantly compared the desired set point with the process value, changing the output to the system (in this case the TEC modules) so that the desired set point was acquired. Set point values for each zone could be entered by the user via the program graphical user interface (GUI). Each module had two dedicated PID controllers, one PID loop handling heating operations, while the other controlled cooling. This setup was essential in this case as the thermal response of each TEC unit was very different depending on whether the unit was in heating or cooling mode. By using this approach, the user could very effectively "tune" the control loops for heating and cooling,

and so high ramp rates and fast thermal response were possible while obtaining high precision with minimal overshoot.

The control and management program for the device was created in the LabView virtual instrument (VI) environment and allowed complex gradients and temperature programming to be carried out. This environment also allowed the user to acquire data from each of the temperature controlled zones. Figures 2.7(a) and (b) show the two screens on the GUI, the main page where temperature set points and programs can be entered, and the parameters page which allows control settings to be input.

Figure 2.7(a) – Column heater, graphical user interface, page 1 (main screen).

Figure 2.7(b) – Column heater, graphical user interface, page 2 (parameter screen).

Due to the complexity and power of this system, additional control circuits and a power supply were constructed. These can be seen in Figure 2.8.

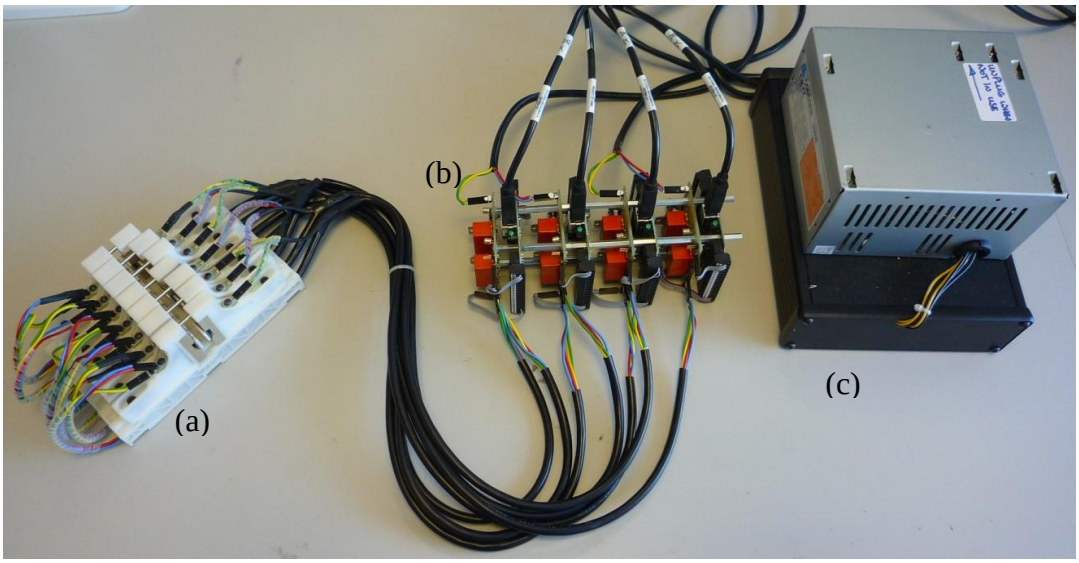

Figure 2.8 – Mk.2 column heater showing column heater unit (a), control and I/O boards (b), and power supply (c).

One of the main advantages of the Mk.2 column heater was its modular design which allowed the user to tailor the device to accommodate the specific dimensional requirements of the column or micro-fluidic chips they are using. By using this approach the user simply attaches the required number of heating/cooling zones, up to a maximum of 10 modules, which equates to a column heater length of 150 mm. Figure 2.9 shows some of the heating/cooling modules separated from one another. The 'quick-click' mechanism for joining the modules together is show in Figure 2.10.

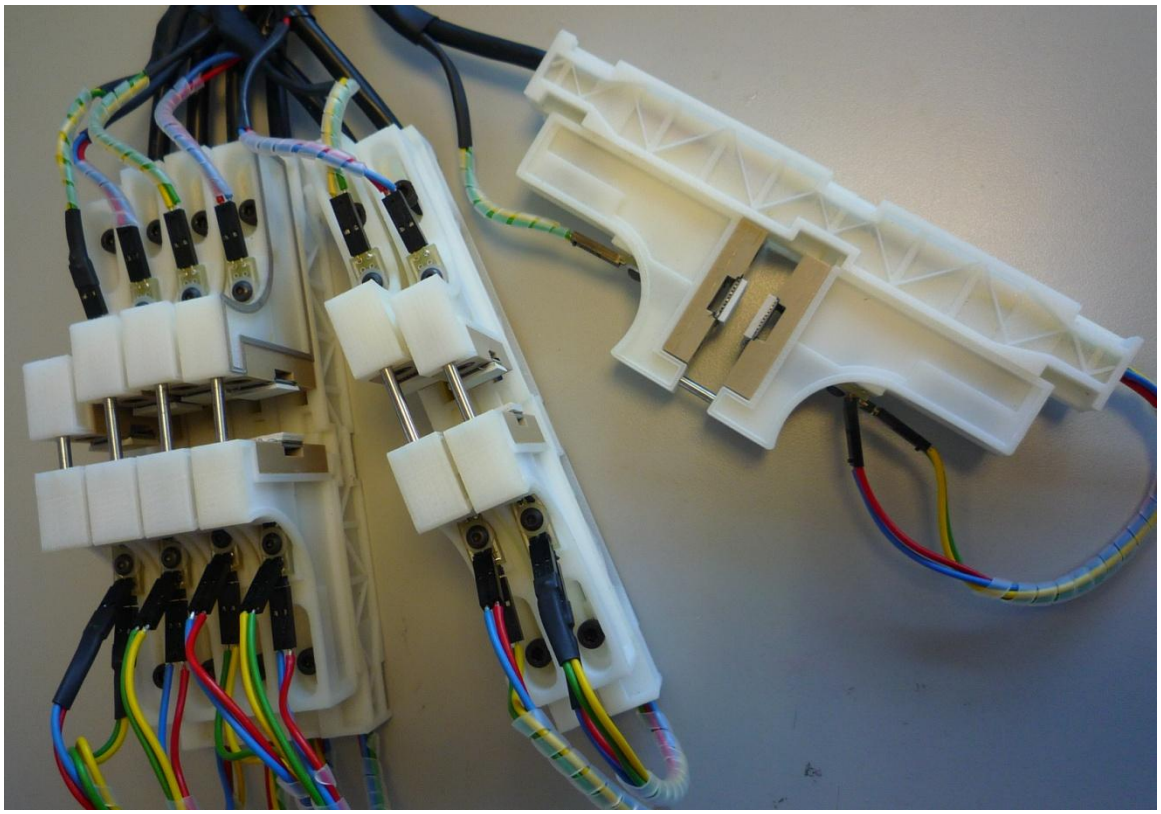

Figure 2.9 – Image of column heater showing individual modules including some that have been removed from the assembly.

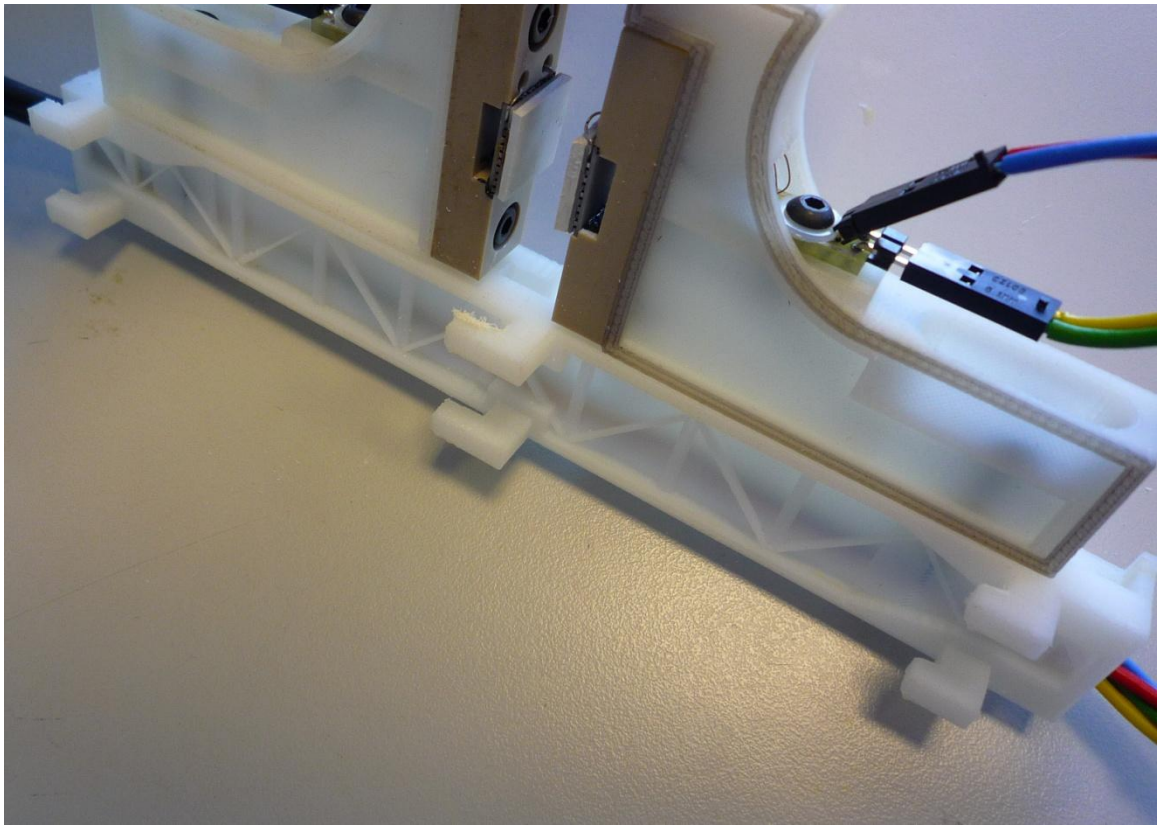

Figure 2.10 – Detail of 'quick-click' mechanism which allows individual heating/cooling modules to be joined together as required by the user.

For low temperature or extended cooling operations another type of module could be substituted. This module is designed with an aluminium heatsink which draws and dissipates heat away from the TEC allowing cooler temperatures to be achieved.

Details on the design and construction of these systems and of the column heater itself can be found in Appendix A.

2.4 Testing - Results and discussion

Initial testing of the device was achieved through thermal imaging of the array during heating and cooling operations and also through system response measurements, i.e. ramp rates, upper and lower temperatures, extended operations at temperature, etc.

2.4.1 Thermal imaging

The thermal response of the assembled systems was recorded using a thermal imaging camera. This approach allows the detection of any temperature variations between each of the heating zones and the attached capillary, whilst also allowing real-time monitoring of the thermal equilibration of the column. Any variation in colour would indicate that thermal transfer between the TEC units and the column was inefficient and that the column temperature was lower than the TEC modules. It was also possible to measure surface temperatures at various spot locations using this approach. This was crucial for validating the control function of the device. An example of spot measurement can be seen in Figure 2.11. It is important to note that thermal imaging was used only in the testing of the system and was not subsequently used or required during chromatographic studies carried out with the device.

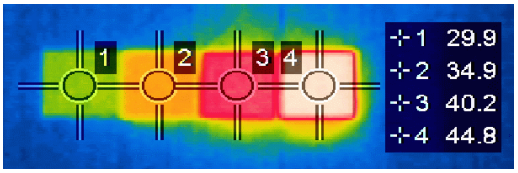

Figure 2.11 – Spot location measurement of four TECs at 30, 35, 40 and 45 °C respectively.

Figure 2.12 shows a typical set up with the thermal imaging camera and Mk.1 TEC column heater.

Figure 2.12 – Typical set up of thermal imaging camera and TEC column heater during initial testing.

Figures 2.13(a) to (c) show examples of thermal images taken during different heating and cooling modes for the TEC column heater, each with a capillary column attached. Figure 2.13(a) shows the column heater operating in isothermal mode at 45 °C. Figures 2.13(b) and 2.13(c) show two thermal gradients along the length of the column, from 30 °C to 50 °C and from 23 °C to 20 °C. Images (b) and (c) shows that there was no heat transfer

between zones which radically distinguishes the TEC based column heater from traditional contact column ovens.

(a)

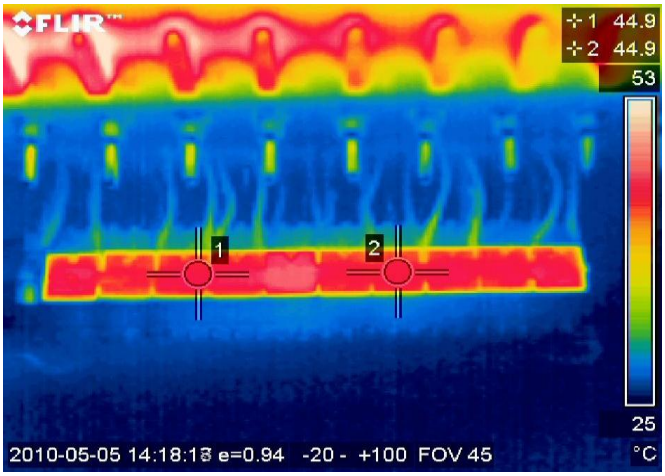

(b)

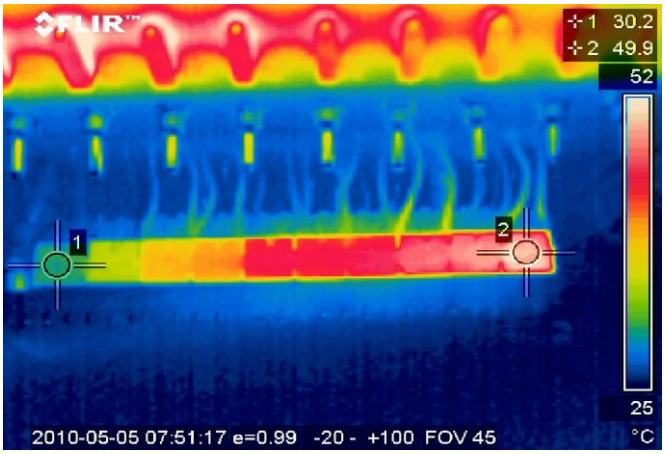

(c)

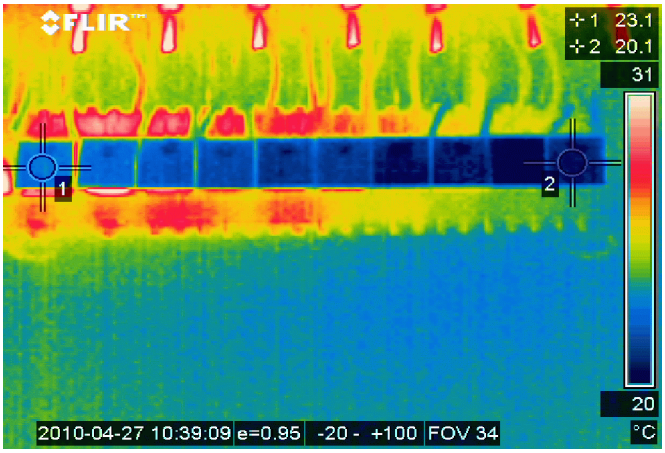

Figure 2.13 – Thermal images of isothermal operation at 45 °C (a), gradient mode operation, from 50 to 30 °C (b), and cooling mode gradient from 20 to 23 °C (c).

Most importantly these images show that the heat generated by each TEC module is transferred directly to the column itself, as the column in each image, and on each individual unit, is not distinguishable from each TEC.

2.4.2 System response

The working temperature ranges of the Mk.1 and Mk.2 prototype TEC arrays were restricted to 15 – 150 °C and 5 – 200 °C, respectively. It was found that the system response for both devices was extremely fast, with heating and cooling rates of almost 400 °C/min. To place this in context, a direct comparison of these devices and a leading commercial air bath column oven (Dionex TCC-3000SD) was made, with the latter exhibiting a maximum heating rate of just 9 °C/min. With comparison to the commercial column oven, the response of the TEC column heaters was approximately 40 times faster. Figure 2.14 shows this comparison graphically, comparing the rate of change (ROC, °C/min) against response time (sec) for the TEC column heater (a) and a leading commercially available air bath oven (b). The graphs show the heating rates of both column heaters, and it can be seen that the TEC column heater reaches its maximum rate of heating after only 2.2 sec, while the commercial system only reaches its maximum rate of heating after 300 sec. The performance of the system was also tested by measuring the individual response of each of the units against time and by also monitoring their thermal stability over time.

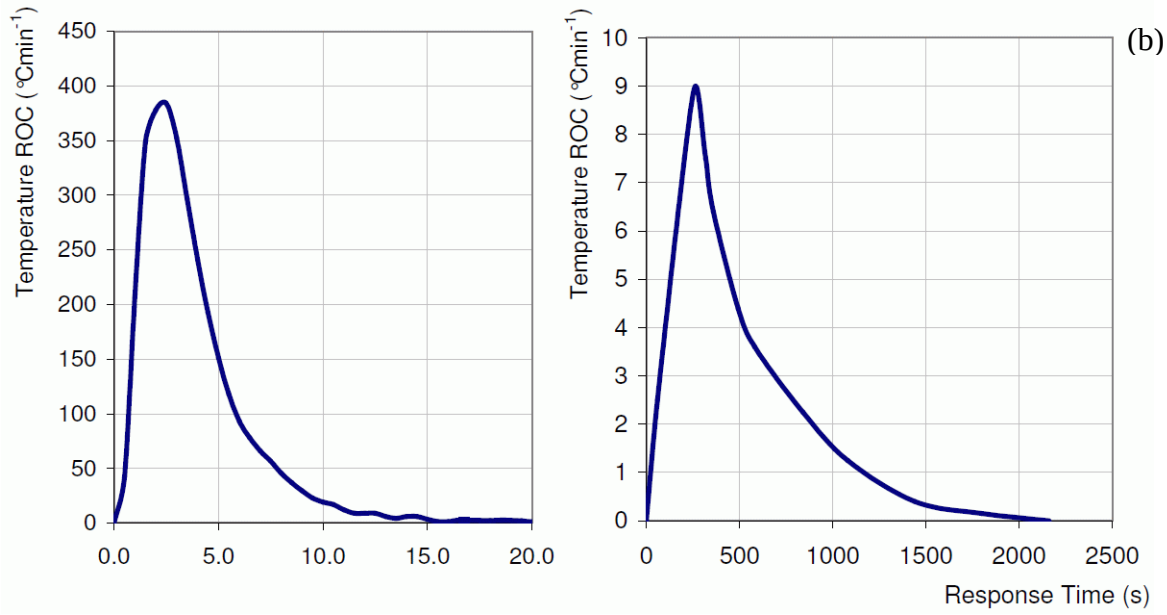

Figure 2.14 – Comparison of heating rates between the TEC column oven (a), and a leading commercially available air bath oven (b).

The system response and stability were investigated while continuously cycling between two set point temperatures of 16 and 40 °C (see Figure 2.15, inset shows temperature stability at 40 °C over approximately a 15 min period).

It was found that the deviation from steady state temperature was in the region of ±0.2 °C over a 1 hr period and ±0.5 °C over 24 hrs. In the initial Mk.1 design, units which were operating in cooling mode and then subsequently "switched off", would automatically return to heating mode (default state). Thus residual current in the circuit causes a slight heating effect for an instant, the result of which can be seen at 3200 sec in Figure 2.15.

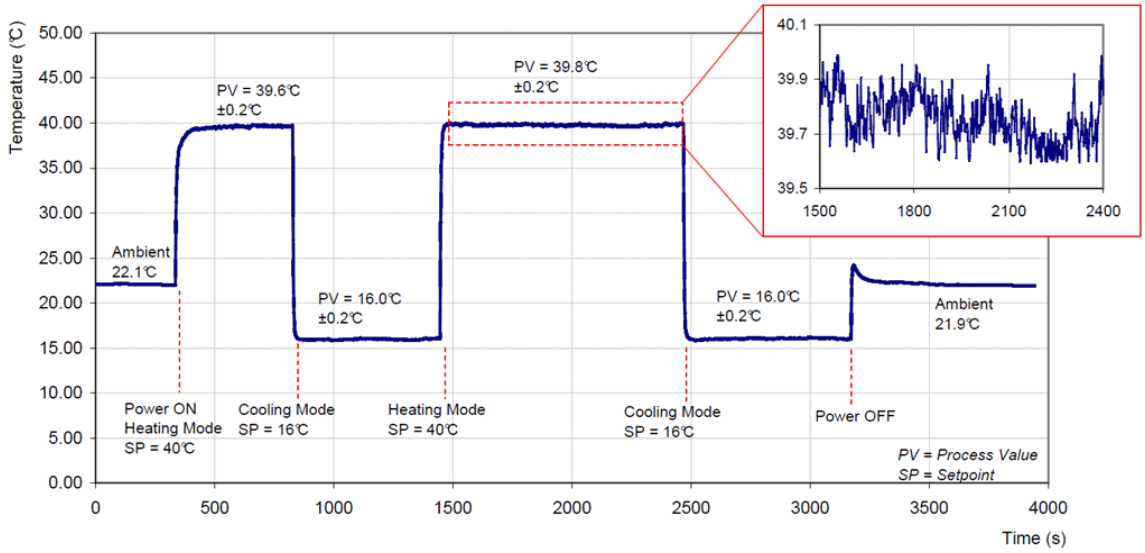

Figure 2.15 – TEC unit response over 1 hr, cycling between 16 and 40 °C.

The actual column heating/cooling effectiveness of the TEC column heater was evaluated through measurement of the rate of change of column back-pressure with a change in temperature. For this study, a single step thermal gradient program was applied and the column backpressure change was recorded. These results were again compared to those obtained for a commercial air bath oven, for which the same temperature program was used and the backpressure change was studied on the same column (LMA-EDMA polymer monolithic column, 150 mm x 100 µm ID). For the example shown in Figure 2.16, the flow rate was set to 4 µL/min (pumping 50% ACN) and the starting temperature was 25 °C. A flow rate of 3 µL/min was used for the examples shown in Figures 2.17 and 2.18. The temperature was ramped up to 60 °C in a single step, and once the column temperature reached 60 °C, the temperature was set to return directly to 25 °C. Figure 2.16 shows the temperature and pressure response of the column for the air bath oven, which had a maximum heating rate of 9 °C/min, taking 28 min to reach set point temperature. This compared with the TEC column heater which took less than 30 sec to reach the desired set

point (see Figure 2.17). The completion of the full heating/cooling cycle took approximately 60 min for the air bath oven, compared to less than 4 min for the TEC column heater.

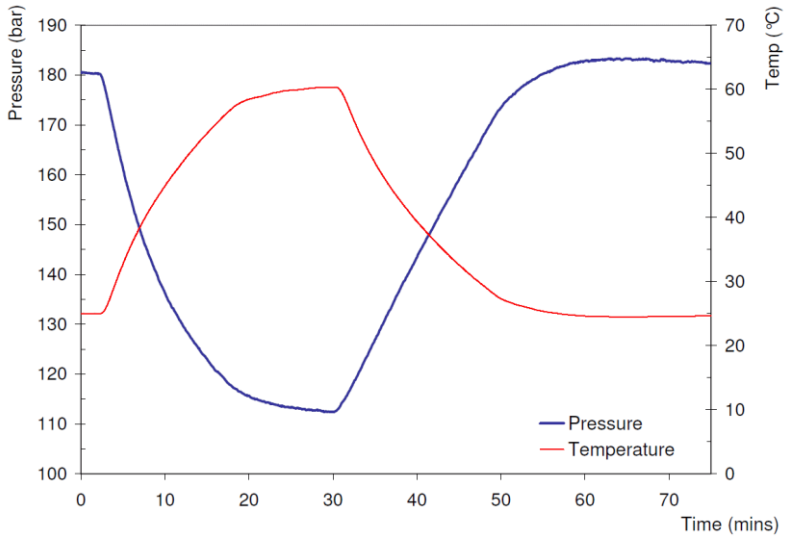

Figure 2.16 – Comparison of column temperature and pressure under maximum heating rates for a leading commercially available air bath oven.

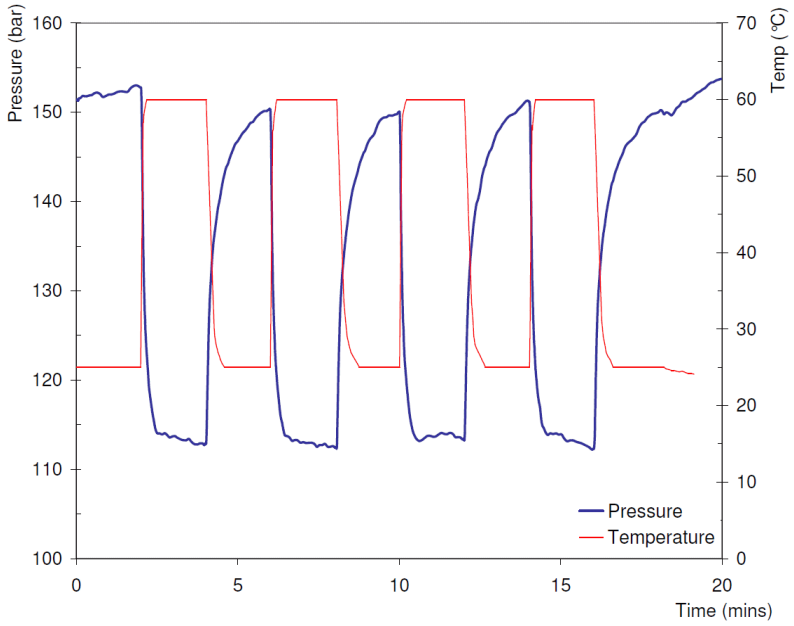

Figure 2.17 – Comparison of column temperature and pressure under maximum heating rates for the TEC column oven.

This simple demonstration highlights the fact that current commercial air bath type ovens can support only very shallow gradients, outside of which the programmed temperature profile does not match that experienced by the column. Column back pressure profiles, as shown in Figures 2.16 and 2.17 are a convenient way of graphically visualising the rate and degree of actual column temperature change (which is directly related to mobile phase viscosity and therefore column back-pressure), in response to changes in the programmed column temperature. A further graphical representation of this can be seen in Figure 2.18. In this case the temperature was cycled between 27 and 62 °C and the corresponding column back pressure recorded.

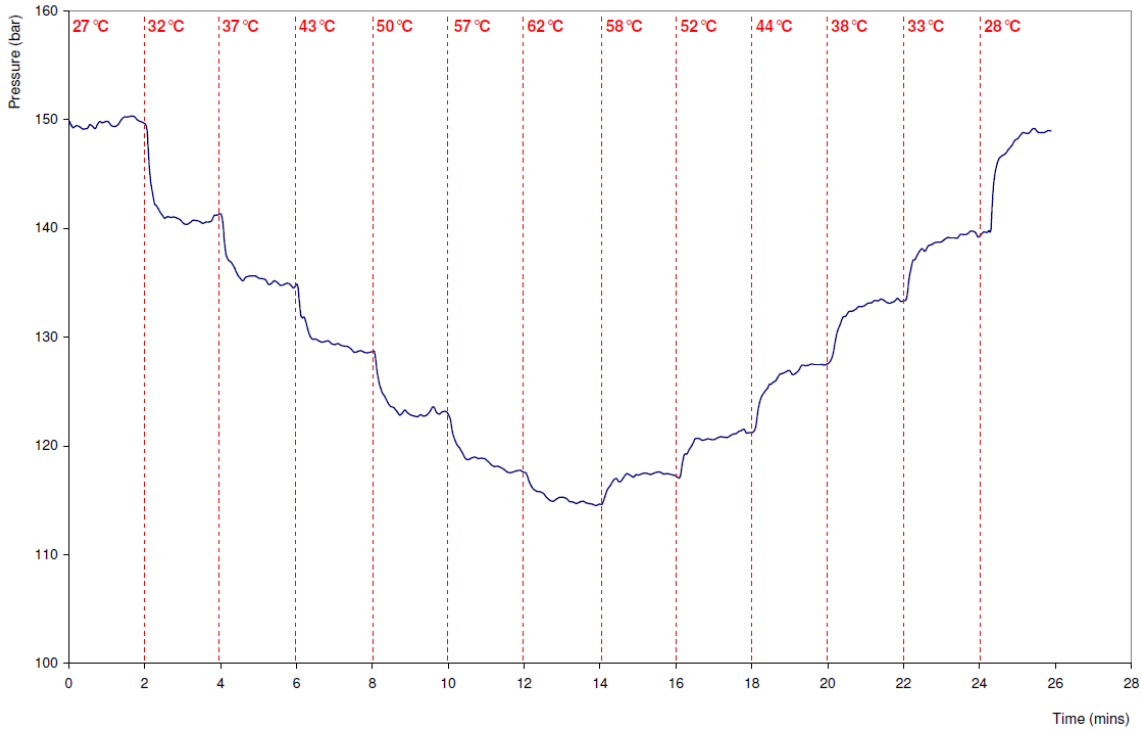

Figure 2.18 – Comparison of column temperature and pressure during temperature cycling.

2.5 Further development

2.5.1 Mk.3 Column heater

The Mk.3 column heater was developed and built under a Technology Innovation Development Award (TIDA) from Science Foundation Ireland (SFI). The purpose of the award was to develop and characterise the next generation of miniaturised column heater, demonstrating its significant advantages and enhanced functionality relative to conventional column heating devices. As part of this award funding was also received to employ a research assistant for 6 months.

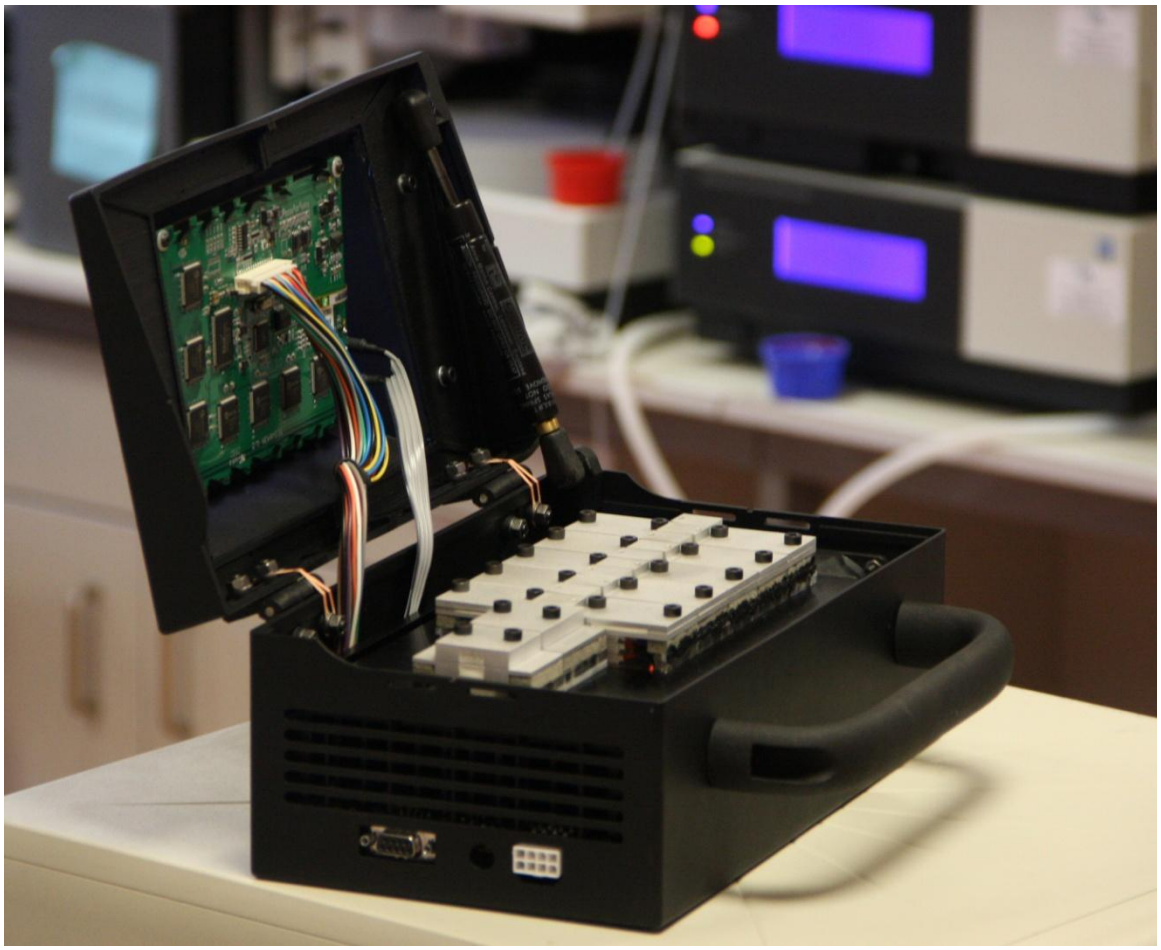

Figure 2.19 – Mk.3 TEC column heater.

The Mk.3 TEC column heater was designed to be a completely standalone device which can be used with any LC instrument and so the footprint of the unit is a mere 295 x 166 mm, with an overall height of 150 mm. The unit is designed with an eluent and fitting preheater (30 mm and 40 mm long respectively) making the total useful length 226 mm and can accommodate columns and fittings up to 8 mm in diameter. The Mk.3 device was designed with a touch screen interface and a serial communication port allowing the temperature data to be downloaded directly to a PC. In addition, complex temperature programs can be uploaded to the instrument.

Like the Mk.2 design, the Mk.3 column heater uses flexible thermally conductive silicon to ensure excellent thermal contact between the column and the heating/cooling elements. In this instance however, the module or zone width has been increased to 15 mm. The heating/cooling zones are made up from aluminium plates which contact much larger 30 mm TEC piles. The TEC piles are constructed from three 30 mm TECs which has a two-fold effect on performance.

Firstly, by using TEC piles such as this, the maximum temperature difference (ΔT) between the hot and cold side of the pile will be much larger, three times that of a single TEC of the same type. This means that there is much less heat transfer into the heatsink during heating and (more importantly) cooling operations. The net effect of this is that much lower temperatures can be reached.

Secondly, by employing TECs in piles, the overall heating and cooling power is greatly increased. This has the effect of increasing the rates of heating and cooling whilst also

improving the low end cooling capability. Currently this prototype is awaiting further commercial development to make the device more flexible thus allowing its application to standard bore LC columns. As such, characterisation and application of the device are beyond the scope of the current thesis. An exploded view of the Mk.3 column heater is shown in Figure 2.20.

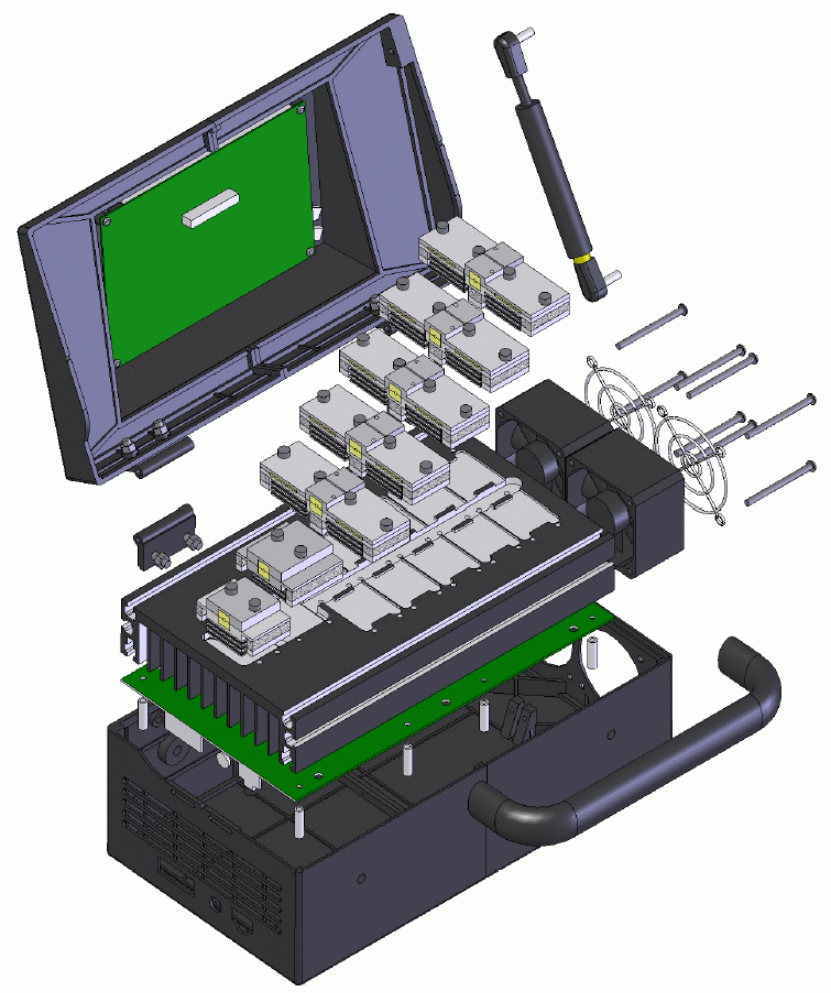

Figure 2.20 – Exploded view of Mk.3 column heater.

2.6 Conclusions

The work presented in Chapter 2 shows the development of a new type of direct contact heating/cooling platform for the precise thermal control of capillary and microbore columns. Three prototypes were presented, from an initial concept device built for proof of principle to a standalone commercial prototype designed for ease of integration with chromatographic instrumentation. It was shown that the developed systems have a broad temperature range, from 5 to 200 °C with a ramp rate of approximately 400 °C/min. Steady state response was also measured and found to be within ±0.2 °C over a 1 hr period and ±0.5 °C over 24 hrs. The devices were also monitored using thermal imaging to ensure thermally isolated zones were not sinking into cooler areas of the device. Finally, the performance of the devices was compared to that of a leading commercially available column heater.

Reference list

1. Teutenberg, T.; Goetze, H.J.; Tuerk, J.; Ploeger, J.; Kiffmeyer, T.K.; Schmidt, K. G.; Kohorst, W.G.; Rohe, T.; Jansen, H.D.; Weber, H., *J. Chromatogr. A,* (2006), 1114, pp. 89.
2. www.jascoinc.com/Products/Chromatography/HPLC-Systems/ HPLC-Components/Versatile-Column-Ovens-and-Support-Modules.aspx, (accessed October 2010).
3. www.zirchrom.com/metalox.asp, (accessed October 2010).
4. www.sim-gmbh.de/index.php?option=com_content&task=view&id=64 &Itemid=502&lang=en, (accessed October 2010).
5. www.selerity.com/main/main_products_hplc_9000.html, (accessed October 2010).
6. Causon, T.J.; Shellie, R.A.; Hilder, E.F. *Analyst,* (2009), 134, pp. 440.
7. Sgro, A.E.; Allen, P.B.; Chiu, D.T., *Anal. Chem.,* (2007), 79, pp. 4845.
8. Bazargan, V.; Stoeber, B.J., *Microelectromech. Syst*., (2010), 19, pp. 1079.
9. Luo, Q.Z.; Mutlu, S.; Gianchandani, Y.B.; Svec, F.; Frechet, J.M.J., *Electrophoresis,* (2003), 24, pp. 3694.
10. Li, Z.M.; He, Q.H.; Ma, D.; Chen, H.W., *Anal. Chim. Acta,* (2010), 665, pp. 107.
11. Maltezos, G.; Gomez, A.; Zhong, J.; Gomez, F.A.; Scherer, A., *Appl. Phys. Lett*., (2008), pp. 93.
12. Li, Z.M.; He, Q.H.; Ma,D.; Chen, H.W.; Soper, S.A., *Anal. Chem*., (2010), 82, pp. 10030.
13. Eeltink, S.; Geiser, L.; Svec, F.; Frechet, J.M.J., *J. Sep. Sci.*, (2007), 30, pp. 2814.

CHAPTER 3.

CHROMATOGRAPHIC EVALUATION AND APPLICATION OF A CAPILLARY AND MICROBORE SCALE COLUMN HEATER BASED ON A THERMOELECTRIC ARRAY

Relevant publications:

Collins, D.; Connolly, D.; Macka, M.; Paull, B., *Chromatography Today*, (Aug/Sep 2010), pp 30–31.

Collins, D.; Nesterenko, E.; Connolly, D.; Vasquez, M.; Macka, M.; Brabazon, D.; Paull, B., *Anal. Chem.*, (2011), 83, 11, pp. 4307–4310.

Collins, D., "The Heat Is On", *LCGC, E-Separation Solutions*, January 2012

Collins, D., "Exploring High Temperature LC", *Laboratory News*, Oct 2012.

Abstract

Having a high degree of temperature control is extremely important in various modes of liquid chromatography, as is fast thermal equilibration. Two developed TEC based column heaters providing direct contact heating, rapid response, and precise control of temperature were evaluated in a number of modes of chromatography. A dual temperature and flow rate gradient was utilised for the separation of a mixture of five alkylbenzenes. This approach resulted in the significant improvement of peak shape and the reduction of the overall retention time by 66% while still maintaining baseline resolution. A dual rapid temperature and solvent gradient separation of polyaromatic hydrocarbons (PAHs) was successfully carried out with five PAHs separated within 8 min.

The TEC column heater was also applied to several thermally initiated polymerisation reactions to form in-capillary monolithic phases. The formation of these in-capillary monolithic stationary phases with gradient polymerisation through precise temperature control was investigated. It was possible to achieve very fine control over the polymer morphology, the formation of which was extremely temperature dependent. The in-chip polymerisation of a polymer monolith phase was also performed and it was shown that by using segmented heating and cooling, a very fine monolith boundary could be formed despite a large thermal mass. This achievement can be of great importance for production of stationary phases within a micro-fluidic device which cannot be fabricated through photo-initiated polymerisation. This Chapter also discusses a preliminary investigation into thermally initiated monolithic porous layer open tubular (monoPLOT) columns using the TEC column heater to finely control the temperature during the polymerisation process.

Aims

The aim of the work presented in Chapter 3 was to apply the Mk.1 and Mk.2 TEC column heaters to different chromatographic and synthetic applications. The work aimed to investigate various reversed-phase and ion exchange separations. Furthermore, it was envisaged that the flexibility of the column heater could also be applied to several fabrication applications through thermal initiation in both capillary and micro-fluidic chip format.

3.1 Experimental

3.1.1 Reagents and materials

For the fabrication of monolithic stationary phases the following reagents and chemicals were used:

- Lauryl methacrylate, ethylene dimethacrylate, butyl methacrylate, 1-propanol, 1,4-butanediol, styrene, divinylbenzene (DVB), 3-methoxysilylpropyl methacrylate, 1-decanol, benzophenone, and UV-initiator dimethoxy-2-phenyacetophenone were purchased from Sigma-Aldrich (Gillingham, U.K.).
- The thermal initiator, azobisisobutyronitrile (AIBN), was obtained from DuPont (Le Grand Sacconex, Switzerland).
- Standard solutions of ethylbenzene, propylbenzene, butylbenzene, and pentylbenzene were purchased from Sigma Aldrich (Gillingham, U.K).
- All solvents which were used for the preparation of HPLC mobile phases and for the synthesis and washing of prepared monoliths, namely, tetrahydrofuran, acetonitrile, toluene, and methanol, were purchased from Lab Scan (Gliwice, Poland).
- Deionised water purified by a Milli-Q system (Millipore, Bedford) was utilised throughout the experiments.
- Teflon coated (15 μm thickness) fused silica capillary, 100 μm ID, 0.375 mm OD was purchased from Composite Metal Services Ltd. (Charlestown, U.K.).
- A 26 mm long glass/silica chip micro-fluidic chip with rectangular channel dimensions of 50 x 100 μm was fabricated and provided by the Tyndall Institute (Cork, Ireland).

3.1.2 Instrumentation

- Capillaries were filled with monomer mixture and washed using a KDS-100-CE syringe pump (KD Scientific, Inc., Holliston, MA, USA).
- For the chromatographic studies, a Dionex Ultimate 3000 nano-HPLC system (Dionex, Sunnyvale, CA) was used, incorporating an FLM3100 column compartment which was used only for the performance comparison with the Mk.1 and Mk.2 TEC column heaters. For data acquisition, Chromeleon 6.8 software (Dionex, Sunnyvale, CA) was utilised. Chromatography was performed with a flow rate of 1 μL/min, and detection was by UV at 254 nm using a 3 nL flow cell.
- A SputterCoater S150B (BOC Edwards, Sussex, U.K.) was utilised for coating capillary monolithic stationary phase samples with a 60 nm gold layer.
- Scanning electron microscopy (SEM) analysis was performed on a S-3400N instrument (Hitachi, Maidenhead, U.K.).
- Optical microscopy evaluation of micro-fluidic chip samples was performed on a Meiji Techno EMZ-8TR stereomicroscope (Meiji Techno UK Ltd., Somerset, U.K.).

3.1.3 Experimental procedures

The experimental procedures used for the silanisation and fabrication of reversed-phase columns in a capillary format are as detailed in Section 2.2.5.

3.1.3.1 Fabrication of reversed-phase column with gradient of pore size

Gradient polymerisation was performed on a butyl methacrylate monomer mixture. The monomer mixture consisted of 24 %wt BuMA, 16 %wt EDMA, 60 %wt 1-decanol, and 1

%wt AIBN. The monomer mixture was prepared as per the procedure described by Nesterenko *et al.* [1]. As per this procedure, AIBN was first dissolved in the porogen, then monomers were added to the mixture, which was then vortexed, deoxygenated under the flow of nitrogen for 10 min, and centrifuged. A length of silanised capillary was filled with the monomer mixture and exposed to a profiled heating program on the TEC array module.

3.1.3.2 Fabrication of reversed-phase columns (micro-fluidic chip format)

A polystyrene-divinylbenzene stationary phase was fabricated by on-chip thermal polymerisation in a micro-fluidic channel. The monomer mixture consisted of 20.3 %wt styrene, 20.5 %wt DVB, 51.2 %wt 1-decanol, 8 %wt THF, and 1 %wt AIBN (with respect to monomers). The initiator (AIBN) was weighed out into the mixture vessel and the porogen mixture (1-decanol and THF) was added, followed by the monomers. The mixture was vortexed and deoxygenated under a flow of nitrogen for 10 min. The micro-fluidic chip was filled with the monomer mixture and exposed to a heating program on the TEC unit array module.

3.1.3.3 Fabrication of reversed-phase monoPLOT columns

A LMA-EDMA monoPLOT column was fabricated by thermal polymerisation by placing a 150 mm length of capillary filled with monomer mixture in the TEC column heater. The monomer mixture consisted of 24 %wt LMA, 16 %wt EDMA, 45.5 %wt 1-propanol, 14.5 %wt 1,4-butanediol, and 0.4 %wt of AIBN (with respect to monomers). The initiator (AIBN) was weighed out into the mixture vessel, and the porogen mixture (1-propanol and 1,4-butanediol) was added, followed by the monomers. The mixture was vortexed and deoxygenated under a flow of nitrogen for 10 min. A 150 mm length of 50 μm ID silanised

capillary was filled with the monomer mixture and was placed in the Mk.2 TEC column heater. One end of the capillary was left open, while the other end of the capillary was attached to a 1 mL syringe filled with monomer mixture. The column heater temperature was set to 60 ºC and heat was applied for 30 min. After 30 min the flow rate of the syringe pump was set to 1 µL/min and monomer mixture was allowed to flow through the capillary for 2 min. The purpose of this was to ensure that complete polymerisation was not allowed to occur by constantly removing short chain polymers which had formed in the middle of the capillary. This process was repeated for 3 hrs. The resultant monoPLOT column was washed with MeOH to remove residual porogen and unreacted monomers.

3.1.3.4 Fabrication of ion-exchange columns

Firstly a 150 mm x 100 µm ID LMA-EDMA column was prepared according to the procedure described in Section 2.2.5.2. The column was then washed with MeOH for 1 hr. Benzophenone (50 mg) was weighed out into the mixture vessel and 1 mL of MeOH was added. The mixture was vortexed until all of the benzophenone had dissolved and then deoxygenated under a flow of nitrogen for 10 min. The column was then filled with this mixture and exposed to 2 J cm^2 of UV radiation. Once treated with benzophenone the column was washed with MeOH for 1 hr at 3 µl/min flow rate. A 6% solution of sulfopropyl methacrylate was then prepared in MeOH, vortexed until all of the sulfopropyl methacrylate had dissolved and deoxygenated under a flow of nitrogen for 10 min. The capillary column was then filled with this mixture and exposed to 2 J cm^2 of UV radiation. The column was washed again with MeOH for 1 hr at 3 µL/min flow rate and then washed overnight with 10 *mM* ethylenediamine made up in H_2O.

3.1.3.5 Preparation of standard solutions

Standard solutions were prepared as per Table 3.1.

Table 3.1 – Preparation of standard solutions.

Analyte	**Solvent**	**Concentration** *(mg/mL)*
thiourea	50:50 ACN/H_2O	0.05
ethylbenzene	50:50 ACN/H_2O	0.05
propylbenzene	50:50 ACN/H_2O	0.05
butylbenzene	50:50 ACN/H_2O	0.05
pentylbenzene	50:50 ACN/H_2O	0.05
Mg^{2+}	H_2O	0.005
Ca^{2+}	H_2O	0.012
Ba^{2+}	H_2O	0.025
phenol	H_2O	0.05
p-cresol	H_2O	0.05
2-nitrophenol	H_2O	0.05
2,4-dichlorophenol	H_2O	0.05
diethylphthalat	Acetone	340
benz(*a*)anthracene	Acetone	0.04
chrysene	Acetone	0.04
benzo(*a*)pyrene	Acetone	0.04
diethylhexylphthalate	Acetone	670

3.2 Results and discussion

In order to demonstrate the practical application of the TEC colum heater for capillary HPLC, a number of separations were carried out in both reversed-phase and ion exchange modes. Furthermore, thermally initiated polymerisation applications were investigated in both capillary and micro-fluidic chip formats.

3.2.1 Reversed-phase separations

3.2.1.1 Separation of alkylbenzenes on a LMA-EDMA monolithic column at elevated temperatures

A simple mixture of alkylbenzenes (ethylbenzene, butylbenzene, and pentylbenzene) and thiourea was separated on a reversed-phase LMA-EDMA monolithic capillary column (150 mm x 100 μm ID) attached to the TEC unit array. The purpose of this experiment was to demonstrate that the device could operate effectively as a simple column heater.

The performed separations are presented in Figure 3.1, with all parameters (flow rate, analyte concentration, injection volume, and mobile phase composition) other than temperature were kept constant. The separation was performed initially at 20 ºC at a constant flow rate of 1 μL/min. The separation was repeated a further 6 times, each time the temperature being increased by 5 ºC. Peak parameters (resolution, selectivity, width at half height, asymmetry, and theoretical plates per meter) were calculated under different temperature conditions for each separation and are presented in Table 3.2. As expected, retention times for each analyte dropped with the temperature increase and improvements were observed in peak widths. Column efficiency for all analytes was found to be

maximum at 35 ºC (Table 3.2), after which it began to decrease possibly due to conformational changes of the polymer chain structure of the stationary phase at higher temperatures. However, the effectiveness of the device as a simple column heater was demonstrated by the expected peak data shown in Table 3.2, with column equilibration time between injections being a matter of just seconds.

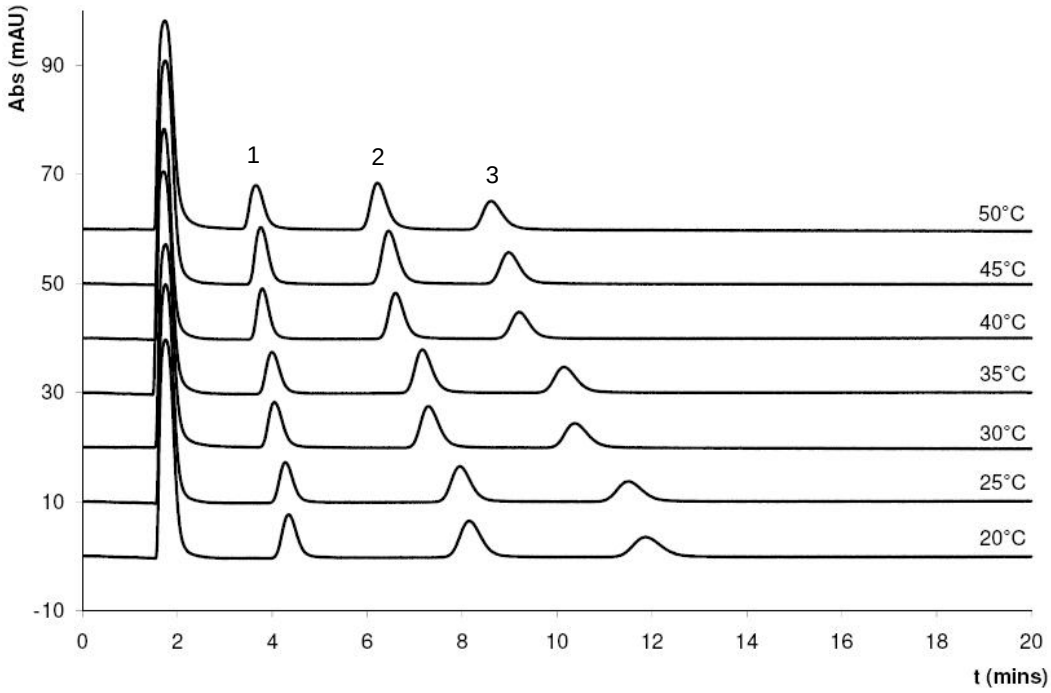

Figure 3.1 – Separation of three alkylbenzenes (1. ethylbenzene, 2. butylbenzene, and 3. pentylbenzene) at varying temperatures performed on Mk.1 column heater. Column: 150 mm x 100 µm ID LMA-EDMA monolithic column. Mobile phase: 50:50 ACN/H_2O, flow rate 1 µL/min. UV detection at 254 nm.

Table 3.2 – Comparative peak data for Figure 3.1 at varying temperatures, flow rate 1 µL/min.

Method	*Temperature 20 °C*					*Temperature 25 °C*					*Temperature 30 °C*				
Analyte	R_s	α	$W_{1/2}$	Asy	*N*/m	R_s	α	$W_{1/2}$	Asy	*N*/m	R_s	α	$W_{1/2}$	Asy	*N*/m
ethylbenzene	-	-	0.34	1.32	6100	-	-	0.33	1.34	6200	-	-	0.31	1.37	6400
butylbenzene	2.31	2.48	0.49	1.20	10300	2.36	2.46	0.45	1.25	11600	2.25	2.40	0.41	1.29	12000
pentylbenzene	1.63	1.58	0.65	1.19	12400	1.70	1.57	0.60	1.22	13600	1.62	1.55	0.53	1.25	14300
	Temperature 35 °C					*Temperature 40 °C*					*Temperature 45 °C*				
	R_s	α	$W_{1/2}$	Asy	*N*/m	R_s	α	$W_{1/2}$	Asy	*N*/m	R_s	α	$W_{1/2}$	Asy	*N*/m
ethylbenzene	-	-	0.31	1.40	6600	-	-	0.30	1.43	6100	-	-	0.30	1.46	5800
butylbenzene	2.27	2.38	0.40	1.33	12400	2.19	2.42	0.38	1.36	12000	2.01	2.34	0.37	1.39	11300
pentylbenzene	1.66	1.55	0.51	1.27	15200	1.61	1.54	0.48	1.32	15100	1.54	1.54	0.45	1.36	14700
	Temperature 50 °C														
	R_s	α	$W_{1/2}$	Asy	*N*/m										
ethylbenzene	-	-	0.30	1.48	5700										
butylbenzene	1.95	2.34	0.36	1.43	11100										
pentylbenzene	1.50	1.54	0.44	1.39	14200										

3.2.1.2 Separation of phenols on a LMA-EDMA monolithic column at sub-ambient, ambient, and elevated temperatures

The practical application of the Mk.1 TEC column heater was also tested by separating a mixture of phenols (phenol, *p*-cresol, 2-nitrophenol, and 2,4-dichlorophenol) at both sub-ambient, ambient, and elevated temperatures. The purpose of this experiment was to demonstrate that the device could operate effectively in all modes (cooling, thermostatting at room temperature, and heating) and in a stable fashion. The mixture of phenols was separated on a reversed-phase LMA-EDMA monolithic capillary column (150 mm x 100 μm ID) that was directly attached to the TEC unit array.

The performed separations can be seen in Figure 3.2, where all parameters (flow rate, analyte concentration, injection volume, and mobile phase composition) other than temperature were kept constant. The separation was performed initially at 15 ºC at a constant flow rate of 1 μL/min. The separation was repeated a further 2 times at room temperature (25 ºC) and at 50 ºC. Peak parameters (resolution, selectivity, width at half height, asymmetry, and theoretical plates per meter) were calculated for each separation at different temperature conditions and are presented in Table 3.3. As before, a drop in retention for each analyte was observed, with improvements in column efficiency and peak widths at increased temperatures. These effects can be attributed both to decrease of mobile phase viscosity and to an increase of diffusion and mass transfer in the stationary phase.

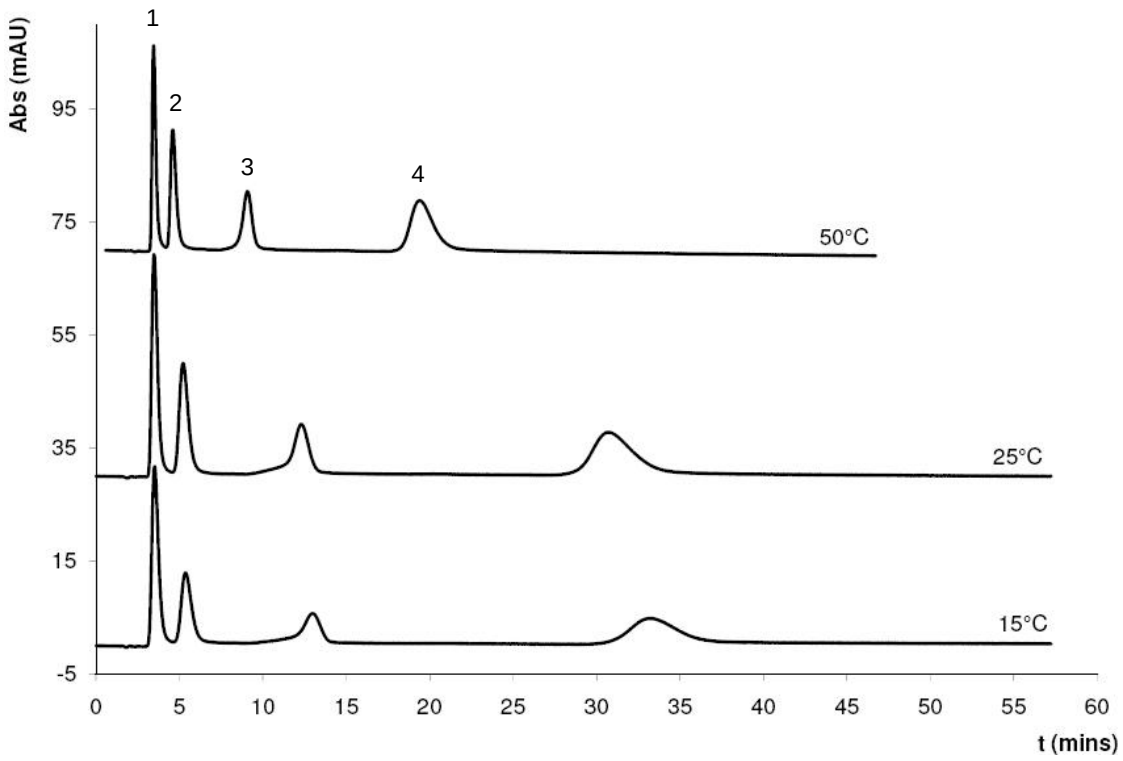

Figure 3.2 – Separation of four phenols (1. phenol, 2. p-cresol, 3. 2-nitrophenol, and 4. and 2,4-dichlorophenol) at varying temperatures performed on Mk.1 column heater. Column: 150 mm x 100 µm ID LMA-EDMA monolithic column. Mobile phase: 50:50 ACN/H_2O, flow rate 1 µL/min. UV detection at 254 nm.

Table 3.3 – Comparative peak data for Figure 3.2 at vaying temperatures, flow rate 1 µL/min.

Method	*Temperature 16 °C*					*Temperature 25 °C*					*Temperature 50 °C*				
Analyte	R_s	α	$W_{1/2}$	Asy	*N*/m	R_s	α	$W_{1/2}$	Asy	*N*/m	R_s	α	$W_{1/2}$	Asy	*N*/m
phenol	-	-	0.44	1.52	2400	-	-	0.39	1.55	3000	-	-	0.25	1.67	5100
p-cresol	1.98	2.09	0.68	1.27	2400	2.08	2.04	0.59	1.38	2900	2.20	2.07	0.37	1.54	4400
2-nitrophenol	5.07	3.14	1.10	0.67	5200	5.40	3.08	0.95	0.74	6200	5.47	3.01	0.59	0.89	7600
2,4-dichloro-phenol.	5.74	2.81	3.06	1.22	4400	6.15	2.76	2.59	1.31	5200	5.91	2.54	1.47	1.37	6100

3.2.1.3 Separation of alkylbenzenes on a LMA-EDMA monolithic column at elevated temperatures under isothermal and isofluentic conditions

This experiment was carried out to test the ability of Mk.1 TEC column heater to operate at higher temperatures (85 °C) and also in temperature programmed mode. The separation was performed under both isothermal and isofluentic conditions and with various combinations of single and dual temporal gradients of temperature and flow rate. The performed separations are presented in Figure 3.3, with all other parameters, such as analyte concentration, injection volume, and mobile phase composition kept constant. The peak parameters (area, height, resolution, width at half height, and asymmetry) were calculated for all the separations shown under each of the applied conditions (see Table 3.4). Initially, the separation was performed at ambient temperature at a set flow rate of 1 μL/min. As shown in Figure 3.3(a), under these conditions a complete resolution of all five analytes was achieved in approximately 20 min. Using the TEC array module set to a constant 85 °C, while maintaining the flow rate at 1 μL/min, resulted in a faster overall separation, complete in just 12 min, see Figure 3.3(c). However, simply increasing the temperature also resulted in decreased resolution, leaving toluene and ethylbenzene peaks unresolved. Neither was any significant beneficial increase in peak height or area observed, with peak shape (peak width and asymmetry) for both separations approximately the same. Combining the application of high temperature (85 °C) and increased flow rate (4 μL/min) significantly shortened the analysis time to just 4 min. In this case, although peak width and asymmetry improved, resolution between early eluting peaks deteriorated further, leaving toluene and ethylbenzene unresolved, with both peak area and height also significantly reduced, see Figure 3.3(f). In order to speed up the separation while maintaining peak resolution, a series of gradient conditions were investigated. Single gradients of

temperature and flow rate were applied separately and were then compared to a dual temperature/flow gradient. In the first instance, a single temperature gradient from 25 to 85 °C was applied from 3.5 to 6.5 min while maintaining a constant flow rate of 1 μL/min. The start of the temperature gradient was delayed to ensure complete separation of the first two peaks.

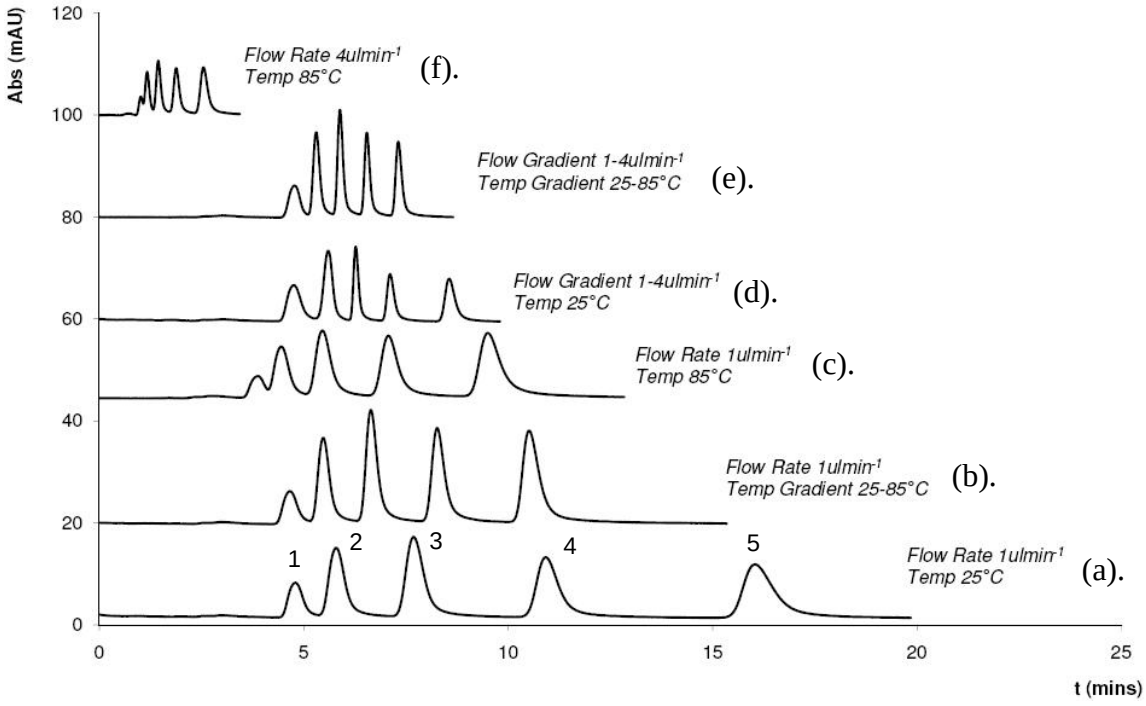

Figure 3.3 – Separation of five alkylbenzenes (1. toluene, 2. ethylbenzene, 3. propylbenzene, 4. butylbenzene, and 5. pentylbenzene) at varying flow rate and temperature performed on Mk.1 column heater: (a) temperature 25 °C, flow rate 1 μL/min, (b) temperature gradient 25-85 °C from 3.5 to 6.5 min, flow rate 1 μL/min, (c) temperature 85 °C, flow rate 1 μL/min, (d) temperature 25 °C, flow gradient 1-4 μL/min from 5.3 to 6.3 min, (e) temperature gradient 25-85 °C from 3.5 to 6.5 min, flow gradient 1-4 μL/min from 4.3 to 8.0 min, (f) temperature 85 °C, flow rate 4 μL/min. Column: 150 mm x 100 μm ID LMA-EDMA monolithic column. Mobile phase: 50:50 ACN/H_2O. UV detection at 254 nm.

During the application of the gradient, the column backpressure change was recorded, confirming that the shape of the programmed gradient was identical and simultaneous to that generated by the TEC array module. With comparison of chromatograms obtained using the temperature gradient, shown as Figure 3.3(b), to the isothermal separations at 25 °C (Figure 3.3(a)) and 85 °C (Figure 3.3(c)), a reduction in peak width was observed, causing an increase in peak height while simultaneously maintaining asymmetry values and resolution between peaks. It can also be seen that overall separation time decreased by 40% compared with the separation at ambient temperature (Figure 3.3(a)). In the second instance, a flow gradient from 1 μL/min to 4 μL/min was applied from 5.3 to 6.3 min, while maintaining a constant temperature of 25 °C, shown as Figure 3.3(d).

Table 3.4 – Comparative peak data for Figure 3.3 under varying applied flow and temperature gradients.

Method	*Temperature 25 °C, flowrate 1 μL/min*				*Temperature gradient 25 - 85°C from 3.5 min to 6.5 min, flowrate 1 μL/min*				*Temperature 85 °C, flowrate 1 μL/min*			
Analyte	R_s	α	$W_{1/2}$	Asy	R_s	α	$W_{1/2}$	Asy	R_s	α	$W_{1/2}$	Asy
toluene	-	-	0.39	1.30	-	-	0.38	1.18	-	0.39	0.39	-
ethylbenzene	1.45	1.57	0.42	1.37	1.4	1.51	0.31	1.50	0.84	1.68	0.39	1.24
propylbenzene	2.51	1.70	0.47	1.50	2.26	1.48	0.3	1.59	1.51	1.72	0.4	1.45
butylbenzene	3.64	1.70	0.58	1.56	3.02	1.45	0.34	1.56	2.29	1.68	0.43	1.58
pentylbenzene	4.38	1.65	0.8	1.70	3.44	1.44	0.43	1.71	2.92	1.61	0.55	1.77
	Temperature 25 °C, flow gradient 1 - 4 μL/min from 5.3 min to 6.3 min				*Temperature gradient 25 - 85 °C from 3.5 mins to 6.5 min, flow gradient 1 - 4 μL/min from 4.3 min to 8.0 min*				*Temperature 85°C, flowrate 4 μL/min*			
	R_s	α	$W_{1/2}$	Asy	R_s	α	$W_{1/2}$	Asy	R_s	α	$W_{1/2}$	Asy
toluene	-	-	0.37	1.16	-	-	0.31	1.05	-	-	-	-
ethylbenzene	1.61	1.39	0.24	1.09	1.33	1.24	0.18	1.30	0.25	0.12	0.12	-
propylbenzene	2.11	1.22	0.14	1.47	2.07	1.22	0.15	1.45	1.32	0.13	0.13	1.31
butylbenzene	3.04	1.23	0.19	1.49	2.69	1.20	0.14	1.41	1.91	0.15	0.15	1.35
pentylbenzene	3.75	1.32	0.26	1.55	2.96	1.20	0.16	1.45	2.33	0.19	0.19	1.44

In this case, the start of the flow gradient was delayed to ensure complete separation of the first two peaks. With comparison of the peak shapes and overall chromatogram to those achieved under isofluentic conditions at 25 °C (Figure 3.3(a)) and 85 °C (Figure 3.3(c)), an improvement was observed in peak resolution (compared with Figure 3.3(c)), with peaks for toluene and ethylbenzene being fully resolved while width and asymmetry values noticeably improved. In addition, the application of a flow gradient reduced the time separation by 48% compared to the separation at 25 °C. Finally, in order to achieve the complete resolution of all peaks, yet maintaining a fast run time, a rapid dual gradient of both flow and temperature was applied, shown in Figure 3.3(e). In this case, the applied temperature gradient was run from 25 to 85 °C over 3.5 to 6.5 min, while a simultaneous flow gradient was applied from 1 μL/min to 4 μL/min over 5.3 to 6.3min. With comparison of this separation with the individual gradient runs, namely, the temperature gradient (Figure 3.3(b)) and flow rate gradient (Figure 3.3(d)), it can be seen that the overall separation time has been further reduced to just under 8 min, equaling a 66% reduction compared to the isofluentic separation at 25 °C (Figure 3.3(a)). Furthermore, the applied dual gradient resulted in the complete resolution of all sample components, with both peak width and asymmetry improved compared to each of the previous runs and peak heights (thus signal to noise ratio) generally unaffected.

3.2.1.4 Separation of polyaromatic hydrocarbons using rapid temperature programming

In past decades considerable work has been done in the area of separation of polyaromatic hydrocarbons (PAHs). This interest and need are attributed to their carcinogenic and mutogenic properties and their effect on human health is a matter of international concern. The US Environmental Protection Agency lists 16 PAHs as "priority pollutants" and which are most frequently used for environmental PAH studies [2]. These include, naphthalene, acenaphthylene, acenaphthene, fluorene, phenanthrene, anthracene, fluoranthene, pyrene, benzo[*a*]anthracene, chrysene, benzo[*b*]fluoranthene, benzo[*k*]fluoranthene, benzo[*a*]pyrene, dibenz[*a,h*]anthracene, benzo[*g,h,i*]perylene, and indeno[*1,2,3-cd*]pyrene. PAHs form during the incomplete combustion of organic materials and can exist in coal-tar, soot, pitch, crude oils, and oil products such as rubber tyres and plastics [3]. Of more significance however is the occurrence of PAHs in environmental conditions which can have a direct impact on human health such as tobacco smoke and automobile exhaust fumes. Additionally, land usage that might lead to contamination with PAHs (land fills, vehicle scrap yards, oil refineries, coal and gas plants, petrol filling stations) often results in that land becoming useless for redevelopment due to environmental or health concerns. Reliable and accurate methods are crucial to the detection of these compounds and indeed much work has previously been done on the separation of PAHs through high performance liquid chromatography[4-11]. However, the separation of many PAHs, especially isomers, remains extremely difficult, and often resolution between eluting analytes is poor.

This more complex separation was carried out to demonstrate the effectiveness of the device during rapid gradient operation and to utilise the Mk.2 TEC column heater with a commercial particle packed reversed-phase column. A mixture of PAHs (diethylphthalate,

benz(*a*)anthracene, chrysene, benzo(*a*)pyrene, and 2,4-diethylhexylphthalate) was successfully separated on a Waters X-Bridge BEH130 C_{18} 100 mm × 300 µm column (d_p 3.5 µm) using a combination of solvent and rapid temperature gradients. The column (including fittings) was encased in thermally conductive silicon in order to aid in heat transfer between the TEC column heater and column.

In previous sections, the rate of the temperature gradients was approximately 20 °C/min, however during this experiment the rates of heating was increased to 55 °C/min. Initially, a separation of five PAHs was performed at ambient temperature with an ACN concentration gradient only. However, in these conditions no resolution for benz(*a*)anthracene and chrysene was achieved, see Figure 3.4(a). A further separation was carried out employing a temperature gradient from 25 to 80°C over 3 min. It can be seen from Figure 3.4(b) that no resolution could still be achieved for benz(*a*)anthracene and chrysene and indeed benzo(*a*)pyrene was observed to co-elute with these analytes. On the contrary, the application of a rapid temperature gradient allowed the complete separation of the test mixture, as it can be seen from Figure 3.4(c).

These changes in selectivity may be attributed to a few factors. Firstly, peak efficiency increases at elevated temperatures due to the change of mass transfer and distribution coefficients of the analytes between the phases. The approximate dependence of the diffusion coefficient on temperature in liquids can be found using the equation:

$$\frac{D_{MT1}}{D_{MT2}} = \frac{T_1}{T_2}\frac{\mu_{T1}}{\mu_{T2}}$$

(eq. 3.1)[12]

where T_1 and T_2 are temperatures 1 and 2 respectively (kelvin). D_m is the diffusion coefficient in the liquid phase (m^2/sec) and μ is the dynamic viscosity of the solvent (Pa.s). Subsequently, the diffusion into the porous media of the stationary phase is also dependent on the diffusion in the liquid phase:

$$D_S = \frac{D\varepsilon_t\delta}{\tau}$$

(eq. 3.2)[12]

Where D is the diffusion coefficient in liquid filling the pores (m^2/sec), ε_t is the porosity, δ is constrictivity and τ is tortuosity (the last three parameters are dimensionless).

Efficiency, as described by the van Deemter equation, is dependent on both diffusion in the mobile phase and diffusion in the stationary phase (through term B and C) so it is clear that efficiency is a temperature dependent parameter.

Selectivity, α (eq. 3.3) is a function of the relative mobility of analytes and is a thermodynamic parameter that is dependent on temperature. At a particular given temperature it will depend only on the nature of the separated compounds and properties of the mobile and stationary phases.

$$\alpha = \frac{V_{R2}}{V_{R1}} = \frac{k_2}{k_1} = \frac{D_2}{D_1}$$

(eq. 3.3.)[13]

It can be concluded that temperature has a significant effect on selectivity, thus application of temperature gradient can facilitate an improvement in selectivity. As a result, application of a very rapid temperature gradient with the stationary phase that was suitable for fast heat transfer allowed complete baseline separation of all five PAHs of interest.

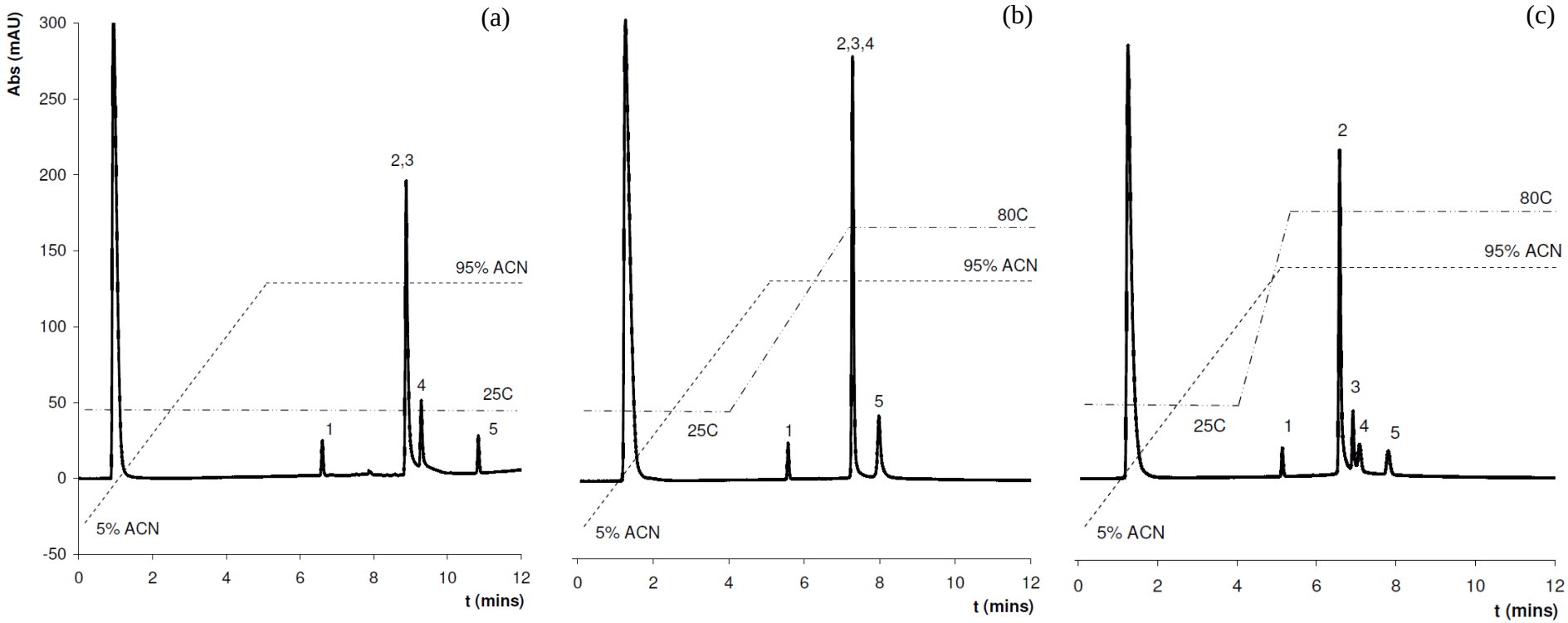

Figure 3.4 – Separation of five polyaromatic hydrocarbons (1. diethylphthalate, 2. benz(a)anthracene, 3. chrysene, 4. benzo(a)pyrene, and 5. 2,4-diethylhexylphthalate) at (a) 25 °C using a solvent gradient of 5% to 95% ACN applied from 0.0 to 5.0 min, (b) using a temperature gradient from 25 – 80 °C applied from 4.0 to 7.0 min and solvent gradient of 5% to 95% ACN applied from 0.0 to 5.0 min, and (c) using a rapid temperature gradient from 25 – 80 °C applied from 4.0 to 5.0 min and solvent gradient of 5% to 95% ACN applied from 0.0 to 5.0 min. Column: Waters X-Bridge BEH130 C_{18} 100 mm × 300 µm column (d_p 3.5 µm). Mobile phase: 5 – 95% ACN/H_2O gradient, flow rate 10 µL/min. UV detection at 254 nm.

3.2.2 Ion-exchange separations

3.2.2.1 Separation of cations on a lauryl methacrylate column functionalised with sulfo groups at elevated temperatures

Although temperature effects in ion chromatography are rather small [14], it was considered interesting to evaluate the performance of the Mk.2 column heater with a polymer-based grafted strong cation exchanger for the separation of selected cations at elevated temperatures. A mixture of cations (magnesium, calcium, and barium) was separated on a sulfonated LMA-EDMA monolithic capillary column (150 mm x 100 μm ID) at varying temperatures, from 20 °C to 40 °C, and at a constant flow rate of 1 μL/min. The performed separations are presented in Figure 3.5. As expected, the temperature effect on the retention and was overall very slight, yet most profound for the strongest retained cation, Ba^{2+}. For all cations it was found that the efficiency increased with the increase of temperature, which can be attributed to the change in distribution coefficients and increased mass-transfer. Peak data for Figure 3.5 is shown in Table 3.5.

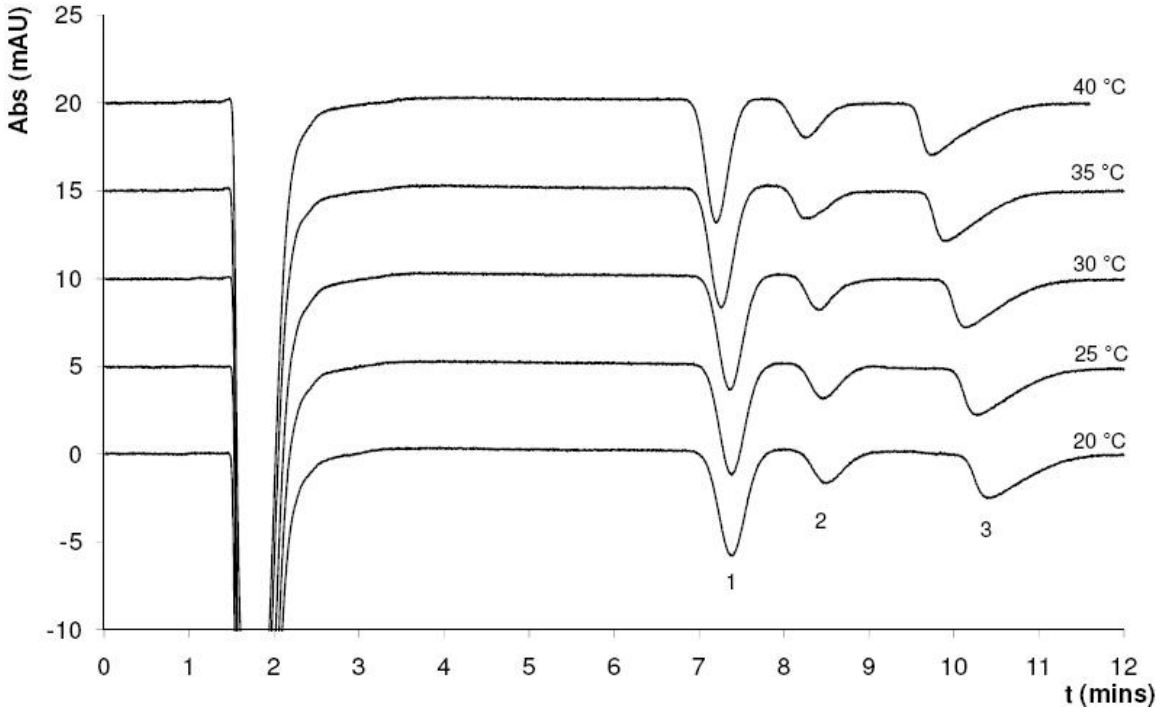

Figure 3.5 – Separation of three alkali earth metals (1. magnesium, 2. calcium, 3. barium) at varying temperatures. Column: 150 mm x 100 µm ID LMA-EDMA monolithic column functionalised with sulpho groups. Mobile phase: 10 mM $CuSO_4$, flow rate 1 µL/min. Indirect UV detection at 214 nm.

Table 3.5 – Comparative peak data for Figure 3.5 at varying temperatures, flow rate 1 µL/min.

Method	*Temperature 20 °C*					*Temperature 25 °C*					*Temperature 30 °C*				
Analyte	R_s	α	W_b	Asy	*N*/m	R_s	α	W_b	Asy	*N*/m	R_s	α	W_b	Asy	*N*/m
Magnesium	-	-	0.97	1.06	10600	-	-	0.97	1.05	11600	-	-	0.96	1.05	14100
Calcium	1.72	1.20	0.87	1.25	11800	1.77	1.20	0.84	1.21	11700	1.83	1.19	0.80	1.25	12000
Barium	2.14	1.28	1.573	2.21	7200	2.13	1.27	1.51	2.16	7600	2.13	1.26	1.39	1.52	9100
	Temperature 35 °C					*Temperature 40 °C*									
	R_s	α	W_b	Asy	*N*/m	R_s	α	W_b	Asy	*N*/m					
Magnesium	-	-	0.94	1.07	15200	-	-	0.91	1.06	16800					
Calcium	1.65	1.19	0.76	1.38	13200	1.85	1.20	0.72	1.10	15100					
Barium	1.86	1.25	1.33	2.00	9900	2.11	1.23	1.26	1.92	10900					

3.2.3 Fabrication of reversed-phase stationary phases

3.2.3.1 Gradient of porosity

It is well-known that in order to obtain fine control of monolith porosity during thermal polymerisation, the precise control of the reaction temperature is crucial. The polymerisation process itself is a complex series of reactions, each affected to some degree by the exact system temperature. The most important of these is the initiation rate, which is highly dependent on temperature, since the half-life of initiators decreases with increases in temperature. As a result, the rate of the formation of free radicals and, subsequently, the speed of the chain growth and formation of globules and the overall polymerisation rate are each higher at elevated temperatures [15]. As the formation of new polymerisation centres is faster than the growth of globules, the supply of monomers runs low fast and the number of globules is large, but their size stays small, leading to smaller voids between globules. Essentially, the entire pore size distribution is shifted smaller with an increase in temperature, although most obviously seen for the larger flow-through pores. Therefore, the ability of the designed column heater to precisely control the temperature of separate zones within a capillary was exploited to optimise and better understand the fabrication of porous polymer monoliths within capillary columns. In this experiment, the TEC array module was used to polymerise a monolithic column with a longitudinal density (pore size) gradient. To achieve this, a capillary filled with BuMA-EDMA polymerisation mixture was attached to the TEC units and a heating profile from 60 to 54 °C programmed over six distinct thermal zones, with 1 °C spatial increments. Polymerisation of the complete monolith was performed for 16 hrs, after which the monolith was washed with MeOH for 1 hr, cut into segments, corresponding to each temperature zone, and dried.

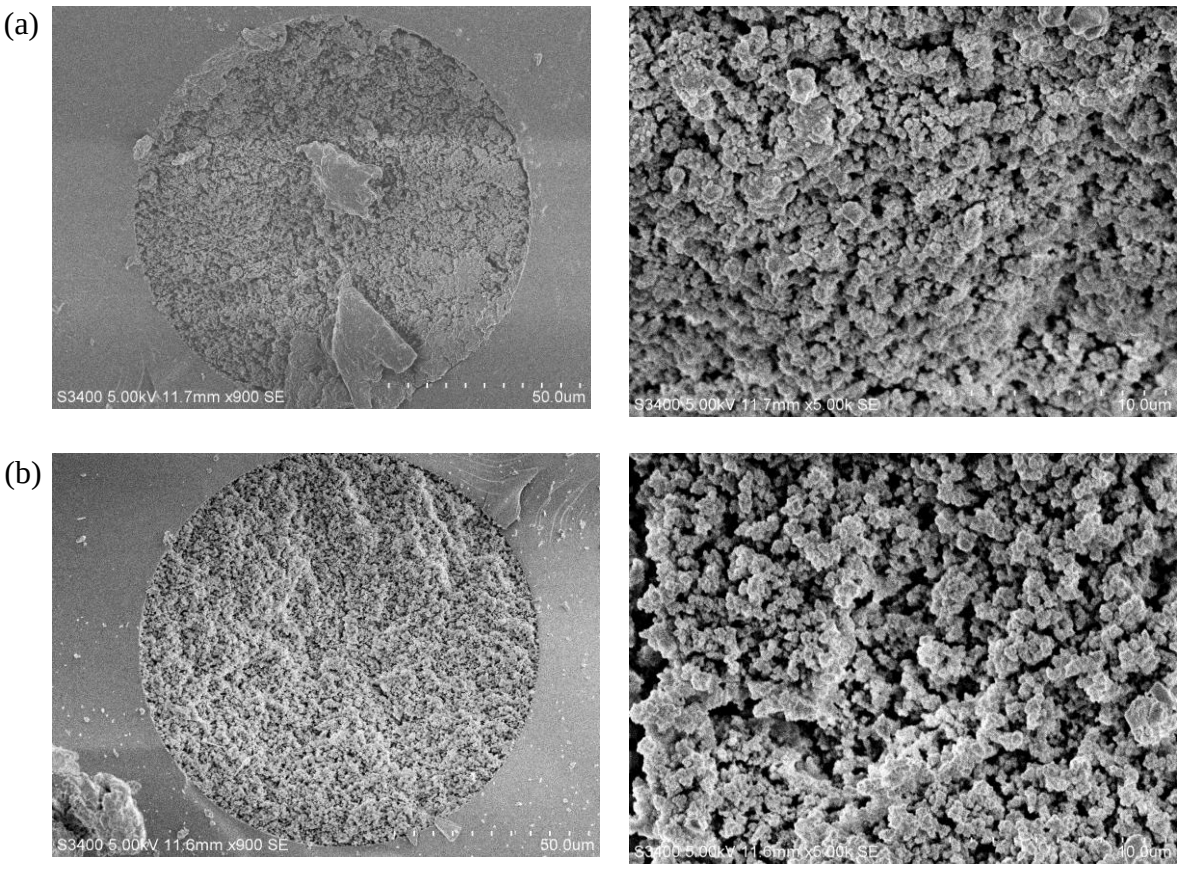

Figure 3.6 – SEM images of a BuMA-EDMA monolith formed using a thermal gradient for 16 hrs at (a) 60 °C and at (b) 54 °C.

The porous structure of each of these segments was characterised using SEM. Figure 3.6 shows SEM images of two selected zones of the monolith polymerised at (a) 60 °C and (b) 54 °C. It can be clearly seen that the size of polymer globules and flow-through pores differ for these sections. From each of the six sets of SEM images, the average size (n = 30) of the pores were determined and plotted against the exact polymerisation temperature. This relationship is presented as Figure 3.7.

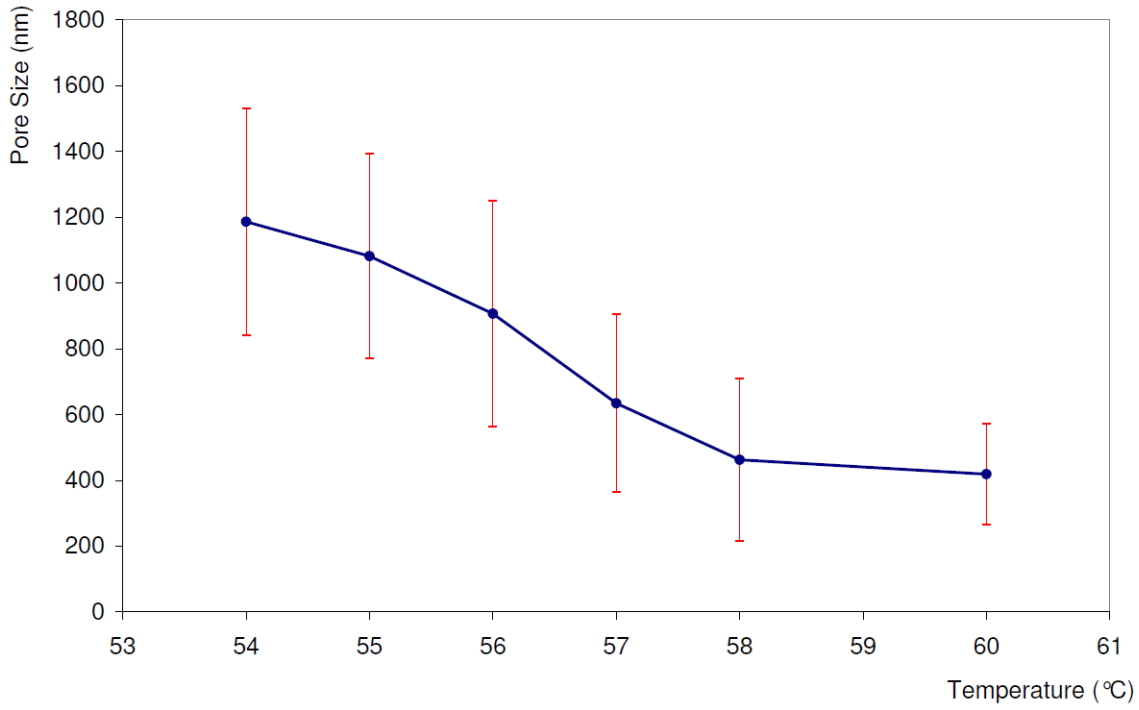

Figure 3.7 – Plot of average pore sizes against increasing polymerisation temperatures for a single capillary housed BuMA-EDMA monolith, polymerised over 16 hrs on the TEC column heater.

The plot clearly shows an increase in pore size with a decrease in polymerisation temperature. The graph also shows how the TEC array can also be utilised to produce polymer monoliths of relatively predictable porous structure resulting in the controlled formation of axial gradients of porosity, something very much more difficult to achieve using alternative air heaters, water baths, or indeed UV polymerisation approaches.

3.2.3.2 On-chip fabrication

With the on-going interest in the development of micro-fluidic based separations, considerable interest has been focused on the packing and formation of various types of stationary phases in such devices, including monolithic stationary phases [16]. Although there have been various methods established to house such phases into micro-fluidic

channels [17-18], often it is required to polymerise only a specific zone of the channel, and depending on the chip material (which eliminates application of traditional heating systems such as water, oil baths, or air circulated ovens) the entire micro-fluidic chip must be immersed. Additionally, depending on the desired chemistry of the stationary phase, UV polymerisation may not be possible as some monomers (for example, polystyrene and divinylbenzene) absorb in the UV region thus inhibiting the reaction.

As the TEC column heater can provide both heating and cooling of specific and subsequent zones, its application to the on-chip thermal polymerisation of polystyrene monolithic stationary phases in fixed zones of micro-fluidic channels was investigated. In order to achieve selective polymerisation such as this, the channel was exposed to a well defined thermal profile, which allowed polymerisation to occur in the appropriate heated area, while the area(s) where polymerisation was not desired were simultaneously cooled. Since the individual TEC unit dimensions were 12 x 12 mm, the polymerised zone in the channel was 12 mm long.

For this experiment, a single pre-treated channel (see Section 3.1.3.2) of a glass/silica chip (26 mm long with channel cross-section dimensions of 50 × 100 μm) was filled with the styrene monomer mixture. The chip was then attached to the TEC column heater by applying a thin layer of thermally conductive silicon paste between the contact surfaces to ensure a good thermal transfer between the chip and the heater. Due to the large thermal mass of the glass chip, a temperature program was applied to facilitate uniform radial porosity as described by Nesterenko *et al.* [1]. Specifically, the temperature of the heating zone on the TEC array module was slowly ramped up to the initial dwell temperature of 50

°C over a period of 30 min. This temperature was held for a further 30 min, after which the set point was again increased to the final polymerisation temperature of 60 °C at a rate of 2 °C every 10 min. On either side of the heating zone two cold areas were programmed with a temperature setpoint of 25 °C to prevent thermal polymerisation outside the selected zone. Polymerisation was performed for a period of 24 hrs after which the fabricated monolithic stationary phase in the channel was washed with MeOH. The formed monolith was then inspected under an optical microscope and the boundary between the polymerised and unpolymerised zones was found to be approximately 100 µm (see Figure 3.8). This application further demonstrates how the TEC array module is capable of generating very well defined thermal profiles, even when attached to objects with a relatively large thermal mass and high thermal conductivity, such as the glass/silica chip.

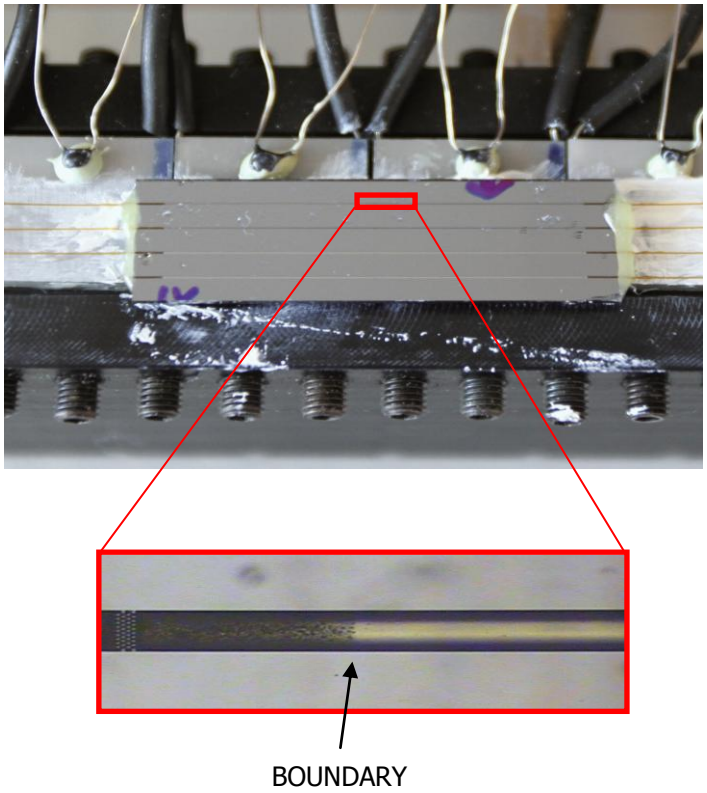

Figure 3.8 – On-chip selective polymerisation of a polystyrene monolith showing the boundary. The boundary was measured at approximately 100 µm.

3.2.3.3 Thermally initiated monoPLOT columns

MonoPLOT columns possess a porous layer of stationary phase on the inner surface of the capillary tubing, maintaining an open-tubular structure after the completion of all column preparation steps [1]. This type of column has many benefits and applications – these are discussed in detail in Chapters 4 and 5. Chapter 5 deals exclusively with thermally initiated monoPLOT columns, however a part of this work is included here as the columns detailed in this Section were fabricated using the TEC column heater.

A 150 mm length of 50 µm ID capillary filled with PS-DVB polymerisation mixture was placed in the TEC column heater. One end of the capillary was left open while the other end was connected to a 1 mL syringe which was also filled with polymerisation mixture. The syringe was held in a syringe pump so that polymerisation mixture could be pumped through the capillary. A heating profile was created which would slowly bring the column heater temperature up to 60 °C at a rate of 15 °C/min. After 30 min polymerisation mixture was pumped through the capillary at a rate of 1 µL/min for 2 min. This process was repeated for a total of 3 hrs after which the capillary was washed with MeOH for 1 hr, dried, and then cut into segments for SEM analysis. Two SEM images of the monoPLOT column are shown in Figure 3.9. Average layer thickness was measured at 60 locations at 10 places along the column and was found to be approximately 2.5 µm. However, the RSD of the monoPLOT layer was calculated to be unacceptably high at 67.5%.

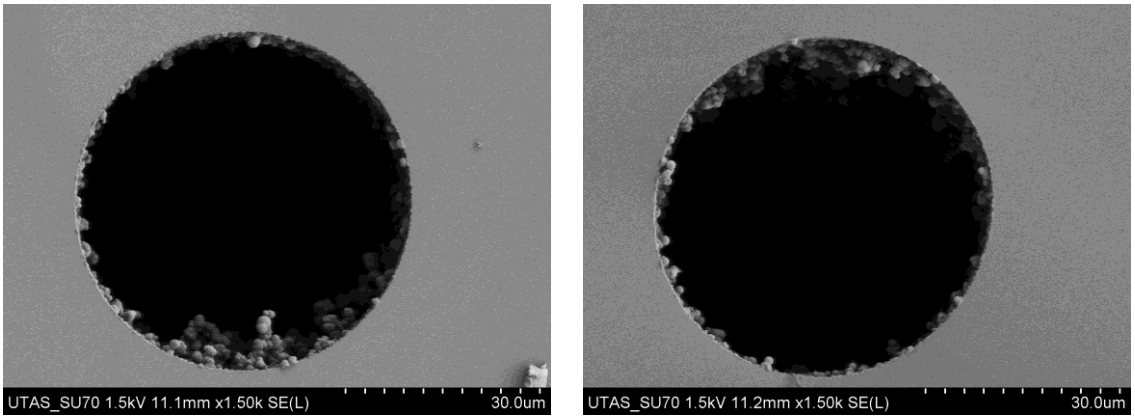

Figure 3.9 – SEM images of a PS-DVB monoPLOT column fabricated in the Mk.1 TEC column heater. Average layer thickness was measured at 2.5 µm (n = 60), RSD = 67.5%.

As can be seen from Figure 3.10, the layer thickness is non-uniform resulting in a high RSD value. Maximum and minimum layer thickness was measured at approximately 26 µm and 2 µm respectively. The wide distribution of layer thickness is largely due to the way that the capillary was attached to the TEC column heater. This polymerisation was carried out on the Mk.1 column heater, and so the capillary was attached to the TEC array using thermally conductive paste. The Mk.1 column heater could only apply heat from one side, and so there was more layer growth on the bottom side of the capillary that was closest to the TEC modules. However, this experiment was only a preliminary one to survey the purpose of demonstrating additional capability of the developed heating platform.

3.3 Conclusions

The results presented in Chapter 3 have demonstrated the design, versatile capabilities, and applications of a novel direct contact column heating/cooling platform based on TEC arrays. It was shown that the developed systems can provide very rapid heating/cooling with rates of up to 400 °C/min, with further rapid thermal equilibration of the capillary or microbore column attached. The unique platform was demonstrated with several chromatographic separations involving the application of dual temperature/flow rate gradients and also rapid temperature programming, with beneficial results. Due to the specific features of thermoelectric modules (precise temperature control, fast response), further demonstrative applications were investigated and presented, such as the fabrication of monoliths incorporating a gradient of porosity (in capillary format) and the precise positioning of monoliths with well-defined boundaries in chip formats, where in both instances the precise spatial control of temperature during polymerisation is essential. Further, the fabrication of thermally initiated monoPLOT columns using the column heater was presented.

Reference list

1. Nesterenko, E. P.; Nesterenko, P. N.; Connolly, D.; Lacroix, F.; Paull, B., *J. Chromatogr., A*, (2010), 1217, pp. 2138.
2. US Environmental Protection Agency (1984). Screening methods for PAH priority pollutants in waste water (http://nepis.epa.gov/), (accessed 05 Oct 2012).
3. International Agency for Research on Cancer (1983) IARC monographs on the evaluation of the carcinogenic risk of chemicals to humans. Polynuclear aromatic compounds, Part 1, chemical, environmental and experimental data, Volume 32. International Agency for Research on Cancer, Lyon.
4. Heudorf, U.; Angerer, J., *Int Arch Occup Environ Health*, (2001), 74, pp. 177.
5. Hagedorn, H.W.; Scherer, G.; Engl, J.; Riedel, K.; Cheung, F.; Errington, G.; Shepperd, J.; McEwan, M., *J Anal. Toxicol*, (2009), 33, pp. 301.
6. Benowitz. N.L.; Jacob. P. III; Bernert. J.T.; Wilson. M.; Wang. L.; Allen. F.; Dempsey. D., *Cancer Epidemiol. Biomark. Prev*., (2005), 14, pp. 1376.
7. Chetiyanukornkul, T.; Toriba, A.; Kameda, T.; Tang, N.; Hayakawa, K., *Anal. Bioanal. Chem.*, (2006), 386, pp. 712.
8. Jacob, P. III; Wilson,, M.; Benowitz, N.L., *Anal. Chem*., (2007), 79, pp. 587.
9. Rossbach, B.: Preuss, R.; Letzel, S.; Drexler, H.; Angerer, *J.*, *Int. Arch. Occup. Environ. Health*, (2007), 81, pp. 221.
10. Xu, X.; Zhang, J.; Zhang, L.; Liu, W.; Weisel, C.P., *Rapid Commun. Mass Spectrom*., (2004), 18, pp. 2299.
11. Onyemauwa, F.; Rappaport, S.M.; Sobus, J.R.; Gajdosova, D.; Wu, R.; Waidyanatha, S., *J Chromatogr. B.*, (2009), 877, pp. 1117.

12. Haynes, W.M., CRC Handbook of Chemistry and Physics, 91st edition, Taylor & Francis Group: Oxford, (2010), 2610 p.
13. Harris, D.C., Quantitative Chemical Analysis, 6th edition, Macmillan: New York, (2002), 928 p.
14. Paull, B.; Bashir, W., *Analyst*, (2003), 128, pp. 335.
15. Svec, F.; Tennikova, T.B.; Deyl, Z., Monolithic materials: Preparations, Properties and Applications, 1st edition,. Amsterdam: Elsevier, (2003), 773 p.
16. Svec, F., *J. Chromatogr. B*, (2006), 841, pp. 52.
17. Rohr, T.; Yu, C.; Davey, M.H.; Svec, F.; Frechet, J.M.J. *Electrophoresis*, (2001), 22, pp. 3959.
18. Rohr, T.; Hilder, E.F.; Donovan, J.J.; Svec, F.; Frechet, J.M.J., *Macromolecules*, (2003), 36, pp. 1677.
19. Nesterenko, E.P.; Yavorska, O.; Macka, M.; Yavorskyy, A.; Paull, B., *Anal. Methods*, (2011), 3, pp. 537.

CHAPTER 4.

PHOTO-INITIATED MONOPLOT COLUMN FABRICATION AND EVALUATION

Relevant publications:

Collins, D.; Nesterenko, E.; Brabazon, D.; Paull, B.; *Anal. Chem.*, (2012), 84, 7, pp. 3465–3472.

Abstract

PLOT columns possess a porous layer of stationary phase covering the inner surface of the capillary tubing, preserving an open-tubular structure after the completion of all column preparation steps. One of the main difficulties in the fabrication of photo-initiated monoPLOT columns is achieving a uniform porosity in the monolith, or across the porous layer. In most commercially available UV reactors, the light source is commonly located on the top at the oven, thereby providing UV light from one direction only. Such ovens rely heavily on diffuse reflection and scatter within the oven to effectively polymerise the target. For such UV reactors, it has been shown that the layer thickness and polymer density of the monolith are higher on the side of the column facing the light source [3].

In the work presented in the current Chapter, automated monoPLOT column fabrication techniques, based upon both UV and IR-induced photo-initiation are presented. As part of this work, several novel pieces of instrumentation were developed to aid in the fabrication process. The developed approaches allow the preparation of columns of varying length due to an automated capillary delivery method, with precisely controlled and uniform layer thickness and monolith morphology, from controlled optical power and exposure time.

For the technique involving UV-initiated polymerisation, the relationships between direct exposure times, intensity and layer thickness were determined, as were the effects of capillary delivery rate (indirect exposure rate), and multiple exposures on the layer thickness and axial distribution. Layer thickness measurements were taken by scanning electron microscopy (SEM), with the longitudinal homogeneity of the stationary phase confirmed using scanning capacitively coupled contactless conductivity detection (sC4D).

The new automated UV polymerisation technique presented in this work allows the fabrication of monoPLOT columns with a very high column-to-column production reproducibility, displaying a longitudinal phase thickness variation within ± 0.8% RSD. Preliminary work in the development of IR-initiated polymerisation of monoPLOT columns and the optimisation of the technique relative to the polymerisation and porogen mixtures is also investigated. Chromatographic test separations of proteins on columns produced by both UV and IR photo initiation are also presented.

Aims

The aim of the work presented in this chapter was to develop a reproducible method for the controlled photo-initiated polymerisation for the production of PLOT chromatographic columns in both the UV and IR range. The method offers a simple, highly controllable solution to the complex task of manufacturing bonded phase porous layer open tubular columns by photo polymerisation.

4.1 Introduction

Porous layer open-tubular capillary columns possess a porous layer of stationary phase attached to the inner surface of the capillary tubing, maintaining an open-tubular structure after the completion of all column fabrication steps. Chromatographic separations on modern PLOT columns can result from various solute−sorbent interactions, in addition to simple partitioning, involving a wide variety of functionalised surfaces. Over the past few decades, numerous PLOT columns have been developed and applied in many different areas of separation science. In GC, open tubular columns offer many advantages over their packed counterpart, notably high efficiencies, low back pressure, and fast analysis times. Typically, open tubular columns are produced by applying a layer of stationary phase onto the inner wall of the capillary. Since in many cases it is not chemically bonded to the capillary, the stability of this stationary phase layer ultimately depends on the constant nature of the surface tension forces that hold it to the column wall. These surface tension forces can be reduced with an increase in temperature or by the solutes passing through the column. As a consequence, the stationary phase film can suddenly break up and wash off the column – this is known as column bleed.

Bonded (or immobilised) wall coated stationary phases (where the stationary phase is polymerised in-situ), are highly desirable as the stationary phase is extremely stable and much less prone to column bleed. PLOT structures provide high capacity separations due to their higher surface area as compared with non-porous, wall-coated polymeric coatings (WCOT). The commercial techniques used in the immobilisation of stationary phases on the walls of capillary columns are highly proprietary and there are few bonded porous layer polymeric stationary phases commercially available. The lack of bonded polymeric PLOT

columns for GC is due to the many problems associated with the manufacture of such a column. Firstly, as suggested, the stationary phase must be bonded to the wall of the capillary, ideally polymerised in-situ. This is extremely difficult to do even on a short column, and so producing long columns as might be used in GC (>10 m) presents even more difficulties.

Open tubular columns were initially proposed for GC by Golay [1] and, following this pioneering development, OT capillary GC has practically replaced packed-column GC for most analytical applications, with PLOT columns now well-established as a common OT column format [2]. Furthermore, electrophoretic methods, such as capillary zone electrophoresis (CZE), are predominantly OT capillary-based, with related techniques, such as capillary electrochromatography (CEC), having been developed using not only particle-packed and monolithic-type stationary phases, but also now commonly with PLOT columns [3-6]. In addition to the above techniques, the application of PLOT columns to micro-solid phase extraction (μ-SPE) has also been reported [7,8]. As far back as the late 1970s, there have been attempts to apply OT format columns to LC separations [9-11], although, in most early cases, practical and instrumental restrictions meant that only limited interest was generated. Over the past decade, most instrumental issues have been largely resolved, and sensitive small volume detectors, compatible with capillary format, together with gradient pumps capable of sub μL/min flow rates, have become readily available. This has seen OT capillary-LC, and, in particular, the use of PLOT columns in LC attracting considerable attention. Indeed, recently, the use of PLOT capillary columns for high-efficiency and high-peak-capacity separations, coupled with mass spectrometric detection, in areas such as proteomics, has been reported by several leading groups [12-14]. In

addition, recent studies into the optimal structures for PLOT columns in liquid chromatography for high-efficiency separations have also been reported [15]. One approach to produce the stationary phase within PLOT columns is to immobilise a thin layer (usually <10 μm) of small particles to the inner surface of the capillary column. This has been shown with metal oxides [16], carbon, molecular sieves [2], metal nano-particles [17], and various derivatives of styrene [7,18] However, a potential disadvantage of this approach is the leaching or bleeding of particles from the wall over time, which affects not only the separation performance, but also may result in damage of detectors, especially mass spectrometers. An alternative approach is the direct covalent attachment of a porous polymer layer to the inner surface of the capillary tubing. This type of stationary phase can provide a highly developed surface area, as required for chromatographic performance and capacity, and is also both physically and chemically stable, for example, being compatible with both basic and acidic buffer systems. In addition, the use of such porous polymeric stationary phases provides the substrate upon which surface chemistry can be relatively easily varied, through simple surface modification procedures, which can be carried out in-situ. To date, the majority of PLOT columns produced, based on immobilisation of a polymeric phase as a single porous layer (monolithic structure) onto the inner surface of the column tubing, have been obtained through the application of thermally initiated polymerisation [14,5,6,19-22]. A thermally initiated approach to polymerisation is discussed in detail in Chapter 5.

4.1.1 UV initiated monoPLOT columns

Recently, several research groups have presented PLOT columns produced by UV-initiated polymerisation [3,25,26]. Eeltink *et al.* [3] prepared capillary columns with methacrylate ester-based monolithic-type porous polymer coatings via UV initiated free-radical polymerisation of butylmethacrylate and a cross-linker (ethylene dimethacrylate), using 1-octanol as a porogen. However, it was shown that obtaining a uniform polymer layer is a non-trivial task. If the capillary filled with the polymerisation mixture was placed under a UV light source, where it remained motionless during all the irradiation time, the resulting polymer coating was found to be non-uniform. Rotation of the capillary at 100 rpm during polymerisation resulted in the formation of a more uniform layer; however, the overall technique could only produce relatively short PLOT columns, restricted by the UV chamber dimensions. Abele *et al.* [25] recently introduced a novel evanescent wave (EW)-initiated photo-polymerisation technique, using a single light-emitting diode (LED) for the fabrication monolithic PLOT columns. The EW photo-polymerisation was induced by the evanescent field created at the inner wall of a transparent polytetrafluoroethylene-coated fused silica capillary illuminated axially and acting as a light waveguide. The authors proposed the resultant PLOT columns for use as capillary reactors, within nano-liquid chromatography (nano-LC), CEC, and related separation methods. It was shown that columns with a layer thickness ranging from 2 μm to 25 μm were obtained; however, again, only short columns (<11 cm) could be produced using this approach, as layer thickness would vary along the column length, decreasing with the increase of distance from the light source increased, because of attenuation within the silica medium. Following this work, Nesterenko *et al.* [26] reported the preparation of slightly longer monoPLOT columns using an automated UV scanning technique. In this work, capillaries filled with polymerisation

mixture were repeatedly exposed to light from the scanning source at a wavelength of 365 nm. The UV source was moved along the length of the capillary column at a uniform scan rate and for an optimized length of time (up to 25 min). The monolithic phase was formed during this perpendicular illumination. This method resulted in the fabrication of columns with a very uniform layer thickness which was confirmed using sC4D. However, using this method, it was only possible to produce columns as long as 30−40 cm. Therefore, it can be seen that the preparation of surface bonded porous phases within open-tubular columns, of a uniform layer thickness and able to provide sufficient phase capacity for application within capillary-LC, still remains a considerable challenge. It should be noted that sC4D is not suitable for characterising the pore morphology of the monolith and is only sensitive to large scale morphological features such as layer thickness, voids, etc.

4.1.2 IR initiated monoPLOT columns

There have been very few works reported on the fabrication of polymer monolithic phases at wavelengths > 400 nm. Dulay *et al.* [34] performed the first monolithic synthesis at wavelengths outside the UV region by forming a sol-gel stationary phase in polyimide coated capillary at 470 nm. More recently, Walsh *et al.* [35] also produced polymer monoliths using 470 nm and also in polyimide coated media using LED sources at 660 nm [37].

4.2 Experimental

4.2.1 Materials

For the development and construction of the UV/IR reactor unit and flow-through curing oven, and the fabrication of photo-initiated monoPLOT columns the following materials were used:

- Boxes and enclosures were purchased from Radionics Ltd., (Dublin, Ireland).
- Rapid prototype parts were produced as per Section 2.2.1.
- Raw materials (aluminium, stainless steel, etc) were purchased from Alperton Engineering Ltd., (Dublin, Ireland).
- Fabricated parts (such as reactor chamber, feed through mechanism, motor mounts, etc) were manufactured in-house.
- Electronic components were purchased from Radionics Ltd., (Dublin, Ireland) and Farnell Ltd., (Leeds, United Kingdom).
- Circuit boards were designed in-house and fabricated by Beta Layout Ltd., (County Clare, Ireland).
- Fabrication of system board, circuits and enclosure were done by Heery Technologies (Kells, Co. Meath, Ireland).
- Teflon and polyimide coated (15 μm thickness) fused silica capillary, 25, 50, 75, and 100 μm ID, 0.375 mm OD was purchased from Composite Metal Services Ltd., (Charlestown, United Kingdom).

4.2.2 Reagents

All chemicals were reagent or analytical grade purity. For the fabrication of monolithic stationary phases, reagents and chemicals used were as per Sections 2.2.2 and 3.2.1. Additional reagents used during the IR fabrication of monoPLOT columns included:

- 4-vinylbenzyl chloride, isopropanol, trifluoroacetic acid, and *N*-methoxy-4-phenylpyridinium tetrafluoroborate (MPPTFB) were purchased from Sigma-Aldrich (Gillingham, U.K.).
- N,N Dimethylacrylamide was purchased from Spectra Group Ltd., (Millbury, Ohio, United States).
- The IR initiator, 2-[2-[2-chloro-3-[(1,3-dihydro-1,1,3-trimethyl-2*H*-benz[e]indol-2-ylidene) ethylide- ne]-1-cyclohexen-1-yl]ethenyl]-1,1,3-tri-methyl-1*H*-
- benz[e]indolium (H-Nu 815), and co-initiator, (butyltriphenyl-borate) borate V, were purchased from Spectra Group Ltd., (Milllbury, Ohio, United States).

4.2.3 Instrumentation

- For the evaluation of column longitudinal homogeneity, a TraceDec capacitively coupled contactless conductivity Detector (Innovative Sensor Technology GmbH, Strasshof, Austria) was used. Settings for scanning the column were as follows: frequency, 3× HIGH; voltage, −6 dB; gain, 50% and offset, 0.
- Additional instrumentation used during the fabrication process are as listed in Section 3.2.2.

4.2.4 Software

- Design software used during the development of the UV/IR ovens are as listed in Section 2.2.4.
- For the data acquisition TraceDec Monitor V. 0.07a software (Innovative Sensor Technology GmbH, Strasshof, Austria) was used.

4.2.5 Experimental procedures

4.2.5.1 Capillary silanisation

Capillary silanisation was carried out as per the procedure in Section 2.2.5.1.

4.2.5.2 Formation of free-radical layer on capillary wall

In order to facilitate the formation of a more uniform layer during UV polymerisation, silanised capillaries were further treated with benzophenone to introduce a layer of free radicals on the inner surface of the capillary. For this, a solution of 50 mg of benzophenone in 1 mL of MeOH was prepared, vortexed and deoxygenated under a flow of nitrogen for 10 min. The desired length of silanised capillary was filled with the mixture and exposed to 1 J/cm2 of UV radiation at 254 nm. The capillary was subsequently washed with MeOH for 30 min at a flow rate of 3 μL/min.

4.2.5.3 Fabrication of reversed-phase BuMA-EDMA monoPLOT columns by UV photo-initiation

The monomer mixture used consisted of 24 %wt BuMA, 16 %wt EDMA, 60 %wt 1-decanol, and 0.4 %wt dimethoxy-2-phenyacetophenone, with respect to monomers. The mixture was prepared by first dissolving initiator in the porogen, followed by the addition of the monomers. The solution was vortexed and deoxygenated under a flow of nitrogen for 10 min. The desired length of pretreated capillary was filled with the monomer mixture and the ends of the capillary were sealed with rubber septums. The filled capillary was loaded and aligned into the flow-through UV reactor, and the speed and intensity settings on the device were set to the desired values. For static tests, the capillary was kept stationary and was subjected to the desired amount of UV radiation through timed exposures and irradiation intensity variation. For dynamic tests and fabrication of monoPLOT columns, the UV LEDs were first switched on and then the capillary was fed at a fixed rate through the UV chamber, the linear rate being chosen to give the desired exposure time. For multiple exposures, the capillary was passed through the chamber the appropriate number of times in order to provide the required amount of radiation. After each pass, the feed motor was reversed once the end of the capillary was reached and the next run was then started. After the completion of all desired steps, the capillary was drawn out from the UV chamber and both ends of the capillary were removed as the last few centimetres of capillary at each end received higher doses of radiation, due to the way the capillary was loaded into the device. Post curing, the resultant monoPLOT column was washed with MeOH at a flow rate of 1 μL/min for 1 hr to remove residual porogen and unreacted monomers.

4.2.5.4 Fabrication of reversed-phase PS-DVB monoPLOT columns by IR photo-initiation

The monomer mixture consisted of 12 %wt styrene, 12 %wt 4-vinylbenzenyl chloride, 16 %wt divinylbenzene; the composition and ratio of both the porogen mixture and initiator was varied during the experiment, see Section 4.4.2. The mixture was vortexed, centrifuged for 1 min at 13,000 RPM, the supernatant removed, and deoxygenated under a flow of nitrogen for 10 min. The desired length of silanised capillary was filled with the monomer mixture and the ends of the capillary were sealed with rubber septums. The capillary was coiled and loaded into the UV/IR chamber. Chamber power was set to 2 mW/cm^2 for each polymerisation and curing time varied. Post curing, the resultant monolithic column was washed with MeOH at 1 μL/min for 1 hr to remove residual porogen and unreacted monomers.

4.2.5.5 Preparation of standard solutions

Standard solutions were prepared as per Table 4.1.

Table 4.1 – Preparation of standard solutions

Analyte	**Solvent**	**Concentration** *(mg/mL)*
Insulin *(INS)*	0.1 % TFA in H_2O	0.01
Ribonuclease B *(RNase B)*		0.005
Trypsin *(TRY)*		0.02
Ribonuclease A *(RNase A)*		0.01
Cytochrome C *(Cyt C)*		0.01
Myoglobin *(MB)*		0.012
Horseradish Peroxydase *(HRP)*		0.04
Phosphatase B *(PP2)*		0.08
Carbonic Anhydrase *(CA)*		0.02
Concanavalin A *(Con A)*		0.01

4.3 Theory

There have been many studies devoted to the mechanism of the formation of polymer phases within PLOT columns [27−29]. Various parameters, such as surface-to-volume ratio, polymerisation kinetics, surface tension at the capillary inner wall, and wettability with the polymerisation mixture affect the formation of the monolith in capillaries with ID < 10 μm, resulting in deviation from the bulk porous structure and leading to the formation of PLOT columns.

The classical equation for the polymerisation rate is given as:

$$R_P = \frac{k_P}{k_t^{0.5}}[M]\left(\frac{R_i}{2}\right)^{0.5}$$

eq. (4.1)[30]

where:

$[M]$ = concentration of monomer

R_i = initiation rate

k_p = coefficient of propagation rate

k_t = coefficient of termination rate

However, in the case of photo-initiated reactions, this equation takes the form:

$$R_P = \frac{k_P}{k_t^{0.5}}[M](\Phi\, I_a)^{0.5}$$

eq. (4.2)

or

$$R_P = \frac{k_P}{k_t^{0.5}}[M](\Phi\, I_O[1-\exp(-\varepsilon[\ln]b)])^{0.5}$$

eq. (4.3)

where:

Φ = quantum yield for initiation

I_a = absorbed light intensity

I_O = incident light intensity

ε = extinction coefficient

[In] = photo-initiator concentration

b = layer thickness

It can be seen from eq. (4.3) that the rate is directly proportional to the light intensity, I_a. As a result, variation of light becomes a key factor to the control of polymer layer growth.

4.4 Design and development

4.4.1 UV/IR reactor

A UV/IR reactor comprised of 60 LEDs (30 of each type) with wavelengths of 365 and 830 nm respectively was developed, shown in Figure 4.1. LEDs were chosen as a light source as they are available in many different wavelengths, they are cheap, and although providing less optical power compared with bulbs, their intensity may be varied or indeed the light can be pulsed; using bulb light sources neither of these is possible. The reactor was constructed from a standard electrical acrylonitrile butadiene styrene (ABS) enclosure with dimensions of 190 x 110 x 65 mm and allowed both static and flow-through

polymerisation. The latter one is performed when the polymerisation mixture is pumped through the stationary capillary. The UV/IR oven was capable of supplying 1.8 – 2.4 mW/cm^2 of IR light at 830 nm and 12 – 37 $\mu W/cm^2$ of UV light at 365 nm.

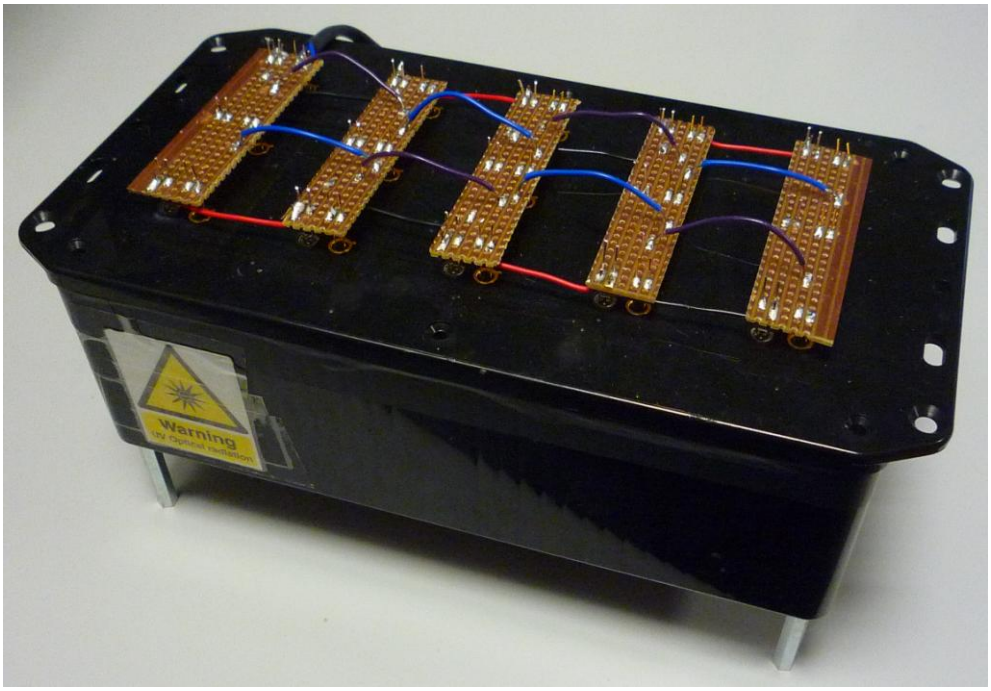

Figure 4.1 – Exterior of UV/IR oven.

The inside of the oven (Figure 4.2) was lined with aluminium foil in order to provide highly reflective surfaces and improve homogeneity of light intensity in the centre of the box. However, this arrangement proved to be problematic during polymerisation of IR initiated monoliths (see Section 4.5.2) as the majority of the incident light was above and below the capillary resulting in a non-uniform polymer layer structure.

Figure 4.2 – Interior of UV/IR reactor.

Small apertures were made in the centre of each side of the reactor for the introduction of the capillaries into the chamber and for supporting capillaries equidistant from the light sources in order to ensure as homogeneous irradiation as possible. This system was tested for the fabrication of both fully polymerised and monoPLOT columns by IR and UV initiation in both static and flow through conditions. This oven was developed as a proof of principle device and precursor to the feed through oven which is described in Section 4.4.2.

4.4.2 UV/IR feed-through curing oven

A prototype feed-through UV curing oven was designed and built for the fabrication of monoPLOT columns of variable length and phase thicknesses. The design of the oven unit takes into consideration the different media that may be polymerised through UV and IR initiation, i.e. capillary columns etc., thus it was necessary to provide a means by which capillary columns of extended length may be polymerised, such as columns that may be used in GC. The oven uses a polar array of UV and IR LEDs mounted around the circumference of a hollow tube (the reaction chamber), see Figure 4.3. These LEDs have a wide viewing angle, meaning that they emit light from the face of the light source at a highly divergent angle. The oven was capable of supplying 12.5 – 16.5 mW/cm^2 of IR light at 830 nm and 50 – 172 $\mu W/cm^2$ of UV light at 365 nm.

The device was equipped with guides allowing the capillary to be passed through the centre of the oven in order to provide most uniform exposure along the length of the capillary from all sides. A simplified schematic of the assembly is shown in Figure 4.4. Feeding the capillary through the chamber allows the manufacture of columns of various length, even over dozens of meters. The internal surfaces of the oven were coated with highly reflective paint, to ensure the emitted light is directed towards the centre of the oven where the capillary is fed through. The capillary is fed through the oven using a set of motorised guide rollers. The speed of the guide rollers can be adjusted allowing the exposure time per unit length of the capillary to be very accurately set. In addition to the draw speed, the intensity of the light can be adjusted and irradiating light can also be pulsed. These configurable settings give a high level of control to the polymerisation process.

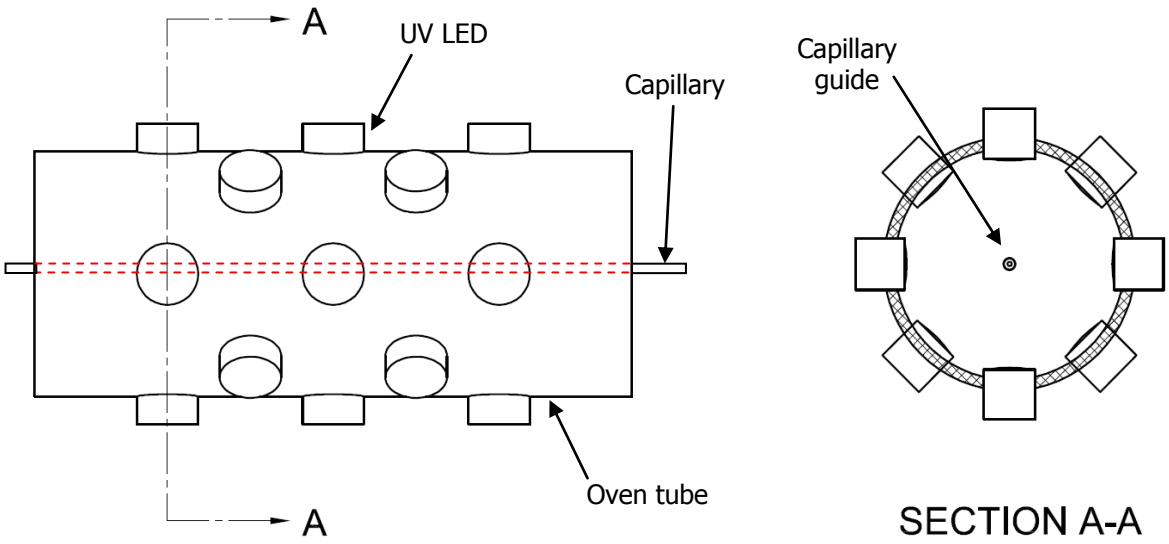

Figure 4.3 – Schematic of UV/IR reactor chamber constructed from a polar array of UV LEDs.

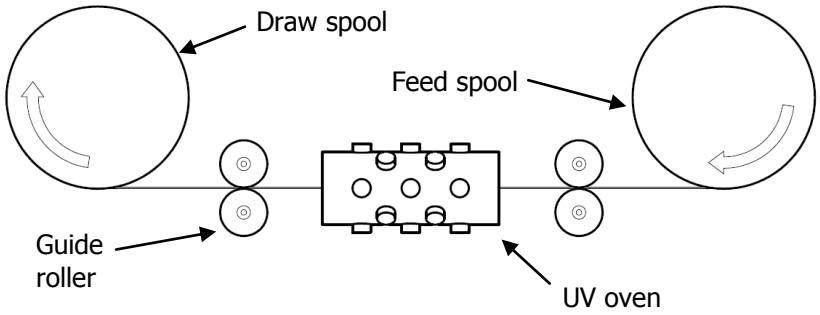

Figure 4.4 – Schematic of UV/IR oven, guide rollers and spool assembly.

A photodiode for monitoring the intensity of the light was mounted inside the UV oven and provided constant feedback. This input was brought back to the control board and used to control the output to the LEDs (i.e. the intensity of the light) through a PID loop.

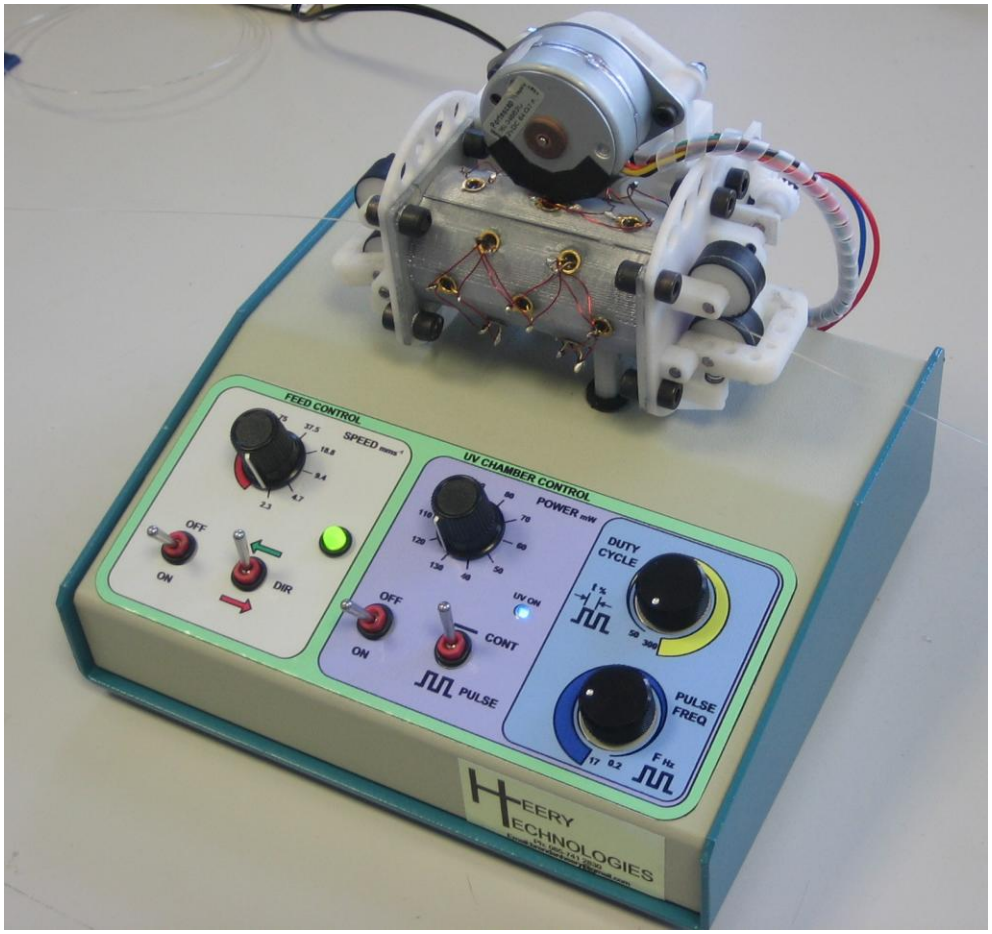

Figure 4.5 – UV/IR oven showing chamber, feed mechanism, and control unit.

The system was tested in both static and dynamic conditions for fabrication of both short (<10 cm) and long (>1 m) monoPLOT columns and the effect of light intensity and exposure time on layer thickness in both modes was studied. The work shows that, by altering the intensity and exposure time, and through repeated exposures, it was possible to fabricate monoPLOT columns with uniform layer thicknesses ranging from <100 nm to several micrometers.

4.5 Results and discussion

4.5.1 monoPLOT fabrication by UV initiation

Within a fused-silica capillary, particularly where the inner surface has been pretreated with initiator, polymer growth is thermodynamically favoured to occur from the capillary wall inward. This is even more so with photo-initiated polymerisation, because light intensity will decrease radially toward the center of the capillary. Where polymerisation conditions are limited by either time or dynamic flow, a porous layer structure results, rather than complete polymerisation throughout the capillary. Early attempts to produce photoinitiated monoPLOT columns [26] were conducted while using simple silanisation of the capillary walls with trimethoxysilylpropyl methacrylate. Although showing promising results, this approach would often lead to the formation of a non-uniform layer or areas of the capillary wall, where little or no polymerisation would occur (Figure 4.6(a)). For columns with a thicker polymer layer, this problem was more pronounced and clearly visible. In the production of PLOT columns, it is important that homogeneity is maintained as the layer thickness increases. If the layer does not grow at the same rate around its circumference, the thicker regions will continue to grow at a faster rate than the rest of the layer, which can eventually result in a partially blocked column or structural weakness within the monolith.

As a number of side reactions, such as recombination, may take place during the polymerisation process and due to inefficient synthesis of the radical species, chain reaction initiation never occurs 100% efficiently. In order to increase the efficiency of the initiation reaction and to facilitate more uniform layer growth, it was decided to introduce an additional capillary pretreatment step, namely the grafting of benzophenone, a radical polymerisation initiator, directly onto the surface. This ensured initiation of the

polymerisation reaction with equal probability along and around the inner walls of the capillary column. For the proof of this concept, two sample monoPLOT columns were prepared under similar conditions; however, one column was subjected to a benzophenone pretreatment, while the second one was only silanised. As it can be seen from the Figure 4.6(b), pretreatment with benzophenone led to the formation of a far more uniform monolithic layer.

(a) 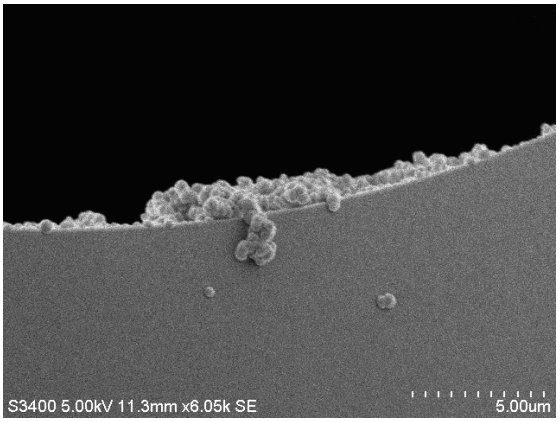

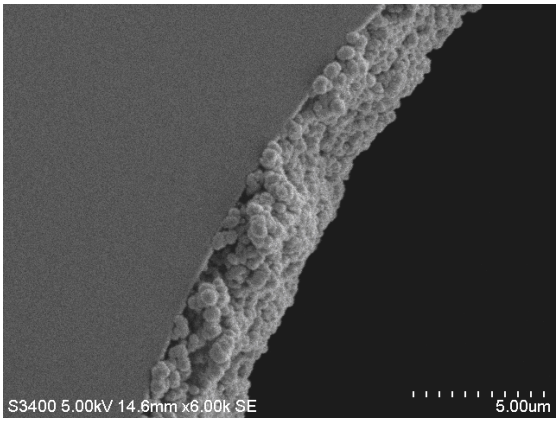

(b)

Figure 4.6 – SEM images of a polymer layer formed (a) on a silanised surface and (b) on a silanised surface also treated with benzophenone.

The effects of light intensity and exposure time were investigated in a series of static tests. It is known that the kinetics of the UV initiated reaction (and, as a result, its speed) is dependent on the light intensity [30], as it was shown earlier eq. (4.3) in Section 4.3. Initial studies were carried out to determine the useful operating limits of the device, with respect to the intensity setting of the UV LEDs and the exposure time to which the capillary was subjected. These limits were determined through fabricating monolithic layers within 100 μm ID capillary, varying both UV light intensity and exposure time. It was found that the optimum range for the optical power of the chamber was 5−7 mW (66 – 92 μW/cm^2). At low power settings, below 4 mW, polymerisation was very slow and the resulting layer was

very fragile. Above 7 mW, polymerisation occurred at such a fast rate that it was almost impossible to control it, making the fabrication of a uniform layer extremely difficult. It was also observed that fabrication at high power settings often resulted in partial or complete over polymerisation of the capillary. It was found that the morphology of the polymer layer can also be varied through the adjustment of the UV light intensity. Thus, at 2 mW, polymerisation was extremely slow and the resultant polymer layer exhibited larger pore sizes, namely, 1.25 ± 0.38 μm (measured from SEM images, n = 15) and a less-uniform structure (see Figure 4.7a).

(a) 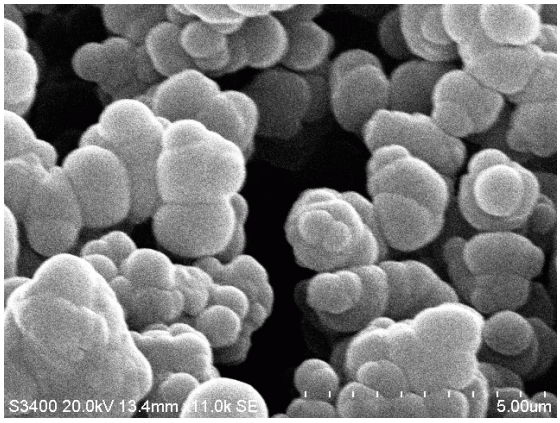

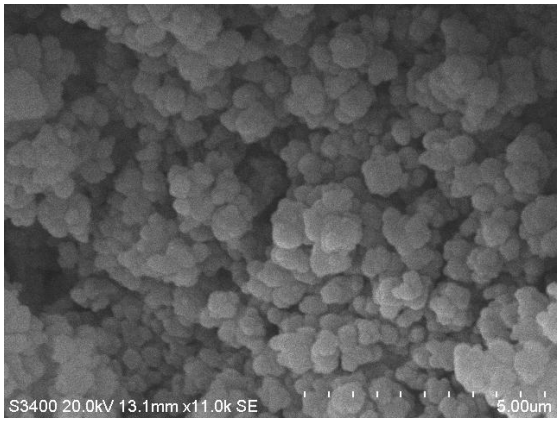

(b)

Figure 4.7 – SEM images showing the different morphology of the polymer monolith layer at two different power settings: (a) 2 mW and (b) 7 mW.

However, the use of higher power settings provided the formation of pores of smaller dimensions: 0.68 ± 0.17 μm at 6 mW, and 0.47 ± 0.16 μm at 7 mW (Figure 4.7(b)). This shows that the UV light intensity has an effect on polymerisation thermodynamics similar to that of temperature in thermally initiated polymerisation, where the reaction rate is slower at lower temperature and increases with higher temperature [31]. First, the initiation rate in the case of non-chain initiator decay is proportional to the efficiency of the initiator (*f*, which is usually between 0.5 and 1.0), the constant of the initiator decay, k_d, and the

initiator concentration, [*In*].

$$R_i = 2 f k_d [\ln]$$

eq. (4.4)[30]

However, the rate of polymerisation is dependent on light intensity (eq. (4.3)), providing a higher polymerisation rate at higher intensity. Since the formation of new polymerisation centers is faster than the growth of globules, the supply of monomers runs low more rapidly and the number of globules is large, but their size remains small, which leads to smaller voids between globules. Two sample SEM images showing the layers formed at two different power settings but with the same exposure time are also shown in Figure 4.8(a) and (b). The difference in layer thickness is clear; however, it was also possible to see a variation in the morphology of the polymer layer, with a larger globule and pore size for the 6 mW exposure (Figure 4.8(a)), compared to the higher power 7-mW exposure (Figure 4.8(b)).

(a) 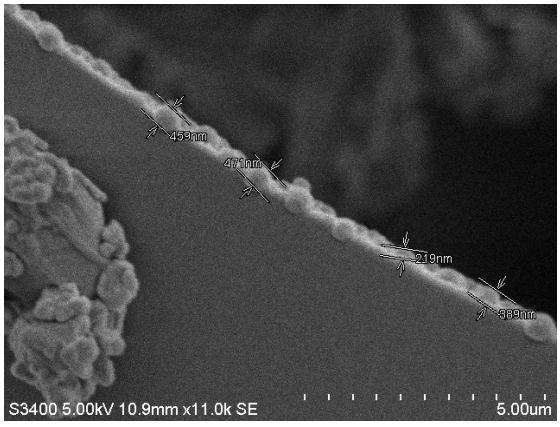

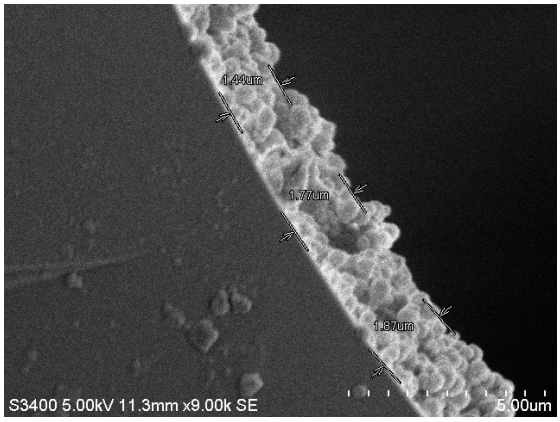

(b)

Figure 4.8 – SEM images of the monoPLOT layer prepared via UV irradiation at (a) 6 mW for 18 s and (b) 7 mW for 18 s.

The next experiments were carried out to measure the average thickness of the monolith layer at increasing exposure times, and this was performed at three different power settings

between 5 and 7 mW. Exposure times were varied from 7 s to 25 s. For each monoPLOT column fabricated under a particular condition, the layer thickness was determined from SEM images. Figure 4.9 shows the relationship between exposure time and layer thickness for different power and time settings. It can be seen that the thickness of the polymer layer grows exponentially with time. Such behavior can be explained from consideration of reaction kinetics. Eq. (4.3) also shows that the rate of the reaction is dependent on the layer thickness, *b*; thus, the thicker the layer, the more negative the exponent value becomes, and, as a result, the reaction rate increases. However, the variation in layer thickness homogeneity also increases at higher exposure times and with increasing intensity of the incident light. This creates a problem, because, in order to achieve the optimum morphology in the polymer layer, it is necessary to polymerise within this given intensity range; however the rate of polymer growth at these intensities

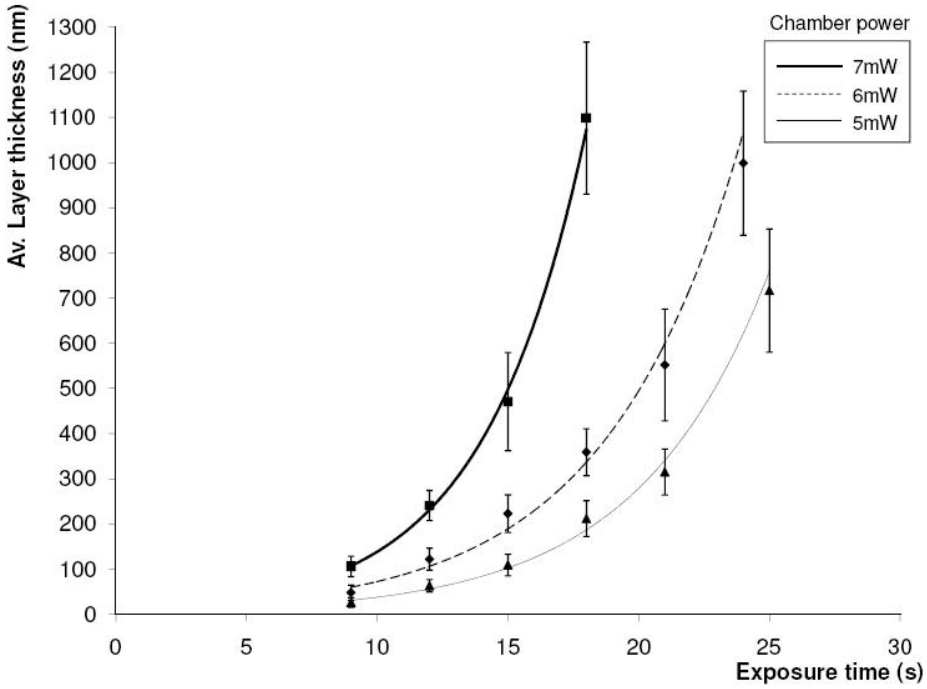

Figure 4.9 – Plot of average layer thickness against exposure time for power settings of 5, 6, and 7 mW.

is extremely high, and, therefore, control of exposure time must be very precise. The developed approach to column fabrication was readily amenable to both flow-through polymerisation and timed exposure experiments. Therefore, to investigate the possibility to more precisely control monoPLOT layer formation (without changing the composition of the monomer mixture), two new polymerisation approaches were investigated using the device. These were (1) pumping the monomer mixture through the capillary during polymerisation, "flow-through polymerisation", and (2) multiple exposures, irradiating the monomer filled capillary with several repeated short exposures. Flow-through polymerisation was investigated as an approach, because the liquid flow would remove short polymer chains and supply fresh monomer mixture, facilitating polymerisation specifically on the sites that are already attached to the capillary walls, providing more-uniform layer growth. The monomer mixture was pumped through the capillary at a fixed flow rate of 1 μL/min, corresponding to a linear velocity of 2.1 mm/s in a 100-μm capillary. This low flow rate was chosen to minimise any damage to the monolithic layer forming during polymerisation by other polymerised particles that could be caught in the flowing stream. It was observed that flow-through polymerisation greatly reduced the rate of growth of the polymer layer, giving a more linear relationship between exposure time and layer thickness. Comparative images for monoPLOT columns prepared in flow-through and static conditions can be seen in Figures 4.10(a) and 4.10(b), respectively.

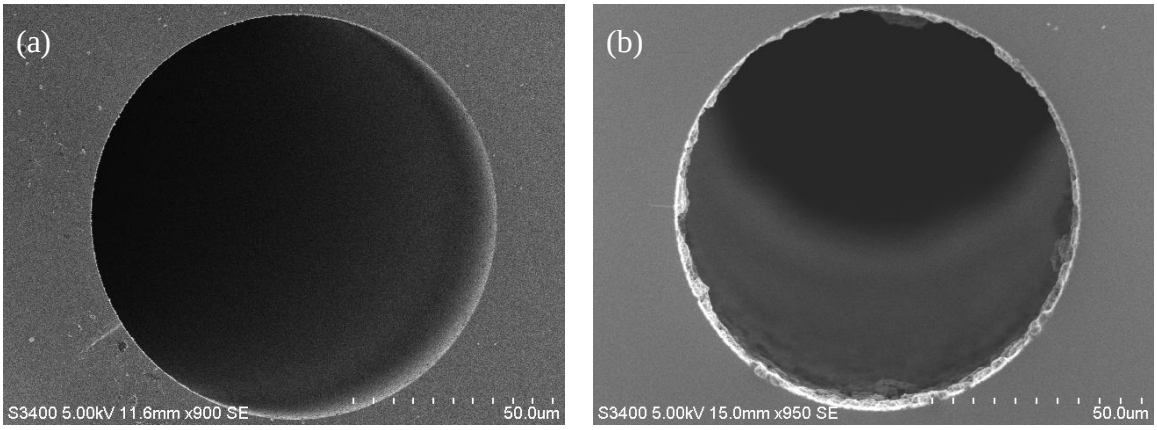

Figure 4.10 – Comparison of two monoPLOT columns polymerised under (a) static and (b) flow-through conditions.

The columns produced under flow-through conditions were exposed to UV light at 7 mW for 65 s, receiving a total dosage of 455 mJ. However, static exposure to 455 mJ would result in complete polymerisation across the capillary. The column produced under static conditions was exposed to light, also at 7 mW, but for just 13 s, giving a dosage of 91 mJ. The average layer thickness for the column prepared by flow-through polymerisation was 332 nm, whereas for the static approach, it was 1.4 μm. It is worth noting that the flow-through approach produced a polymer layer, which, although thinner, was extremely uniform along the length and circumference of the column. It is also worth noting here that the monomer mixtures used in both the static and flow-through polymerisation were identical. In both instances, the monomers were used without removal of any polymerisation inhibitors; as such, the changes in the rate of polymerisation observed could only be attributed to the physical differences in the polymerisation process using the two approaches. One of the advantages of the photo-initiated polymerisation is the ability to initiate and halt the reaction relatively rapidly, compared to thermally initiated polymerisation approaches [30]. Applying this approach, in which radicals are generated

over short periods of time, it was hoped that this situation would facilitate a more controlled polymerisation process and thus allow the fabrication of a more homogeneous layer. For multiple exposures, the polymerisation mixtures were similar to those discussed previously during static testing. However, in this instance, the full dose of radiation would be delivered in smaller discrete doses, thus controlling the duration of the reaction. Since the minimum draw speed of the device was 7.2 mm/s and the chamber length was 65 mm this gave a minimum dynamic exposure time of ~9 s. In order to record useful data at parameters that could be further used in dynamic testing, it was decided to use 9 s as the exposure time for each dose of UV energy. For the static study, a length of capillary was filled with a monomer mixture, as before, and aligned within the UV chamber. The polymerisation study, as described earlier, was repeated for three power settings; 5, 6, and 7 mW. However, in this case, the dose of radiation was given in 9 s doses, and the number of doses was varied. The resultant polymer layers were inspected and their thickness was measured as done previously, using SEM. A comparison of constant exposures against multiple short exposures (passes) for chamber powers of 6 and 7 mW is shown in Figure 4.11. It can be seen that, for a given total energy supplied, the rate of polymer growth for multiple exposures was considerably slower and therefore more controlled. In addition, when compared with the data shown in Figure 4.9, it can be seen that the variation in layer thickness is also much lower, compared to long single exposures.

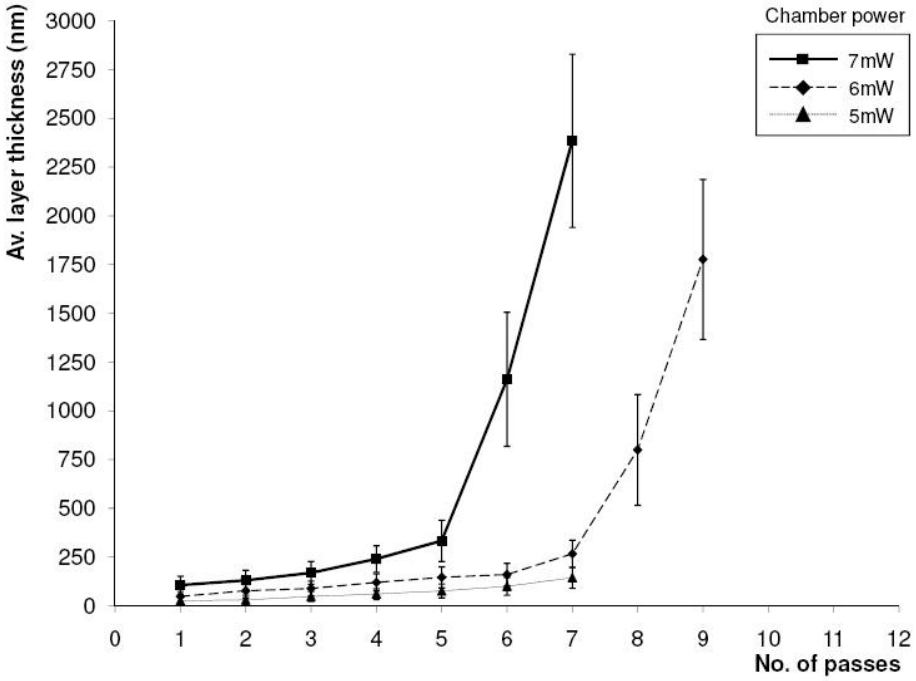

Figure 4.11 – Comparison of layer thickness for multiple exposures (passes) at 5, 6, and 7 mW for dynamic tests.

Using the results obtained from the above static tests, it was possible to determine the range of best parameters for dynamic tests and for polymerisation of longer monoPLOT capillary columns. Therefore, a length of pretreated capillary was filled with monomer mixture, and its ends were capped, and then the capillary fed into the UV reactor. For dynamic studies, the capillary was exposed to UV radiation while, at the same time, being drawn through the UV chamber at a fixed speed. In this case, the linear speed was set to its minimum value of 7.2 mm/s, giving each unit length of capillary an exposure time of 9 s for each pass. At a power setting of 7 mW, this corresponds to 63 mJ of energy per pass. A setting of 6 mW will yield 54 mJ per pass, and 5 mW will give 45 mJ. The results of this dynamic study can be seen in Figure 4.12.

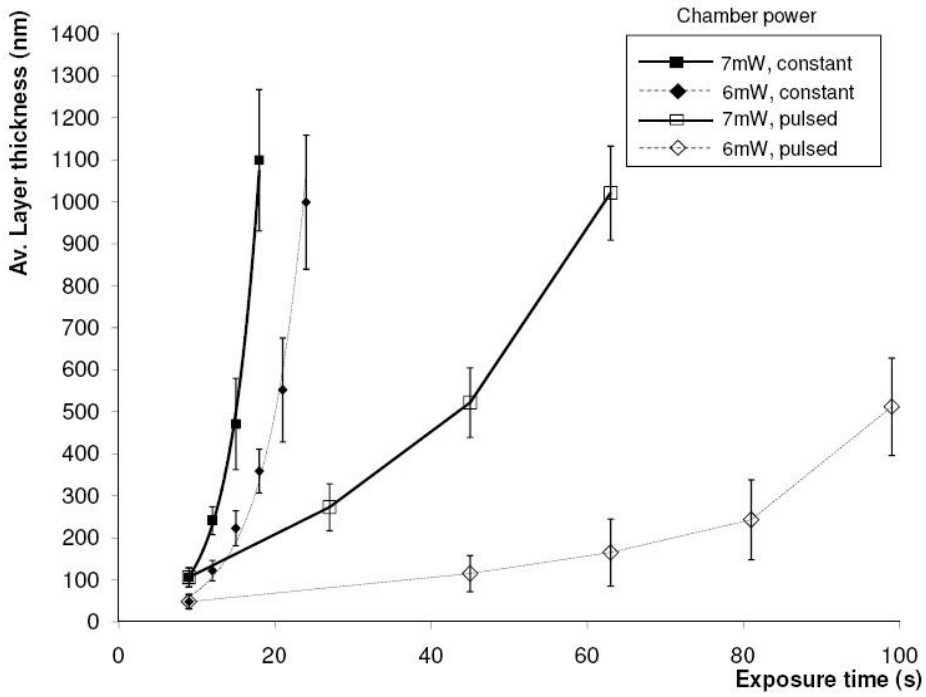

Figure 4.12 – Comparison of layer thickness at two different power levels, 6 and 7 mW, for both continuous and 9-s multiple exposures.

It was interesting to observe that the layer thicknesses obtained were considerably thicker compared to static tests, which were carried out under the same conditions and indicated that there was a far higher rate of polymer growth with longer capillaries. The reason for the increased rate of polymer growth is assumed to be from light scattering within the capillary. The propagation of light through fused-silica capillaries has already been well-documented [25,32] and it has been shown that the capillary can transmit a considerable amount of light along its length. During dynamic fabrication, the capillary was exposed to some UV radiation before being drawn into the UV chamber, because of light propagation along the capillary.

The same effect will also be present on the other side of the UV chamber, where the post exposure capillary was also further irradiated. This results in an overall thicker polymer layer, because the total dosage per unit length is higher. As part of the dynamic study, several long monoPLOT columns were formed, with lengths ranging from 300 mm to 1750 mm. All of these columns were characterised using sC4D, which is known to be a non-destructive technique for the characterisation of capillary stationary phases [33] and several were further evaluated via SEM analysis. The layer thickness measurements and homogeneity of one such 300-mm example is presented in Figure 4.13. The layer thickness was determined from the SEM images of the cross sections of the monoPLOT column. For this, a 300-mm-long monoPLOT column (after sC4D scan) was cut into thirty 10-mm-long sections and the layer thickness was measured from the SEM images (n = 30). Although layer thickness measurements were intermittent, it can be seen that the average thickness of the polymer layer is ~310 nm and it is consistent along the column. At the same time, the sC4D scan showed that the layer was homogeneous (sC4D RSD = 0.22%) and confirmed that there were no voids or blockages along the length of the column. Further work yielded a 1750-mm column and the sC4D characterisation of this column is shown in Figure 4.14. The RSD of layer thickness for this column is 0.78%. A 10-mm segment from the end of the column was removed and was further inspected via SEM, showing the resultant polymer layer to be very uniform with an average layer thickness of ~400 nm.

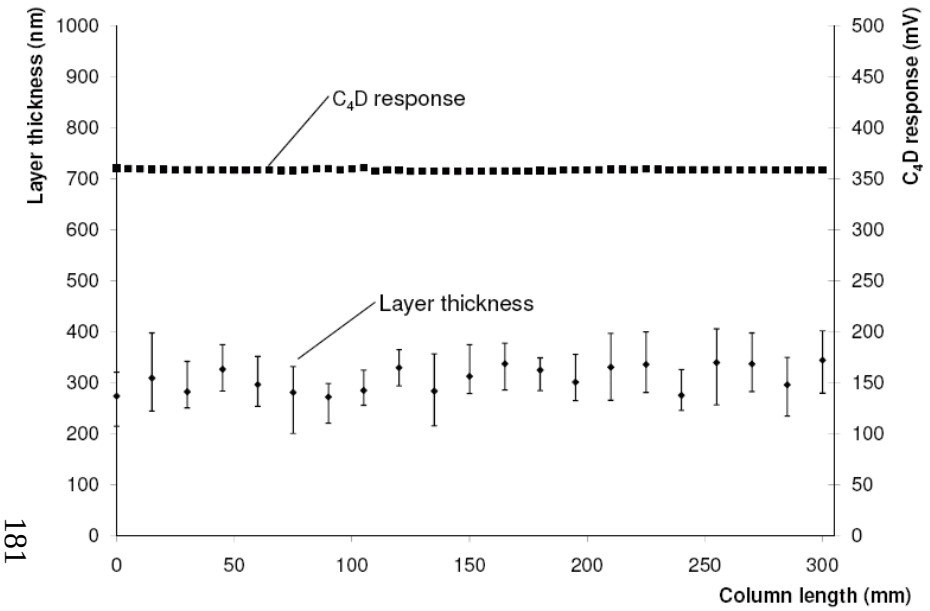

Figure 4.13 – Layer thickness and sC4D characterisation of a 300 mm column produced over five exposures at 7 mW.

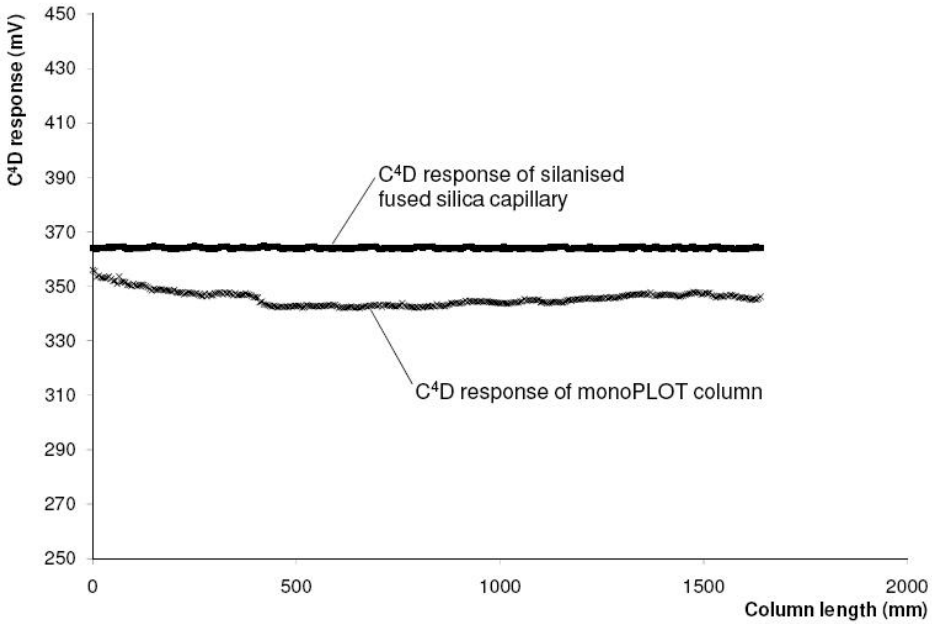

Figure 4.14 – sC4D characterisation comparison between a 1750 mm monoPLOT column produced over five exposures at 7 mW and a silanised silica capillary. Capillary feed rate was 7.2 mm/s, giving an exposure time of 9 s.

4.5.2 monoPLOT fabrication by IR initiation

As discussed earlier, very little work has been carried out on the fabrication of porous monolithic materials via IR-initiated polymerisation, yet photo-initiation by IR has many benefits. Polymerisation using IR light is advantageous mostly due to the fact that monolithic phases can be produced in polyimide coated capillary; this is not possible using UV light as polyimide absorbs strongly in the UV region and up to approximately 600 nm. Furthermore, compounds such as styrene also absorb in the UV region, thus making photo-initiation of styrene based stationary phases impossible using UV light. These limitations are discussed in further detail in Chapter 5. Exposure to IR light is also less damaging to the human eye or tissue making it far safer than UV. Thus, here the possibility of monoPLOT production via photo-initiation in the near IR range (830 nm) was investigated.

Another advantage of IR initiated reactions over UV initiated, particularly with regard to the manufacture of monoPLOT columns, is the high extinction coefficient, ε > 250,000 L/mol/cm (and thus corresponding high absorptivity) of the photo initiators used; in this case H-Nu 815. Light in the visible and IR region has a higher penetration ability compared to UV light [38], however, the use of an initiator with a high extinction coefficient leads to the absorbance of significantly more light and so the amount of light penetrating deep into the cavity of the capillary is greatly reduced. A high percentage of the incident light is absorbed by the polymerisation mixture at the walls of the capillary ID and so the growth of the polymer occurs almost exclusively from the capillary wall inwards. Using the Beer-Lambert Law an approximate comparison of the percentage of light transmitted ($\%I_O$) through a 100 μm ID capillary for three different photo initiators can be made – see Table 4.2.

Table 4.2 – Comparison of percentage of light transmission for three photo initiators

Initiator	*%wt*	*ε (L mol^{-1} cm^{-1})*	*Abs (AU)* *@1 μm* / *@100 μm*	*%I_O* *@1 μm* / *@100 μm*
DAP* *λ = 342 nm*	0.4	1.2 x 10^3	1.873 x 10^{-4} / 1.873 x 10^{-2}	99.9% / 95.7%
H-Nu 635† *λ = 635 nm*	0.4	2.3 x 10^5	1.242x 10^{-2} / 1.242	97.1% / 5.7%
H-Nu 815 *λ = 815 nm*	0.4	>2.5 x 10^5	1.324 x 10^{-2} / 1.324	96.9% / 4.7%

** 2,2-Dimethoxy-2-phenylacetophenone*

† 2,4,5,7-Tetraiodo-3-hydroxy-9-cyano-6-fluorone

From Table 4.2 it can be seen that for DAP used at a wavelength of 342 nm, the optical power of the light transmitted through to the opposite side of a 100 μm ID capillary is 95.7% of that of the incident light. This is highly problematic for the fabrication of a monoPLOT column since the optical power of the light at any location within the capillary is almost the same as that which is incident at the boundary of the capillary ID. However, for H-Nu 815, the intensity of the light at the opposite capillary wall has fallen to just 4.7% that of the incident light. Compared with photo initiation using DAP, this approach is much more favorable for the fabrication of open tubular formats. However, this method requires the use of a light source capable of providing an even coverage of light on all areas of the capillary since the penetrating ability of the IR light in such polymerisation mixtures is low. Figure 4.15 represents a good example of a PS-DVB polymer layer formed using this method with a non-homogenous light source. In this case the IR light was provided from above and below the capillary using the device described in Section 4.3.1 and the effect on the monolith growth can be clearly seen.

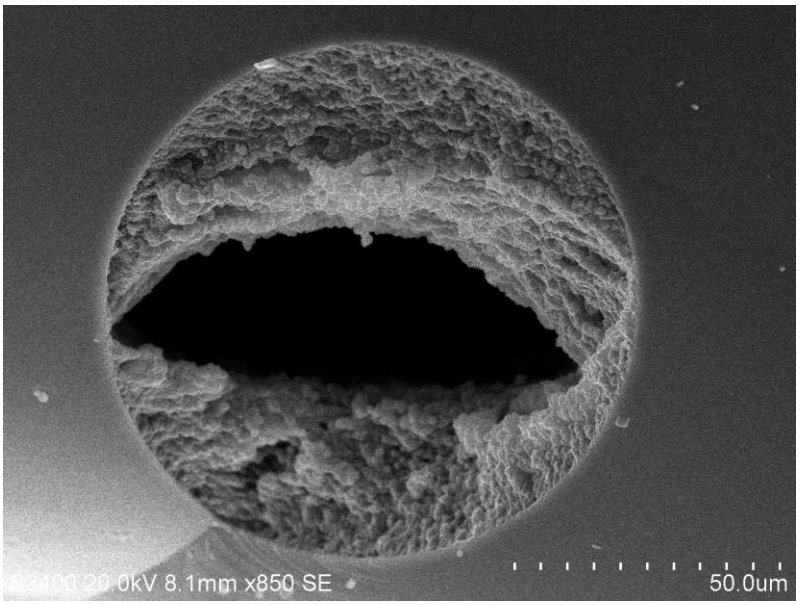

Figure 4.15 – SEM image of a non-uniform porous PS-DVB layer inside a 100 µm ID polyimide coated capillary due to non-homogenous light.

The initiator used in this work is a new and experimental compound and so very little was known about its reactive properties. According to manufacturer's instructions [40], to enhance initiator performance, H-Nu 815 had to be used as a two-component mixture with co-initiator butyltriphenyl-borate (borate V), further complicating the system. Structures for these two compounds are shown in Figure 4.16(a) and (b).

(a)

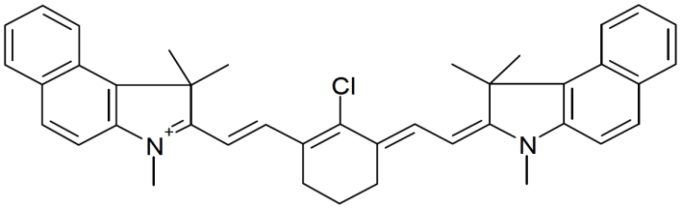

(b)

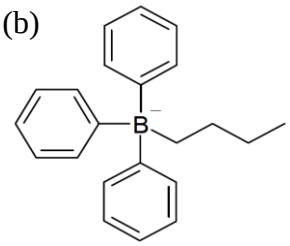

Figure 4.16 – Chemical structure of (a) H-Nu 815 and (b) borate V.

The mechanism for the formation of free radicals from H-Nu 815 and borate V can be given by:

$$Cy^{\oplus}[RB(Ph)_3]^{\ominus} \xrightarrow{h\nu} [Cy^{\bullet}] + R^{\bullet} + (Ph)_3B \qquad \text{eq. (4.5)[39]}$$

where *Cy* is H-Nu 815 and *RB(Ph)$_3$* is borate V.

During the initial experiments problems with solubility of the initiator were discovered. According to the manufacturer's guidelines it was expected that the initiator would be soluble in methacrylate type monomers and although the recommended solvents (1-decanol, 1,4-butanediol, 1-propanol, and N,N Dimethylacrylamide) were used, a gold flake type precipitate was observed. However, change of the colour of the solution to dark green indicated that some initiator was getting into the solution. In early studies the supernatant of the solution was utilised for polymerisation, but it was found that results were not reproducible and in almost all cases no (or very little) polymerisation was observed. However, when it was possible to fabricate a monolithic phase the porosity was extremely low and the phase itself was not homogenous. Heating or sonication of the polymerisation mixture did not improve solubility of the initiator.

In their work, Kabatc and Paczkowski [39], studied two- and three-component photo-initiator systems that are used in visible light induced polymerisation, where five cyanine dyes were investigated as photo-sensitisers in combination with one or two co-initiators. It is known that irradiation of cyanine organoborate salts with visible light results in efficient generation of free radicals [41]. However, for the systems containing dye and *N*-alkoxypyridinium salt, it was found that the latter one also acts as a source of free radicals

formed in the second photochemical reaction between dye radical and *N*-alkoxypyridinium salt. So Kabatc and Paczkowski found that the use of three-component systems comprising of cyanine dye, organoborate and *N*-alkoxypyridinium salts were 4.05 to 8.25 times more efficient as photoinitiators compared to the systems consisting of the dye and organoborate only. Based on these findings, the same approach in the case of H-Nu 815 and borate V system was applied, and 2.5 %wt *N*-methoxy-4-phenylpyridinium tetrafluoroborate (with respect to monomers) was added to the polymerisation mixture. However, solubility of the initiator and co-initiators remained poor and as before little or no polymerisation was observed to occur even after exposure to 2 mW/cm^2 of IR light for 24 hrs.

Walsh *et al.* [36], in their work on fabrication of polymer monoliths photoinitiated at 660 nm using a sensitiser dye with a structure similar to H-Nu 815, suggested the use of a mixture of acetonitrile, isopropanol and 1-decanol as the porogen mixture for polymerisation. As no problems with solubility were reported, it was decided to use a similar porogen mixture, comprising of 15 %wt acetonitrile, 20 %wt isopropanol, 22 %wt 1-decanol. After vortexing the mixture it was observed that the colour of solution turned clear deep emerald green, with no visible precipitate. This effect is expected to be attributed to the increase in polarity of the porogen mixture.

This time complete polymerisation of the mixture was achieved, however, the resultant monolith was extremely dense. The use of polar solvents as porogens in styrene and methacrylate systems is well known to produce smaller pores, smaller globules, and denser monolith [41], precisely what was observed in this case. In Figure 4.17(a) a section of monolith formed using this mixture and possessing extremely dense structure is shown.

The porogen mixture was then experimentally optimised to ensure that solubility was maintained while monolith porosity was increased. The resultant optimal polymerisation mixture consisted of 12 %wt styrene, 12 %wt vinylbenzene chloride, 15.5 %wt divinylbenzene, 18 %wt acetonitrile, and 39 %wt 1-decanol. In both cases the amount of initiator was the same, 0.5 %wt H-Nu 815, 0.5 %wt borate V, and 2.5 %wt MPPTFB (with respect to monomers).

(a) 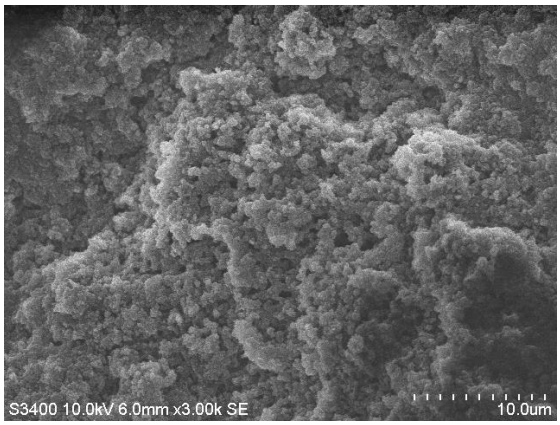

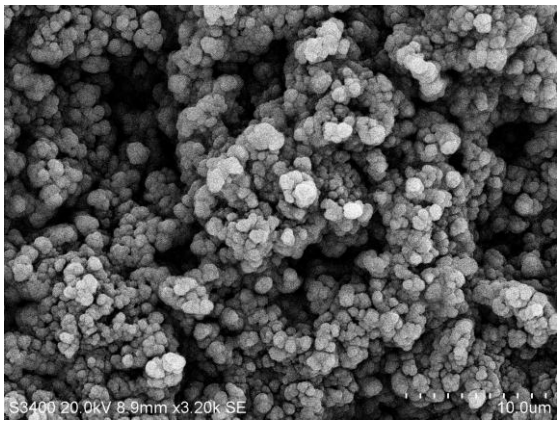

(b)

Figure 4.17 – SEM images of porous PS-DVB layers formed inside a 100 µm ID polyimide coated capillary. Polymerisation mixture: 12 %wt styrene, 12 %wt vinylbenzene chloride, 15.5 %wt divinylbenzene, (a) 15 %wt acetonitrile, 20 %wt isopropanol, 22 %wt 1-decanol, and (b) 18 %wt acetonitrile, 39 %wt 1-decanol. In both cases the amount of initiator was the same, 0.5 %wt H-Nu 815, 0.5 %wt borate V, and 2.5 %wt MPPTFB (with respect to monomers). Polymerisation conditions: Exposed to 2 mW/cm^2 of IR light at 830 nm for 4 hrs.

From Figure 4.17(a) and (b) the difference in porosity can be clearly seen; by removing isopropanol from the porogen mixture and optimising the amount of acetonitrile it was possible to produce a more porous monolithic structure with larger pores and globules. From the work carried out by Kabatc *et al.* [39], it is clear that the amount of MPPTFB has a significant effect on the efficiency of the polymerisation. A further study was carried out to observe the effects of the amount of MPPTFB present in the mixture, the aim being to

further optimise the growth of the polymer layer by altering the amount of MPPTFB. The experiment was performed using between 0.5 and 2.5 %wt of MPPTFB in the same PS-DVB polymerisation mixture; other than the percentage of MPPTFB the polymerisation mixture remained the same, and the efficacy of the system was calculated by measuring the layer growth. Samples of capillary were filled with polymerisation mixtures containing 0.5, 1.0, 1.5, 2.0 and 2.5 %wt MPPTFB and were exposed to 2 mW/cm^2 of IR light at 830 nm for 4 hrs. The samples were then washed and the layer thickness measured for each was measured from SEM images (n = 6 – 12). The relationship between %wt MPPTFB in the solution and layer thickness is shown in Figure 4.18.

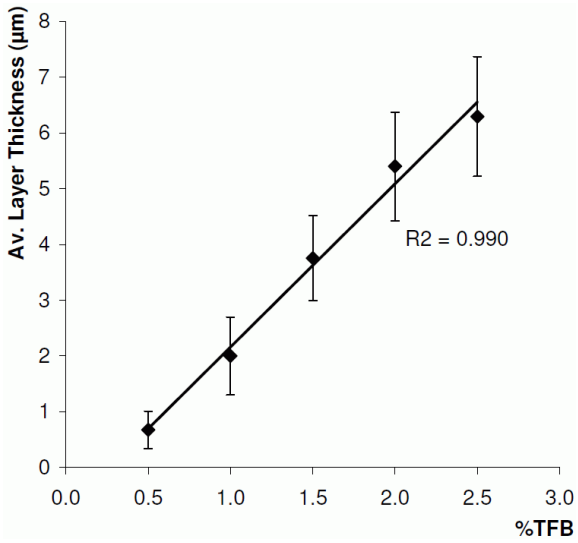

Figure 4.18 – Comparison of polymer layer thickness and %wt of MPPTFB *in the polymerisation mixture. Polymerisation mixture: 12 %wt styrene, 12 %wt vinylbenzene chloride, 16 %wt divinylbenzene, 18 %wt acetonitrile, 40 %wt 1-decanol, 0.5 %wt H-Nu 815, 0.5 %wt borate V, and varying %wt TFB (with respect to monomers). Polymerisation conditions: Exposed to 2 mW/cm^2 of IR light at 830 nm for 4 hrs.*

As expected, with an increased amount of MPPTFB in the polymerisation mixture, the layer formation was observed to be faster, showing a linear relationship between the layer

thickness and the percentage of MPPTFB. It is interesting to note that the percentage of MPPTFB in the polymerisation mixture had no noticeable effect on the morphology of the monolithic structure with pore and globule sizes being comparable across the range of MPPTFB used. This occurs due to the fact that the MPPTFB simply acts as a secondary source of free radicals [39]. Figure 4.19 shows three sample SEM images of polymer layers formed using (a) 0.5 %wt, (b) 1.5 %wt, and (c) 2.5% wt MPPTFB, where it can be seen that the morphology of the monoliths was the same.

(a)

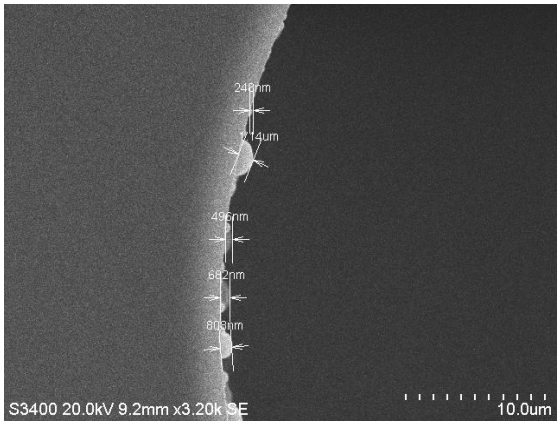

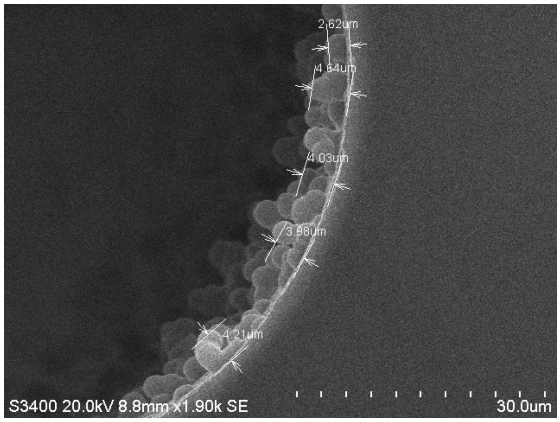

(b)

(c)

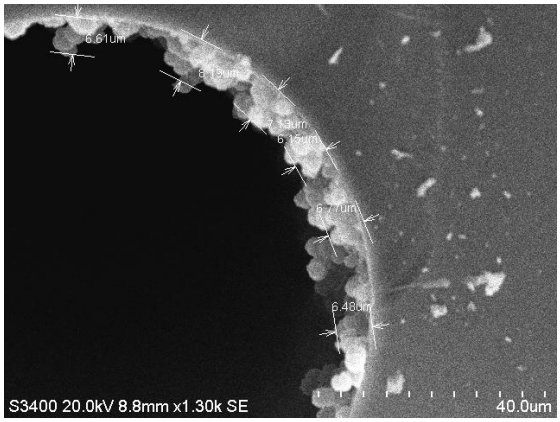

Figure 4.19 – SEM images of PS-DVB polymer layer formed within a 100 µm ID capillary using (a) 0.5% wt, (b) 1.5 %wt, and (c) 2.5% wt TFB. Polymerisation mixture and conditions as per Figure 4.18.

Although only preliminary experiments were carried out in relation to the fabrication of IR-initiated monoPLOT columns, the results were found to be very promising, as it was possible to tailor the conditions easily in order to obtain the desired layer thickness.

4.5.3 Chromatographic applications

4.5.3.1 Separation of proteins on a BuMA-EDMA monoPLOT column

Initial chromatographic performance of the UV prepared monoPLOT column was evaluated by separating a mixture of proteins (Insulin, Ribonuclease B, Trypsin, Ribonuclease A, Cytochrome C, Myoglobin, Horseradish Peroxydase, Phosphatase B, Carbonic Anhydrase, Concanavalin A). The column used was a reversed-phase BuMA-EDMA monoPLOT column, 50 µm ID x 60 cm long with a layer thickness ~2 µm. The first step was the optimisation of the flow rate. For this study, a simple 45 min, acetonitrile-water (0.1% TFA constant) mobile phase gradient was applied from 1 to 90% acetonitrile. This study was carried out at flow rates from 0.1 to 0.5 µL/min. This flow rate range was chosen based on the work by Nesterenko *et al.* [26] where the authors studied the effect of flow rate between 0.1 and 1.5 µL/min, showing that the optimal flow rate was between 0.2 and 0.4 µL/min for a column of similar dimensions. From figure 4.20 it can also be seen that the optimal flow rate was 0.2 µL/min. This figure also correlates well to the optimal flow rate range calculated relative to the internal diameter of the column [43]. As previously mentioned, one of the expected advantages of this type of column is a reduced backpressure. Luo and co-authors [44-46] used Darcy's law [47] to calculate permeability of long (4.2 m x 0.01 mm ID) PLOT columns using:

$$k = \upsilon\,(\mu\,.\,\Delta x / \Delta \mathrm{P}) \qquad \text{eq. (4.5)}$$

where:

k = permeability

υ = linear velocity

μ = solution viscosity

Δx = column length

ΔP = pressure drop.

Their column provided a backpressure of ~20MPa at a flow rate of 20 nl/min and the permeability was calculated to be 1.3 x 10^{-12} m^2, which was 4 times lower than for the corresponding bare capillary with an ID of 10 µm. The same approach was applied in this study; in this case, the back pressure for the 600 x 50 µm ID monoPLOT column varied

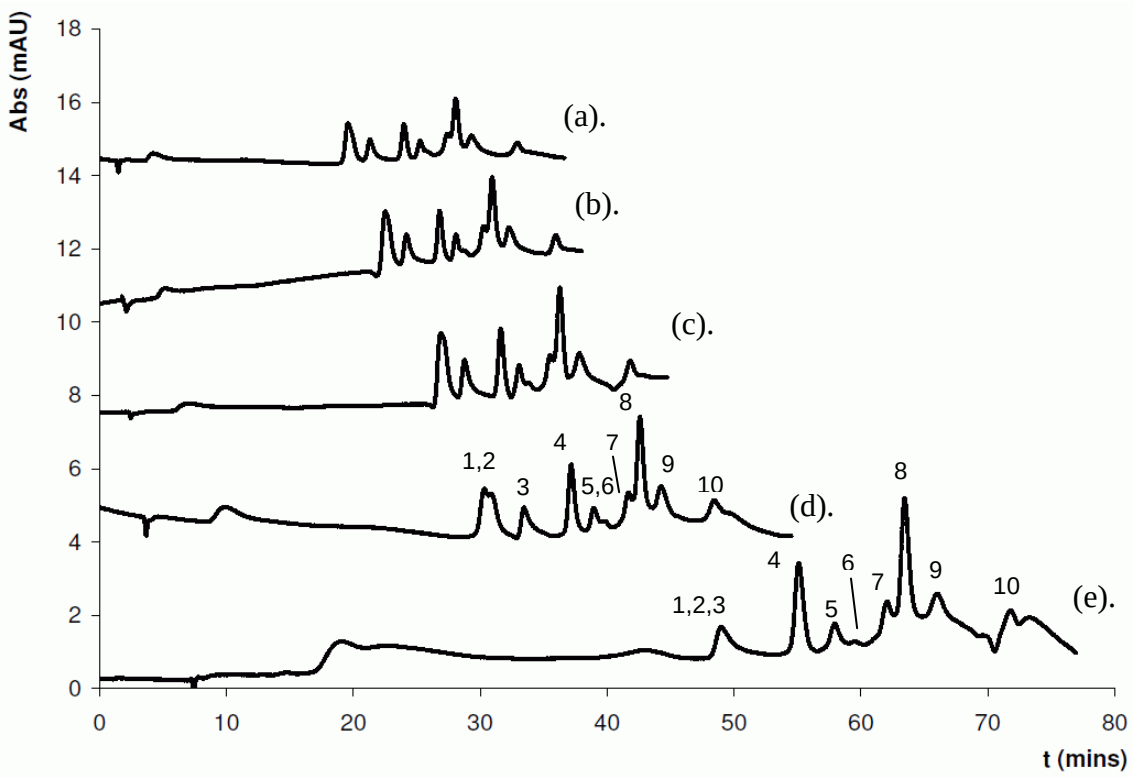

Figure 4.20 – Separation of ten proteins (1. INS, 2. RNase B, 3. TRY, 4. RNase A, 5. Cyt C, 6. MB, 7. HRP, 8. PP2, 9. CA, and 10. Con A) at varying flow rates using a 45 min gradient from 1 to 90% acetonitrile: flow rate (a) 0.5 µL/min, (b) 0.4 µL/min, (c) 0.3 µL/min, (d) 0.2 µL/min, and (e) 0.1 µL/min. Column: 60 cm x 50 µm ID BuMA-EDMA monoPLOT column, layer thickness ~2 µm. Mobile phase: ACN/H_2O gradient from 1 to 90% with 0.1% TFA. UV detection at 214 nm.

from 0.15 MPa at 0.1 µL/min to just 1.35 MPa at 0.9 µL/min when water was used as mobile phase. This gives a permeability of approximately 4 x 10^{-10} m^2. These findings show great potential for faster low pressure separations above this flow rate. For further chromatographic evaluation of this column the flow rate of 0.2 µL/min was used. In the next experiment, the optimisation of the gradient slope was performed, varying the gradient over 20 min, 35 min, 45 min, and 55 min. A comparison of the obtained chromatograms is shown in Figure 4.21, and again it can be seen that the optimal gradient conditions were achieved for chromatogram (b) (35 min gradient).

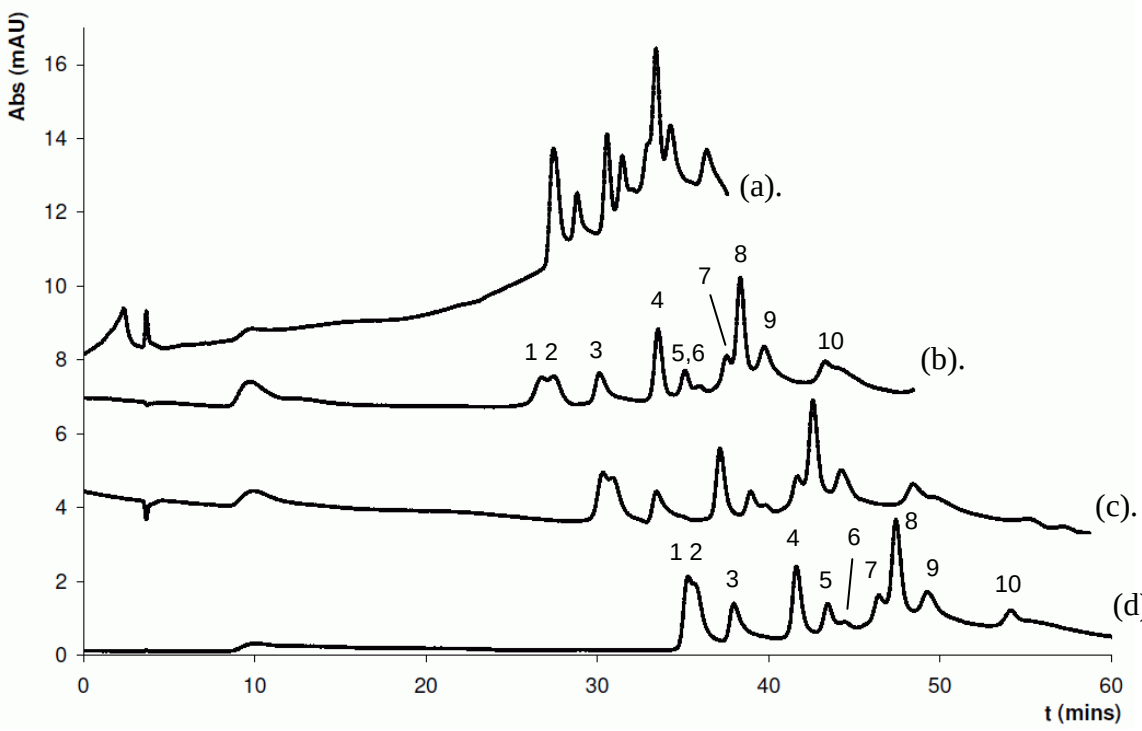

Figure 4.21 – Separation of ten proteins (1. INS, 2. RNase B, 3. TRY, 4. RNase A, 5. Cyt C, 6. MB, 7. HRP, 8. PP2, 9. CA, and 10. Con A) using a constant flow rate of 0.2 µL/min with different gradients from 1 to 90% acetonitrile: (a) 20 min (b) 35 min, (c) 45 min, and (d) 55 min. Column: 60 cm x 50 µm ID BuMA-EDMA monoPLOT column, layer thickness ~2 µm. Mobile phase: ACN/H_2O gradient from 1 to 90% with 0.1% TFA at a flow rate of 0.2 µL/min. UV detection at 214 nm.

One of the most important factors to examine for this type of stationary phase is the stability of the phase and how robust it is over time. During the course of this chromatographic study a stationary phase stability test was carried out by injecting a standard mixture using the same separation conditions. A total of 30,000 column volumes was passed through the column between the first and last injection in this test. The %RSD of the t_R of the last peak on this chromatogram (Con A) was found to be only 0.9% showing excellent column stability. Figure 4.22 shows an overlay of five separations of the protein test mixture recorded over the duration of the study.

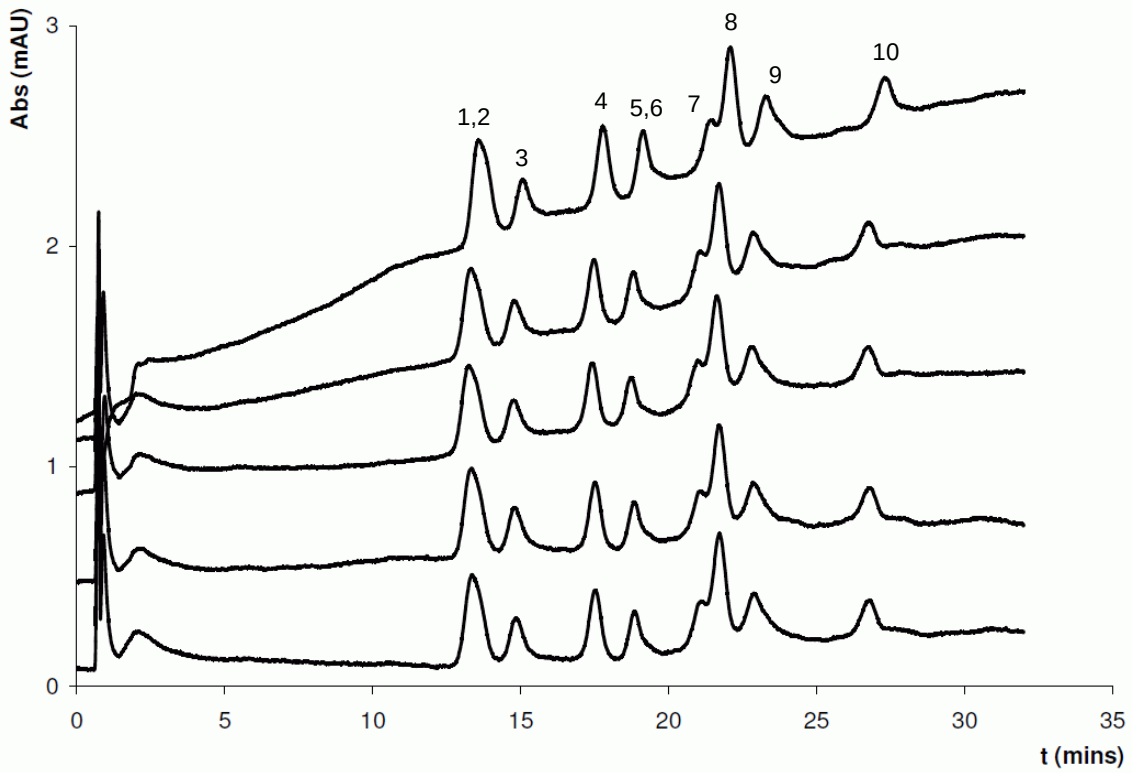

Figure 4.22 – Stability study showing chromatograms recorded over a total of 30,000 column volumes (approx. 6000 column volumes between each separation). The %RSD of the t_R of the last peak (Con A) = 0.9%. Column: 60 cm x 50 µm ID BuMA-EDMA monoPLOT column, layer thickness ~2 µm. Mobile phase: ACN/H_2O gradient from 1 to 90% over 45 min (constant 0.1% TFA) at a flow rate of 1.0 µL/min. UV detection at 214 nm.

4.5.3.2 Separation of proteins on a PS-DVB monoPLOT column

Initial chromatographic evaluation of an IR prepared monoPLOT column was also carried out by separating the same mixture of proteins as per Section 4.4.4.1. The column used was a reversed-phase PS-DVB monoPLOT column, 100 µm ID x 30 cm long with a layer thickness ~1-2 µm.

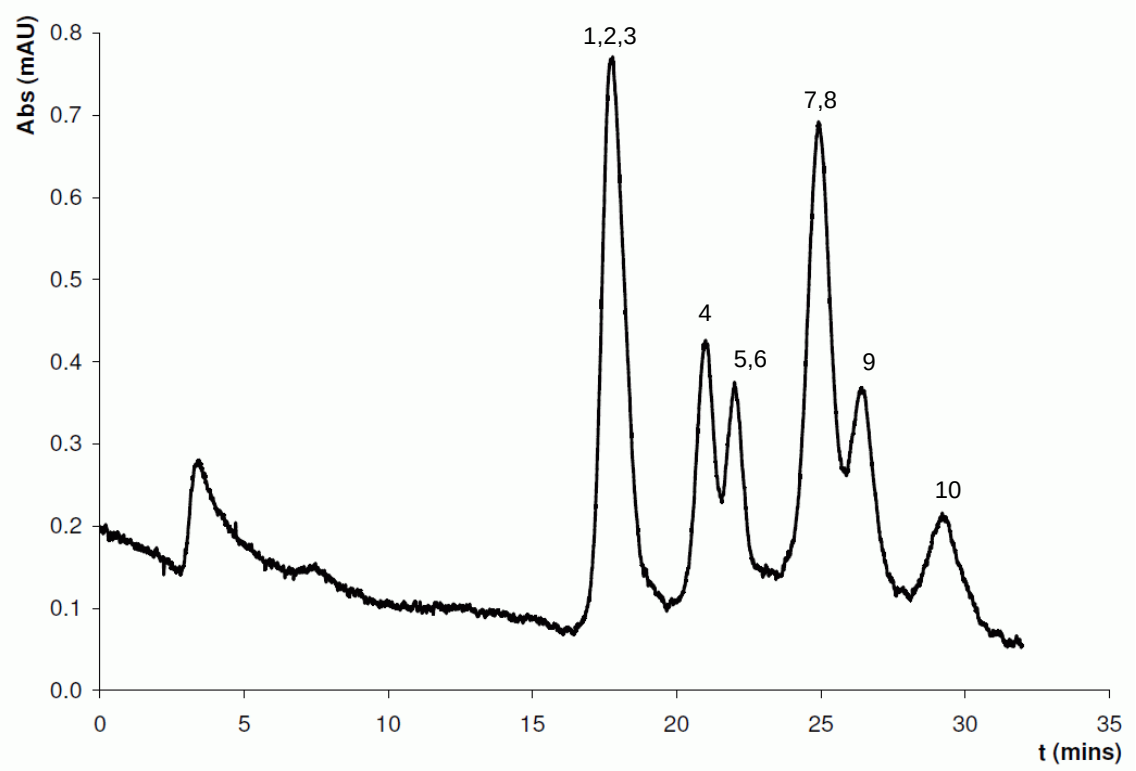

Figure 4.22 – Separation of ten proteins (1. INS, 2. RNase B, 3. TRY, 4. RNase A, 5. Cyt C, 6. MB, 7. HRP, 8. PP2, 9. CA, and 10. Con A) using a constant flow rate of 0.9 µL/min with a 45 min gradient from 1 to 90% acetonitrile. Column: 30 cm x 100 µm ID PS-DVB monoPLOT column, layer thickness ~1–2 µm. Mobile phase: ACN/H_2O gradient from 1 to 90% with 0.1% TFA at a flow rate of 0.9 µL/min. UV detection at 214 nm.

The purpose of this experiment was not to optimise the separation, it was simply to confirm that a viable reversed phase layer existed in the capillary and that a separation of a simple

mixture was possible. The observed results were quite impressive considering the wide bore of the monoPLOT column and its very short length compared to those usually used for LC separations [44-46].

4.5 Conclusions

The results presented herein demonstrate a new technology and approach for the fabrication of monoPLOT columns by photo-initiation with precisely controlled layer thickness and length. The fine control of the monolith morphology and the formation of polymer layers have been demonstrated at several intensities of UV light at 365 nm, at various exposure times and also using IR light at 830 nm. These novel methods have a great potential and open up many more possibilities for the fabrication of monoPLOT columns and provide some interesting insights into the polymerisation process and the various user-controlled effects that can be employed during polymerisation. Although the application of the prepared columns was to the separation of relatively simple test mixtures of proteins, their potential to low pressure separations was further demonstrated.

Reference list

1. Golay, M.J.E., *Gas Chromatography*, Coates, V.J., Ed. Academic Press: New York, (1958), pp. 1.
2. de Zeeuw, J., *LC-GC*, (2011), 24, pp. 38.
3. Eeltink, S.; Svec, F.; Frechet, J.M.J. *Electrophoresis*, (2006), 27, pp. 4249.
4. Yu, C.; Svec, F.; Frechet, J.M.J., *Electrophoresis*, (2000), 21, pp. 120.
5. Zaidi, A.; Cheong, W. J., *Electrophoresis*, (2009), 30, pp. 1603.
6. Chen, J.L.; Lin, Y.C., *J. Chromatogr. A*, (2010), 1217, pp. 4328.
7. Bakry, R.; Gjerde, D.; Bonn, G.K.J., *Proteome Res*., (2006), 5, pp. 1321.
8. Hirayama, Y.; Ohmichi, M.; Tatsumoto, H.J., *Health Sci*., (2005), 51, pp. 526.
9. Niessen, W.M.A.; Poppe, H., *J. Chromatogr*. (1985), 323, pp. 37.
10. Escoffier, B.H.; Parker, C.E.; Mester, T.C.; Dewit, J.S.M.; Corbin, F.T.; Jorgensen, J.W.; Tomer, K.B., *J. Chromatogr. A*, (1989), 474, pp. 301.
11. Swart, R.; Kraak, J.C.; Poppe, H., *TrAC*, (1997), 16, pp. 332.
12. Yue, G.; Luo, Q.; Zhang, J.; Wu, S. L.; Karger, B. L., *Anal. Chem.*, (2007), 79, pp. 938.
13. Rogeberg, M.; Wilson, S. R.; Greibrokk, T.; Lundanes, E., *J. Chromatogr. A*, (2010), 1217, pp. 2782.
14. Wang, D.; Hincapie, M.; Rejtar, T.; Karger, B. L., *Anal. Chem.*, (2011), 83, pp. 2029.
15. Causon, T. J.; Shellie, R. A.; Hilder, E. F.; Desmet, G.; Eeltink, S., *J. Chromatogr. A*, (2011), 1218, pp. 8388.
16. Abi Jaoude, M.; Randon, *Anal. Bioanal. Chem*., (2011), 400, pp. 1241.

17. Yang, L.; Guihen, E.; Holmes, J. D.; Loughran, M.; O'Sullivan, G. P.; Glennon, J. D., *Anal. Chem*. (2005), 77, pp. 1840.
18. de Zeeuw, J.; de Nijs, R. C. M.; Buyten, J. C. J.; Peene, A.; Mohnke, M., *J. High Res. Chromatogr*. (1988), 11, pp. 162.
19. Ruan, Z.; Liu, H., *J. Chromatogr. A*, (1995), 693, pp. 79.
20. Luo, Q.; Yue, G.; Valaskovic, G.A.; Gu, Y.; Wu, S.L.; Karger, B.L., *Anal. Chem*. (2007), 79, pp. 6174.
21. Luo, Q.; Ge, Y.; Wu, S.L.; Rejtar, T.; Karger, B.L., *Electrophoresis*, (2008), 29, pp. 1604.
22. Luo, Q.; Wu, S.L.; Rejtar, T.; Karger, B.L., *J. Chromatogr. A*, (2009), 1216, pp. 1223.
23. Xu, L.; Sun, Y., *Electrophoresis*, (2008), 29, pp. 880.
24. Kuban, P.; Dasgupta, P.; Pohl, C.A., *Anal. Chem.*, (2007), 79, pp. 5462.
25. Abele, S.; Smejkal, P.; Yavorska, O.; Foret, F.; Macka, M., *Analyst*, (2010), 135, pp. 47.
26. Nesterenko, E.; Yavorska, O.; Macka, M.; Yavorskyy, A.; Paull, B., *Anal. Methods*, (2011), 3, pp. 537.
27. Nischang, I.; Svec, F.; Frechet, J.M.J., *Anal. Chem*., (2009), 81, pp. 7390.
28. He, M.; Zeng, Y.; Sun, X.J.; Harrison, D.J., *Electrophoresis*, (2008), 29, pp. 2980.
29. Nischang, I.; Brueggemann, O.; Svec, F. *Anal. Bioanal. Chem*., (2010), 397, pp. 953.
30. Andrzejewska, E., *Prog. Polym. Sci*., (2001), 26, pp. 605.
31. Svec, F.; Tennikova, T. B.; Deyl, Z., *J. Chromatogr. Libr*., (2003), pp. 19.

32. Piasecki, T.; Macka, M.; Paull, B.; Brabazon, D., *Opt. Lasers Eng*., (2011), 49, pp. 924.

33. Gillespie, E.; Connolly, D.; Macka, M.; Nesterenko, P.N.; Paull, B., *Analyst*, (2007), 132, pp. 1238.

34. Dulay, M.T.; Choi, H.N.; Zare, R.N., *J. Sep. Sci.*, (2007), 30, pp. 2979.

35. Walsh, Z.; Levkin, P.; Jain, V.; Paull, B.; Svec, F.; Macka, M., *J. Sep. Sci*., (2010), 33, pp. 61.

36. Walsh, Z.; Abele, S.; Lawless, B.; Heger, D.; Klan, P.; Breadmore, M.; Paull, B.; Macka, M., *Chem. Commun*., (2008), pp. 6504.

37. Walsh, Z.; Levkin, P.; Abele, S.; Scarmagnani, S.; Heger, D.; Klan, P.; Diamond, D.; Paull, B.; Svec, F.; Macka, M., *J. Chrom. A*, (2011), 1218, pp. 2954.

38. Burged, D.; Grotzinger, C.; Fouassier, J.P., *Trends Photochem. Photobiol*., (2001), 7, pp. 71.

39. Kabatc, J.; Paczkowski, J., *J. Photochem. and Photobiol. A*, (2006), 184, pp. 184.

40. www.sglinc.com, (accessed Feb 2013).

41. Svec, F.; Tennikova, T.B.; Deyl, Z., Monolithic Materials: Preparations, Properties and Applications, 1st edition, Elsevier: Amsterdam, (2003), 773 p.

42. Chatterjee, S.; Gottschalk P.; Davis, P.D.; Schuster, G.B., *J. Am. Chem. Soc.*, (1988), 110, pp. 2326.

43. http://www.restek.com/Technical-Resources/Technical-Library/General-Interest/general_A018, (accessed Feb 2013).

44. Luo, Q.Z.; Rejtar, T.; Wu, S.L.; Karger, B.L., *J.Chromatogr. A*, (2009), 1216, pp. 1233.

45. Yue, G.H.; Luo, Q.Z.; Zhang, J.; Wu, S.L.; Karger, B.L.; *Anal. Chem.*, (2007), 79, pp. 938.

46. Luo, Q.Z.; Gu., Y.; Wu, S.L.; Rejtar, T.; Karger, B.L., *Electrophoresis*, (2008), 29, pp. 2604.

47. Hlushkou D.; Tallarek, U., *J. Chromatogr. A*, (2006), 1126, pp. 70.

CHAPTER 5.

FABRICATION OF MONOPLOT COLUMNS IN WIDE BORE CAPILLARY BY LAMINAR FLOW THERMAL INITIATION

Relevant publications:

Collins, D.; Nesterenko, E.; Brabazon, D.; Paull, B.; *Chromatographia*, (2013), 76, pp. 581-589.

Abstract

A novel scalable procedure for the thermally initiated polymerisation of bonded monolithic porous layers of controlled thickness within open tubular fused silica capillaries (monoPLOT columns) is presented. Porous polymer layers of either polystyrene-divinylbenzene or butyl methacrylate-ethylene dimethacrylate, of variable thickness and morphology were polymerised inside fused silica capillaries utilising combined thermal initiation and laminar flow of the polymerisation mixture. The procedure enables the production through thermal initiation of monoPLOT columns of varying length, internal diameter, user defined morphology and layer thickness for potential use in both LC and GC. The morphology and thickness of the bonded polymer layer on the capillary wall is strongly dependent upon the laminar flow properties of the polymerisation mixture and the changing shear stress within the fluid across the inner diameter of the open capillary. Due to the highly controlled rate of polymerisation and its dependence on fluid shear stress at the capillary wall, the procedure was demonstrably scalable, as illustrated by the polymerisation of identical layers within different capillary diameters.

Aims

The aim of the work presented in Chapter 5 was to develop a method for the production of monoPLOT columns in polyimide coated capillary through thermal initiation which also allowed fine control over polymer layer thickness and morphology. The work aimed to investigate the effect of laminar flow on the polymerisation process, specifically on the rate of layer growth and also on the structure of the formed layer.

5.1 Introduction

A technique for the production of monoPLOT columns in capillaries of large internal diameter was presented in Chapter 4. The technique utilised photo-initiated in-situ polymerisation, however, its application was limited to polymers, and resultant polymer structures, which could be produced by photo-initiation within the UV region, and within UV transparent media. Polystyrene-based materials are commonly used as reversed phase and hydrophobic substrates in both LC and GC. PS-DVB based stationary phases are considered advantageous in GC due to their high thermal stability compared with alternative hydrophobic polymers. However, there are a number of difficulties related to the fabrication of open tubular columns with a PS-DVB stationary phase. Firstly, photo-initiated polymerisation within the UV region is not possible due to the strong UV absorbance of styrene itself. Additionally, fused silica capillary, of the type commonly used in GC, is coated with polyimide for strengthening and supporting the brittle fused silica capillary. This coating also absorbs in the UV region, and further upwards to approximately 600 nm (see Figure 5.1), thus making in-situ polymerisation by UV photo-initiation impossible regardless of the polymerisation mixture. Thermal initiation of polymers such as PS-DVB, although unrestricted by UV absorbance limitations, is notoriously difficult to control in the production of open tubular or layered structures. Earlier studies [3-7] have demonstrated that the fabrication of thermally initiated PLOT type columns is possible; however, stationary phase layers could only be obtained in capillaries of small ID, typically less than 25 µm, but these dimensions are too small for application in GC and of limited application in capillary LC [4] due to high column backpressures. Chuang *et al.* [8] has reported the thermal polymerisation of a polystyrene ‘monolithic’ layer inside a 75 µm ID capillary, however the layer thickness achieved was only 300 nm with little or no porosity.

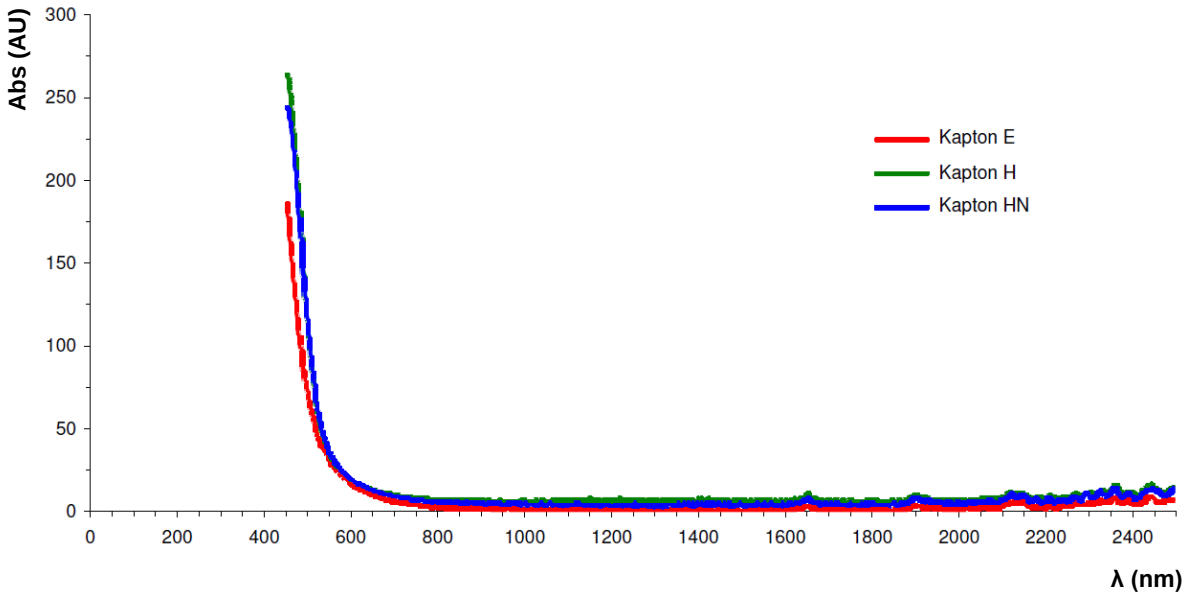

Figure 5.1 – Optical absorbance of some common polyimide polymers.

In all other studies dealing with the thermal polymerisation of porous polymer layers within capillaries, the resulting porosity has also been shown to be poor with layer thicknesses achieved only equalling that of the polymer globule size. The limited successes detailed above, can be mainly ascribed to the difficulty in controlling the thermal polymerisation process as compared to photo-initiated polymerisation. More often than not, attempts to form polymeric PLOT columns through thermal initiation will result in over polymerisation across the entire section of the capillary [4].

As mentioned above, there are very few studies which have succeeded in producing highly porous polymer layers (typical monolithic porous polymer structures) within capillaries of ID >25 µm. The difficulty in the polymerisation of porous layers in larger diameters stems from the increased number of parameters in such systems, including for example, surface tension. However, porous layer structures have been successfully polymerised in much

larger diameter tubing. In the work by Shen [9], the in-situ polymerisation of divinylbenzene in a 762 µm ID stainless steel tube was shown, with the layer formed through static polymerisation at 80 °C for 7 hr. Stainless steel has a high thermal conductivity compared with silica, and the polymerisation mixture at the tube walls would reach polymerisation temperature very quickly, as compared with the centre of the tube. However, having such a thermal gradient in the tube results in a highly non-uniform layer, with low porosity and globule size at the wall, which increases dramatically towards the centre. In this study it was demonstrated that it was possible to control neither the pore size, morphology nor the thickness of the layer.

Very little work has been done on laminar flow polymerisation within capillaries, and no prior studies have been reported on the fabrication of porous polymer 'monoPLOT' type columns by either 'flow through', or laminar flow thermal polymerisation. Prior reports on laminar flow polymerisation describe exothermic reactions in large scale reactors [10-12] for the bulk manufacture of polymers, which have limited relevance in regard to polymerisation within micro-bore capillaries of the type discussed herein. In Chapter 4 flow-through photo-initiated polymerisation was attempted with mixed results. From analysis of results herein, it would appear that within this early study the flow velocities used were excessively high, resulting in turbulent flow, less than ideal phase morphology, and loss of pore structure.

Therefore within this current study, the development of a highly controlled thermally initiated method for the fabrication of PS-DVB monoPLOT columns in large ID capillary (from 50 to 200 µm) is presented. Precise control over layer thickness and morphology was

delivered through the application of laminar flow within the monomer mixture through the capillary during polymerisation.

5.2 Experimental

5.2.1 Reagents and materials

All chemicals used within this study were of reagent or analytical grade purity.

- Ethylene dimethacrylate, butyl methacrylate, styrene, divinylbenzene, 4-vinylbenzyl chloride, 1-decanol, toluene, and 3-methoxysilylpropyl methacrylate, trifluoroacetic acid and proteins used for chromatographic evaluation of prepared column (Insulin, Ribonuclease B, Trypsin, Ribonuclease A, Cytochrome C, Myoglobin, Horseradish Peroxydase, Phosphatase B, Carbonic Anhydrase, Concanavalin A) were all purchased from Sigma-Aldrich (Gillingham, UK).
- The thermal initiator, azobisisobutyronitrile (AIBN), was obtained from DuPont (Le Grand Sacconex, Switzerland).
- All solvents which were used for the preparation, or for the synthesis and washing of prepared monoliths, namely, sodium hydroxide, hydrochloric acid, acetonitrile, acetone, and methanol, were purchased from Lab Scan (Gliwice, Poland).
- Deionised water was supplied from a Milli-Q system (Millipore, Bedford, MA, USA).
- Polyimide coated (15 μm thickness) fused silica capillary, 25, 50, 75, and 100 μm ID, 0.375 mm OD was purchased from Composite Metal Services Ltd. (Charlestown, U.K.).

5.2.2 Instrumentation

- Capillaries were filled with monomer mixture and washed using a KDS-100-CE syringe pump (KD Scientific, Inc., Holliston, MA, USA).
- Formation of the monolithic layer was carried out in a water bath, using a Yellow Line MST Basic hotplate with TC1 temperature controller and glassware (VWR Ltd., Dublin, Ireland).
- A Rheodyne 6-port switching valve (Rheodyne, Cotati, CA, USA) was used to switch between the polymerisation mixture and MeOH flows.
- Laminar flow studies were carried out using a PHD2000 syringe pump, purchased from Harvard Apparatus (Holliston, MA, USA).
- An Upchurch Model # 565 flow cell (IDEX Health & Science LLC, Washington, USA) was used to measure flow rates.
- Additional experiments using flow gradients used a Dionex Ultimate 3000 nano-HPLC system (Dionex, Sunnyvale, CA, USA).
- A SputterCoater S150B (BOC Edwards, Sussex, UK) was used for coating capillary monolithic stationary phase samples with a 60 nm gold layer.
- Scanning electron microscopy (SEM) analysis was performed on an S-3400N instrument (Hitachi, Maidenhead, UK).
- Optical microscopy evaluation of samples was performed on a Meiji Techno EMZ-8TR stereomicroscope (Meiji Techno UK Ltd., Somerset, United Kingdom).
- Fluid viscosities were measured using an Anton Paar MCR 301 Rheometer (Anton Paar GmbH, Graz, Austria).

5.2.3 Experimental procedures

The experimental procedures used for the silanisation and fabrication of reversed-phase columns in a capillary format are as detailed in Section 2.2.5.

5.2.3.1 Fabrication of BuMA-EDMA monoPLOT columns

The BuMA-EDMA monomer mixture consisted of 24 %wt BuMA, 16 %wt EDMA, 59.6 %wt 1-decanol, and 0.4 %wt AIBN (with respect to monomers). The initiator (AIBN) was weighed out into the mixture vessel, and the porogen mixture (1-propanol and 1,4-butanediol) was added, followed by the monomers. The mixture was vortexed and deoxygenated under a flow of nitrogen for 10 min.

5.2.3.2 Fabrication of PS-DVB monoPLOT columns

The PS-DVB monomer mixture consisted of 12 %wt styrene, 12 %wt 4-vinylbenzyl chloride, 16 %wt divinylbenzene, 18 %wt toluene, 41.6 %wt 1-decanol, and 0.4 %wt AIBN (with respect to monomers). The mixture was prepared as described in Section 5.2.3.1.

5.2.3.3 Laminar flow polymerisation

For the in-column polymerisation, the desired length (from 30 cm to 1.5 m) of silanised capillary was coiled and one end connected to a port on the switching valve which was mounted above a heated water bath. The two inlet ports of the switching valve were connected to a syringe filled with polymerisation mixture and another syringe filled with MeOH, respectively. Both syringes were placed in a syringe pump. The coiled capillary was immersed in the water bath and the other end was left open so that the polymerisation mixture could flow through it. A typical experimental set-up is shown in Figure 5.2.

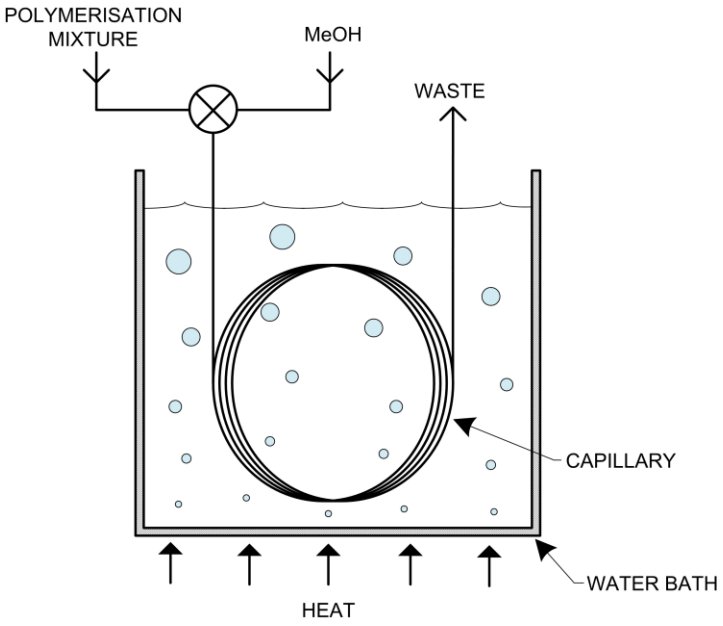

Figure 5.2 – Polymerisation process experimental set-up.

The polymerisation mixture was pumped through the capillary at the desired linear flow velocity, namely 0.25, 0.5, or 1.0 mm/s. After flow was established the water bath was brought up to a polymerisation temperature of 60 °C.

The formation of the porous polymer layer was allowed to continue for the desired length of time, after which the water bath was evacuated and the hot water was replaced with cold water to quench any further reaction. The switching valve was also switched over to flush the capillary with MeOH in order to remove all unreacted monomer. Once the capillary had been thoroughly washed it was removed and dried with nitrogen. In the above polymerisation set-up, thermal gradients, both axial and longitudinal, were avoided, as the dimensions of the capillary permitted almost instant thermal equilibration of the monomer mixture [18]. Additionally, the linear flow velocity was very low, further facilitating faster

thermal equilibration. Given the high thermal conductivity of fused silica, capillary dimensions and flow rate, a longitudinal thermal gradient could exist only at the very column entrance, which for each column produced was later removed and discarded. Therefore, in the current work, thermal gradients could have no measurable effect upon monolithic layer thickness.

5.3 Theory

The method proposed herein uses the effect of laminar flow to build up a porous polymer layer on the inside of a fused silica capillary through thermal polymerisation. Due to the small diameter of the fused silica capillaries (typ. 10 – 400 µm ID), fluids flowing through them exhibit extremely low Reynolds numbers. Furthermore, these types of capillary possess remarkably smooth inner surfaces, with root-mean-square roughness values of approximately 0.4 – 0.5 nm [14]. The combination of such a narrow, smooth bore and low Reynolds number, results in highly laminar flow within the capillary, causing the effective formation of ‘stream tubes’ within the flowing liquid (see Figure 5.3).

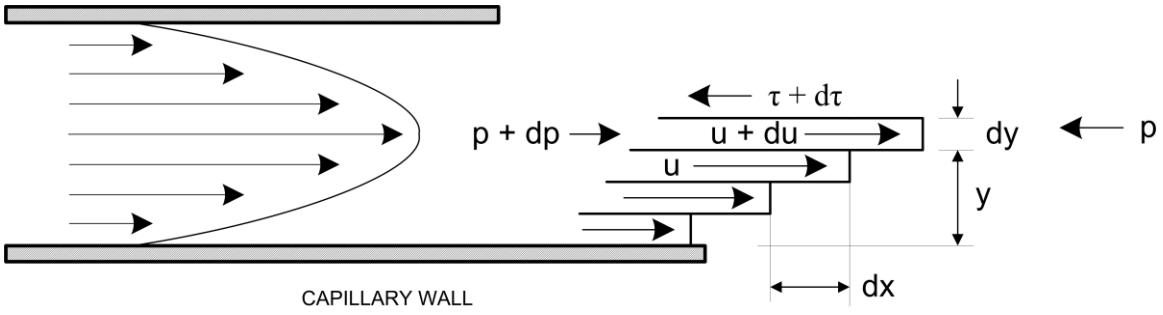

Figure 5.3 – Laminar flow model for a narrow bore capillary (adapted from [15]).

Figure 5.3 shows a schematic of fluid flowing through a capillary and the various forces affecting its flow structure and profile, where:

y = distance above capillary wall

dy = thickness of each shearing layer

dx = distance moved by each shearing layer relative to the adjacent layer

u = linear velocity of any layer

du = increase in linear velocity between any two adjacent layers

p = force due to pressure

dp = capillary pressure drop between up and downstream end

τ = shear stress

dτ = increase in shear stress over adjacent layer

When a fluid flows over a surface, the layer in contact with the surface will have a linear flow $\cong$ 0 mm/s, since the fluid is effectively attached to the surface. The layers of fluid above the surface are moving and so shearing layers will exist within the fluid, each layer moving a distance, dx, in a time, dt, relative to the layer outside it. The ratio dx/dt will vary with the change in linear flow velocity between layers, giving du = dx/dt, inducing a shear stress (τ) between the layers which corresponds to a shear strain, γ. Shear strain can be defined as [15]:

$$\gamma = \frac{\text{deformation of layer}}{\text{thickness of layer}} = \frac{\mathrm{d}x}{\mathrm{d}y}$$

eq. (5.1)

It follows that the rate of shear strain will be:

$$\dot{\gamma} = \frac{\gamma}{\mathrm{d}t} = \frac{\mathrm{d}x}{\mathrm{d}t \cdot \mathrm{d}y} = \frac{\mathrm{d}u}{\mathrm{d}y}$$

eq. (5.2)

For Newtonian fluids the rate of shear strain is directly proportional to the shear stress between the layers in the fluid. The constant of proportionality in this case is the dynamic viscosity of the fluid, μ, giving:

$$\tau = \dot{\gamma} \times \mu$$

eq. (5.3)

Thus, the dynamic viscosity of the fluid can be defined as:

$$\mu = \frac{\text{shear stress}}{\text{rate of shear}} = \frac{\tau}{\dot{\gamma}} = \tau \frac{\mathrm{d}y}{\mathrm{d}u}$$

eq. (5.4)

From equation (4) it can be seen that for a given dynamic viscosity, μ, and linear flow velocity, u, the shear stress, τ, will change across the radius of the capillary, reaching a maximum at the capillary wall, where the effective linear flow velocity, $u \approxeq 0$ mm/s (see Figure 5.4).

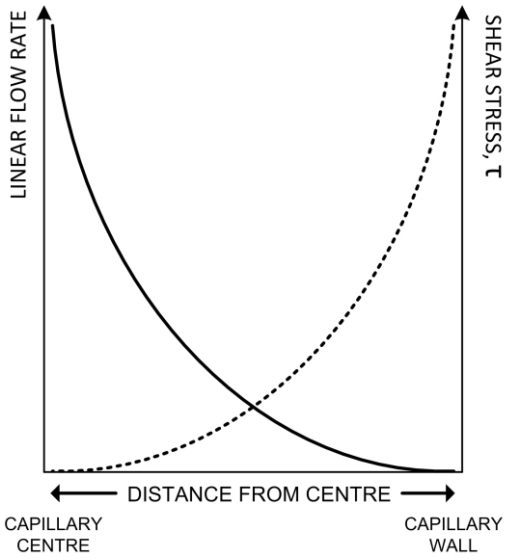

Figure 5.4 – Relationship between fluid linear flow velocity and shear stress, τ, across the bore of a capillary column.

During polymerisation, the rate of polymer growth at the wall of the capillary is heavily dependent on the liquid shear stress at the capillary walls. During no-flow conditions polymer growth will initially start at the capillary walls as the silica has a high thermal conductivity (~1.4 Wm/k) [16]. However, since there is no flow, the shear stress in the fluid will be zero and provided the entire capillary has equilibrated to polymerisation temperature, polymer growth will occur throughout the mixture. Under laminar flow conditions, this cannot occur and net growth of the polymer layer is from the capillary walls inwards towards the centre of the capillary, as shown in Figure 5.5. Applying heat energy to the outside of the capillary with a flowing polymerisation mixture will subject the outer streams of the mixture to more energy due to the lower linear flow velocity at the capillary walls. Since the linear flow velocity decreases radially in the capillary due to laminar flow, free radicals and short polymer chains are also removed more slowly at the capillary wall zones than at its centre.

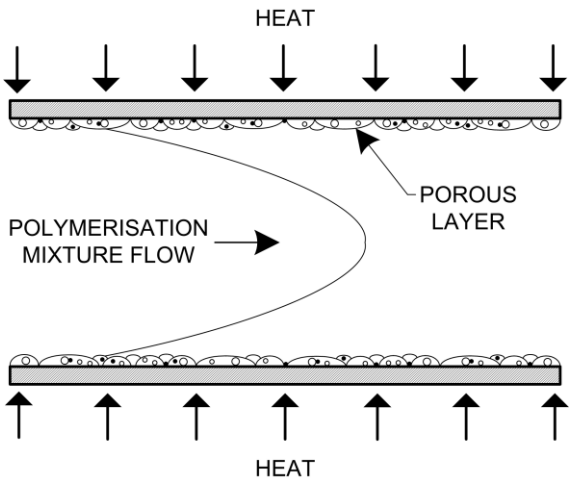

Figure 5.5 – Growth of porous polymer layer upon capillary walls under laminar flow polymerisation conditions.

Theoretically this polymerisation process should be scalable between capillaries of different diameters. However, although the scaling process is straightforward, it is first necessary to calculate the linear flow velocity which provides the optimum relative shear stress at the capillary walls for the desired layer thickness and morphology. This can be done experimentally, but once calculated the process can be scaled for any given polymerisation mixture.

Figure 5.6 shows a comparison between shear stresses within the liquid in a 50 µm ID (solid black line) and 100 µm ID (broken black line) capillary for a given volumetric flow rate, F_R = N. The shear stress in the 100 µm ID capillary at the desired flow rate, F_R = n, is also shown. In scaling from a 50 µm ID capillary to 100 µm ID, the relative shear stresses in the polymerisation liquid must be considered. Assuming that the polymerisation mixture and temperature are held constant (and thus the liquid viscosity), then the volumetric flow rate for the larger diameter capillary must be adjusted to ensure that the shear stress at the

capillary wall for the larger bore capillary (broken red line) equals that of the smaller diameter capillary. This should give approximately the same thickness and porosity of layer coating for the larger capillary as for the smaller capillary.

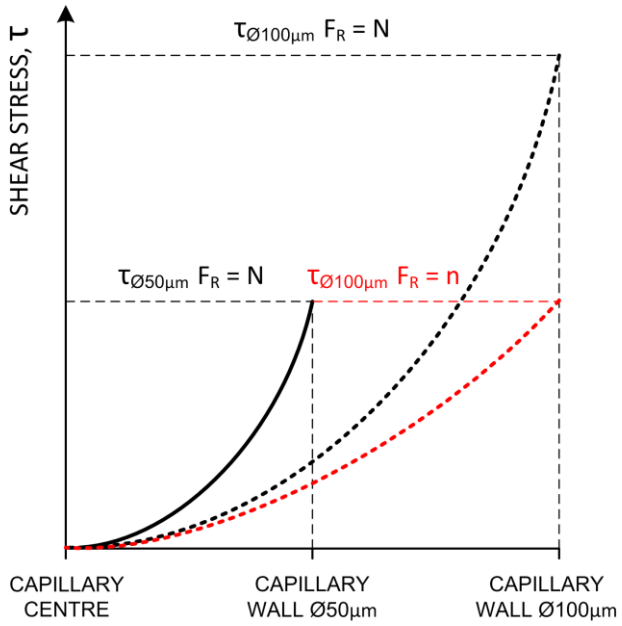

Figure 5.6 - Comparison between shear stress, τ, across capillary bore sizes of 50 and 100 µm ID at a given flow rate, $F_R = N$.

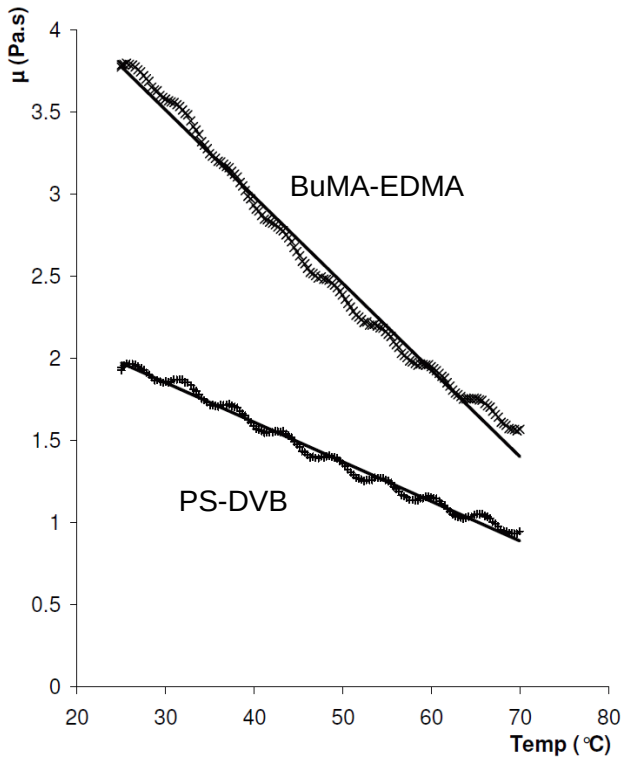

Figure 5.7 – Comparison of dynamic viscosities, μ, for BuMA-EDMA and PS-DVB polymerisation mixtures between 25 and 70 °C.

Figure 5.7 shows a comparison of the dynamic viscosities for the BuMA-EDMA and PS-DVB mixtures. The influence of fluid viscosity on the formation of the porous layer will be discussed later.

5.4 Results and discussion

5.4.1 Porous layer morphology

Following each polymerisation experiment, 10 samples of the capillary were removed, washed, and evaluated via SEM. The average pore and globule sizes were measured (n = 50) and plotted against linear flow velocity, u. This was carried out for both BuMA-EDMA and PS-DVB polymerisation mixtures. Figure 5.8 shows the recorded pore and globule sizes in response to linear flow velocity for these two polymer phases. The responses show a very clear rapid decrease in the layer porosity with increasing linear flow velocity, and at velocities of 1.0 mm/sec and above, the layers contained no observable pore structure whatsoever.

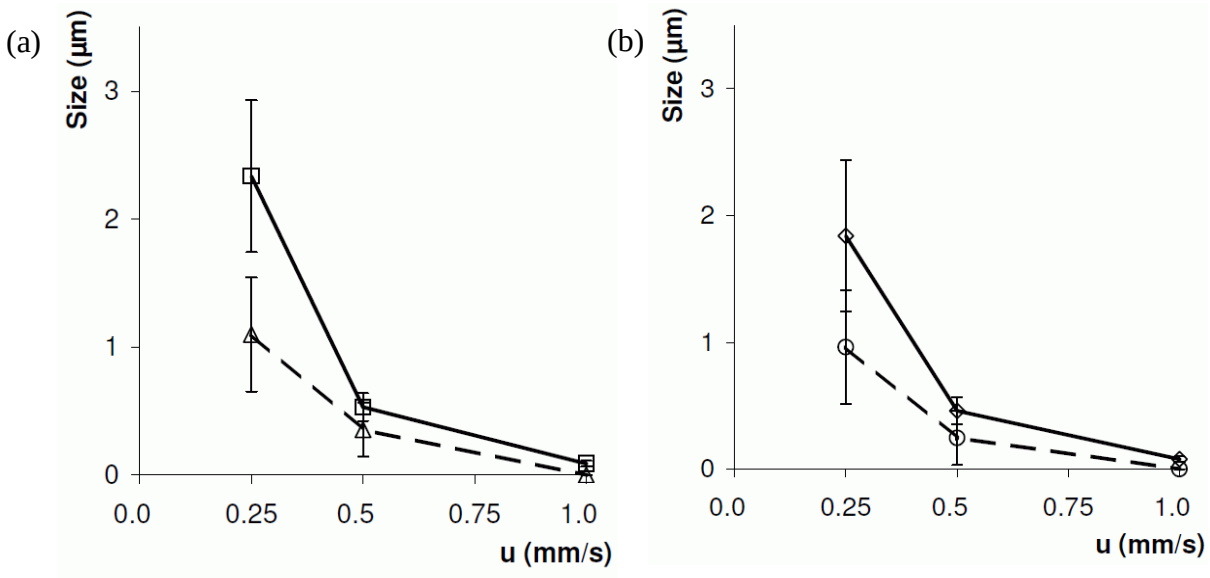

Figure 5.8 – Pore and globule sizes (dashed and solid lines respectively) for (a) BuMA-EDMA and (b) PS-DVB porous layers in relation to various linear flow velocities of the polymerisation mixture.

Figure 5.8 also shows how the average globule size similarly decreases with increased flow velocity. However, it is also interesting to note that the variability (%RSD) of the pore structure decreases significantly for both polymers from 0.25 to 0.5 mm/s, showing that it was possible to tightly control the layer morphology under these conditions. Figure 5.9 shows SEM images of two 100 µm ID capillaries containing porous PS-DVB layers obtained at different linear flow velocities, (a) 0.5 mm/sec and (b) 0.25 mm/sec, each polymerised for 90 mins at a temperature of 60 °C.

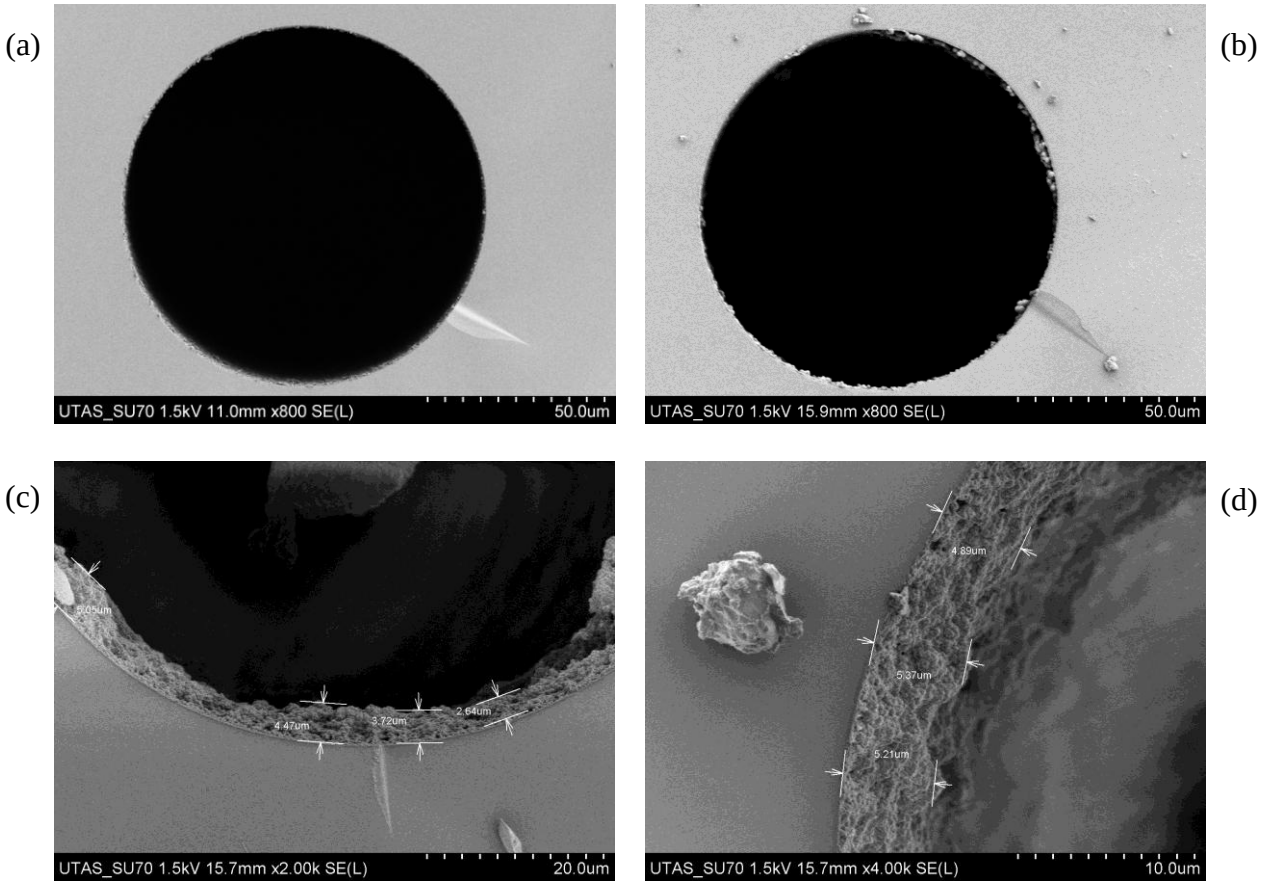

Figure 5.9 – SEM images of porous PS-DVB layers formed within 100 µm ID at different linear flow velocities, (a) 0.5 mm/sec and (b) 0.25 mm/sec. Polymerisation time was 90 mins for each sample at a temperature of 60 °C. Insets (c) and (d) show SEM images of 4 and 5 µm layers formed at a linear flow rate of 0.5 mm/sec in 100 µm ID capillary at a temperature of 60 °C. Polymerisation time was 135 mins.

Layer thicknesses were measured to be in the order of 1.2 µm and 3 µm, respectively. The difference in layer morphology is clear from close inspection of Figure 5.9(b), which shows that although 0.25 mm/sec produces a much larger pore and globule structure, it also develops a much less homogenous layer. The layer thickness %RSD for (b) was measured at 51%, compared to just 20% for (a). Figures 5.9(c) and (d) illustrate the more homogeneous phase coverage which can be achieved at the linear flow velocity of 0.5 mm/sec within the 100 µm ID capillary (temperature of 60 °C). Under these conditions homogenous PS-DVB layers of 4 and 5 um, with desired porous monolithic type polymer structure were obtained.

It is clear that once a layer of polymer begins to form on the surface of the capillary two further factors will begin to affect the polymerisation process. Firstly, the layer (regardless of its porosity) will reduce the effective ID of the capillary, causing the linear flow velocity to increase for a given volumetric flow. Figure 5.10 shows a simple comparison of the percentage change in linear flow velocity, *u*, for layer thicknesses between 1 and 10 µm within capillaries of ID between 50 and 200 µm. For simplicity, here the effects of layer porosity and increased surface friction have been ignored; however, these additional effects would be negligible.

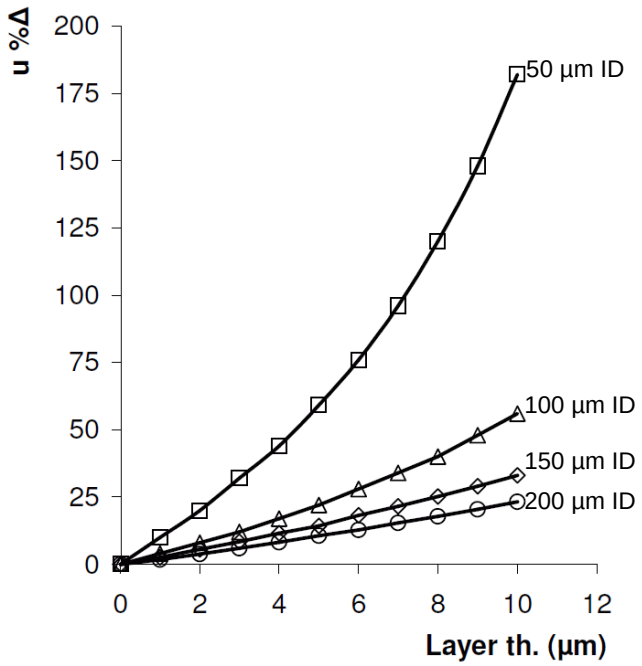

Figure 5.10 – Comparison of the % change in linear flow velocity, u, for layer thicknesses between 1 and 10 µm in capillaries between 50 and 200 µm ID.

Figure 5.10 shows how this increase in linear velocity with stationary phase growth will be most apparent in smaller ID capillaries, making this approach difficult to control for capillaries smaller than 50 µm ID. It can be seen that a layer of 4 µm thickness will result in a 44 % increase in the fluid linear velocity for a 50 µm ID capillary, and just a 17 % increase in a 100 µm ID capillary. The increased linear flow velocity will negatively affect the rate of layer growth and the morphology of the layer structure. If the linear flow velocity increases too much, it may cause part of the stationary phase layer to break away, potentially blocking the column. Should this take place, complete polymerisation will rapidly occur with the process no longer in control. For these reasons it is recommended that a flow gradient be used for capillaries with an ID less than 75 µm, the volumetric flow rate being reduced as the layer builds to ensure a constant linear flow velocity.

(a) 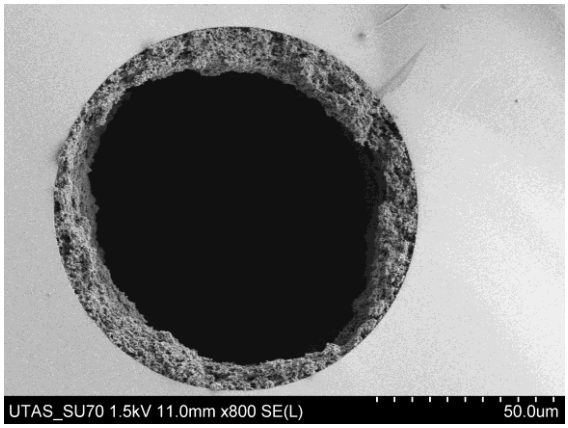

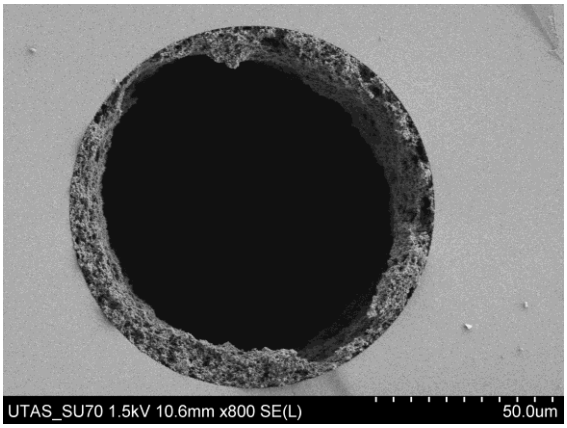

(b)

Figure 5.11 – 100 µm ID column with a 10 – 15 µm PS-DVB porous layer, showing layer non-uniformity.

A secondary effect of layer growth is a reduction in laminar flow and an increase in turbulent flow, which will also have an increasingly negative impact on the further growth of the layer. Turbulent flow will result in a loss of layer homogeneity, and this can be seen from the high %RSD (typically > 35%) obtained for thicker layers. Figures 5.11(a) and (b) illustrate this phenomenon, showing examples of a 100 µm ID column with a 10 – 15 µm layer which exhibited layer non-uniformity, possibly due to turbulent flow during the polymerisation process. Layer homogeneity is lost since turbulent flow may remove shorter polymer chains that are weakly attached to the layer and deposit them elsewhere, resulting in a non-uniform structure. Once this process begins it will continually worsen as the layer becomes less and less uniform resulting in increased turbulence within the polymerisation mixture.

5.4.2 Controlling layer thickness

A study showing the possibility of precise control of layer thickness of two types of monolithic phases, fabricated in capillaries of various ID and using different flow velocities was performed. In Figures 5.12 and 5.13, comparisons between layer thickness and linear flow velocity for PS-DVB in 50, 100 and 150 µm ID capillaries and BuMA-EDMA in 50 and 100 µm ID capillary are presented respectively.

For both figures it can be seen that the rate of layer growth increases dramatically above 60 mins for PS-DVB, and above approximately 90 mins for BuMA-EDMA. Moreover, for Figure 5.12(a), (b), and (c) that there is good correlation between the layer thicknesses, illustrating how the process is easily scalable to larger diameter capillaries. Figures 5.12(a-c) also confirm that the optimum linear flow velocity was 0.5 mm/sec, giving a homogenous PS-DVB layer thicknesses of approximately 18 and 14 µm after 150 mins in the 100 µm ID and 150 µm ID capillaries, respectively. As the layer size decreases so too does the %RSD showing that not only is the process scalable, but is also very reproducible for layers up to 5 µm.

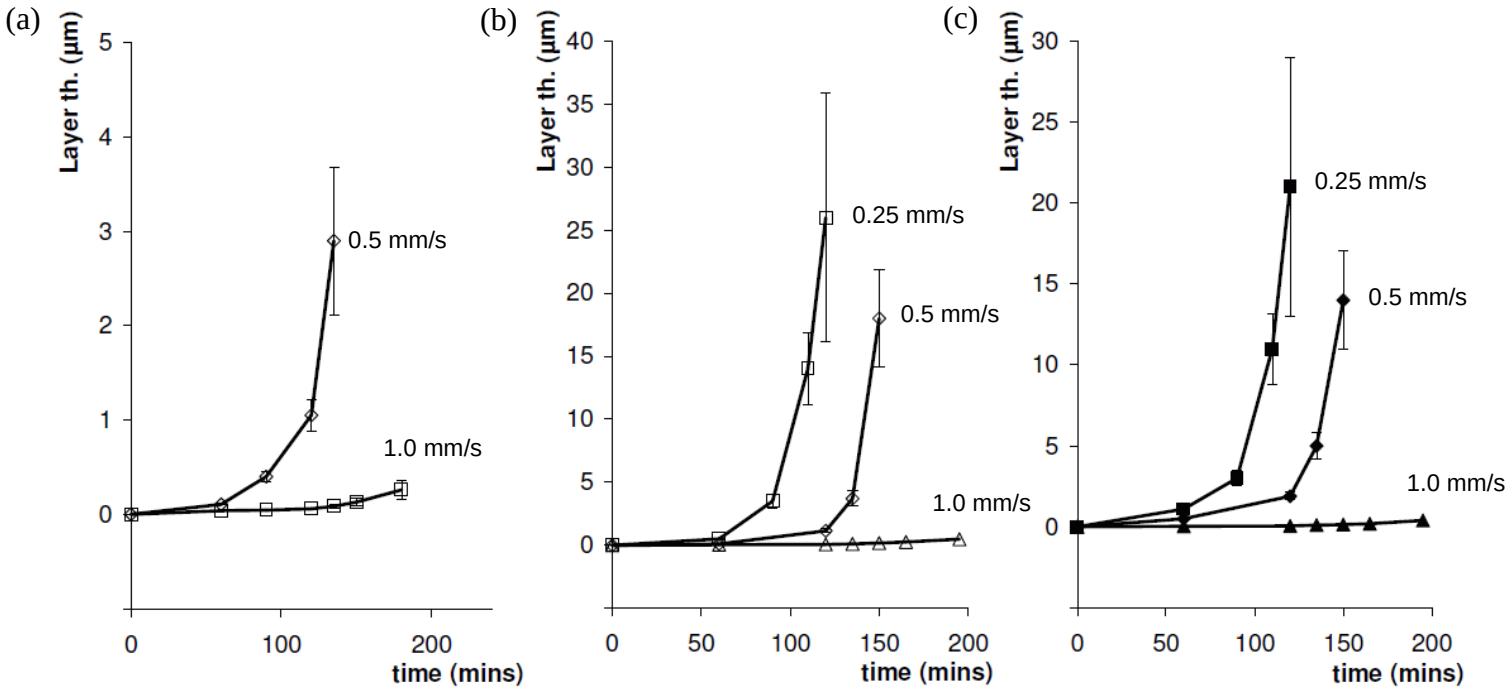

Figure 5.12 – Comparison of layer thickness against linear flow rate for a PS-DVB porous layer fabricated in a (a) 50 µm ID, (b) 100 µm ID and (c) 150 µm ID capillary at linear flow rates of 0.25, 0.5, and 1.0 mm/sec. Polymerisation temperature was 60 °C.

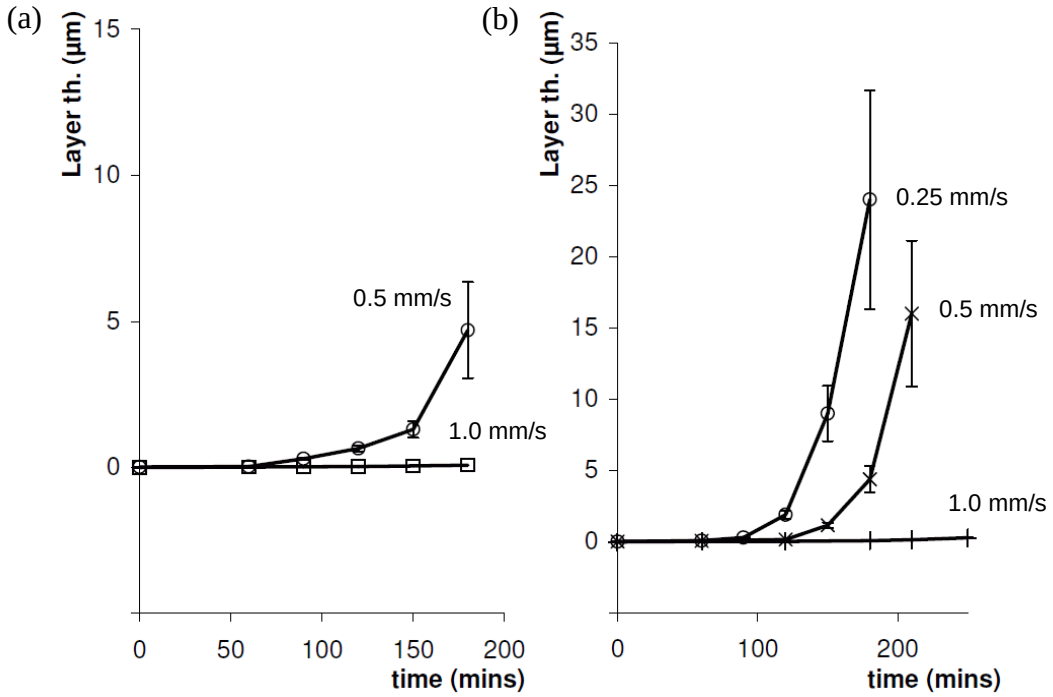

Figure 5.13 – Comparison of layer thickness against linear flow rate for a BuMA-EDMA porous layer fabricated in a (a) 50 µm ID and (b) 100 µm ID capillary at linear flow rates of 0.25, 0.5, and 1.0 mm/sec. Polymerisation temperature was 60 °C.

The relationship between linear flow velocity and layer thickness for a BuMA-EDMA layer in 50 and 100 μm ID capillaries is shown in Figure 5.13(a) and (b). Again, there is good correlation between the rates of layer growth in the two capillary sizes. As per the PS-DVB layer, the %RSD value for the 50 μm ID capillary is slightly higher (35% compared with 21% for the 100 μm ID capillary) at 0.5 mm/sec flow, probably due to increased turbulence in the fluid due to layer build up.

It is interesting to note that the layer formation occurred more slowly in case of the BuMA-EDMA phase, as compared to PS-DVB. The formation of a 3 μm layer in 50 μm ID capillary at a flow velocity of 0.5 mm/s took ~180 min for BuMA-EDMA, and only ~120 min for PS-DVB. This may be partially related to the BuMA-EDMA polymerisation mixture exhibiting a higher viscosity (see Figure 5.7), which causes an increase in shear stress (see eq. (5.3)) and slows down the layer formation compared with the PS-DVB mixture. Clearly, the viscosity of the polymerisation mixture plays a significant role, as generally methacrylate based monomers are characterised by a higher reaction rate of the chain growth step, compared to styrene based monomers [17].

5.4.3 Initial chromatographic performance evaluation

One of the key advantages of monoPLOT columns is high flow-through permeability, which makes them a promising type of stationary phases for low pressure chromatography. Although PLOT columns have been applied in LC separation [4], the PS-DVB columns were based upon 10 μm ID fused silica capillary of 4.2 m length. These long PLOT columns showed great efficiency and peak capacity for the separation of protein digests, however, the separation time and backpressure were extremely high.

Herein, as expected, a significant reduction in column length and increased internal diameter (300 x 0.1 mm ID, layer thickness 2 μm), compared to the above study [4], obviously resulted in much lower peak capacities and efficiencies. However, the low pressure liquid chromatographic separations obtained demonstrate considerable potential for further optimisation, including the formation of columns of greater length. Initial chromatographic performance was investigated by separating a mixture of 10 proteins using a simple 35 min acetonitrile-water gradient (0.1% TFA) from 1 to 90% ACN. Column temperature was kept constant at 22 °C. The flow rate applied was 1 μL/min, and importantly the backpressure was only 0.6 MPa. This initial low pressure separation obtained on the above column is shown in Figure 5.14.

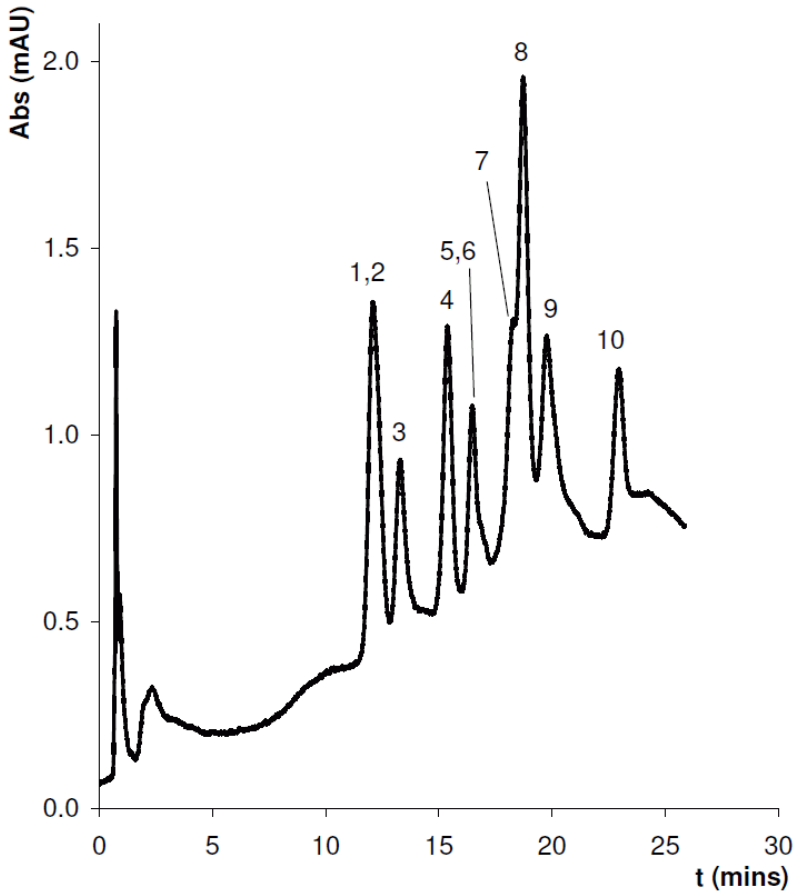

Figure 5.14 – Separation of ten proteins (1. Insulin, 2. Ribonuclease B, 3. Trypsin, 4. Ribonuclease A, 5. Cytochrome C, 6. Myoglobin, 7. Horseradish Peroxydase, 8. Phosphatase B, 9. Carbonic Anhydrase, and 10. Concanavalin A) under ACN-water gradient conditions: from 1 to 90% acetonitrile (0.1% TFA) over 35 min, flow rate 1 µL/min. Column: 300 mm x 50 µm ID PS-DVB monoPLOT column, layer thickness ~2 µm. UV detection at 214 nm.

5.5 Conclusions

A new method for the fabrication of thermally initiated monoPLOT columns with fine control over the polymerisation process was described. The proposed method allows precise control of both layer thickness and morphology, and is potentially applicable to a variety of polymer phases within a large variety of capillary formats, significantly expanding the range of monoPLOT columns available for application within both GC and LC. Herein, the process was demonstrated with two polymers, namely PS-DVB and BuMA-EDMA, and on three column sizes, showing the process to be scalable and with a high dependency on fluid shear stress within the capillary. The relationship between linear flow velocity of the fluid and both layer thickness and morphology was demonstrated at a polymerisation temperature of 60 °C. An initial chromatographic evaluation was shown for the low pressure separation of a test mixture of proteins.

Reference list

1. Golay, M. J. E; *Gas Chromatography*; Coates, V.J., Ed. Academic Press: New York, (1958), pp. 1.
2. de Zeeuw, J.; *LC-GC*, (2011), 24, pp 38.
3. Nischang, I.; Brueggemann, O.; Svec, F.; *Anal. Bioanal. Chem*. (2010), 397, pp. 953.
4. Luo, Q.; Rejtar, T.; Wu, SL.; Karger, B.; *J. Chromatogr., A*, (2009), 1216, pp. 1223.
5. Huang, X.; Zhang, J.; Horvath, C.; *J. Chromatogr., A*, (1999), 858, pp. 91.
6. Tan, Z.J.; Remcho, V.T.; *J. Microcolumn Sep.*, (1998), 10, 1, pp. 99.
7. Tan, Z.J.; Remcho, V.T.; *Anal. Chem*., (1997), 69, 4, pp. 581.
8. Chuang, S.C.; Chang C.Y.; Liu C.Y.; *J. Chromatogr., A*, (2004), 1044, pp. 229.
9. Shen, T.C.; *J. Chromatogr. Sci.*, (1992), 30, 6, pp. 239.
10. Banu, I.; Bildea, S.; Bozga, G.; Puaux, J.P.; *Stud. Univ. Babes-Bolyai, Chem.*, (2009), 54, 1, pp. 227.
11. Castro, J.M.; Lipshitz, S.D.; Macosko, C.W.; *AIChE J.*, (1982), 28, 6, pp. 973.
12. Wehner, J.F.; *Chemical Reaction Engineering - Houston*, (1978), DOI: 10.1021/bk-1978-0065.ch012.
13. Nesterenko, E. P.; Nesterenko, P. N.; Connolly, D.; Lacroix, F.; Paull, B.; *J. Chromatogr., A*, (2010), 1217, pp. 2138.
14. Cifuentes, A.; Diez-Masa, J.C.; Fritz, J.; *et al*.; *Anal. Chem*., (1998), 70, 16, pp. 3458.
15. Fox, R.; McDonald, A.; Pritchard, P.; Introduction to Fluid Mechanics, 7th edition, Wiley: New York, (2009), 768 p.

16. www.polymicro.com, (accessed November 2012).

17. Odian,G., Principles of Polymerisation, 4th edition.; Wiley: New York, (2004), 832 p.

CHAPTER 6.

IN-PROCESS LAYER MEASUREMENT FOR MONOPLOT COLUMN FABRICATION

Relevant publications:

Collins, D.; Nesterenko, E.; Brabazon, D.; Paull, B.; *The Analyst*, (2013), 138, pp. 2540-2545.

Abstract

Although several techniques for the fabrication of monoPLOT columns have been developed, they all rely on empirical and experimental data and require re-optimisation once transferred between capillary housings of different dimensions. Therefore, there is a need for an in-process method for the control of the polymer layer growth.

Two techniques for the in-process measurement of polymer stationary phase growth inside fused silica capillaries during the fabrication of monoPLOT columns are introduced, based on optical absorbance in the IR range and C4D. In the first case, the relationship between optical absorbance and polymer layer thickness was investigated for BuMA-EDMA polymers, formed inside 100 µm ID Teflon and polyimide coated capillaries by photo- and thermal-initiation. The optical absorbance for a range of layer thicknesses was measured and the effect of the optical aperture size was evaluated through the use of 8 and 100 µm optical fibres. The success of the technique proved to be highly dependent on the alignment of the capillary between the optical fibres and crucially on the surface quality of the capillary coating, resulting in %RSD values for layer thickness of between 22 and 27%. The technique was also limited by the optical power of the light source, requiring long data integration times for the 8 µm optical fibre. Secondly, the relationship between effective capillary diameter and C4D response was investigated for two polymers, BuMA-EDMA and PS-DVB over a range of capillary diameters and layer thicknesses. The technique was shown to be very precise, with a measured %RSD for layer thickness of < 10%.

The described methods can be used with both photo- and thermally-initiated approaches for monoPLOT fabrication and in the case of C4D provide an accurate, real-time measurement

of the porous layer growth within the capillary, which should vastly improve column-to-column reproducibility.

Aims

The aim of the work presented in Chapter 6 was to develop methods for the non-destructive, in-process measurement of the polymer layer growth during the fabrication process of monoPLOT columns. This worked aimed to develop two online measurement methods, namely optical absorbance and capacitively coupled contactless conductivity defining their relationship with polymer layer thickness.

6.1 Introduction

Several techniques for the manufacture of PLOT columns exist [1-7] and include both thermal- and photo-initiated methods. However, in the majority of these techniques, it is difficult to precisely control layer thickness and morphology. In Chapters 4 and 5 two methods which allow the fine control of both layer thickness and morphology were presented. In Chapter 4 the capillary was subjected to repeated exposures to UV light, slowly building up the required layer thickness while also maintaining the desired morphology. The main disadvantage of such an approach was the need for the optimisation of the reaction conditions (number of passes and UV light intensity) when the polymerisation mixture was changed, or capillary of different ID or length were used, which can be quite laborious. In Chapter 5 this problem was addressed by the introduction of laminar flow polymerisation which uses the laminar flow properties of the polymerisation mixture as it is pumped through the capillary to control layer growth and morphology.

Although the above methods have shown good column to column reproducibility for fully polymerised monoliths, there is still a significant amount of experimental work which must be done to achieve the required layer thickness and pore morphology in case of monoPLOT columns. Changing the pore structure and/or layer thickness usually means the development of new procedures, and so the manufacture of monoPLOT columns in different capillary sizes, with different layer thickness and structure creates a lot of additional experimental work. As a result, there is a significant need for in-process checks during the fabrication process simply as a quality control measure.

In this Chapter, two non-invasive, in-process methods for measurement of the layer growth, involving optical absorbance and C4D are presented and their application to existing approaches to the fabrication of monoPLOT columns through both photo- and thermal-initiation is discussed. Additionally, the advantages, disadvantages, and suitability of the methods are discussed, particularly in relation to the accuracy of the method and with respect to the reproducibility of the fabrication process which is being employed.

6.2 Experimental

6.2.1 Reagents and materials

Materials used for in-process layer measurements during monoPLOT fabrication were as described in Sections 4.2.1 and 5.2.1. Additional materials used in this Chapter are listed below:

- Rapid prototype parts were produced as per Section 2.2.1.
- Boxes and enclosures were purchased from Radionics Ltd., Dublin, Ireland.
- Fabricated parts were manufactured in-house.
- Electronic components were purchased from Radionics Ltd., Dublin, Ireland, and Farnell Ltd., Leeds, United Kingdom.
- For the absorbance measurements using the precision aperture, 20 µm precision pinholes were purchased from Edmund Optics, York, UK.
- Fibre optic cables (8 & 100 µm) and connectors were purchased from Fibre Pulse Ltd., Mayo, Ireland.

All chemicals were reagent or analytical grade purity. For the fabrication of monolithic stationary phases reagents and chemicals used were as per Sections 2.2.2 and 3.2.1.

6.2.2 Instrumentation

- Capillaries were filled with monomer mixture and washed using a KDS-100-CE syringe pump (KD Scientific, Inc., Holliston, MA, USA).
- Fabrication of thermally-initiated monoPLOT columns for off-line optical and C4D characterisation was carried out in a water bath, using a Yellow Line MST Basic hotplate with TC1 temperature controller and glassware (VWR Ltd., Dublin, Ireland).
- Thermal-initiation of monoPLOT columns using C4D as an in-process measurement was carried using a Dionex Ultimate 3000 nano-HPLC system (Dionex, Sunnyvale, California, United States).
- A PHD2000 syringe pump, purchased from Harvard Apparatus (Holliston, MA, United States) was also used to pump polymerisation mixture during the fabrication process.
- A Rheodyne 6-port switching valve (Rheodyne, California, United States) was used to switch between the polymerisation mixture and MeOH flows.
- The light source used during absorbance measurements using fibre optics was a DH-2000-FHS Deuterium Tungsten Halogen Light Source purchased from Ocean Optics, Dunedin, Florida, USA.

- Optical absorbance was measured using a USB650 spectrometer purchased from Ocean Optics, Dunedin, Florida, USA.
- For the measurement of layer growth by C4D during thermal-polymerisation, a TraceDec capacitively coupled contactless conductivity Detector (Innovative Sensor Technology GmbH, Strasshof, Austria) was used. Settings used during the measurement were as follows: frequency, 3× HIGH; voltage, −6 dB; gain, 50% and offset, 0.
- A purpose built, C4D sensor head, designed to operate at elevated temperatures was specially made for these experiments by Innovative Sensor Technology GmbH.
- Data acquisition was done via TraceDec Monitor V. 0.07a software, also supplied from Innovative Sensor Technology GmbH.
- A SputterCoater S150B (BOC Edwards, Sussex, United Kingdom) was utilised for coating capillary monolithic stationary phase samples with a 60 nm gold layer.
- Scanning electron microscopy (SEM) analysis was performed on a S-3400N instrument (Hitachi, Maidenhead, United Kingdom).

6.2.3 Software

- Absorbance measurements were taken using SpectraSuite (version 2008), purchased from Ocean Optics, Dunedin, Florida, USA.

- C4D measurements were taken using eDAQ Chart (version 5.2.18) purchased from eDAQ Pty Ltd., NSW, Australia.
- C4D measurements were also taken using TraceDec Monitor (version 0.07a) purchased from Innovative Sensor Technology GmbH, Strasshof, Austria.
- Pressure data acquisition was made using Chromeleon 6.8 software purchased from Dionex, Sunnyvale, CA, USA.

6.2.4 Experimental procedures

6.2.4.1 Capillary silanisation

Capillary silanisation was carried out as per the procedure in Section 2.2.5.1.

6.2.4.2 Fabrication of BuMA-EDMA monoPLOT columns

The fabrication of BuMA-EDMA monoPLOT columns by photo-initiation was carried out as per the procedure in Section 4.2.5.3. Thermally-initiated fabrication of BuMA-EDMA monoPLOT columns was carried out as per the procedure in Section 5.2.3.1.

6.2.4.3 Fabrication of PS-DVB monoPLOT columns

The fabrication of PS-DVB monoPLOT columns by thermal-initiation was carried out as per the procedure in Sections 5.2.3.2 and 5.2.3.3. For studies carried out with C4D, a solution of 1 %wt 10 m*M* NaCl prepared in H_2O was added to the PS-DVB polymerisation mixture to increase its conductivity.

6.2.4.4 Measurement of monoPLOT layer thickness by optical absorbance

A previous work by Florea *et al.* [8] successfully characterised a spiropyran coating inside fused silica capillaries using optical absorbance. In this work, the author used micro-fluidic connectors and couplings to align 100 µm fibre optic cables with 100 µm ID Teflon coated capillaries. The same arrangement was employed for the measurement of the monoPLOT layer thickness, see Figures 6.1 and 6.2.

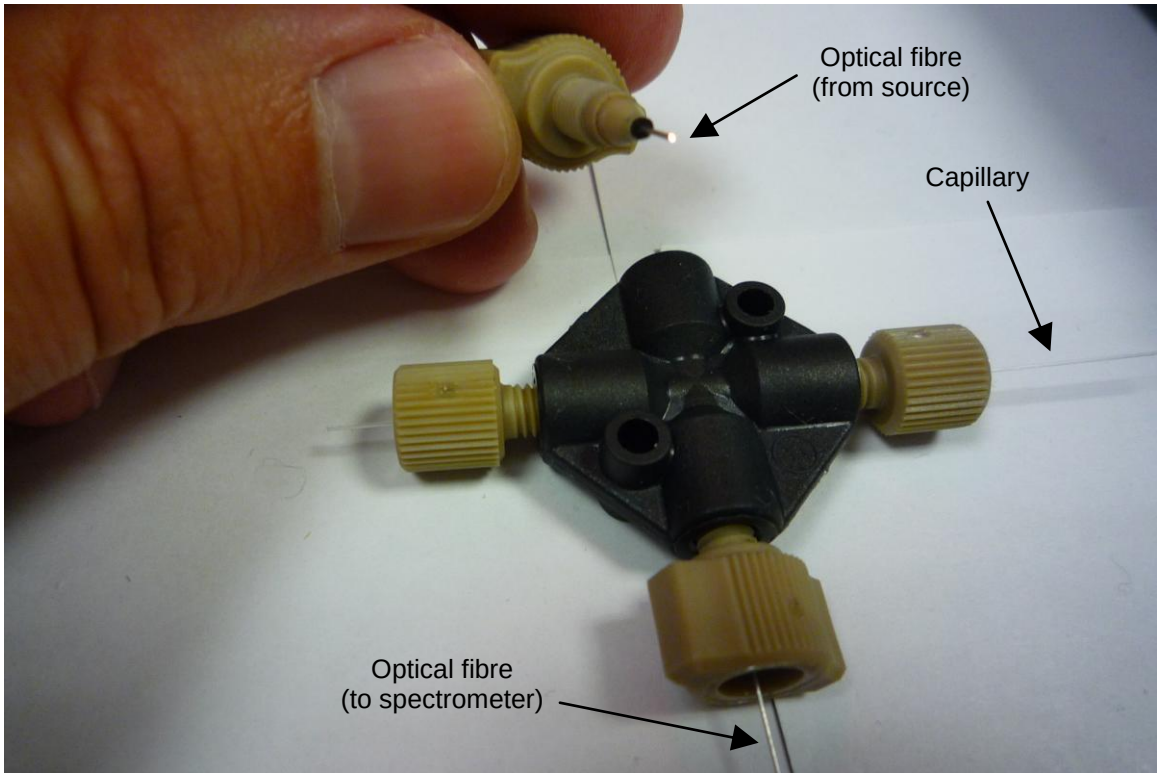

Figure 6.1 – Arrangement of fibre optic and coupling assembly for the in-process measurement of monoPLOT layer thickness using optical absorbance.

In order to accurately measure the absorbance across the monoPLOT column, it was first necessary to align the optics precisely with the centreline of the capillary. This was achieved using a 4-port coupling which aided in the alignment of the optical fibres and

capillary. Standard 1/16th OD micro-fluidic connectors were used to connect and hold the optical fibres in place as shown in Figure 6.1. For online studies, this arrangement was mounted next to a feed through UV curing oven which allowed the capillary to be fed through the device, facilitating the in-process measurement of the layer growth (see Figure 6.2). Optical power of the light source was approximately 1100 µW/cm^2 at 700 nm. This wavelength was used for all optical absorbance studies.

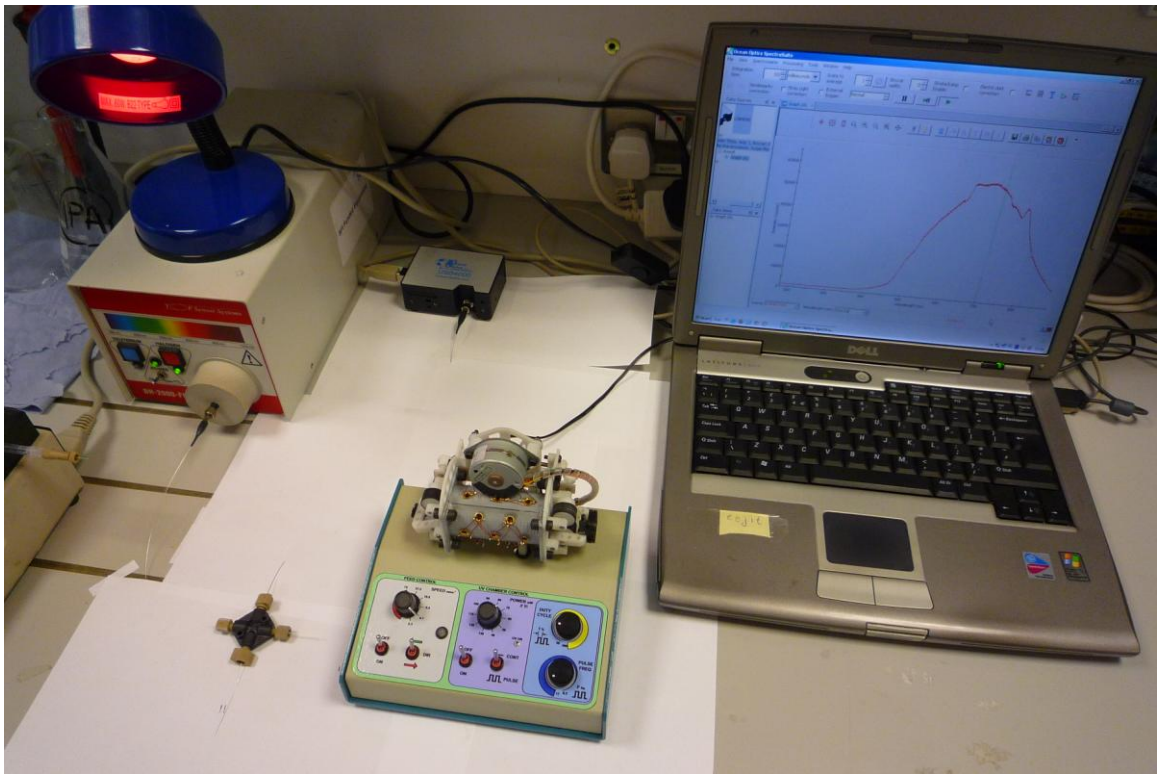

Figure 6.2 – Instrumentation set-up during the in-process measurement of monoPLOT layer thickness.

6.2.4.5 C4D measurements during thermally-initiated polymerisation

C4D measurements can be applied to both thermal- and photo-initiated polymerisation. It was noted that in both cases the signal-to-noise ratio (SNR) of the output signal was

dramatically improved by pumping the polymerisation mixture through the capillary during the fabrication process. Two inlet ports of the switching valve were connected to two syringes filled with polymerisation mixture and with MeOH, respectively. Both syringes were placed in a syringe pump. The desired length of silanised capillary was coiled and one end connected to an outlet port on the switching valve which was mounted outside an air oven. The coiled capillary was mounted in the air oven and the other end was left open so that the polymerisation mixture could flow through it to waste. The C4D cell was attached to the capillary so that it was also mounted within the air oven.

The polymerisation mixture was pumped through the capillary at a linear flow rate of 0.5 mm/s. After flow was established and the C4D response had stabilised the air oven temperature was increased to 60 °C. The C4D response rose with an increase in temperature and once the oven temperature stabilised the C4D response also became steady state. After some time, formation of the porous polymer layer began and thus the effective internal diameter of the capillary reduced causing the C4D response to fall. The formation of the porous polymer layer was allowed to continue until the desired C4D output was reached, after which the capillary was removed from the oven. The switching valve was also switched over to flush the capillary with MeOH in order to remove all unreacted monomer. Once the capillary had been thoroughly washed it was removed and dried with nitrogen.

6.3 Theory

6.3.1 Optical absorbance

Several methods exist for the measurement of thin film thickness, ranging from β- and X-ray techniques [9,10], electrical impedence and conductivity [11,12], to tactile methods such as atomic force microscopy (AFM) [13,14,16]. Various optical techniques can also be applied [10,13,15], including optical absorbance. Optical absorbance is a commonly used method and finds application in a wide variety of detection and measurement techniques [17]. It should be noted that in this case the measured absorption is due to attenuation of the light signal, caused by both absorption of the layer material and scattering of the light.

Using Lambert's absorption law it is possible to directly apply optical absorption to the measurement of the polymer layer thickness within a monoPLOT column. The fractional change in intensity of the incident beam, $-dI_O/I_O$, will be proportional to the thickness and density of the polymer layer. This relationship can be represented as:

$$-\mathrm{d}I_O = \mu I_O \,\mathrm{d}x \qquad \text{eq. (6.1)}$$

where:

I_O = intensity of incident light

μ = linear attenuation coefficient of the layer

$\mathrm{d}x$ = layer thickness

The linear attenuation coefficient, μ, is related to the density of the material, ρ, which in turn is related to the porosity.

Integrating eq. (6.1) gives:

$$\ln(I_O / I) = \int_0^d \mu \, \mathrm{d}x$$

eq. (6.2)

The transmission of light through the polymer layer can also be expressed in terms of absorbance, *A*:

$$A = -\log_{10}(I / I_O)$$

eq. (6.3)

Since the intensity of the incident light drops due to absorption within the polymer layer, and the level of absorption is relative to the thickness and density (porosity) of the layer, then it is possible to relate absorption to the physical properties of the polymer layer.

6.3.2 C4D response

Early reports on contactless conductivity detection were published in 1980 by Gas *et al.* [18,19], however, C4D as we know it today was developed by two independent research groups in 1998 [20,21] as a detection method for small inorganic ions in capillary electrophoresis. Two radial electrodes (which are placed around the capillary at approximately 2 - 5 mm apart) supply and detect an induced current in the solution within the capillary. The magnitude of the detected signal is proportional not only to the magnitude of the excitation signal, but also to the concentration and mobility of the ionic charge carriers within the solution. A complete explanation of the fundamental concept behind C4D is beyond the scope of this work but can be found in the excellent review by Kuban [22].

C4D has been previously used to characterise stationary phase homogeneity of packed columns [23,24] polymer monoliths formed within capillaries [25] and layer thickness of preformed monoPLOT columns in off-line approaches [1]. The application of C4D to the detection of polymer layer growth with a capillary is technically relatively straightforward; however, there are some considerations which must be taken into account. First of all the polymerisation mixture must contain a charged species in order to generate any kind of useful signal and so a 1 %wt solution of 10 m*M* NaCl prepared in H_2O was added to the polymerisation mixture. Secondly, the type of polymerisation is important – for photo-initiated polymerisation the C4D cell must be placed outside the reaction chamber, or else the electrodes should span the chamber so as not to mask any area of the capillary. For thermally-initiated polymerisation the C4D cell must be immersed in the air or water bath, and so some additional considerations must be made for this setup, these will be discussed later.

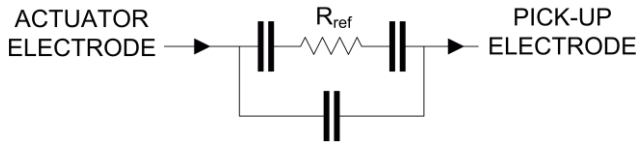

Figure 6.3 – Equivalent circuit diagram of a typical C4D cell.

An equivalent circuit diagram of the C4D cell is shown in Figure 6.3. In this model, R_{ref} represents the resistance of the solution between the electrodes. When a charged species passes through the detector the resistance of R_{ref} decreases due to the increased conductivity

and thus the corresponding voltage drop across the cell, V_{Rref} will change. There is an inverse relationship between resistance and conductivity:

$$\sigma = \frac{1}{\rho}$$

eq. (6.4)

where:

σ = conductivity of the conductor material

ρ = resistivity of the conductor material

Resistance is not only a function of the electrical resistivity of the conductor material (in this case the polymerisation solution) but also depends on the geometry of the conductor. The resistance, R, of a conductor of uniform cross section is given by:

$$R = \rho \frac{L}{A}$$

eq. (6.5)

where:

L = length of conductor

A = cross sectional area of conductor

As can be seen from eq. (6.5), the resistance of a conductor is inversely proportional to its cross sectional area. The volume of polymerisation mixture that exists between the excitation and pick-up electrodes (separated by a distance, L) can be viewed as the resistor

in the case above. At the start of the polymerisation process, no porous polymer layer exists within the capillary and so the effective cross sectional area, A_{eff}, of the resistor is equal to the capillary cross sectional area (see Figure 6.4). As the layer grows, the effective capillary cross sectional area, A_{eff}, will get smaller, increasing the resistance, R_{Ref}, and causing a larger voltage drop across the C4D cell. By measuring the change in voltage drop, ΔV_{Rref}, it is possible to measure the porous layer build up inside the capillary. Since the conductivity (and hence the resistance) of the volume between the electrodes is proportional to the ionic mobility of the solution, pumping the mixture through the capillary during the polymerisation process results in a very stable response.

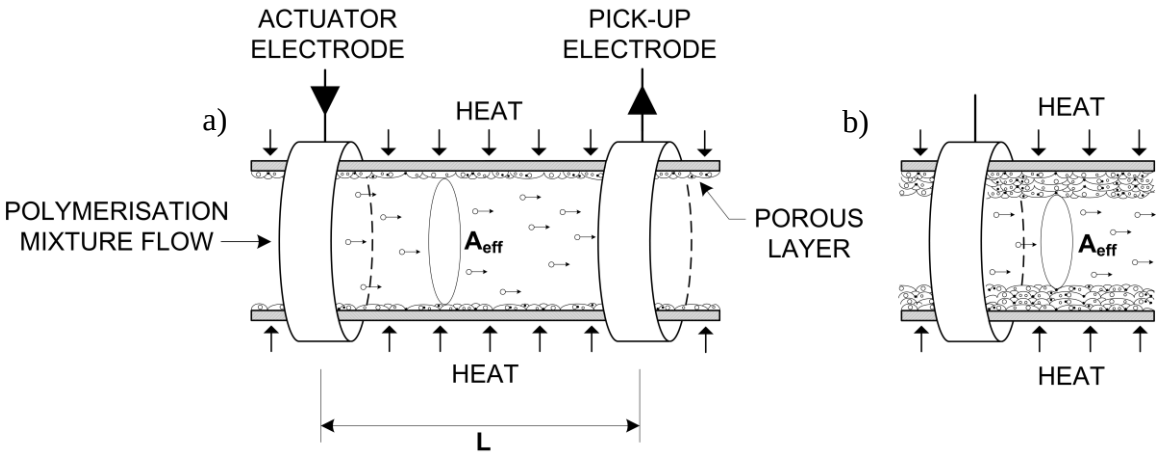

Figure 6.4 – (a) Section view of capillary and C4D electrodes during the polymerisation process and (b) the reduction in the cross sectional area, A_{eff}, due to layer growth.

6.4 Results and discussion

6.4.1 Measurement of layer by optical absorbance

Prior to optical absorbance measurements it was first necessary to choose a suitable wavelength which could be used for both Teflon and polyimide coated capillaries and a range of different polymers. From Figure 5.1 (Section 5.1) it can be seen that polyimide absorbs strongly up to approximately 600 nm.

An initial experiment was carried out to measure the near-IR absorbance spectra of the BuMA-EDMA polymerisation mixture and a 4.2 µm BuMA-EDMA polymer layer, both in Teflon coated capillary, see Figure 6.5. Based on the absorbance spectra, 700 nm was selected as the optimal wavelength for the measurement of optical absorbance. This wavelength was chosen as it is suitable for both Teflon and polyimide coated capillary.

Studies of layer thickness were initially carried out on a BuMA-EDMA layer formed in Teflon coated capillary by photo-initiated polymerisation. This experiment attempted to measure monoPLOT layer growth during the fabrication process, by feeding the capillary through the optical detector (see Figure 6.2). However, these early results had a low SNR and repeatability due to poor alignment. In order to allow the capillary to pass freely through the optical detector a small amount of clearance was required between the sleeve and the capillary which had a negative impact by allowing the capillary to move relative to the axis of the optical fibres.

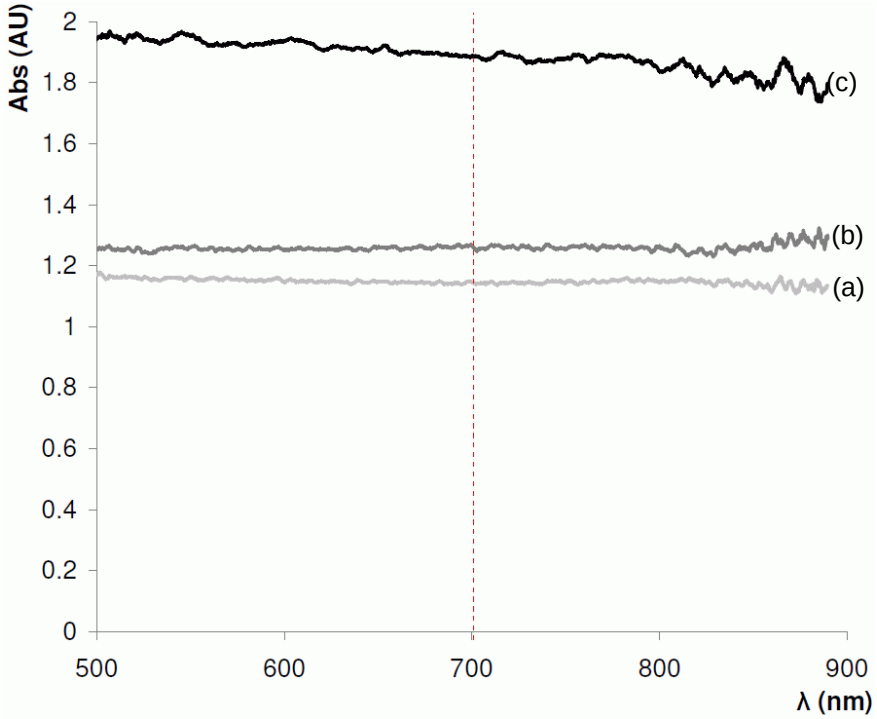

Figure 6.5 – Absorption spectra for a 100 µm ID Teflon coated fused silica capillary in the near-IR range (500 – 1000 nm) using a 100 µm optical fibre; (a) empty, (b) filled with BuMA-EDMA monomer mixture, and (c) with a 4.2 µm BuMA-EDMA polymer layer.

A second study was carried out to measure layer monoPLOT layer thickness off-line. This was achieved by forming a BuMA-EDMA monoPLOT column using the laminar flow polymerisation technique already described (see Sections 5.2.3.1 and 5.2.3.3) and removing samples at different periods during the process. A total of 10 samples were taken, with layer thicknesses ranging from 100 nm up to ~5 µm. The samples were immediately placed in the optical detector and the level of absorbance recorded at 30 locations along the sample. The samples were then washed with MeOH and a precise

a)

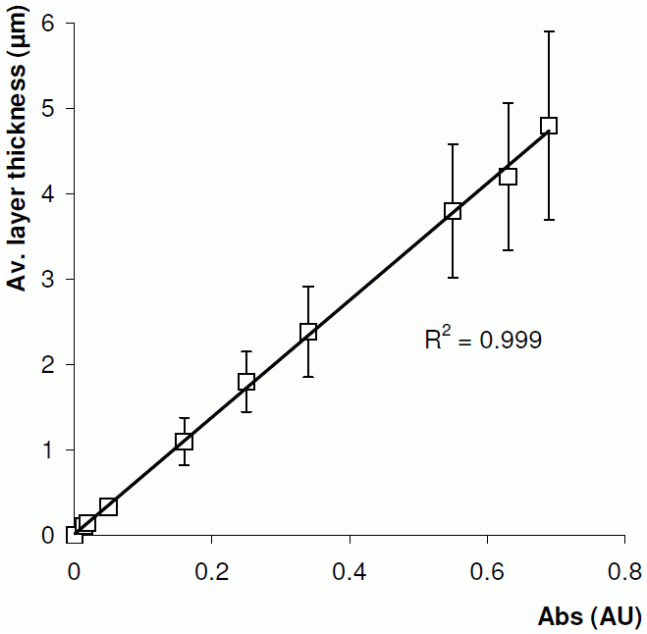

b)

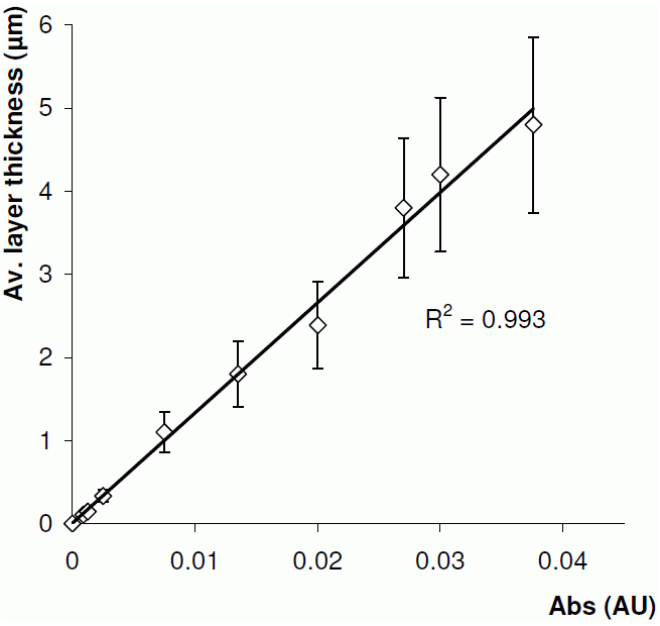

Figure 6.6 – Relationship between monoPLOT layer thickness and optical absorbance at 700 nm for PS-DVB formed inside a 100 µm ID polyimide coated fused silica capillary using (a) 100 µm and (b) 8 µm optical fibre.

measurement of the layer thickness was made using SEM analysis. The results are presented in Figure 6.6(a). The results show excellent linearity between the optical absorbance and layer thickness, however, %RSD was measured at approximately 27%.

Clearly, using a 100 µm optical fibre would have serious limitations in the measurement of layer thicknesses in capillaries with internal diameters smaller than 100 µm, and so the experiment was repeated with a modified optical cell using a 8 µm optical fibre. The results for the 8 µm fibre are presented in Figure 6.6(b). Again, excellent linearity was observed and a %RSD of 22%. However, using an optical fibre with such a small diameter meant that the measured response was extremely low. In order to improve the response, a spectrometer integration time of approximately 10 sec was required. Since each measured thickness was made up of n = 30 samples, it took several minutes to record each data point. From Section 5.4.2 it can be seen that the rate of polymer growth is exponential and the layer thickness can more than double over several minutes making this technique difficult to employ, particularly for thicker layers where the polymer growth is fast. However, the technique could be improved in terms of speed and sensitivity by using a higher power light source. A further drawback of the technique is that optical absorbance will be sensitive to the morphology of the polymer layer, with denser, less porous layers absorbing more light than more porous structures.

6.4.2 In-process measurement of monoPLOT layer using C4D

Prior to using C4D response as an in-process measurement for layer thickness, it was necessary to show that the C4D cell was stable during repeated long exposures to elevated temperatures. Initial studies had shown that after some time the C4D response displayed excessive baseline drift and decreased SNR. Further exposure to elevated temperatures (60 °C) resulted in a permanently damaged C4D cell which exhibited poor SNR and sensitivity. Using a purpose built C4D cell designed to operate at 60 °C the stability tests were repeated. Figure 6.7 compares stability of the standard and high temperature C4D cells over a 20 hr period.

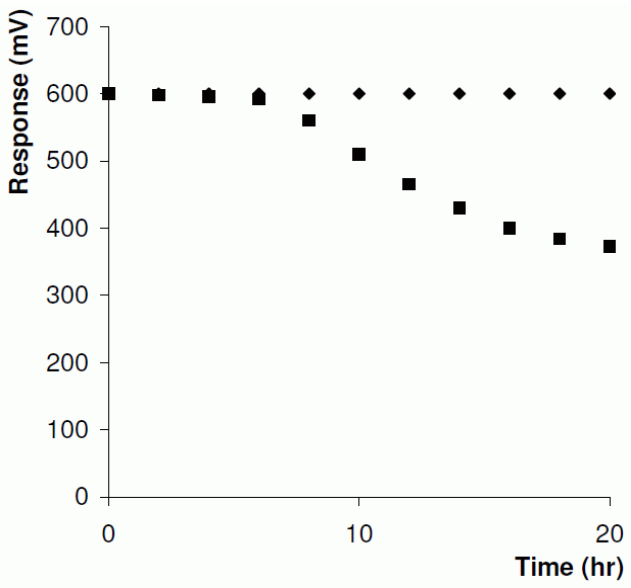

Figure 6.7 – Comparison of baseline drift for a standard TraceDec C4D cell (■) *and a purpose built high temperature C4D cell* (◆) *over a 20 hr period at 60 °C.*

As can be seen from Figure 6.7, the C4D cell designed to operate at high temperatures remained stable even after 20 hrs of repeated exposure to 60 °C. Secondly, it was necessary to demonstrate that the technique was repeatable, regardless of the position of the C4D cell on the capillary. In order to achieve this, polymerisation mixture without the thermal

initiator (AIBN) was pumped through a 30 cm length of empty 100 µm ID capillary at a temperature of 60 °C. The C4D response was measured every 5 mm (60 locations) along the column. This was repeated for another 30 cm length of 100 µm ID capillary with a known layer thickness of ~2 µm, again at a temperature of 60 °C. The linear flow rate was varied between 0.25 and 1.5 mm/s with no change in the response observed. Figure 6.8 represents the C4D response for both capillaries at each location, showing a very stable signal for both scans. The difference in the magnitude of signal between empty capillary and monoPLOT with 2 µm layer is clear.

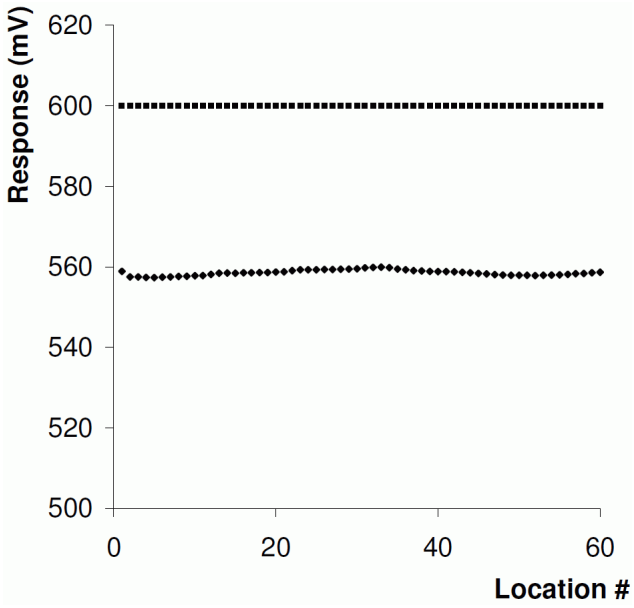

Figure 6.8 – C4D response recorded at 60 locations for an empty 100 µm ID capillary (■) *and for a 100 µm ID capillary with a 2 µm porous layer* (◆)*. Output is approximately 601 and 557 mV respectively.*

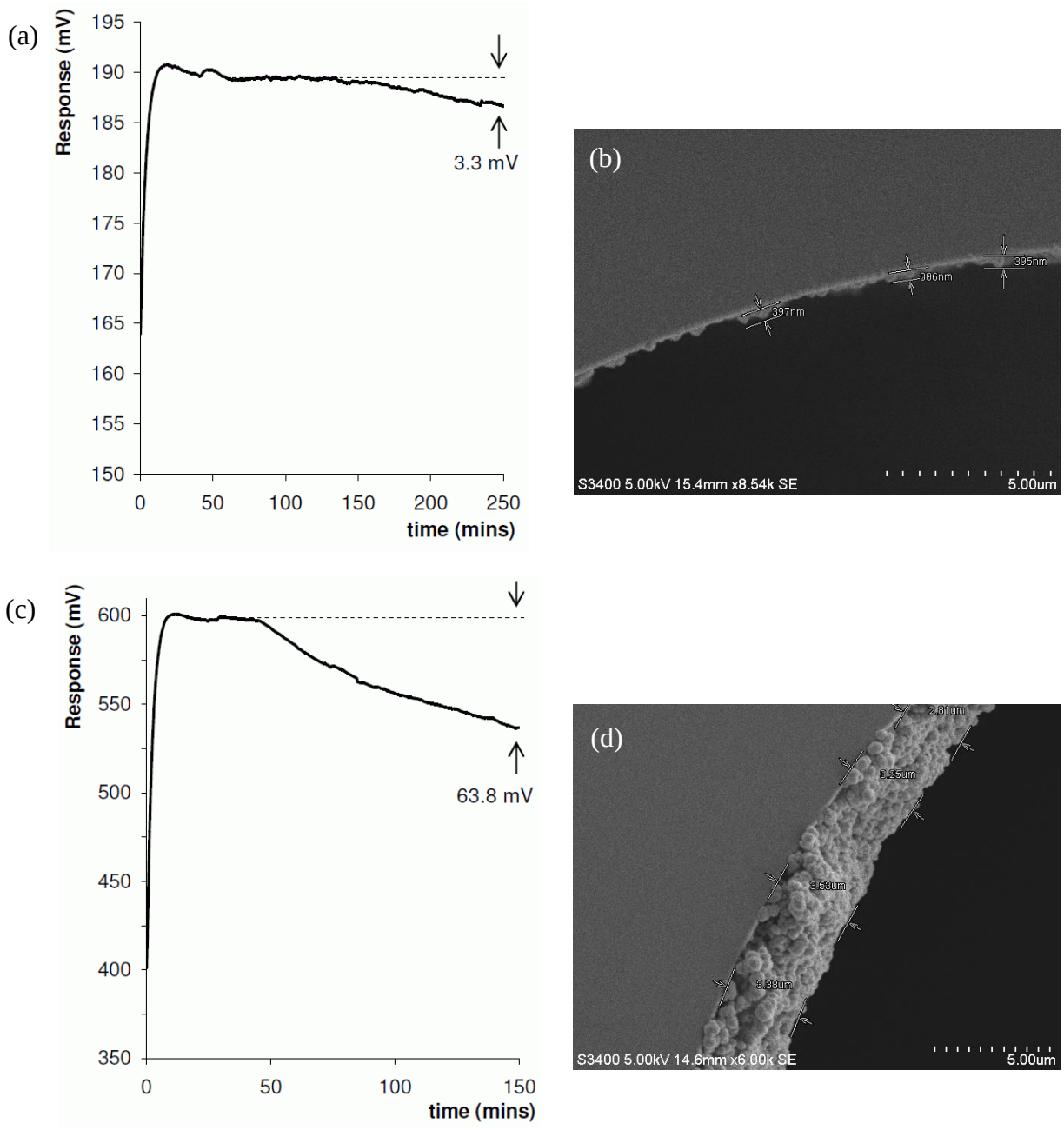

Figure 6.9 – (a) C4D response recorded during polymerisation of a ~400 nm layer inside a 50 µm ID capillary and (b) SEM image of fabricated layer. Polymerisation conditions: mixture = BuMA/EDMA with 1% 10 mM NaCl, temperature = 60 °C, linear flow rate = 1.0 mm/s. Change in C4D response was recorded as 3.3 mV, corresponding to a theoretical layer thickness of 370 nm. (c) C4D response recorded during polymerisation of a ~3.3 µm layer inside a 100 µm ID capillary and (d) SEM image of fabricated layer. Polymerisation conditions: mixture was PS-DVB with 1% 10 mM NaCl, temperature = 60 °C, linear flow rate = 0.5 mm/s. Change in C4D response was recorded as 63.8 mV, corresponding to a theoretical layer thickness of 2.98 µm.

During in-process measurements, the C4D cell was placed inside the air oven and the output was recorded during the polymerisation process. Figure 6.9 shows two examples of layer formation and C4D response during polymerisation of BuMA/EDMA and PS-DVB layers at flow rates of 1.0 and 0.5 mm/s respectively. C4D response fluctuations due to oven temperature instability at the start of the process can be clearly seen in Figure 6.9(a). Figure 6.9(c) shows a more stable C4D response, with only slight overshoot, again due to some variation in oven temperature. It is interesting to note that the porosity of the layer has only a slight, but negligible impact on the measured output. For the example shown in Figure 6.9(a), the drop in C4D response (ΔV_{Rref}) was recorded at 3.3 mV which corresponds to a theoretical layer thickness of 370 nm. The actual average layer thickness (see Figure 6.9(b)) was measured at ~400 nm, %RSD ~7.5 %. For Figure 6.9(c), the ΔV_{Rref} value was 63.8 mV which corresponds to a theoretical layer thickness of 2.98 µm. The actual layer thickness (see Figure 6.9(d)) was measured at ~3.3 µm, %RSD 9.6 %.

A further study of ten samples was carried out for capillaries of both 50 and 100 µm ID with layers of thickness 400 nm up to 15 µm. The measured C4D response for each capillary was plotted against the average measured layer thickness in each case and Figure 6.10 shows the linear relationship between C4D response and effective capillary ID, ID_{eff}.

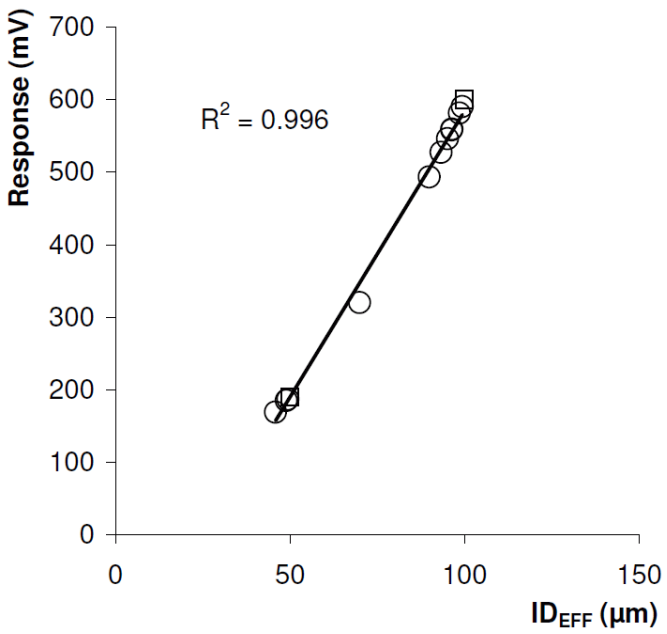

Figure 6.10 – Relationship between effective capillary ID and C4D response, showing both bare capillary (□) *and capillary with monoPLOT layer* (○).

Although this technique has been shown to be very precise, demonstrating a good level of stability and relatively easy to implement, it has some limitations. Firstly, static polymerisation within the capillary is not possible as no useful C4D response is obtained - the polymerisation mixture must be allowed to flow through the capillary. Secondly, it is necessary to 'spike' the mixture with some charged species. For the two polymerisation mixtures presented within this work, the addition of 1 %wt of 10 m*M* NaCl had no noticeable effect on the layer morphology or pore structure, however that is not to say that other types of monomer mixture would not be affected. Indeed, initial work in the development of this technique used 2 %wt of 10 m*M* NaCl, which resulted in the formation of smaller pores and thus lower porosity for the same polymerisation conditions (see Figure 6.11). Average pore and globule sizes for the BuMA-EDMA polymerisation mixture were measured from SEM images. For the polymerisation mixture containing 1 %wt of 10 m*M* NaCl, the pore and globule sizes were found to be 0.69 ±0.24 µm and 0.97 ±0.27 µm

respectively, while using 2 %wt of 10 m*M* NaCl the values were 0.26 ±0.10 µm and 0.60 ±0.14 µm. The observation correlates well with the theory for the formation of methacrylate polymers where the introduction (or increase in %) of a polar solvent in the porogen mixture leads to the formation of smaller pores and globules [26].

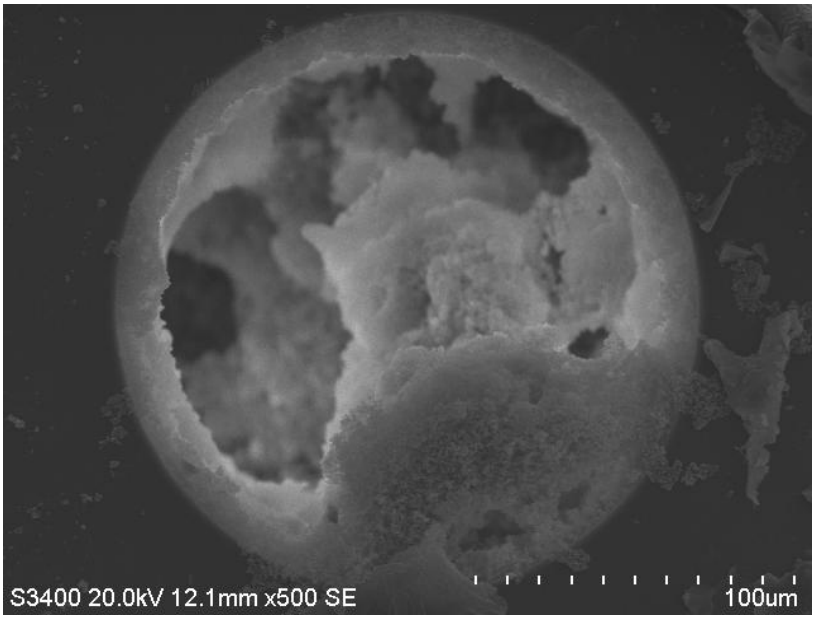

Figure 6.11 – SEM image of overpolymerised BuMA-EDMA monoPLOT column fabricated from a polymerisation mixture containing 2 %wt of 10 mM NaCl.

Perhaps the most difficult aspect of applying C4D as an in-process tool in the fabrication of monoPLOT columns lies with the long term stability of the electronics in the cell itself. From Figure 6.7 it can be seen that for a standard TraceDec C4D cell operated at 60 °C, the device will begin to deteriorate rapidly after approximately 8 hrs use. Even for the high temperature cell, extended use above 60 °C was not advised by the manufacturer.

Lastly, temperature has a large effect on the output signal and it is imperative that the oven is very temperature stable. Ion mobility increases with temperature and so any temperature

fluctuations within the oven will cause signal fluctuations and reduce the overall accuracy of the technique.

6.5 Conclusions

Two novel methods for the in-process measurement of layer growth during fabrication of monoPLOT columns are described and their potential shown. In the case of optical absorbance, a linear relationship between the fabricated monolithic layer and the absorbance was demonstrated for a BuMA-EDMA polymer. This study was carried out on 100 µm ID capillaries over a range of layer thicknesses up to ~4.2 µm. The method was further evaluated for two different types of optical fibre and the application and limitations of the technique to in-process and offline measurements was discussed. In addition, a linear relationship between C4D and effective cross-sectional area of the capillary was also demonstrated. The proposed method was demonstrated with two types of polymer, namely PS-DVB and BuMA-EDMA, on two column diameters, and over a wide range of layer thicknesses, from 400 nm up to 15 µm. The method was also tested for stability and considerations for its implementation were discussed. The application of C4D to the fabrication process allows precise, non-invasive, real time measurement of the growth of the polymer layer, enabling the user to finely control the fabrication process. This method can also be used as a quality control test, allowing the user to characterise the monoPLOT column during production.

Reference list

1. Nesterenko, E.; Yavorska, O.; Macka, M.; Yavorskyy, A.; Paull, B., *Anal. Methods*, (2011), 3, pp. 537.
2. Nischang, I.; Brueggemann, O.; Svec, F. *Anal. Bioanal. Chem*., (2010), 397, pp. 953.
3. Luo, Q.; Wu, S.L.; Rejtar, T.; Karger, B.L., *J. Chromatogr. A*, (2009), 1216, pp. 1223.
4. Huang, X.; Zhang, J.; Horvath, C., *J. Chromatogr., A*, (1999), 858, pp. 91.
5. Tan, Z.J.; Remcho, V.T., *J. Microcolumn Sep.*, (1998), 10, 1, pp. 99.
6. Tan, Z.J.; Remcho, V.T., *Anal. Chem*., (1997), 69, 4, pp. 581.
7. Chuang, S.C.; Chang, C.Y.; Liu C.Y., *J. Chromatogr. A*, (2004), 1044, pp. 229.
8. Florea, L.; Hennart, A.; Diamond, D.; Benito-Lopez, F., *Sens. Actuators, B*, (2012), 175, pp. 92.
9. Veerkamp, T.H.; De Kock, R.J.; Veermans, A.; Lardinoye, M.H.; *Anal Chem*, (1964), 36, 12, pp. 2277.
10. Toney, M.; Mate, M.; Leach, A.; Pocker, D.; *J. Colloid Interface Sci.*, (2000), 225, pp. 219.
11. Macomber, C.; Eastman, M.; Porter, T.L.; Manygoats, K.; Delinger, W., *J. Electrochem. Soc*., (2003), 150, pp. H172.
12. Fitt, A.D.; Owen, J.R., *J. Electroanal. Chem.*, (2002), 538-539,pp. 13.
13. Brand, U.; *et al*., *Meas. Sci. Technol.*, (2011), 22, 094021, pp. 14.
14. Hong, X.; Gan, Y.; Wanga, Y., *Surf. Interface Anal.*, (2011), 43, pp. 1299.
15. Grunlan, J.; Mehrabi, A.; Ly, T., *Meas. Sci. Technol.*, (2005), 16, pp. 153.
16. Lobo, R.; Pereira-da-Silva, M.; Raposo, M.; Faria, R.; Oliveira, O., *Nanotechnology*, (1999), 10, pp. 389.

17. Harris, D., Quantitative Chemical Analysis, 6th edition, W.H. Freeman & Company: New York, (2003), 744 pp.
18. Gas, B.; Demjanenko, M.; Vacik, J., *J. Chromatogr.*, (1980), 192, pp. 253–257.
19. Gas, B.; Vacik, J., *Chem. Listy*, (1980), 74, pp. 652–658.
20. da Silva, J.; do Lago, C., *Anal. Chem.*, (1998), 70, pp. 4339–4343.
21. Zemann, A.J.; Schnell, E.; Volgger, D.; Bonn, G.K., *Anal. Chem.*, (1998), 70, pp. 563–567.
22. Kuban, P.; Hauser, P., *Anal. Chim. Acta*, (2008), 607, pp. 15–29.
23. Connolly, D.; Barron, L.; Gillespie, E.; Paull, B., *Chromatographia*, (2009), 70, pp. 915–920.
24. Connolly, D.; Floris, P.; Nesterenko, P.; Paull, B., *TrAC*, (2010), 29, 8, pp. 870-884.
25. Gillespie, E.; Connolly, D.; Macka, M.; Nesterenko, P.; Paull, B., *Analyst*, (2007), 132, pp. 1238–1245.
26. Svec, F.; Tennikova, T.B.; Deyl, Z., Monolithic Materials: Preparations, Properties and Applications, 1st edition, Elsevier: Amsterdam, (2003), 773 p.

CHAPTER 7.

FINAL CONCLUSIONS AND FUTURE WORK

Several novel instrument developments, platforms, and approaches for capillary chromatography were presented. The aim of the developed platforms was to broaden the horizons of capillary chromatography and facilitate miniaturisation of LC instrumentation.

A new type of direct contact heating/cooling platform for the precise thermal control of capillary and microbore columns was developed. Three prototypes of the device were constructed and thoroughly tested. The developed systems had a broad temperature range, from 5 to 200 °C with a ramp rate of approximately 400 °C/min, and also exhibited excellent steady state response, within ±0.2 °C of the setpoint temperature over a 1 hr period and ±0.5 °C over 24 hrs. Several chromatographic separations involving the application of dual temperature and flow rate gradients, and also rapid temperature programming were performed on the developed systems. Further applications such as fabrication of polymer monoliths in capillary and chip format, monoPLOT columns, and monolithic phases with gradients of porosity were investigated and the precise spatial control of the position of monolithic sections was demonstrated.

Novel technologies for the fabrication of monoPLOT columns using both photo- and thermal-initiation were introduced. In the first case, an approach for photo-initiated fabrication using a feed through in-house built device was developed. This platform allowed the manufacture of long, wide bore monoPLOT columns using light sources in both the UV and IR region. Fine control of the monolith morphology and the formation of polymer layers were demonstrated. The second method developed was based upon the fabrication of thermally initiated monoPLOT columns with fine control over the polymerisation process through the use of thermally initiated laminar flow polymerisation.

The relationship between linear flow velocity of the fluid and both layer thickness and morphology was investigated and the process was shown to be scalable, with a high dependency on fluid shear stress within the capillary.

An initial chromatographic evaluation of the developed monoPLOT stationary phases was also shown. Columns prepared via the fabrication methods described were utilised for the separation of a text mixture of proteins, showing that these novel type of monoPLOT columns exhibit a great potential for low pressure capillary liquid chromatography.

Two methods for the in-process measurement of layer growth during fabrication of monoPLOT columns were developed and their potential and application were investigated. The first approach was based upon the linear relationship between the thickness of the fabricated monolithic layer and optical absorbance, while the second method was based on C4D measurements, using the linear relationship between conductivity and effective cross-sectional area of the capillary. The performance of both methods was tested on a variety of capillary columns of various diameters over a range of layer thicknesses for both PS-DVB and BuMA-EDMA polymer monolithic layers. RSD values for optical absorbance and C4D measurements were observed to be between 22 – 27% and <10% respectively.

Future work will initially focus on the reproducible fabrication of long (>10 m) monoPLOT columns and the impact of column parameters, such as layer morphology (thickness, porosity, etc.) on fundamental chromatographic indicators (retention, selectivity, efficiency). The developed stationary phases will be thoroughly studied for their chromatographic application in GC and in emerging chromatographic modes, such as a low

pressure capillary LC. The work will progress towards the development of miniaturised chromatographic systems based around these new column technologies including the developed heating/cooling platform.

APPENDIX A

Mk. 2 & 3 COLUMN HEATER DESIGN INFO.